IDENTIFICATION OF ISOFLAVONOID CONJUGATES BY HIGH PERFORMANCE LIQUID CHROMATOGRAPHY CONTINUOUS-FLOW LIQUID SECONDARY ION MASS SPECTROMETRY

By

LLOYD W. SUMNER

Bachelor of Science

Cameron University

Lawton, Oklahoma

1989

Submitted to the Faculty of the
Graduate College of the
Oklahoma State University
in partial fulfillment of
the requirements for
the Degree of
DOCTOR OF PHILOSOPHY
December, 1993

IDENTIFICATION OF ISOFLAVONOID CONJUGATES BY HIGH PERFORMANCE LIQUID CHROMATOGRAPHY CONTINUOUS-FLOW LIQUID SECONDARY ION MASS SPECTROMETRY

Thesis Approved:

Horacio A Mottola

Thesis Adviser

Paul W. Flemo

Wad El Rays

Margaret Essenberg

Thomas C. Collins

Dean of the Graduate College

ACKNOWLEDGMENTS

I would like to express my most sincere appreciation to the Noble Foundation for their financial support of this project. Through their continued financial support and the understanding of my graduate committee, I was able to complete my degree in the chosen area of analytical mass spectrometry. I would like to thank Dr. Nancy Paiva of the Noble Foundation for both her scientific input and her help in managing the project. I found that she was always available and willing to help whenever called upon. I would also like to thank her for the unmentionable amount of time contributed in growing and preparing the plant samples used at various points in the project. I would like to thank Dr. Paul Geno for the development of this project and his guidence throughout the project. I would also like to thank him for his continued contributions after his departure from OSU. I would like to thank Dr. Paul Geno, Dr. H. Mottola , and Mr. Tim Smith for their contributions in editing and preparing this thesis. I would like to thank Mr. Paul West for his development of B/E link scans on the ZAB2-SE and for providing the saponin data used for comparision purposes in this thesis. I would like to thank Dr. Ziad ElRassi for the many casual conversations concerning HPLC that provided direction in the nanoscale HPLC study.

I would also like to thank my wife and son, Sherry and Ricky, for their support and sacrifices made while I pursued an advanced degree in analytical chemistry. I

would also like to thank my parents, Mr. and Mrs. Kenneth Sumner, for their encouragement and nurturing of my scientific interests.

Instrumentation support for the VG ZAB2-SE was supplied by NSF Instrumentation Grant BBS-8704089.

TABLE OF CONTENTS

Chapter **Page**

LIST OF TABLES

TABLE **Page**

LIST OF FIGURES

Figure **Page**

CHAPTER 1

INTRODUCTION

I.1 Project Overview and Objectives

Mass spectrometry (MS) has progressively evolved into a powerful analytical tool since its inception in the early 1900's [1]. Its high degree of success can be attributed to the specific chemical information gained from the resultant data. The data provides information such as molecular mass, characteristic fragmentation of functional groups, and "fingerprint" mass spectra that are dependent upon the chemical composition of the analyte [2]. These attributes of mass spectrometry have led us to investigate the use of mass spectrometry to aid in the identification of flavonoid conjugates.

The primary objective of this project was to develop a mass spectrometric method to provide a rapid on-line method for the separation and identification of isoflavonoid conjugates in alfalfa and other plant systems. The objectives were successfully met and the results constitute the major body of this thesis. To attain these goals, several MS techniques were investigated. These included electron-impact mass spectrometry (EI/MS), direct-probe liquid secondary-ion mass spectrometry (DP-LSIMS), continuous-flow liquid secondary ion mass spectrometry (CF-LSIMS), analytical high-performance liquid chromatography continuous-flow liquid secondary

ion mass spectrometry (LC-CF-LSIMS), nanoscale high-performance liquid chromatography continuous-flow liquid secondary ion mass spectrometry (LC-CF-LSIMS), and tandem (LC-CF-LSIMS/MS).

The introduction will present several topics in an attempt to provide the reader with basic information necessary for understanding the project and its rationale. This will begin with selected modern mass spectrometry ionization techniques. Then, an overview of flavonoids and plant response systems will be given. Finally a discussion of the ionization of flavonoid conjugates and the project rationale will be presented to establish the justification for the project.

I.2. *Mass Spectrometry Ionization Techniques*

Mass spectrometry utilizes physical principles to determine the mass-to-charge (m/z) ratio of gas-phase ions. This is accomplished through three generalized processes (i.e. ionization, mass analysis, and detection). Ionization involves the production of gas-phase ions. There are many ionization techniques available which will be discussed in more detail below. Once gas-phase ions have been produced, they are then mass analyzed. Mass analysis can be performed by a number of available instrumental techniques, but the technique used in our experiments utilized a double focusing (magnetic and electric sector) instrument. The mass analyzed ions are then electronically detected and transformed into an observable signal in the form of a mass spectrum. All of the above processes are performed under high vacuum conditions to minimize collisions along the ion trajectories. Collisions lower the number of ions

reaching the detector and, therefore, reduce instrument sensitivity. Active research is performed in each of the above areas, but the more relevant issue for our project was the production of gas-phase molecular ions.

I.3 *Electron Impact Ionization*

The most common and widely used ionization technique today is electron-impact ionization (EI) [3]. EI is achieved by passing a gas-phase molecule through an energetic electron beam. The energy of this electron beam is typically maintained at 70 eV, but can be varied between 20 eV and 70 eV. 70 eV is most commonly used since maximum ionization efficiency occurs at this energy for most organic species [3]. The energy of the electron beam is reported in electron volts where 1 eV (23 kcal/mole) is the energy gained by an electron transversing an electric field sustained at a potential difference of one volt.

The interaction of the molecule and electron beam results in the transfer of energy to the molecular species. The energetic neutral molecule then has sufficient energy to eject one of its own electrons resulting in the formation of a radical molecular cation. After electron ejection, the radical molecular cation still posses excess energy. If the molecular ion is stable enough to sustain the excess energy an intense molecular ion will be observed. If the molecular ion is unstable, fragmentation will occur to dissipate the excess energy. This fragmentation is dependent upon the chemical structure of the molecule and as a result, a spectrum of ion peaks are produced that can be used for identification of an unknown compound [2].

Electron-impact ionization requires that the sample have a significant vapor pressure (10^{-2} mm Hg) or be volatile so that gas-phase molecules can be directed into the ionization source. Promotion of a solid sample to the gas phase is typically performed by heating the sample on a probe until it vaporizes. An alternative sample introduction method for EI/MS is gas chromatography (GC). This sample introduction technique has become a fundamental tool in the analytical laboratory since it allows on-line separation of complex mixtures followed by mass analysis. Both introduction techniques then direct the vaporized sample into a heated source block commonly maintained at 180° to 220° C. The EI/MS source block is maintained at an elevated temperature to prevent the gas phase sample from recondensing in the source housing. Therefore, to observe a molecular ion by EI/MS the analyte must be thermally stable. In addition, the sample must also be energetically stable enough to interact with the 70 eV electrons and still produce molecular ions with limited decomposition.

I.4 *Chemical Ionization*

A short mention should be made of chemical ionization (CI) [3-5]. This ionization technique is similar to EI but utilizes a reagent gas. Ionization is achieved by introducing sufficient reagent gas into a sealed source to produce a pressure of approximately 1 torr. The reagent gas, present in a large excess, is ionized by EI and then reacts with the analyte molecules. This interaction results in a charge exchange between the ionized reagent gas and the analyte molecule and results in the formation of analyte molecular ions. The molecular ions generated are considered

pseudomolecular ions since their ionic nature is achieved by either adduct attachment or abstraction of a charged species originating from the ionized reagent gas and are not true molecular ions. An adduct is the association of a charged chemical species with the analyte molecule resulting in a charged molecular species. An example of a positive pseudomolecular ion is the adduct formed by the addition of a proton $[M+H]^+$. In the negative-ion mode, pseudomolecular ions are commonly generated by the abstraction of a proton $[M-H]^-$, or the capture of an electron to form a radical molecular anion (M^-). Commonly used CI reagent gases include methane, isobutane, and ammonia..

Chemical ionization has the advantage of being a less energetic ionization technique than EI. Thus, more intense molecular ion peaks are typically observed since less fragmentation occurs. Although, CI still requires that the analyte be thermally stable since it is also introduced in the gas-phase by heating prior to ionization.

I.5 *Particle Desorption Ionization*

The need for mass analysis of thermally labile, high molecular weight, non-volatile, and polar species not amenable to EI/MS has led to the development of particle desorption techniques. These techniques are typically considered "softer" or less energetic ionization processes than EI or CI. Several techniques are now available that are capable of generating molecular ions from thermally labile, nonvolatile compounds which are commonly of biological significance. Particle

desorption techniques include secondary-ion mass spectrometry (SIMS) [6], ^{252}Cf-plasma desorption mass spectrometry (^{252}Cf-PDMS) [7], fast atom bombardment (FAB) [8], and liquid secondary-ion mass spectrometry (LSIMS) [9].

Particle desorption techniques achieve ionization by sputtering. However, before an argument can be presented on the benefits of one particle desorption technique over the others, a basic understanding of the mechanisms of sputtering is needed. A relevant, in-depth discussion of the mechanisms of sputtering resulting from particle induced desorption follows. This discussion will provide a basis for future arguments presented in the project rationale section.

I.5.1 *Sputtering Mechanisms*

The proposed mechanisms of sputtering have varied over the years and have been rigorously reviewed [6,10]. The currently accepted mechanism is the cascade model presented by Sigmund [11,12]. This mechanism is based on particle bombardment and is accepted for both solid and liquid sputtering. Sigmund sputtering is based on the concept that an incident particle initiates a series of primary binary collisions which further propagates a series of secondary collisions that continue until an eventual cascade of collisions is achieved. An illustration of sputtering is provided in Figure 2, where the collisional cascade is denoted by the dark lines.

The collisional momentum is dispersed throughout the matrix by the collisional cascade process. The matrix might be the solid sample itself, as in the case of SIMS, or the matrix may be a liquid in which the sample is dissolved, as in the case of FAB

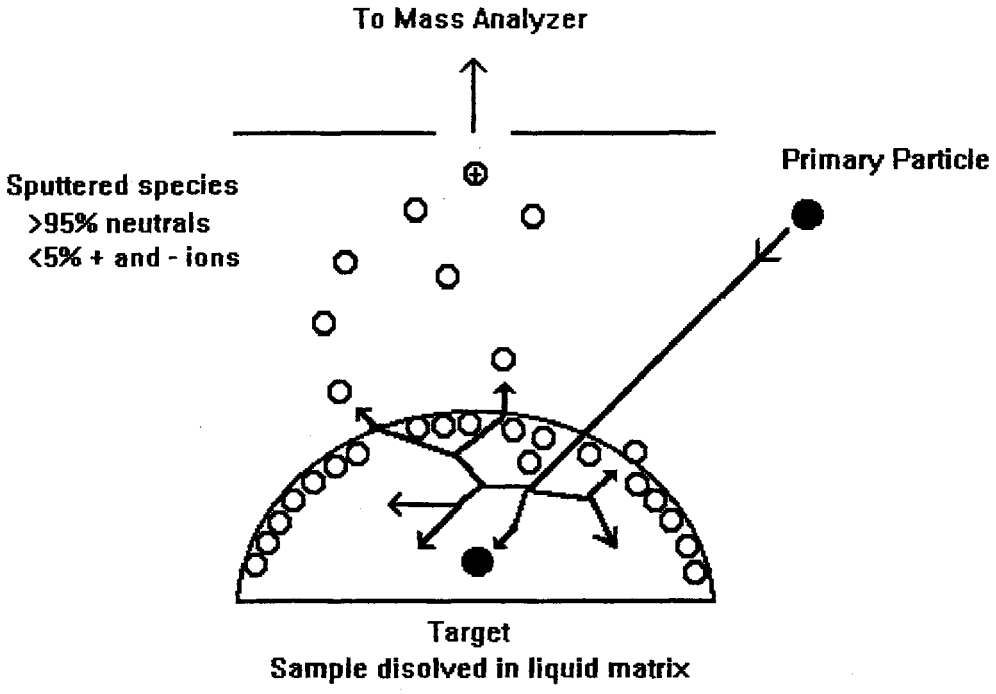

Figure 1 - Schematic illustration of sputtering

and LSIMS. As the cascade expands, a portion of the momentum is deflected back towards the surface of the matrix. The momentum that is deflected back towards the surface of the matrix is also transferred to sample molecules at the surface of the matrix. If the deflected collisions result in sufficient energy transfer to the molecules at the surface, a sample molecule will be desorbed or sputtered from the surface of the matrix . Typically, desorbed sample molecules contain kinetic energies in the range of 1 eV to 5 eV [13].

It is important to realize that sputtering occurs at the surface of the matrix. This fact is supported by theoretical calculations that predict 96% of all species sputtered originate from the surface layer [14]. The relevance of this phenomenon will become apparent in the discussion presented in the liquid matrix section.

The majority of all species sputtered are desorbed as neutral species while a small portion of the species are sputtered as either positive or negative ions. These ions are referred to as secondary ions. After sputtering, the positive or negative ions are then extracted from the source region and mass analyzed. The excess neutral species produced are removed by the vacuum system. Particles that are desorbed are composed of the sample analyte, matrix, and any other modifier or impurity that is present in the matrix/sample solution.

The mechanism of ionization resulting from sputtering is also a currently debated topic. "Sputtering" is simply the ejection or desorption process by which the sample is transferred from the condensed phase to the gas phase. Sputtering in LSIMS results in the production of predominantly neutral species with a low percentage

(0.01% to 5%) sputtered as positive or negative ions. Although desorption is achieved by sputtering, experimental evidence demonstrates that ionization is not a singular mechanism [15]. The reported data illustrate that ionization is not only achieved by sputtering of preformed ions from solution, but also results from gas phase reactions. These reactions occur between sputtered (a) neutral sample molecules and (b) matrix ions and other component ions of the mixture resulting in charge transfer similar to CI [16,17]. Thus, the charge transfer mechanism also contributes to the overall ionization of the analyte.

Sputtering promotes molecules to the gas phase without heating, which eliminates the need for thermal volatilization of the sample. Furthermore, sputtering produces species containing significantly lower internal energies than those encountered in EI/MS. Thus, one can logically expect and actually observe more intense molecular ions of labile molecules by using particle desorption techniques. These attributes have elevated particle desorption techniques to a favorable regard in today's mass spectrometric society. Various particle desorption techniques will now be presented in more detail.

I.5.2 *SIMS*

Originally, particle desorption techniques utilized samples in their solid state. These solid state sample techniques include both ^{252}Cf-PDMS and SIMS. ^{252}Cf-Plasma desorption mass spectrometry utilizes primary particles in the MeV energy range while SIMS utilizes primary ions in the keV range to bombard samples in their solid state

that have been deposited onto a direct insertion probe tip. In SIMS, ionization is achieved as a result of sputtering or desorption as discussed above. Although ionization is achieved by particle bombardment of solids, SIMS has a major disadvantage of low secondary ion currents. These low secondary ion currents are the result of surface damage around the point of primary particle impact. This damage reduces secondary-ion production and lowers the useful sputtering time duration for mass analysis [9].

I.5.3. *FAB and LSIMS*

A large step in overcoming the negative effects of SIMS was accomplished in 1982 by the introduction of a liquid matrix. The first technique developed that used a liquid matrix was fast atom bombardment (FAB) [8]. Soon afterwards, a very similar technique, LSIMS [9], was introduced that also used a liquid matrix. In these techniques, the sample is dissolved in a highly viscous, low vapor pressure liquid. The liquid matrix/sample solution is placed on the direct insertion probe tip and bombarded by keV energetic particles to produce secondary ions.

The principal difference between FAB and LSIMS is the primary particle used for bombardment of the sample/matrix. Fast atom bombardment utilizes neutral Ar or Xe primary particles originating from a gaseous stream fed saddle field gun whereas, LSIMS uses a primary ion beam, such as Cs^+ for bombardment. Typically primary particle energies are 4 keV to 10 keV for FAB, while LSIMS utilizes energies in the 10 keV to 50 keV range with 30 keV being the most common .

Liquid secondary ion mass spectrometry offers several advantages over FAB. One benefit is that LSIMS allows a lower source housing pressure than FAB since the cesium ions are thermally desorbed from a solid as compared to originating from a gaseous beam in FAB. The lower source housing pressure provides better sensitivity due to less collisions along the secondary ion trajectory. In addition, focusing of the primary ion beam is possible in LSIMS due to its ionic nature. This is not possible for the neutral primary beam used in FAB.

Both FAB and LSIMS have developed into powerful techniques for the mass analysis of polar, labile, and nonvolatile species. These techniques have been successfully employed in an extremely broad range of analytical methods for the analysis of compounds such as amino acids and peptides [18,19], oligosaccharides [20,21], and a vast variety of natural products [22].

I.5.3.a Liquid Matrices

As stated, both FAB and LSIMS utilize a liquid matrix in which the sample is dissolved as a means of sample introduction. Commonly used matrices include glycerol, thioglycerol, 2-nitrobenzyl alcohol, diethanolamine, triethanolamine, and various others [23]. Since the mass spectrometer is maintained under high vacuum, the matrix must have a low vapor pressure. This requirement is imposed so that the matrix will maintain its liquid nature for a reasonable amount of time during mass spectral acquisition and not significantly burden the vacuum system.

The liquid matrix serves a unique and important function in the ionization

process associated with FAB and LSIMS. The liquid nature of the matrix allows the surface to be continually replenished by diffusion and convection [20,24] in an attempt to equilibrate the solution concentration. This equilibration process results in higher secondary ion yields than in solid SIMS since it overcomes the problem of surface damage. Furthermore, the use of a liquid matrix provides a longer, more useful data acquisition lifetime than SIMS since as surface molecules are sputtered other matrix/sample molecules replace them. This process eliminates the problem of surface damage previously described in SIMS.

Another important factor in LSIMS performance is the surface activity of the analyte in the liquid matrix. This activity is a measure of the surface concentration of an analyte and therefore, directly affects the secondary ion yield. Surface activity of an analyte molecule is related to the sample's hydrophobicity or its counter measure, hydrophilicity. The degree of hydrophobicity/hydrophilicity can be quantitated by the Bull and Breese index [18]. We will consider the case of both a hydrophobic and a hydrophilic analyte.

Hydrophobicity/hydrophilicity is a measure of the intermolecular forces present between species in an aqueous or aqueous-like solutions and is directly related to entropy [25]. In a polar matrix such as glycerol, hydrophobic species are generally nonpolar or posses a significant nonpolar portion. Since the intermolecular force of hydrogen bonding observed in aqueous/polar solutions such as glycerol, is stronger between the solvent molecules than between the solvent and the hydrophobic species, hydrogen bonding "squeezes" the hydrophobic species out onto the surface of the

matrix. This process maximizes the number of hydrogen bonds. Hydrophobicity can also be explained through entropy. In solution, the hydrophobic species is present as a highly ordered solvated shell. This results in a higher order of the solution and thus decreases the entropy of solution. This is in direct contradiction to the second law of thermodynamics which dictates that spontaneous events only occur when accompanied by an increase in entropy. Since hydrophobic species in a polar matrix have a much higher surface concentration than hydrophilic species, they produce much higher secondary ion yields. To the contrary, hydrophilic species have a lower surface activity and thus, lower secondary ion yields. This is because hydrophilic species typically contain polar groups, such as carbonyls or amines, that are capable of interacting with the hydrogen bonds of the solution. In addition, most highly hydrophilic species contain charged functional groups that form electrostatic interactions with polar matrices that are governed by Coulomb's Law [26]. These physical properties allow and even require that the hydrophilic analytes be dispersed throughout the bulk of the solution which lowers its surface concentration and its secondary ion yields.

I.5.3.b Matrix Modifiers

Matrix modifiers are added to the matrix in an attempt to increase secondary ion intensities. The most common modifiers are volatile organic acids, such as acetic acid and trifluoracetic acid (TFA). These acids are typically added in an attempt to increase positive secondary ion yields by increasing the concentration hydrogen ions in

solution which are necessary for the formation of proton adducts, $[M+H]^+$. In addition to acids, common modifiers also include surfactants. The use of surfactants as matrix modifiers has been reported to increase the surface activity of some hydrophilic compounds and thus increase their secondary ion yields [27].

I.6 Limitations of Particle Desorption Techniques

Although FAB and LSIMS are widely used ionization techniques, they still have limitations and disadvantages. The two most prominent disadvantages are a high background produced by the presence of matrix ions and low ionization efficiencies for hydrophilic analytes. The high background results in lower signal-to-noise ratios and higher detection limits when compared to ionization techniques such as electron impact. The problem of low ionization efficiencies associated with hydrophilic molecules is further magnified by the presence of hydrophobic impurities. These hydrophobic impurities have a higher surface activity and suppress or lower the signal of the hydrophilic analyte.

Since most biological samples are hydrophilic, the limitations of FAB and LSIMS for these analytes warrants further development . Thus, any further advances that could overcome these obstacles would not only result in an improvement in the spectral quality of the already vast quantity of applications, but would also result in improved mass spectral analysis of limited sample quantities often found in most biological or "real world" applications. Some advances have been made in overcoming these obstacles through the use of liquid chromatography interfaced with

mass spectrometry (LC/MS).

I.7 *Liquid Chromatography / Mass Spectrometry*

Some of the largest advances in mass spectrometry in recent years have been associated with the development of unique techniques that interface high performance liquid chromatography (HPLC) with mass spectrometry (LC/MS). These highly innovative techniques introduce the analyte as a liquid solution for mass analysis. The successful interfacing of HPLC and MS has arisen mainly due to improvements made in the pumping capacity of modern vacuum systems and the utilization of differential pumping [3]. The increased pumping capacity allows the introduction of a liquid directly into the mass spectrometer without increasing the source pressure above the operational range. In some techniques, the liquid solution or mobile phase plays an intricate part in the ionization process while in others it serves only as the means for transporting the sample into the mass spectrometer.

Generally, two modes of operation are utilized in LC/MS. The first is flow-injection analysis which is not a true chromatography method since an analytical column is not used. In this mode, fractions collected from an HPLC column or prepared solutions of the analyte may be injected directly into a liquid carrier solution. Typically a low-pulse pump is used to provide an isocratic mobile phase at a constant flow to transport the analyte into the mass spectrometer for mass analysis. This method offers the benefit of much greater source pressure stability. The second mode is the high performance liquid chromatography/mass spectrometry mode which can be

performed using either isocratic or gradient elution. In this mode the eluent from an analytical column is submitted for mass analysis. Many LC/MS techniques can not accommodate the entire flow of eluent typically encountered in HPLC. In these cases the column eluent is split so that an acceptable flow rate is delivered into the mass spectrometer.

The driving force for the development of LC/MS has been twofold. The first driving force was the lack of a universal detector for HPLC. The role of a universal detector can be fulfilled with a mass spectrometer which has the added benefit of a higher degree of selectivity than absorbance detectors. The second driving force for the development of LC/MS was the need for better techniques to ionize thermally labile, nonpolar, high molecular weight, and nonvolatile compounds. Since LC/MS is the basis of this project, a brief review will be given of the various methods with a special emphasis on the more relevant techniques.

I.7.1 Direct Liquid Introduction Techniques

The chronological development of LC/MS began with the direct liquid introduction (DLI) technique in 1973 [28]. The original DLI technique collected fractions from an HPLC column in capillary tubes which were then introduced directly into a CI source. The vaporized solvent from the sample solution served as the necessary reagent gas in the CI source and therefore, aided in the ionization of the sample. The DLI technique yielded best results when used with solvents common to normal-phase HPLC since these solvents produced the best reagent gases.

The original DLI technique was experimentally complex and relied on CI for ionization. This technique further lacked the true interface between HPLC and MS and did not allow on-line LC/MS where the eluent of the HPLC is fed directly into the mass spectrometer. This obstacle was surmounted in 1978 with the use of a specialized splitting probe [29,30]. This probe allowed a fraction of the eluent (0.010 mL/min) to be sprayed into a heated (150° to 350° C) desolvation chamber where the excess solvent was removed. The desolvated sample was then introduced into a CI source where it is ionized.

The DLI technique provided a fundamental introduction into LC/MS. It provided a means of promoting nonvolatile and thermally labile analytes to the gas phase without direct heating. In addition, the DLI was employed using common reverse-phase solvents up to 70% water. This LC/MS interface further permitted the on-line separation and detection of difficult polar species. On the other hand, the DLI technique was limited by the restrictions it placed on flow rates. These restrictions required splitting which results in sample waste which in some cases may not be acceptable. Although the desolvation and CI source were maintained at high temperatures, little thermal degradation was reported for the small molecules (benzanilide, indomethacine, certisol, cytosine, adenine, etc) that were analyzed [30]. This illustrated that the DLI technique could produce molecular ions of thermally labile compounds.

I.7.2 Moving Belt Interface

Soon after the introduction of the DLI techniques, the moving belt interface (MBI) was presented in 1974 [31]. This LC/MS method was based on the removal of HPLC solvents between the column exit and the mass spectrometer's ion source. The MBI interface performed this by depositing the eluent from an HPLC column onto a continuous moving wire. The moving wire was later exchanged for a stainless steel or polyamide belt which provided a much higher solvent uptake [32,33]. After eluent deposition, the belt was fed through a series of desolvation chambers in which vacuum "forepumps" were used to remove the solvent. After desolvation, the analyte remaining on the belt was passed over a flash vaporizer tip that thermally desorbed the sample from the belt for EI or CI ionization. The belt then passed over a cleanup heater and a wiping pad before returning for a fresh supply of eluent. More recently, the MBI interface has been adapted to particle desorption by FAB but without the use of the viscous matrix [34].

The MBI interface offers little advantage for the mass analysis of thermally labile species over EI or CI, but does permit separation by HPLC. It further lacks the ability to mass analyze energetically labile analytes since ionization is typically accomplished by EI. In addition, the MBI interface has the problem of "memory" effects arising from residual analyte remaining on the belt. The MBI interface is best suited for normal phase chromatography, since these solvents are typically more volatile.

I.7.3 Thermospray

Thermospray ionization (TSP) was the next technique in the evolution of LC/MS and was introduced in 1983 [35]. It has since become one of the more popular sample introduction and ionization techniques for LC/MS. Thermospray was the first LC/MS technique to accommodate typical HPLC flow rates in the range of 1 to 2 mL/min. In addition, TSP was the first LC/MS technique capable of producing molecular ions from thermally labile and nonpolar species. These properties gave TSP the advantages of both on-line separation by HPLC and soft ionization MS. As a result, TSP has become one of the most widely commercialized LC/MS sources.

The basic operation of the TSP interface begins with the passage of an HPLC eluent through a heated stainless steel vaporizer capillary into an evacuated region. This process produces a supersonic jet containing a fine mist of droplets composed of solvated analyte molecules. The degree of vaporization has been correlated to the temperature of the heated capillary [36]. When charged analytes are present, the droplets contain either a net positive or negative charge depending on statistical probabilities. The charged droplets continue to evaporate in the high vacuum until a critical point is reached in which the droplet can no longer support the high electrical field generated by the charge and a "coulombic explosion" induces ion evaporation. The resultant ions are then mass analyzed. A volatile salt is often added to the mobile phase to encourage ion formation. It has been shown that molecular ion intensities can be greatly increased by the use of an optimum 0.10M ammonium acetate buffer [37].

Ionization in TSP is achieved by two methods. The first is the ion evaporation process described above. The second process is gas phase ion-molecule reactions that occur between the analyte and components of the mobile phase similar to CI. These reactions result in the formation of adduct ions. Typical positive ion TSP mass spectra contain pseudomolecular ions generalized by $(M+X)^+$ where X can be H^+, Na^+, NH_4^+, H_3O^+, CH_4CN^+, or other cations present in the mobile phase. The dominance of one ionization process over the other is dependent upon many factors including sample volatility, source block temperature, mobile phase composition, repeller voltage, vapor temperature, mobile phase additives, and other instrumental parameters. These instrumental variables also influence the intensity and composition of ions observed in a TSP mass spectrum for a given analyte. More recently, modifications in the TSP technique have been presented that utilize a discharge filament placed at the exit of the vaporizer tip. This modified thermospray ionization technique is known as plasmaspray [38].

I.7.4 Particle Beam

Particle beam LC/MS, or monodisperse aerosol generation interface (MAGIC), was introduced in 1984 [39]. Particle beam LC/MS also has the advantage of being amenable to normal HPLC flow rates and is capable of vaporizing an analyte without the use of heat. Particle beam can be utilized with both normal-phase and reverse-phase HPLC. The particle beam interface sprays an eluent into a desolvation chamber. The spray is then further dispersed into a fine aerosol with a jet of helium. The

solvent vapor and dispersing gas are then removed through a two step process that results in analyte enrichment of the particle beam. The first process removes the bulk of the solvent in a desolvation chamber at a pressure close to ambient by simple evaporation of the solvent from the individual droplets. The excess solvent vapor and dispersing gas are then pumped away by a rotary vacuum pump. The second step involves a momentum separator. The momentum separator separates higher mass sample molecules from lower mass solvent and dispersing gas based on the particles momentum. Lower mass particles have a lower momentum and expand from the core of the expansion jet significantly more than higher mass particles. The lower mass components can thus be skimmed away from the beam core using small apertures. This process creates a beam typically less than 2 mm in diameter that is composed of individual particles less than 100 nm in diameter. These particles then enter the mass spectrometer source region. If the analyte is a solid, the beam is composed primarily of solid particles and if the analyte is a liquid, then the beam is composed primarily of liquid particles. These particles enter the high vacuum ion source and undergo a process of flash vaporization when they hit the interior walls of the heated source block. The vaporized molecules are then ionized.

Particle beam LC/MS has been used primarily with EI and CI ionization [39,40]. This has the benefit of producing mass spectra that can be readily compared to those published in vast libraries for identification. But the use of particle beam with EI has found limited use in the analysis of energetically labile species. Some steps in overcoming this problem have been made by coupling particle beam with

FAB [41]. This has been accomplished by directing the particle beam onto a probe tip containing a matrix. The stream of particles are deposited into the matrix and then ionized by FAB as described previously. Another current research endeavor in its infancy utilizes a laser beam that transverses the particle beam to achieve ionization [42].

I.7.5 Continuous-Flow FAB and Continuous-Flow LSIMS

Another LC/MS sample introduction technique is Continuous-Flow FAB (CF-FAB). This technique was introduced almost simultaneously by Ito and co-workers in 1985 [43] and Caprioli and co-workers in 1986 [44]. The technique used by Ito employed a frit-FAB interface while Caprioli utilized a direct introduction interface. Although CF-FAB was first introduced by Ito, it has been developed in depth by Caprioli [45-52]. The adaptation of the continuous-flow technique to liquid secondary ion mass spectrometry (CF-LSIMS) soon followed [53] and differs only in the nature of the primary particle as described previously.

The CF-LSIMS interface can be operated in the flow-injection mode or directly interfaced with HPLC (LC-CF-LSIMS). Continuous-flow LSIMS uses a low flow-rate (1 to 10 μL/min) of a mobile phase provided by either a syringe pump or an HPLC. The mobile phase, matrix, and sample are transported to the CF-LSIMS probe tip inside the ion source region through a small fused silica capillary. Upon exiting the transfer capillary, the solvents readily evaporate in the high vacuum ion source region and leave the sample and matrix on the probe tip. The matrix solution is then

bombarded to achieve ionization by sputtering as described previously. The sample and matrix are removed by evaporation and desorption at an ideal rate equal to the rate of delivery. To aid in the process of evaporation of the viscous matrix, the probe tip and source block are gently heated to approximately 40° to 60° C to prevent an excess build up of the matrix at the CF probe tip.

The interfacing of HPLC with continuous-flow requires that a portion of the HPLC eluent from an analytical column be split [54] to obtain the desired flow rate into the mass spectrometer. The necessary FAB/LSIMS viscous matrix can be added directly to the mobile phases [44] at concentrations between 1% to 10% or may be delivered post-column by a coaxial capillary design [55,56]. The coaxial design uses dual capillaries in which a smaller capillary is placed inside a larger capillary to provide two separate channels for liquid delivery. The outer capillary delivers a concentrated matrix solution (10% to 25% matrix) which then mixes with the HPLC eluent, that has been supplied through an inner capillary, at the probe tip. A quantitative comparison of these two methods has been presented [57]. The addition of the high concentrations of the viscous matrix directly to the mobile phase produces some chromatographic band broadening [58,59] due to the increased viscosity. This band broadening effect can be minimized by minimizing the concentration of matrix.

CF-LSIMS has some very distinct advantages over regular or static LSIMS which have been summarized by Caprioli [60] and include: (1) the direct introduction of aqueous sample solutions, (2) higher sensitivity, (3) decreased intensity of background matrix cluster ions, (4) decreased ion suppression effects, (5) greater

reproducibility resulting in increased precision and, (6) higher sample throughput. Most of the above advantages can be attributed to the fact that CF-LSIMS is a dynamic process resulting from the constant motion and mixing at the probe tip. The dynamic process results in movement of the bulk solution and allows the surface to be replenished at a rate faster than diffusion through the viscous matrix. Sensitivity is also increased by lower concentrations of the matrix present which reduces the intensity of background matrix ions. Also, the mixing process decreases the ion suppression effects since hydrophilic compounds are brought to the surface by the dynamic process. Greater precision is achieved since the sample introduction probe is stationary and not removed each time a new sample is analyzed. This minimizes minute alterations in instrumental parameters that result from removal and reinsertion of the probe. Higher sample throughput is also achieved since the probe is stationary and does not need to be removed for new samples.

Continuous-flow LSIMS has become a widely utilized technique for the mass analysis of nonvolatile, thermally labile, polar, and ionic species without derivatization. The disadvantages of CF-LSIMS are a high background from the matrix ions and the restrictions placed on the flow rate (1 to 10 μL/min) into the mass spectrometer. In addition, low ionization efficiencies for compounds such as oligosaccharides result in low sensitivities for these molecules. The development of nanoscale HPLC [61-63] has provided a solution to the low flow-rate limitations. Nanoscale HPLC utilizes analytical columns with internal diameters of 50 μm *i.d.* to 500μm *i.d.* These columns operate at significantly lower flow rates and are much more readily adapted to LC/MS

techniques that place limitations on flow rates into the mass spectrometer. The use of nanoscale HPLC has also found significant use in electrospary ionization.

I.7.6 Electrospray Ionization

The foundations of electrospray as a mechanism for the ionization was set forth by Dole and co-workers in the late 1960's and early 1970's [64-66]. The authors demonstrated that large quantities of ions were produced by spraying analyte solutions from a hypodermic needle that was maintained at a high potential. Although Dole and co-workers developed electrospray as a technique for the ionization of dilute polymer solutions, they did not interface it with mass spectrometry due to the lack of MS technology at that time.

The electrospray phenomena operates by applying a high potential to a hypodermic needle into which a flow of an analyte solution is delivered. The high potential of the needle supplies a surface charge to the solution, which is then electrostatically attracted towards a counter electrode of lower or opposite potential. This electrostatic attraction results in the production of a fine mist spray of the analyte solution. Spraying can occur with mobile phases under free-flow conditions (i.e. no pressure applied) but is generally encouraged by applying a slight pressure to the mobile phase using a syringe pump or HPLC. Analyte ionization is achieved by ion evaporation from the small charged droplets similar to thermospray, but ESI has the added advantage of selectivity in the charge state of the analyte (positive or negative). Whereas, the charge state in TSP is statistically determined. ESI further has the

capability of generating charged analytes of molecules that are typically uncharged or neutral in solution. This is performed by imposing a charge onto the droplets which can then be transferred to the neutral species.

In 1984 Fenn and co-workers instituted electrospray ionization (ESI) as an ionization source for MS and demonstrated the production of both positive and negative ions, depending on the polarity of the applied needle potential [67,68]. Fenn and co-workers then followed with the development of electrospray as an interface for LC/MS in 1985 [69]. Since then, ESI has since rapidly evolved into one of the most promising LC/MS ionization sources. Applications of ESI include the analysis of polypeptides, high molecular weight proteins, and many other high molecular weight biological compounds [70].

ESI has earned its popularity as a result of several factors. First, its high ionization efficiency results in extremely sensitive measurements [71]. Second, ESI extends the "mass" range of conventional mass spectrometers through multiple charging. Multiple charging results in the observation of a sequential series of m/z values or peaks corresponding to the molecular species with a sequential number of charges. This phenomena allows the analysis of high molecular weight species in excess of 100 kDa without the demand of a mass analyzer of a high mass-to-charge (m/z) capacity [72-73]. For example, a species with a molecular weight of 100 kDa containing 100 charges (positive or negative) will be observed at a m/z value equal to 1000 (100,000/100). These characteristic m/z values can then be mathematically deconvoluted to determine the molecular weight of the parent analyte [72]. Other

factors that have influenced ESI popularity include cleanliness, flexibility, ease of maintenance, and adaptability to other separation techniques such as capillary electrophoresis. The major limitation of ESI is it's maximum flow rate of approximately 50 μL/min. This, as mentioned before, can be surmounted with the use of nanoscale LC/MS or by splitting the column eluent. Successful alterations of the ESI now exists which allow flow rates in the 1 to 2 mL/min range known as atmospheric ionization (API) and atmospheric pressure chemical ionization (APCI) [74,75]. In addition to API and APCI, other spray ionization techniques have evolved that instrumentally assist the spray process with a drying gas or ultrasonic nebulization to enhance ionization effieciencies.

I.8 Summary of LC/MS Techniques

All of the above sample introduction and ionization techniques have their individual benefits and drawbacks. Each technique has advanced the development of LC/MS by yielding some contribution to the acquisition of mass spectra in the once forbidden area of the mass analysis of nonvolatile, high molecular weight, thermally labile, and polar species. The older and more established techniques have the major advantage of being more fully developed and commercially available. This puts the power of LC/MS into to the hands of the non mass spectrometrist who will ultimately gain by its use. The newer techniques, as they evolve, conquer newer and greater portions of the above described problematic mass spectrometry regions. These techniques have opened wide the doors of biological LC/MS to provide invaluable

information about ourselves and the world around us.

The most promising LC/MS interfaces at the present time are the ESI technique and its derivatives. The ESI techniques encompass most of the benefits of all the other techniques while suffering little from the limitations and restrictions placed on them. The major disadvantages of ESI interfaces are their high cost (i.e. $80,000) and their stringent requirements on vacuum pumps. Electrospray ionization provides a significant increase in sensitivity and does not involve heating which allows for a wider range of analytes. Although ESI is at the forefront of modern mass spectrometry, the older techniques such as CF-LSIMS, TSP, and particle beam still enjoy a significant popularity. This is primarily because these instruments are present in many more laboratories than the ESI and are considerably less expensive. Furthermore, these techniques are still employed to yield solutions to many mass spectrometry problems such as that presented in this thesis. The disadvantages and limitations placed on the DLI and MBI, which were described in the individual sections, have made these techniques almost obsolete.

I.9 Tandem Mass Spectrometry

Tandem mass spectrometry (MS/MS) can be conceptually visualized as two mass spectrometers placed end-to-end with a collision cell between the two mass spectrometers. The first MS selects a single or parent ion by allowing only that ion to pass through to the collision cell. If the collision cell contains a low gas pressure, usually helium , fragmentation is induced by the "collision gas". This form of MS/MS

is known as collisionally induced dissociation (CID) or collisionally activated dissociation (CAD). If the collision cell is empty or void of any collision gas, the ion continues along its original trajectory during which some of the molecules undergo fragmentation to release internal energy. These fragment or product ions are referred to as metastable ions. The product ions from either method of fragmentation are then mass analyzed by the second MS to produce a tandem mass spectrum.

The above conceptional processes can be instrumentally achieved by several means with different mass analyzers [76,77]. The preferred tandem mass spectrometry method for a reverse-geometry, dual sector instrument (i.e. VG ZAB2-SE) is performed by link scanning at a constant ratio of the magnetic field strength to the electrostatic field strength (B/E). Link scanning has the advantage of increased resolution over other MS/MS techniques available on sector instruments. A mathematical derivation of B/E link scans is provided in Appendix A. This derivation mathematically describes the process where only selected parent ion and those product ions of the parent molecule which fragment after acceleration but prior to the magnetic sector are transmitted to the detector to produce a tandem mass spectrum. The tandem mass spectrum yields a true mass spectrum of the analyte by removing other ions originating from the matrix and impurities. This provides a greater degree of certainty in the identification of the fragment ions as true analyte fragments and not matrix or background peaks. In addition, the MS/MS experiment is capable of generating additional fragment ions by CAD or CID that are not typically observed in a normal scanning acquisition mode to further aid in structural determinations.

1.10 Flavonoids

Flavonoids are recognized as one of the most abundant groups of natural products found in plants. To date, some 4,000 flavonoid compounds have been identified and documented [78]. Although the most abundant and prolific sources of flavonoids are flowering plants, they are also found in lower plants such as algae, bryophytes, and ferns. The subclasses of the flavonoid family that are most relevant to this project are provided in Figure 2.

The flavonoid ring systems have been given specific letter designations [79]. The A ring is identified as the benzene ring attached directly to the central benzopyran ring with carbon atoms located in both ring systems. The B ring is identified as the benzene ring attached to the central benzopyran ring through a single carbon-carbon bond. Flavonoids are typically referred to as plant phenolic compounds since they commonly contain hydroxyl groups located on the A and B rings of the flavonoids. In addition to hydroxyl groups, it is common to find methoxy groups on the A and B ring systems. Although not as common, hydroxy and methoxy substituents have been observed on the central benzopyran ring. The combination of the above substituents has provided the vast number of known flavonoids.

The functions of flavonoids vary as much as the structure and include such functions as pigmentation, growth regulators, nodulation inducers, and phytoalexins [79]. It has been further suggested that some flavonoids may even have medicinal properties such as anticancer agents [80]. Our interest in flavonoids focuses on their "phytoalexic" properties which will be discussed in more detail below.

Flavonoid Aglycone Classification

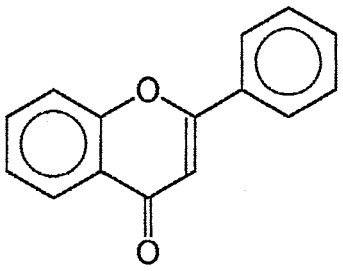

Flavones

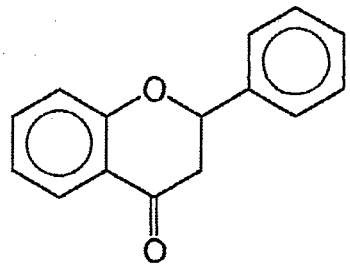

Flavanones

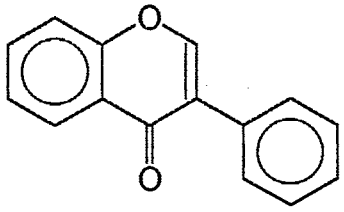

Isoflavones

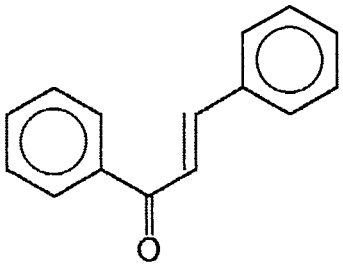

Chalcones

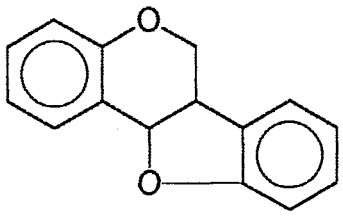

Pterocarpans

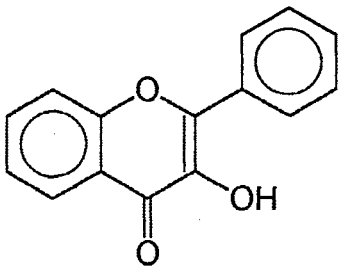

Flavonols

Figure 2- Classification of Relevant Flavonoid Aglycones

I.11 Plant Response Systems

It has been observed that many plant systems have unique defense responses to pathogens. Natural pathogens are considered to be any of a multitude of microorganisms that may attack the plant such as fungi. The resistance to pathogens in specific plant systems has been correlated to the production of secondary metabolites that accumulate to levels sufficient to inhibit microbial growth within the plant cells [81,82]. Secondary metabolites are compounds synthesized from smaller molecules such as phenylalanine. Further, secondary metabolites are not crucial for organism life but serve to enhance it. The secondary metabolites of interest in alfalfa are isoflavonoids and a related class of compounds, the pterocarpans. The pterocarpan medicarpin has been identified as a major phytoalexin present in alfalfa [83,84] and its biosynthetic pathway has been determined [85]. The biosynthetic pathway of medicarpin is presented in Figure 3. Phytoalexins are low-molecular weight, broad-spectrum antimicrobial compounds synthesized in plants in response to infection. Isoflavonoids and pterocarpans are synthesized in response to microbial infection and accumulate to levels sufficient to result in the limitation of microbial growth within the plant cells [81,82]. These responses may be induced experimentally with suspensions of fungi (spores or mycelia) or with biotic or abiotic elicitors. Typical elicitors employed are the cell walls of yeast, bacteria, and heavy metal salts such as $AgNO_3$ or $CuCl_2$ [86].

Although the aglycone form (the basic ring structures given in Figure 3 without any conjugation) of isoflavonoids and pterocarpans have been identified as possessing

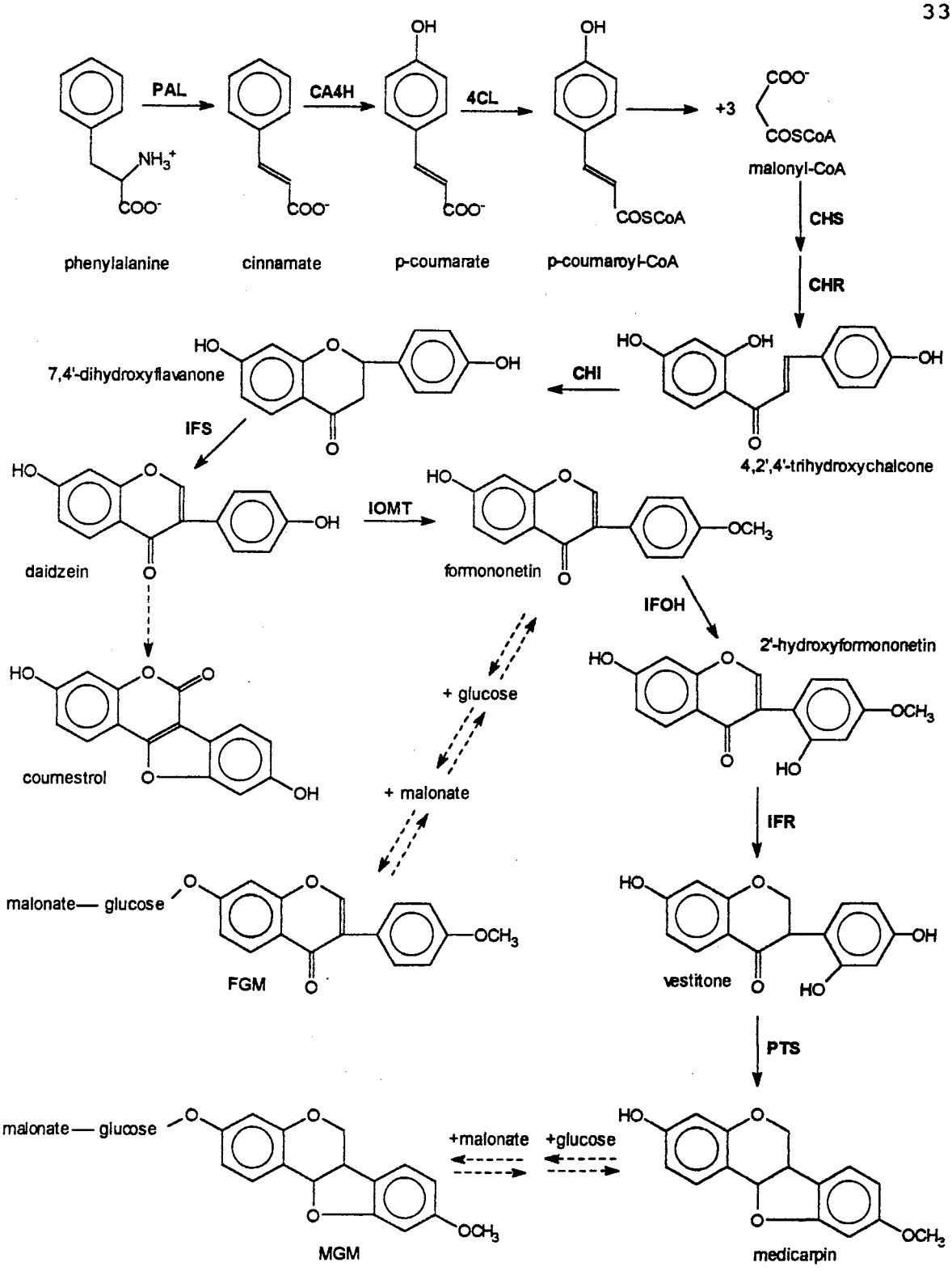

Figure 3- Biosynthetic pathway of medicarpin in Alfalfa (*medicago sativa* L.)

the phytoalexic character, it has been reported that some of these compounds are stored as glycoside conjugates until needed [87,88]. This glycosylation is believed to increase the compound's solubility in the aqueous plant environment. More recently, it has been found that the glucose moiety is also malonated which might further aid in this function. Upon infection of the cell, the isoflavonoid aglycones are synthesized from precursors or are generated by the hydrolysis of conjugates into their phytoalexic form to inhibit microbial growth [87,88].

Further study and identification of these compounds will provide a better understanding of the biochemistry and molecular biology associated with phytoalexins. This information can then be used to help identify the genes responsible for their accumulation. Once isolated and characterized, the gene can then be introduced into other plant systems in an attempt to provide them with the favorable resistance traits.

I.12 Project Rationale

To date, most methods for the identification of flavonoid conjugates are composed of extensive wet chemical methods. Examples of these methods follow. The identification of the sugar is performed by hydrolysis of the sugar from the conjugate with 1N HCl. Following which the aqueous extract is analyzed by gas-liquid chromatography (GLC) after trimethylsilylation [89,90]. Sugar identification has also been performed using β-glycosidase in an attempt to cleave the sugar. HPLC is performed before and after the hydrolysis experiment to confirm or deny the presence of a β-glycoside [91]. Malonic acid substituents have been determined with

p-bromophenacylbromide to yield their chromophoric esters [92]. These derivatives are then identified by co-chromatographing them with esters of standard acids by HPLC. One of the most established methods used for the identification of the aglycones is one and two dimensional thin-layer chromatography [93]. In addition, EI/MS has increasingly become more popular for the identification of flavonoid aglycones. EI/MS is performed after the hydrolysis of the conjugate with 1N HCl [79]. Instrumental analysis such as NMR and UV spectroscopy further aid in the identification of isoflavonoid conjugates. The above illustrates that these methods are very time consuming and labor intensive. Therefore, an easier, faster method is much needed.

These facts have led us to investigate mass spectrometry as a means for the identification of flavonoid conjugates found in alfalfa and other plant extracts. This began with attempts to utilize gas chromatography followed by EI/MS. Mass spectral identification of flavonoid aglycones by EI/MS has been extensively documented [78,79] and a recent survey of EI/MS and CI/MS has been presented [94]. Although EI/MS and CI/MS have been demonstrated as a powerful tool in the analysis of flavonoid aglycones it has found little utility in the mass spectral analysis of flavonoid glycosides without derivatization [95]. This is due to the fact that these techniques are typically unable to produce molecular ions due to thermal decomposition of the glycosides. The development of particle desorption techniques such as fast atom bombardment (FAB) [8] and liquid secondary ion mass spectrometry (LSIMS) [9] has provided the means for lower energetic mass spectral analysis of many natural

products including flavonoid conjugates [96,97]. To date, direct insertion probe FAB has been used almost extensively for the identification of flavonoid glycosides [98-101]. Most MS methods still rely on batch processing which generally includes the collection of HPLC fractions followed by direct insertion probe EI, FAB or LSIMS. Although, a few reports have been made utilizing derivatization followed by GC/MS [102,103].

Our attempts to utilize direct insertion probe LSIMS for the identification of suspect isoflavonoid conjugates in alfalfa had limited success. This was attributed to the eventual decomposition of conjugates as a result of the elapsed time factor and actual procedures associated with fraction collection followed by mass spectrometry. Therefore, the feasibility of an on-line separation and mass analysis method was contemplated.

The literature offers a few reports of such methods. The first employed the moving belt interface in conjunction with CI that was operated at a source temperature of 160° [104]. The mass spectra obtained for rutin and hesperidin produced [M+H]+ ion peaks of very low relative ion intensities, 1.3% for rutin and 5.0% for hesperidin. Additional reports utilized thermospray mass spectrometry [105,106]. Although the authors obtained appreciable mass spectra for several glycosides, no reports were made for malonated glycosides. Malonated conjugates are believed to be significantly more labile. Due to the more labile nature of malonate conjugates and a report that thermally labile molecules have a tendency to decompose at higher TSP vaporizer temperatures [107], TSP was avoided.

We rationalized that an effective solution to the above problem could be achieved by interfacing high performance liquid chromatography with continuous-flow liquid secondary ion mass spectrometry (LC-CF-LSIMS). This method could provide both on-line UV and mass selective detection . We further rationalized that the on-line separation method would overcome the obstacle of sample decomposition. Also, the on-line UV detection would provide us with sample elution times. These elution times could then be used in the method development by providing observable peaks in the UV chromatogram that could be correlated to peaks observed in the mass spectrometry data. Thus, the above described LC-CF-LSIMS interface would provide significant benefits over the previous reported LC/MS methods and provide significant benefits over direct insertion probe LSIMS such as increased sensitivity and reduced hydrophilic effects.

CHAPTER II

EXPERIMENTAL

II.1 Mass Spectrometry

Mass spectral analyses were performed on a VG ZAB2-SE (VG Analytical, Manchester, UK) double focusing mass spectrometer equipped with a slightly modified VG continuous-flow probe. A schematic drawing of the commercial continuous-flow probe is provided in Figure 4. The modification consisted of mounting an adapter plate onto the CF-LSIMS probe that would accept either an internal loop injector (Valco Instrument Co. Inc., model C4UW, Houston, TX) or a splitting device previously described by Kokkonen and co-workers [54]. This splitting system is described in more detail in section II.5. The transfer fused silica capillary was sealed at the end of the probe by wrapping the capillary with teflon tape before installing the stainless steel domed probe tip. The domed probe tip was then tightened down to compress the teflon tape and seal the capillary while leaving approximately 5 cm of the capillary protruding out of the probe tip. The capillary was then pulled back until it was slightly recessed (0.5 mm) below the surface of the probe tip. This slight recess helped prevent the mobile phase from "spitting" from the end of the capillary and provided more stable source pressure conditions.

The LC-CF-LSIMS source was operated using a 30 keV Cs^+ primary ion beam

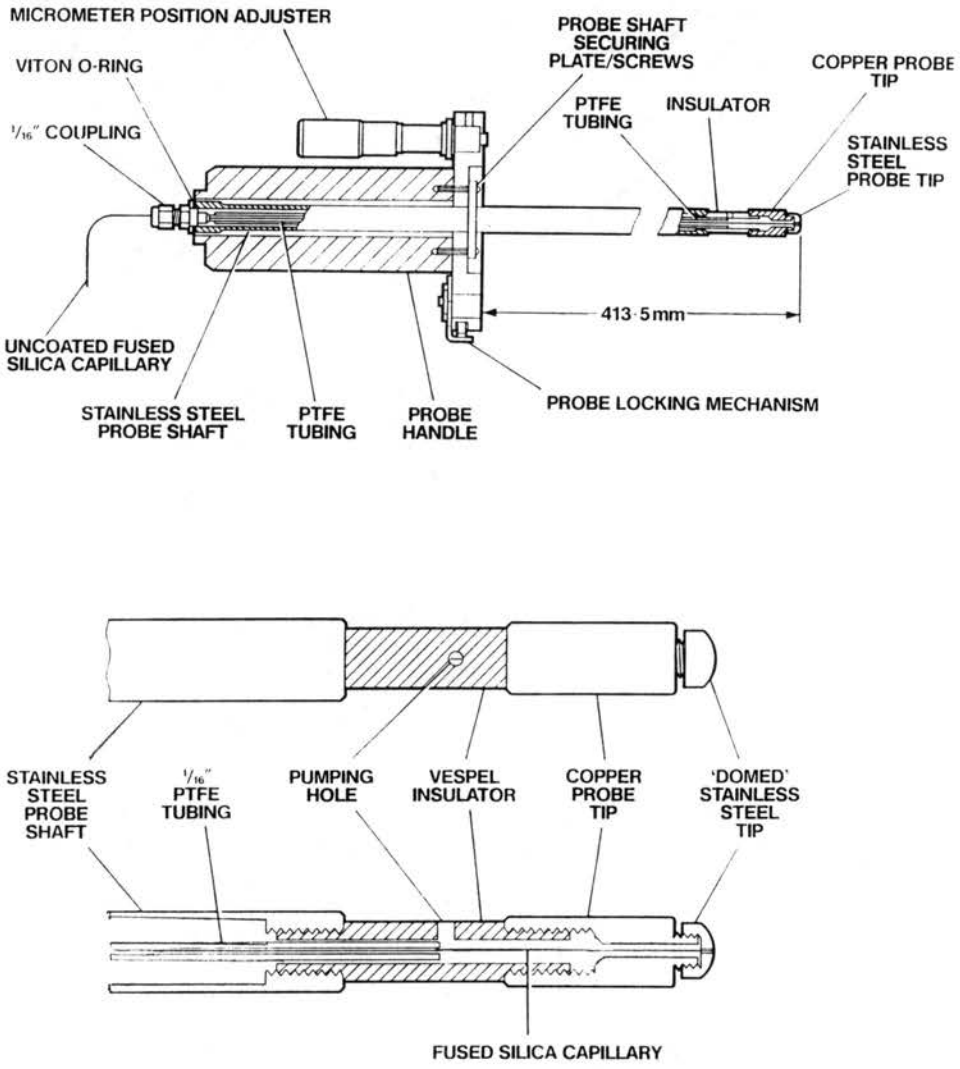

Figure 4- Illustrative Drawings of the Commercial CF-LSIMS Probe.

while the analyzer was typically scanned at a rate of 10 or 15 seconds per decade from m/z = 800 to m/z = 200. Positive or negative secondary ions from LC-CF-LSIMS experiments were extracted and accelerated to 6 keV unless otherwise stated. Optimization experiments were performed to determine the above instrumental parameters which are discussed in detail in chapter 3. All data were acquired using a VG 11-250J data system.

II.1.1 Data Acquisition and Display

Two major modes of data acquisition were utilized in this project which included the selected ion recording (SIR) mode and the full scanning mode. In the SIR mode, the mass analyzer is set at a specified mass and measures its intensity as a function of time. The results are then reported in the form of a chromatogram as intensity versus time with the area of the peak being proportional to the concentration. The scanning mode scans the magnetic sector to encompass the entire mass range selected. The results from scanning experiments are presented in the form of mass spectra which plot relative intensity versus mass-to-charge (m/z) ratio. The summation of all the ion currents in the acquisition mass range for each scan are then displayed as a total ion chromatogram (TIC). Summations of selected individual m/z values can be displayed in the form of a selected ion chromatogram (SIC). Further, summation of several selected m/z values from each scan can be displayed in the form of a reconstructed ion chromatogram (RIC).

The SIR mode is the preferred mode for quantification since it acquires a much

larger number of measurements of the signal intensity per unit time than the full scanning mode. Therefore, SIR provides a more accurate account of the signal intensity. Selected ion recording produces a chromatogram as describe above, but does not yield a mass spectrum. In addition, SIR data is typically obtained at an adjustable dwell time of 80 msec with a delay time of 20 msec. The dwell time is the amount of time of actual data acquisition while the delay time is the time allowed for the magnetic field or acceleration voltage to make slight adjustments. In the full scanning mode for a mass range of m/z = 800 to m/z = 100 and a scan rate of 15 seconds per decade, a mass spectrum is obtained at a rate of one scan every 13.5 seconds [scan time x log (high mass/low mass)].

II.2 Methods of CF-LSIMS

Three sample introduction modes were used in the CF-LSIMS experiments. These modes were (1) flow-injection, (2) analytical HPLC-CF-LSIMS, and (3) nanoscale HPLC-CF-LSIMS. Analytical HPLC experiments were performed with a 4.6 mm *i.d.* column while nanoscale HPLC experiments were conducted with columns with internal diameters of 200 μm or 320 μm. Instrumental illustrations for each mode are presented in Figures 5-7. Optimization experiments were performed in the flow-injection mode. This mode utilized an Isco μLC-500 Micro Flow syringe pump in conjunction with the Valco internal loop injector to deliver an isocratic mobile phase and sample to the probe tip. Experiments with alfalfa extracts utilized analytical reversed-phase high performance liquid chromatography mode (LC-CF-LSIMS).

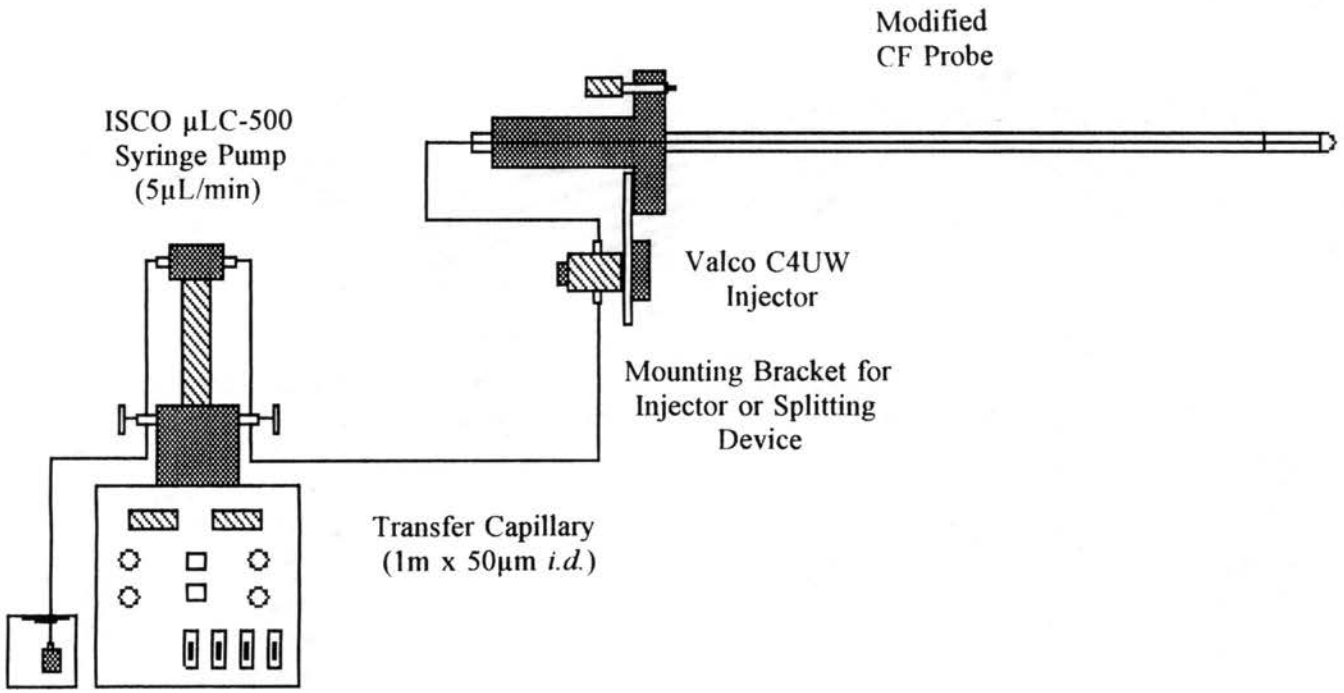

Figure 5- Instrumental Setup for Flow-injection CF-LSIMS

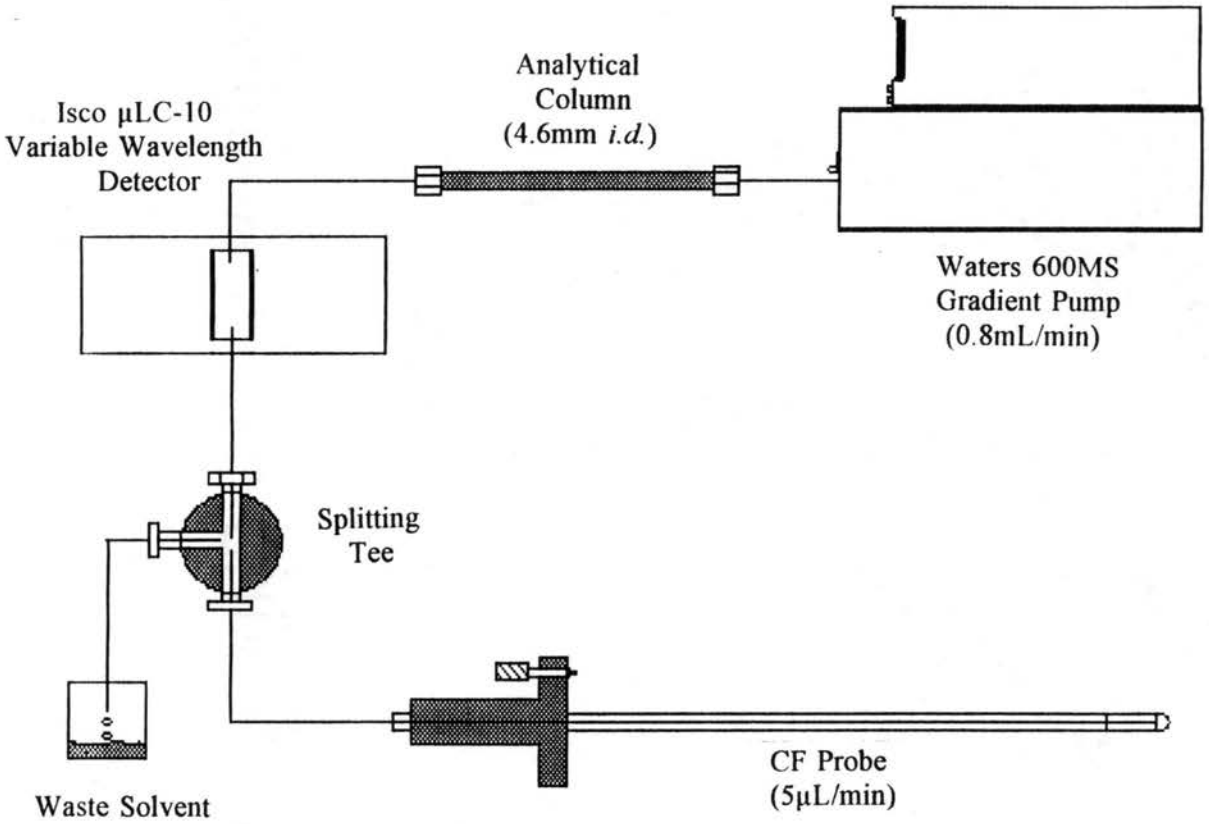

Figure 6- Instrumental Setup for Analytical LC-CF-LSIMS

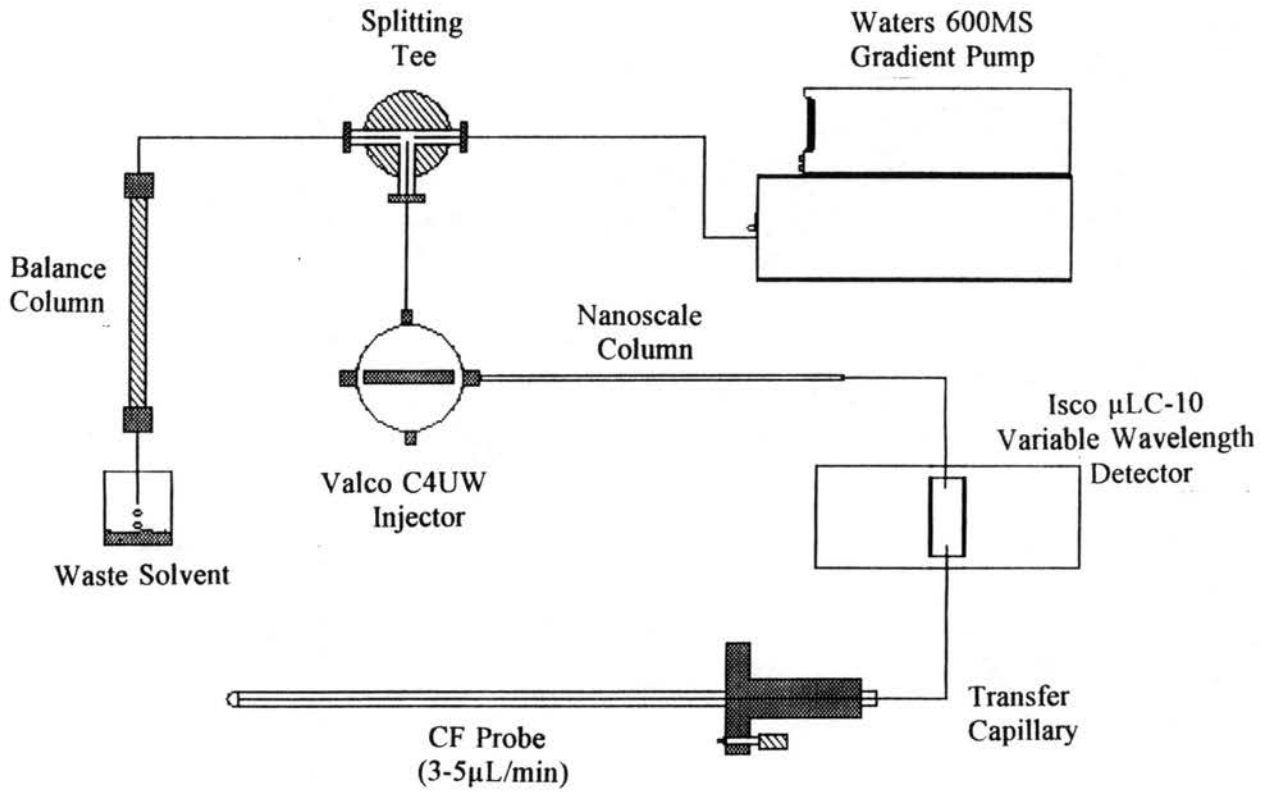

Figure 7- Instrumental Setup of Nanoscale LC-CF-LSIMS

Additional experiments with alfalfa and other plant extracts were performed by nanoscale LC-CF-LSIMS.

II.3 CF-LSIMS Mass Calibration and Tuning

Mass spectra were typically acquired over the mass range of m/z = 200 to m/z = 800 for flow-injection CF-LSIMS experiments. This mass range was too narrow for the commonly used calibration compound CsI since only three ions from CsI are observed in this mass range. It was observed that glycerol produced cluster ions at 92 amu intervals. Therefore, calibration files for both positive and negative ions of glycerol were created on the VG 11-250 J data system which contained the known four decimal value for the cluster ions of glycerol. The mass range of these calibration files ranged from m/z = 17 up to a m/z value of approximately 1500. These calibration files allowed mass calibration using a drop of glycerol placed on a dry CF-LSIMS probe tip or directly from the glycerol in the mobile phase. The addition of acetic acid to the glycerol matrix produced the same series of glycerol cluster ions, but also generated a series of glycerol acetate adduct ions at intervals of 60 mass units higher than the glycerol cluster ions. Thus, an additional mass calibration file was created for the negative ions in the glycerol acetate adduct series (m/z = 91, 151, 183, 243, 275, 335, etc.). This file has the benefit of more calibration points and was used primarily in negative-ion, LC-CF-LSIMS experiments that utilized an acetic acid modifier.

Initially the mass range utilized had an upper limit of m/z = 650 which

presented difficulties in mass calibration. This was because the glycerol cluster ion peak at m/z = 645 for positive-ion and m/z = 643 for negative-ion mode CF-LSIMS was to close to the upper mass limit for adequate mass calibration. Therefore, It was found necessary to calibrate with a higher upper mass limit of preferably m/z = 700 or 800.

The lower mass limit of the acquisition mass range typically used for CF-LSIMS experiments was m/z = 200. This was used since the glycerol matrix yielded relatively intense ions corresponding to the monomer and dimer. Thus, by removing these ions from the acquisition mass range, the relative ion intensities of analyte ions were increased.

Typical tuning of the ion optics of the VG ZAB2-SE was performed on the glycerol cluster around which analyte ions were expected to be encountered. Tuning involves the maximization of ion transmission through the ion optics of the mass spectrometer by adjustment of the applied voltages to focusing lenses. This process generally began with a "rough tune" on the glycerol monomer followed by a "fine tune" on a higher mass glycerol cluster ion such as $[5Gly-H]^-$ at m/z = 459 or $[6Gly-H]^-$ at m/z = 551. These tuning practices provided the best results and were followed throughout all optimization experiments to ensure that discrimination due to instrument tuning was minimized.

Although CsI was not used for mass calibration, it was found ideal for proper alignment of the Cs^+, primary ion gun since CsI illuminates under particle bombardment. Therefore by depositing the salt on the probe tip and bombarding it,

visual perception of the area of impact of the primary ion beam on the CF-LSIMS probe tip could be observed. For proper Cs^+ gun alignment, the primary ion beam was aligned so that it struck the central region around the point of emergence of the liquid flow. This alignment was critical to successful CF-LSIMS analysis.

II.4 Chromatography

A Waters 600MS solvent delivery system was utilized for the analytical LC-CF-LSIMS mode in conjunction with either a 4.6 mm x 150 mm Zorbax™ 5μm, 100Å pore size, octadecylsilane (ODS) column obtained from MAC-MOD Analytical, Inc. (Chadds Ford, PA) or a 4.6 mm x 250 mm Bakerbond (J.T. Baker, Phillipsburg, NJ) 5μm, 120Å pore size, ODS column. A linear gradient of 80:20 (solvent A:B) to 40:60 over forty-five minutes at 0.80 mL/min was used for the separation of all plant extracts. Solvent A consisted of 97.9% water, 2.0% glycerol, 0.10% TFA. Solvent B consisted of 97.9% acetonitrile, 2.0% glycerol, 0.10% TFA. Additional experiments were performed with a varying concentrations of an acetic acid modifier in place of TFA. Similar gradients were used for nanoscale LC-CF-LSIMS. On-line UV detection was performed at 287 nm or 254 nm using an ISCO μLC-10 variable wavelength detector. For analytical HPLC, the eluent from the detector was split 160:1 such that 5μL/min was delivered to the continuous-flow probe tip through a 50 μm *i.d.* fused silica capillary (Polymicro Technologies, Inc., Phoenix, AZ). Nanoscale HPLC also utilized the Waters 600 MS solvent delivery system in which the mobile phase was split prior to the nanoscale column to generate a flow of approximately 3 to

5 μL/min through the column. These splitting methods are described in detail below.

II.4.1 Mobile Phase Preparation

Solvents were vacuum filtered through 0.2μm Nylon 66 membrane filters (Alltech Associates, Inc., Deerfield, IL 60015). This process removed any particulate matter and vacuum degassed the solvents. The degassed solvents were then used to prepare mobile phases. Water was distilled and then deionized using an 8 in. x 44 in. mixed bed ion exchange column (Continental Waters Systems, San Antonio, TX). Mobile phases were prepared by weighing the appropriate mass of glycerol necessary to generate a 2.0% (v/v) solution in water or acetonitrile. Since the density of glycerol is 1.263 g/ml, 25.280 g of glycerol or the equivalent to 20 mL was weighed out and dissolved in 1 L of solvent. This was found to be a more accurate method than volumetric measurements of glycerol due to its high viscosity. The appropriate amount of the acid modifier was then added using a volumetric pipet, followed by the final dilution to 1 L. Acetonitrile solutions of 2.0% glycerol required magnetic stirring for approximately 30 minutes to completely dissolve the glycerol. The mobile phases were then sparged for approximately 15 minutes at 25 mL/min with helium prior to use.

II.5 Mobile Phase Splitting

Two methods of splitting the mobile phase were used. The first was the method described by Kokkonen and co-workers [54]. This method utilized a splitting

tee and differential lengths of fused silica capillaries. Our version of this splitting design is illustrated in Figure 8. The column eluent was delivered from the on-line UV detector or directly from the analytical column to a Valco zero dead volume (ZDV) tee by a 25 cm length of 1/16 inch *o.d.* x 0.178 mm *i.d.* (0.007 inch *i.d.*) stainless steel tubing. Splitting was achieved by using two lengths of fused silica capillaries. The first was the transfer capillary that carried the analyte to the CF probe tip. The length and internal diameter of this capillary were typically 1 m and 50 μm *i.d.* or 75 μm *i.d.* The second capillary varied in length and internal diameter since its only function was to provide a slight backpressure to generate the desired flow through the transfer capillary. The most common splitting system for our experiments used a 3 m x 250 μm *i.d.* backpressure capillary in conjunction with a 1 m x 50 μm transfer capillary. The backpressure generated by the 3 m x 250 μm *i.d.*capillary was sufficient to generate 5 μL/min through the 1 m x 50 μm transfer capillary.

Since dead volumes were extremely detrimental to our CF-LSIMS experiments, the stainless steel capillary was counter bored approximately 1cm. The 50 μm *i.d.* transfer fused capillary was inserted into this counter bore to minimize band spreading. This process prevented mixing in the internal volume of the tee prior to passage into the transfer capillary.

The second splitting method was used in the nanoscale HPLC experiments and is referred to as the balance column method [108]. This method was illustrated in Figure 7. The Waters 600MS gradient pump is operated at flow rates of 0.1 mL/min to 1.0 mL/min and the mobile phase is plumbed to a Valco ZDV tee. Also attached to

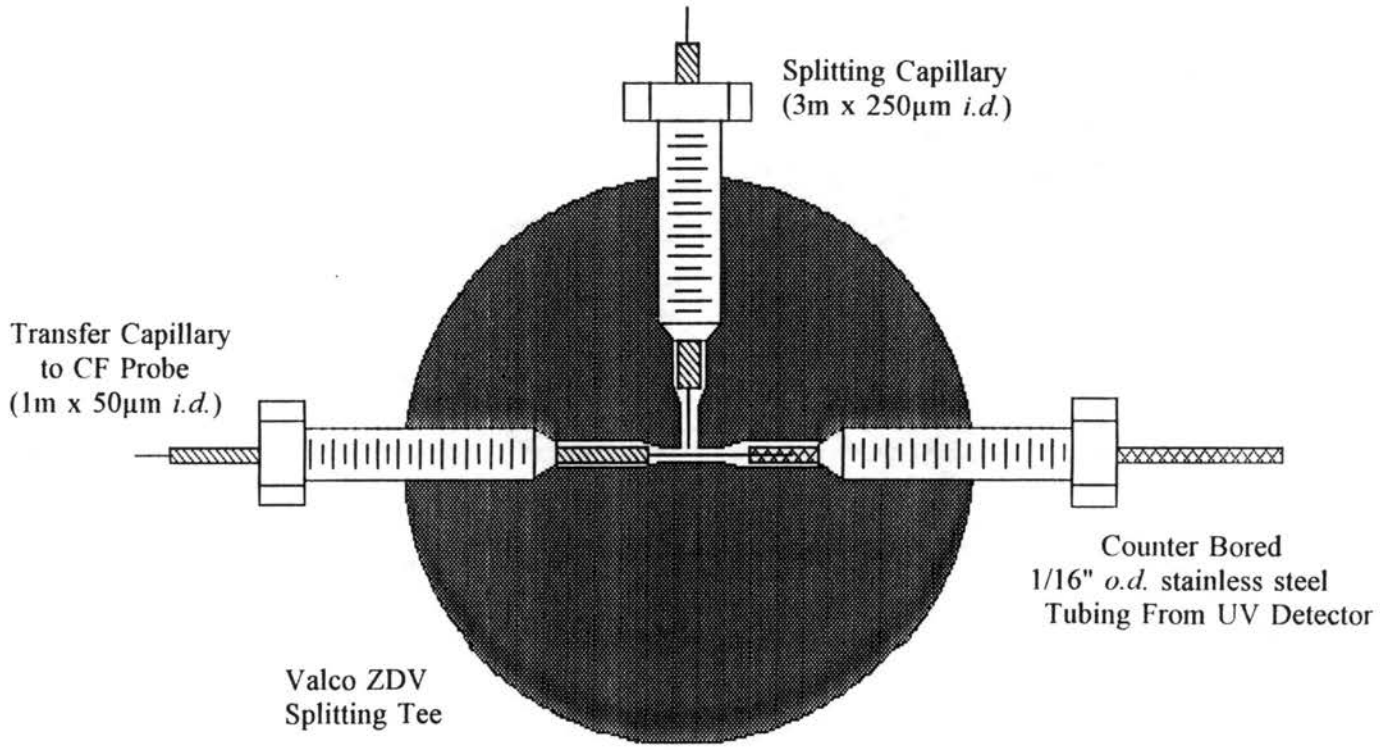

Figure 8- Valco ZDV Splitting Tee utilizing Differential Fused Silica Capillary Lengths

the ZDV tee are the balance column and Valco C4UW internal loop injector. The balance column acts as a backpressure regulator which diverts a portion of the mobile phase through the nanoscale column which is attached to the injector. Splitting is achieved by setting the flow rate on the HPLC pump which produces the desired flow through the nanoscale column.

Flow rates at the μL/min levels were measured with a 10μL Hamilton syringe. The syringe was connected to the transfer capillary and nanoscale column exits using a piece of teflon tubing with the proper internal diameter to fit over both the needle of the syringe and the fused silica capillary. The volume of the eluent was then measured for one minute and recorded. It should be kept in mind that these measurements were performed at atmospheric pressure. When the probe/capillary are placed in the high vacuum, a lower backpressure is present at the exit of the transfer capillary. This lower pressure alters the split ratio, and a higher flow rate is realized in the mass spectrometer than that measured at atmospheric pressure.

II.6 Packing Nanoscale HPLC Columns

All nanoscale HPLC columns were packed in our laboratory. Columns with internal diameters ranging from 0.178 μm to 508 μm were packed. The columns consisted of straight lengths of 1/16" (1.5876 mm) *o.d.* stainless steel tubing (Alltech Associates part #97060 and #97091) or fused silica capillaries obtained from Polymicro (Phoenix, AZ). All columns were slurry packed with octadecylsilane (ODS). Approximately 1 gram quantities of the packing material were obtained from

the following sources: 3μm, 5μm, 10μm Chromanetics Spherisorb ODS particles were obtained from P.J. Cobert (St. Louis, MO), 8 μm Zorbax ODS particles were generously donated by MAC-MOD Analytical (Chadds Ford, PA), 5 μm Bakerbond ODS particles were also generously donated by (J. T. Baker, Phillipsburg, NJ)..

Initially, columns were slurry packed with isopropyl alcohol by suspending approximately 100 mg of the ODS in 1.0 mL isopropyl alcohol. A preferred slurry solvent was later used consisting of water, acetonitrile, and glycerol (39:59:2). The slurry was placed into and empty 3 cm x 1 mm *i.d.* precolumn (Upchurch Scientific, Oak Harbor, WA, part #C-135 B) that served as a reservoir. The capillary to be packed was attached to the terminal end of the reservoir and an ISCO μLC syringe pump filled with the slurry solvent was attached to the forward end of the reservoir. Packing was performed by gradually increasing the syringe pump pressure to 7000 p.s.i. Gentle tapping of the reservoir promoted faster packing. Once the capillary was packed, a constant pressure of approximately 3000 p.s.i. was applied overnight to produces a continuous flow through the column. The pump was then halted and allowed to gradually depressurize undisturbed which generally required a few hours.

One of the more difficult aspects of nanoscale column preparation was "fritting" the columns. Several methods were used and are listed below as Procedures A through D. Mobile phase composition and gradients employed for nanoscale LC-CF-LSIMS were similar to those used for analytical LC-CF-LSIMS.

Procedure A

Procedure A consisted of constructing a glass wool plug that served as the frit for packed fused silica capillaries. The glass wool used had been ground in a mortar and pestle to a fine consistency. Fritting was performed by gluing a glass press fit "butt" connector, commonly used to join two GC columns, (Supelco, Bellefonte, PA, part #2-0479M) or a piece of glass tubing to the end of the fused silica capillary with DURO™ Master Mend 5 minute epoxy. After the epoxy hardened, a small glass wool plug was forced into the union. A 1 meter x 50 μm *i.d.* transfer fused silica capillary was then inserted into the other end of the connector. The transfer capillary was forced down tight against the glass wool plug to minimize dead volume and then secured in place with epoxy. It was eventually determined that glass sleeves with internal diameters close to the outside diameter of the packed fused silica capillaries produced a lower dead volume frit than the press fit connectors.

Procedure B

In this procedure, stainless steel capillaries were fritted with glass wool. This method was similar to Procedure A, except the glass wool frit was placed inside the stainless steel tubing. The glass wool frit was placed approximately 1cm inside the terminal end of the tubing and approximately 1 cm of the fused silica transfer capillary was inserted. The glass wool plug was held in place by a transfer capillary that had been glued with epoxy cement. The packing procedure then compressed the glass wool plug against the fused silica capillary and formed the frit.

Procedure C

This method for fritting fused silica capillary columns used a 1/16" Valco ZDV stainless steel union (Alltech Associates stock # 45834) in which a 1/16" diameter by 1/32" thick stainless steel frit was placed. Commercially available frits with 0.5 μm, 2 μm, and 5 μm pore sizes were obtained but the 0.5 μm (Alltech part# H2746) was preferred since the frit pore size should be approximately one tenth of the particle size. The union of choice had a 0.250 mm bore through its center. The frit was held in place by either a commercial Unchurch 1/16" fused silica capillary connector (Unchurch part # F-218, F-219, F-220, and F-221) or a capillary connector made from a two inch long piece of poly ether ether ketone (PEEK) 1/16" *o.d.* x 0.020" (508 μm) *i.d.* tubing (Alltech Associates stock #35708). Since the PEEK tubing is considerably less expensive than the Unchurch fittings, it was preferred. Both the PEEK tubing and Unchurch sleeve were compatible with conventional Valco's 1/16" nuts and ferrules.

Procedure D

Procedure D was very similar to Procedure C expect that a stainless steel column was used in place of the fused silica capillary. In this method, the stainless steel column to be packed was placed directly into the Valco ZDV union at the end containing the stainless steel frit. This configuration is similar to modern analytical columns. Once the column was fritted it was then washed and packed.

Procedure A

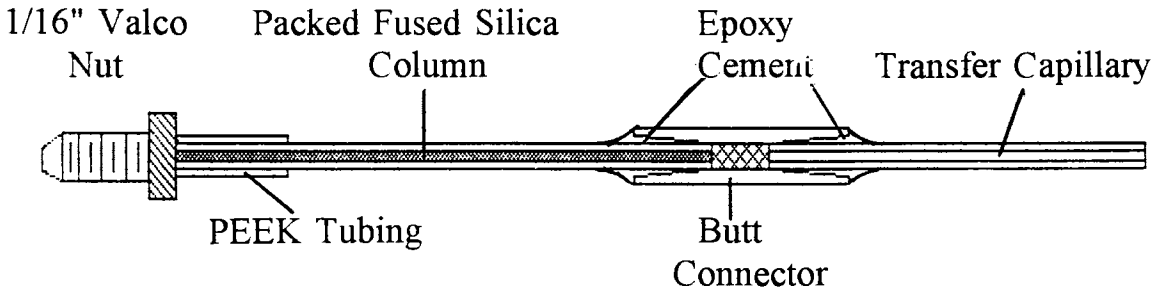

Procedure B

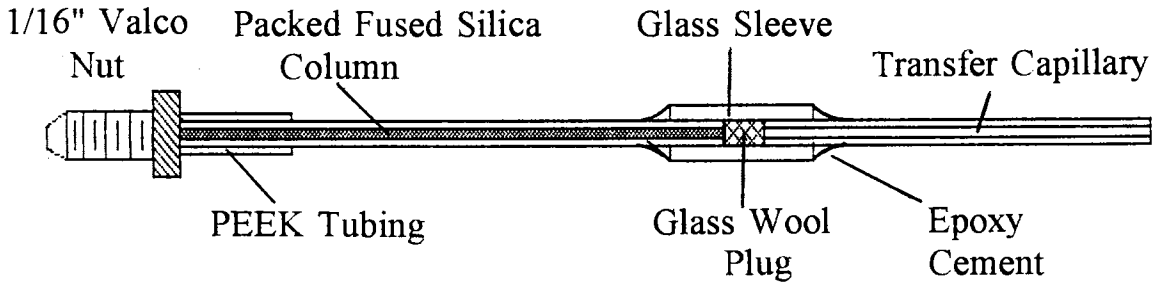

Figure 9- Schematic drawings of Nanoscale Columns packed in our laboratory by Procedures A and B

Procedure C

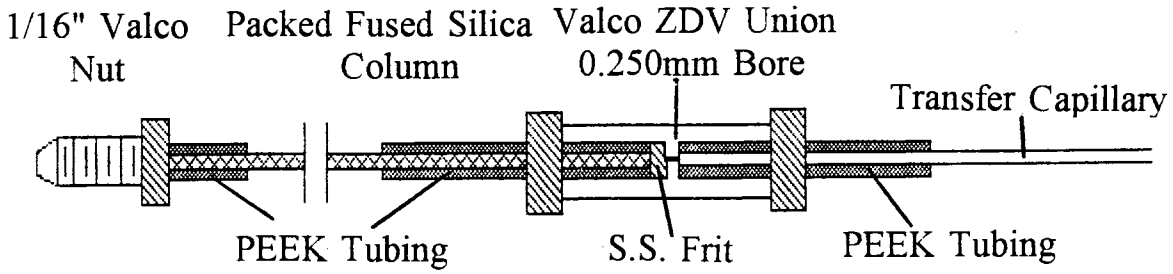

Procedure D

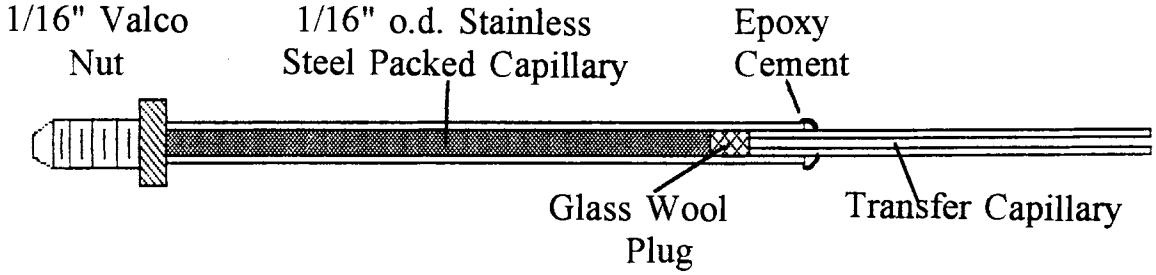

Figure 10- Schematic drawings of Nanoscale Columns packed in our laboratory by Procedures C and D

Procedure E

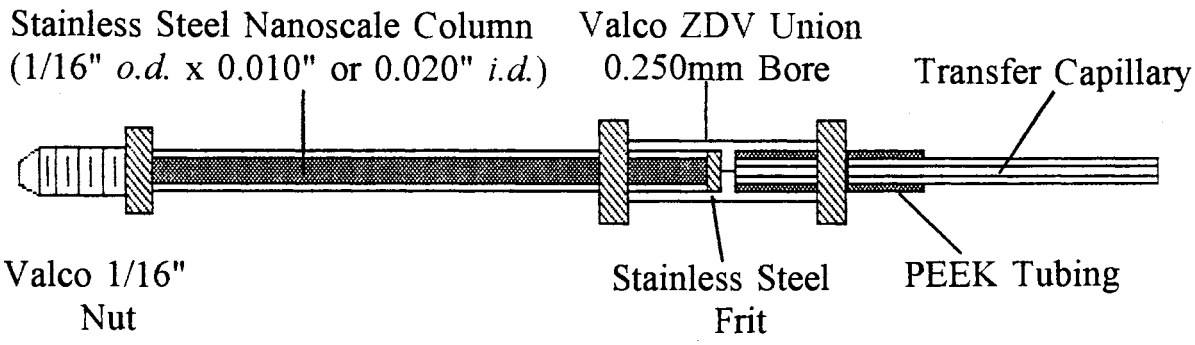

Figure 11- Schematic drawing of a Nanoscale Column packed in our laboratory by **Procedure** E

II.7 CHEMICALS AND REAGENTS

Burdick & Jackson acetonitrile and methanol were obtained from Baxter Health Corporation (McGraw Park, IL). Water was distilled, deionized using an 8 in. x 44 in. mixed bed ion exchange column (Continental Waters Systems, San Antonio, TX), and then filtered with a 0.2μm Nylon 66 membrane filters (Alltech Associates, Inc., Deerfield, IL 60015). Glycerol, trifluoroacetic acid (TFA), rutin, and naringin were obtained from Sigma Chemical Co. (St. Louis, MO). Polyamide 6™ (polyamide particles with 95% of particles with a size < 100μm) and ACS grade glacial acetic acid were obtained from J.T. Baker (Phillipsburg, NJ). Polyclar AT™ (polyamide particles with an average size of 120μm) was obtained from GAF (Wayne, NJ). Reagent ACS grade ammonium hydroxide was obtained from Fisher Scientific (Pittsburgh, PA).

II.8 Nanoscale HPLC UV Detection

A capillary column detection cell was constructed for nanoscale HPLC. The detector cell was constructed with a 3-way axis of alignment to maximize sensitivity. Experiments with this cell indicated a lack of sensitivity. Therefore, the commercial ISCO μLC-10 variable wavelength detector capillary cell designed for capillary electrophoresis was purchased. The main difference between the commercial detection cell and the one built in-house was that the commercial detection cell contained a collimating lens which considerably increased its sensitivity. However, the commercial cell lacked the feature of adjustability. As a result, our in-house

constructed detector cell was modified to accept the collimating lens. The modified cell is discussed in more detail in section *III.7*.

II.9 Sample Preparation

Alfalfa (*Medicago sativa* L.) callus cell culture suspensions were initiated and maintained as previously described [86,91]. Alfalfa roots (cv. Apollo), inoculated with *Rhizobium meliloti*, were harvested from whole plants approximately 2 to 3 months after germination. The plants were grown in a controlled environment while in a perlite medium. Plant material was frozen in liquid N_2 immediately after harvesting and then stored at a maximum of -10°C until extracted.

Isoflavonoid conjugates were isolated from alfalfa cell suspension cultures and alfalfa roots by modification of the method reported by Kessman and co-workers [86]. This method extracted smaller amounts of plant material and was approximately three times faster than the column method reported [86]. The modified isolation method was further preferred since the large amount of extract material generated from the original method could not be used in a timely manner to ensure that isoflavonoid conjugate decomposition was kept to a minimum.

The modified method consisted of freezing approximately 15 g to 30 g of plant material in liquid N_2 followed by immediate homogenization by grinding in a mortar and pestle. The homogenized sample was extracted three times with 200 mL portions of ice-cold acetone for approximately 4 hours each. Extraction was performed with magnetic stirring in an ice bath. The extracts were pooled and sequentially filtered

through Whatman™ #4 filter paper and Whatman™ #40 filter paper. The extract was then concentrated on a rotary evaporator and loaded onto a prewashed polyamide column (Polyamide 6 or Polyclar AT).

The polyamide column was prepared by soaking the polyamide material in water overnight to allow the particles to "swell". The particles were then dispersed in water and allowed to settle for 30 minutes. The finer particles remaining suspended in solution were removed by decanting the supernatant. This process was repeated several times until the supernatant was clear after the settling period. A 25 mL bed volume of polyamide was then added to a Pyrex™ coarse (40 μm to 60 μm pores) fritted disc glass funnel (Fisher Scientific, Pittsburgh, PA). The column was then prewashed with successive 75 mL portions of water, methanol, and a 1:500 (v/v) solution of concentrated (30%) ammonium hydroxide in methanol. A slight vacuum, generated by water aspiration, was used to increase the flow rate through the column. Care was necessary to avoid cavitation of the column by extreme vacuum. The column was re-equilibrated with H_2O and the extract loaded.

The extract was then fractionated with a step gradient of 75 ml each H_2O, CH_3OH, and the basic methanol solution described above. The basic fraction was collected and taken to dryness using a rotary evaporator. The oily residue remaining after evaporation was then resuspended in a minimal amount of CH_3OH for transfer to a vial. The resulting solution was then dried under a stream of Ar or N_2 at 40°C and resuspended in CH_3OH. This basic fraction was then analyzed by LC-CF-LSIMS.

CHAPTER III

RESULTS AND DISCUSSION

III.1 Initial Investigations

Initial investigations into the mass spectrometry of flavonoids began with HPLC fractions collected by the Noble Foundation, which were suspected to contain isoflavonoid glycosides. Attempts to obtain molecular weight information of these glycosylated compounds were made by both direct probe EI/MS and GC/MS using EI ionization without success. However, direct probe EI/MS experiments did provide molecular weight information of aglycones generated by enzymatic hydrolysis of the conjugates. In addition, GC/MS analysis using EI and traditional nonpolar capillary columns such as a DB-1 (100% dimethylpolysiloxane) or a DB-5 (95% dimethylpolysiloxane, 5% dipenylpolysiloxane) from J&W Scientific, Folsom, CA, were unsuccessful since the compounds would not elute from these columns. Further method development was performed using commercially available flavonoid aglycones that had been derivatized using N-methyl-N-trimethylsilyl-trifluoroacetamide (MSTFA) to form trimethylsilyl (TMS) derivatives followed by GC/MS. GC/MS was performed on the derivatized isoflavonoids, daidzein and formononetin, but these derivatives had extremely long retention times on the DB-1 and DB-5 capillary columns. Using a similar approach, the Noble Foundation developed a GC method, which was further

adopted to GC/MS, for the analysis of derivatized precursor aglycones found in the medicarpin synthesis pathway [91].

From the EI studies, it became apparent that molecular weight information of flavonoid conjugates could not be readily obtained by EI/MS. Therefore, investigations were directed towards direct probe LSIMS (DP-LSIMS) of the unknown isoflavonoid conjugates. The results obtained from these experiments were limited and will be discussed in detail later in section III.5.4. However the data obtained from these experiments, along with significant other experimental data such as NMR, UV spectroscopy, and other wet chemical methods described in the project rational section of Chapter 1, were used to identify several conjugates. The conjugates were identified as medicarpin-3-O-glucoside-6"-O-malonate (MGM), afrormosin-7-O-glucoside (AG), and afrormosin-7-O-glucoside-6"-O-malonate (AGM) [91].

III.2 Direct Probe LSIMS of Model Flavonoid Conjugates

The study into the DP-LSIMS analysis of flavonoid conjugates began with the use of commercially available model compounds,which included rutin (3,3',4',5,7-pentahydroxyflavone-3-rutinoside), naringin (4',5,7-trihydroxyflavanone 7-rhamnoglucoside), and esculin (6,7-dihydroxycoumarin 6-glucoside). Other flavonoid conjugates, such as genistin (4',5,7-trihydroxyisoflavone 7-glucoside) and daidzin (4',7-dihydroxyisoflavone 7-glucoside) that supplemented our model compounds, were provided as gifts from the Noble Foundation. Molecular structures of these compounds are provided in Figure 12. The purpose for investigating direct probe

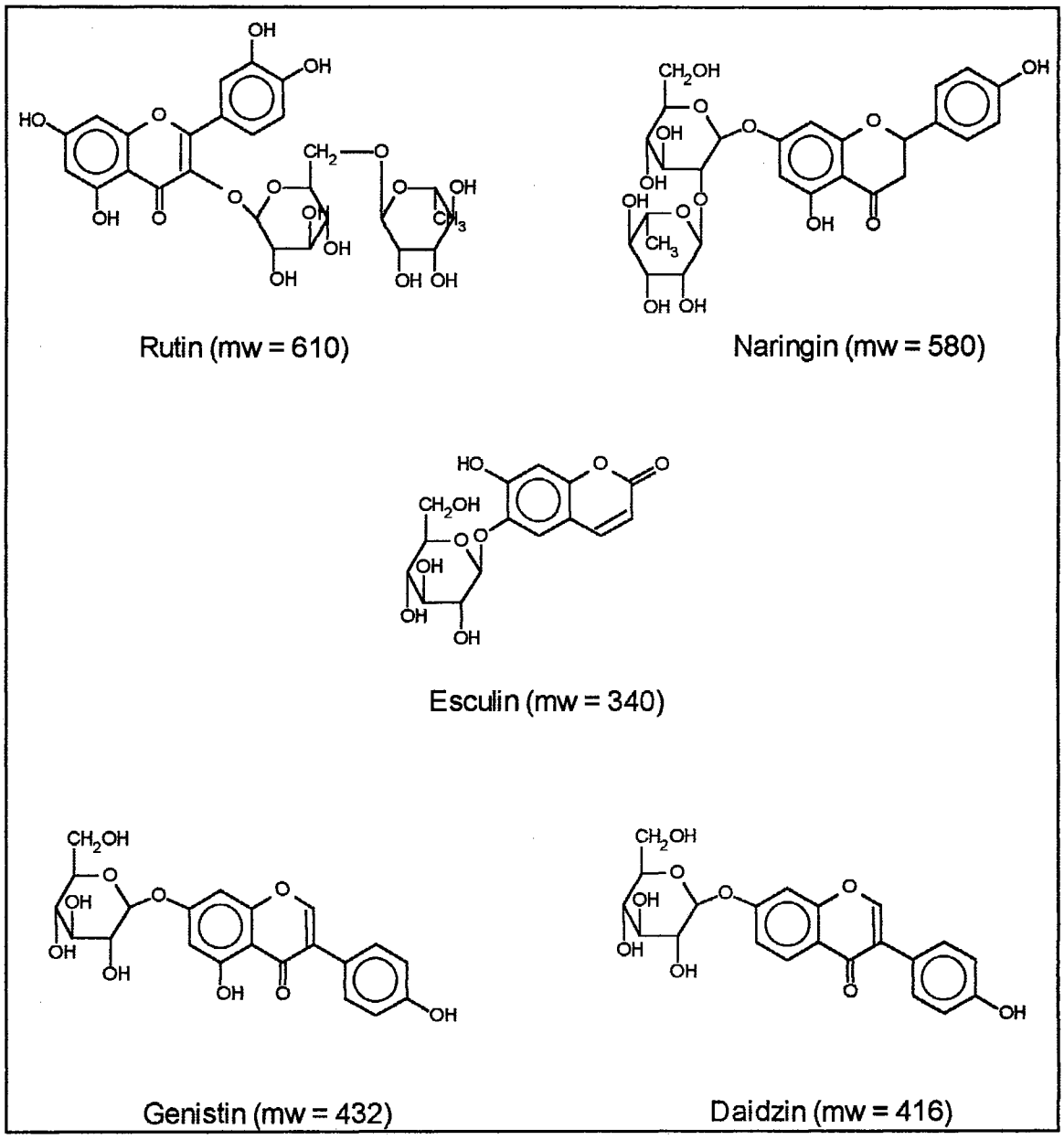

Figure 12- Molecular Structures of the Model Compounds.

LSIMS of these model compounds was to help characterize the LSIMS mass spectra of the model flavonoid conjugates and then use this information for the development and comparison with CF-LSIMS mass spectra. Direct probe FAB mass spectra of the model flavonoid glycosides have been reported in the literature [97-101]. However to perform a valid comparison between direct probe LSIMS and CF-LSIMS, the direct probe experiments were repeated on our instrument. This was done since FAB and LSIMS spectra often vary from instrument to instrument. FAB and LSIMS spectra also differ due to their differences in primary particle and primary particle energies.

The investigation into direct probe LSIMS began with the mass spectrometer operating in the positive-ion mode [(+) DP-LSIMS]. From a survey of common LSIMS matrices, it was experimentally determined that thioglycerol containing 1.0% TFA was the best matrix for positive-ion, direct probe LSIMS since it produced the highest secondary ion yields of the flavonoid conjugates. The survey included other matrices such as glycerol, glycerol with 1.0 % TFA, nitrobenzyl alcohol, and a 50:50 mixture of glycerol and thioglycerol containing 1.0 % TFA.

Mass spectra of rutin, naringin, esculin, and a blank matrix were acquired by (+) DP-LSIMS. Approximately 20 μg to 30 μg of each flavonoid conjugate was dissolved in 1.5 μL of the 1.0 % TFA in thioglycerol matrix and submitted for analysis. Ionization was achieved using a 35 keV, Cs^+ primary ion energy. The mass spectra of rutin, naringin, esculin, and a blank 1.0% TFA in thioglycerol matrix are provided in Figures 13 through 16.

A nomenclature for the identification of flavonoid fragments was first described

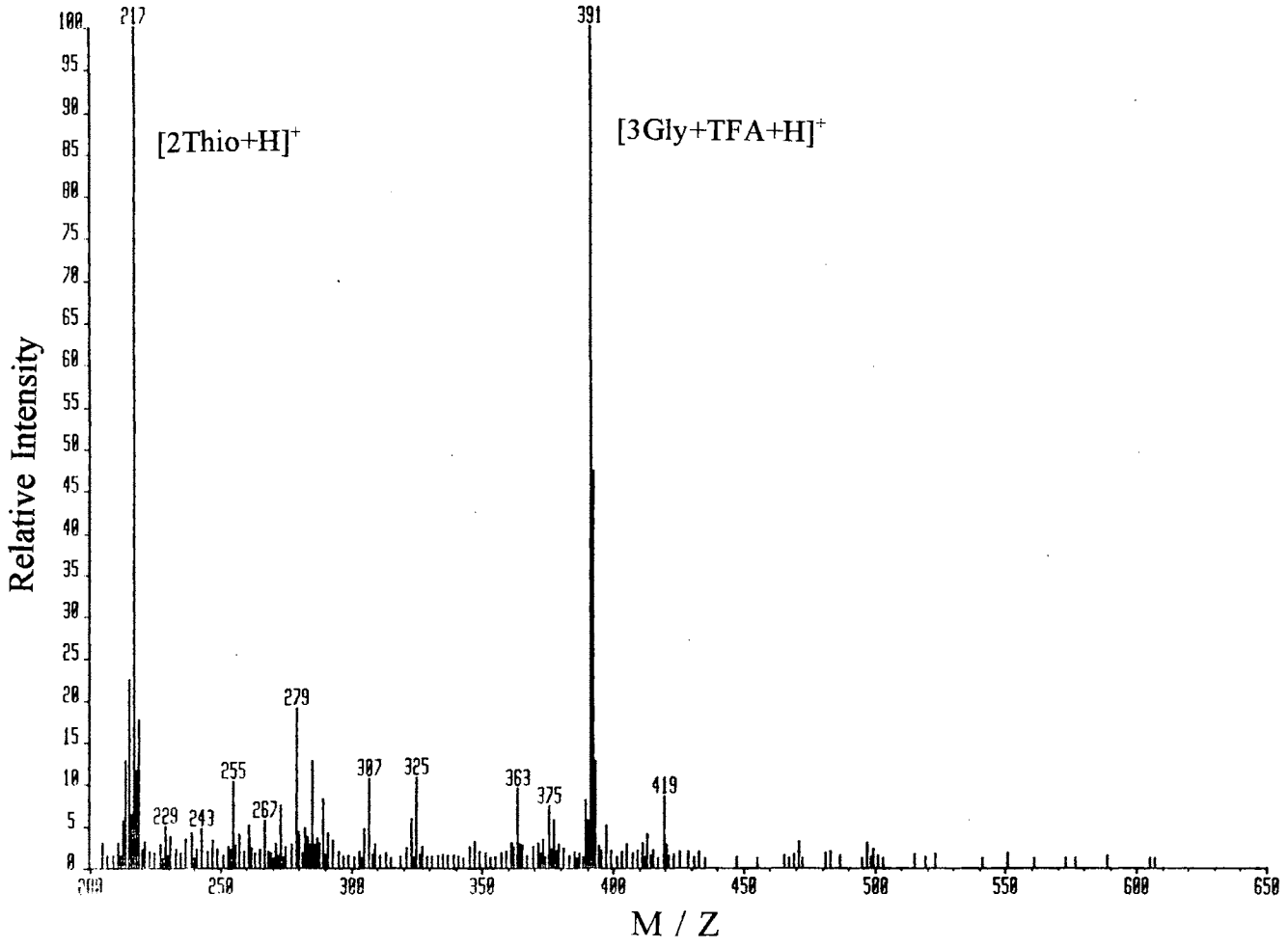

Figure 13- (+) DP-LSIMS Mass Spectrum of 1.0% TFA in Thioglycerol

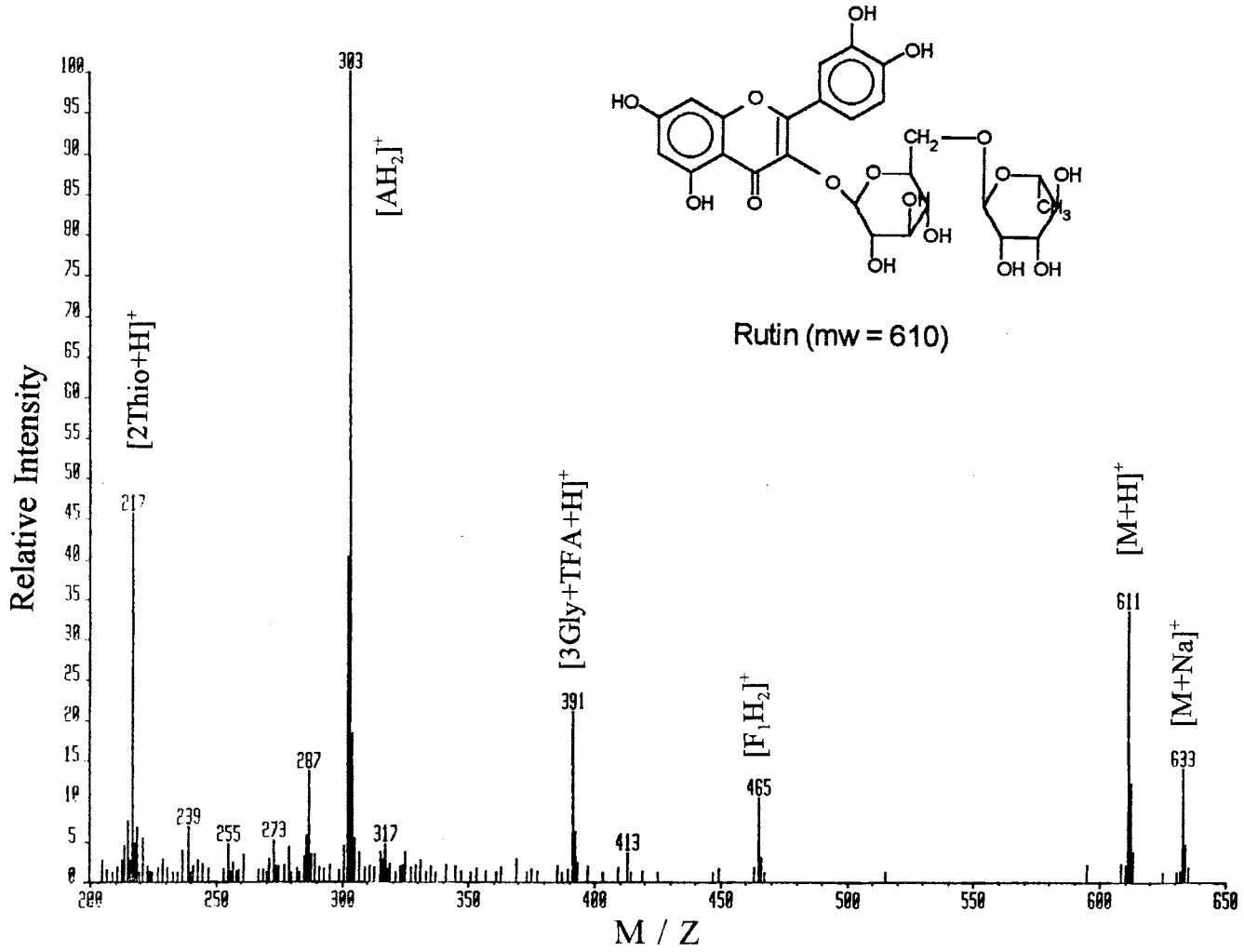

Figure 14- (+) DP-LSIMS Mass Spectrum of Rutin

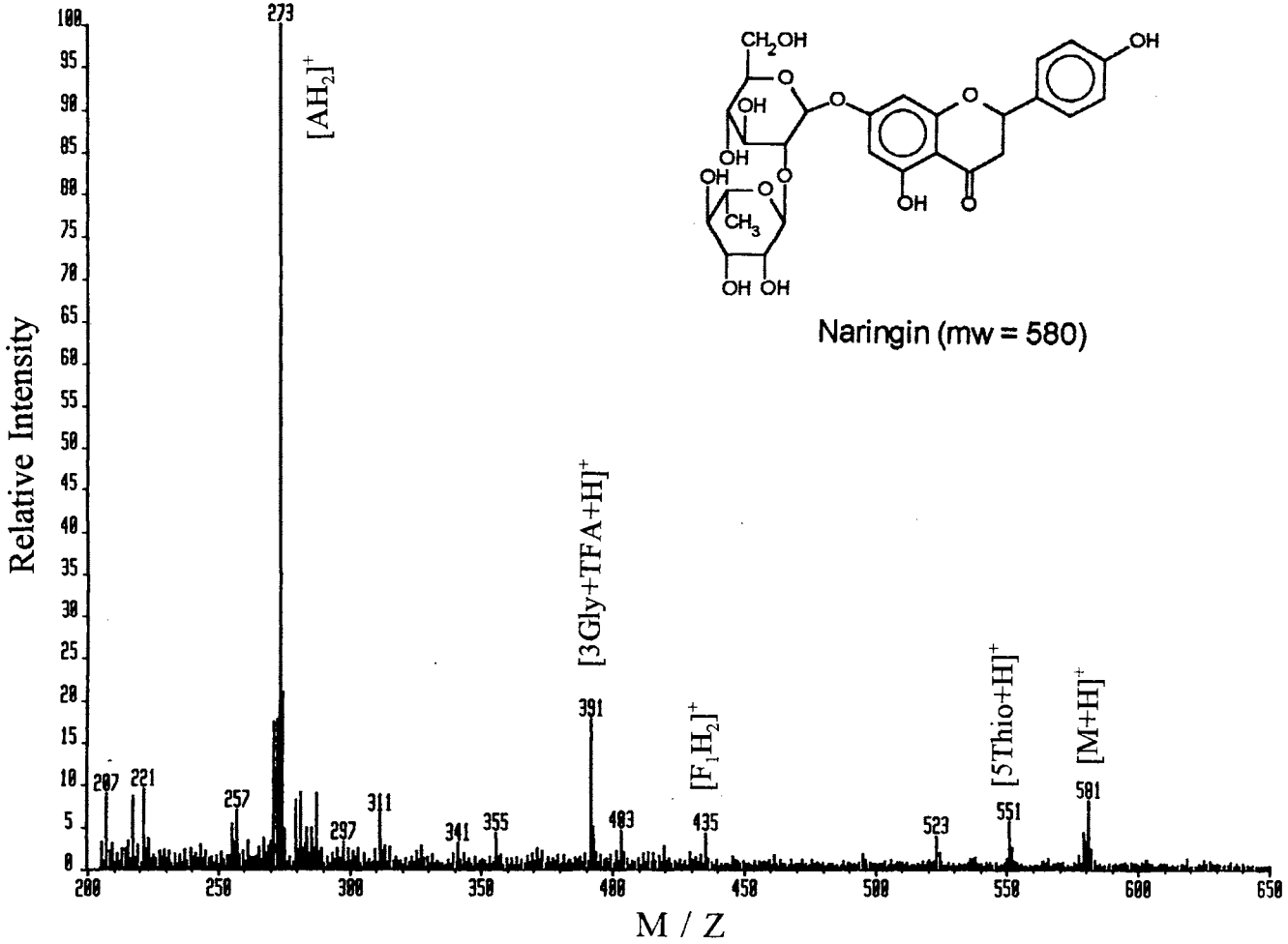

Figure 15- (+) DP-LSIMS Mass Spectrum of Naringin

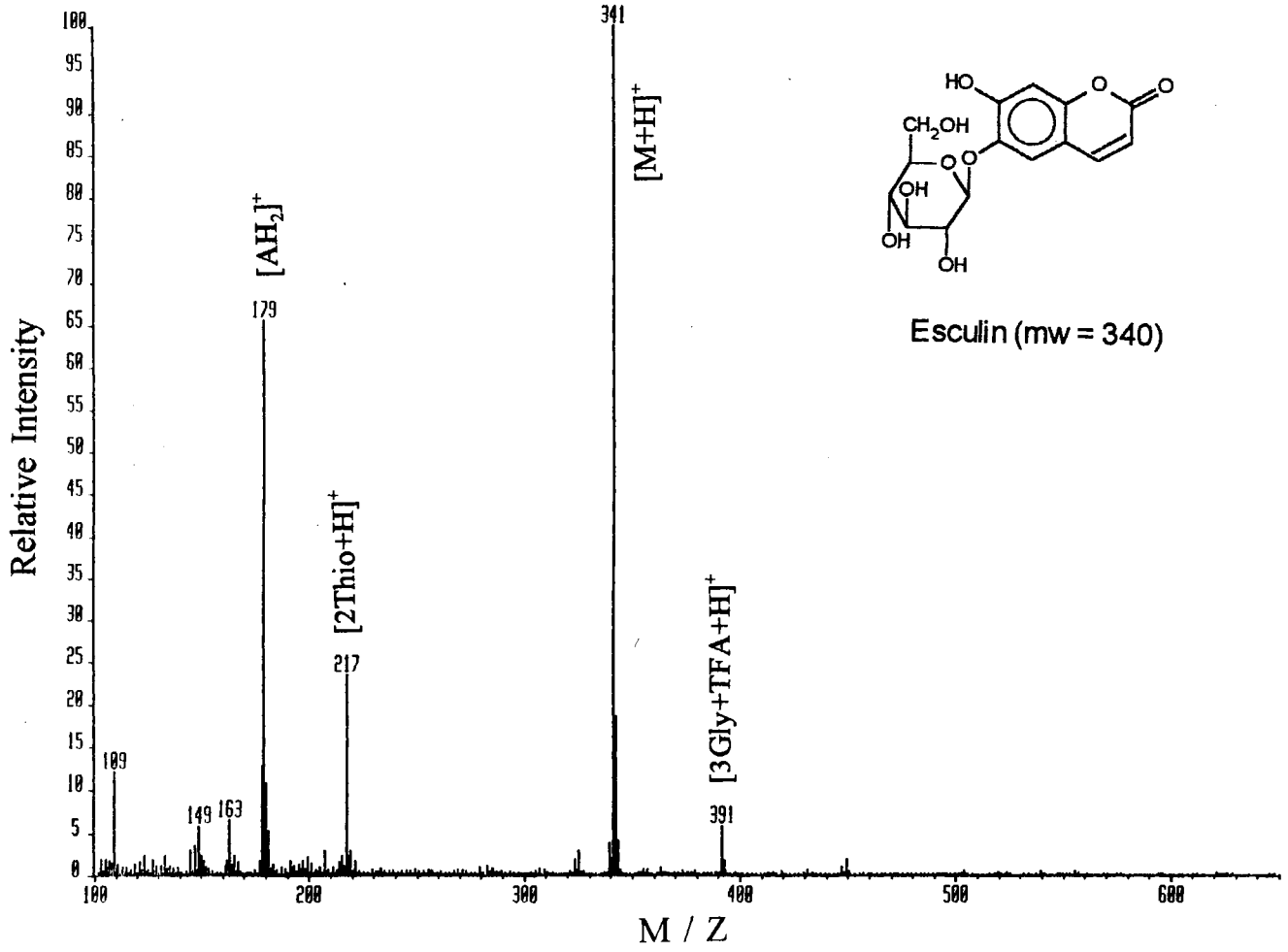

Figure 16- (+) DP-LSIMS Mass Spectrum of Esculin

by Crow and co-workers [98] and is illustrated in Figure 17. The aglycone fragment ion resulting from the cleavage of the glycosidic bond is described as the **A** fragment, while the successive fragmentation of the saccharides are referred to as $\mathbf{F_1}$, $\mathbf{F_2}$,... fragment ions. Positive molecular ions are formed by the addition of a proton which forms an adduct with the molecular species, $[M+H]^+$. The aglycone fragment adduct ion is formed by the addition of two protons $[AH_2]^+$. One proton is added at the site of sugar cleavage, while the second proton generates the charged nature of the adduct. Similarly, the sugar cleavage produces a positive-ion corresponding to $[FH_2]^+$. The protons originate from the matrix and TFA.

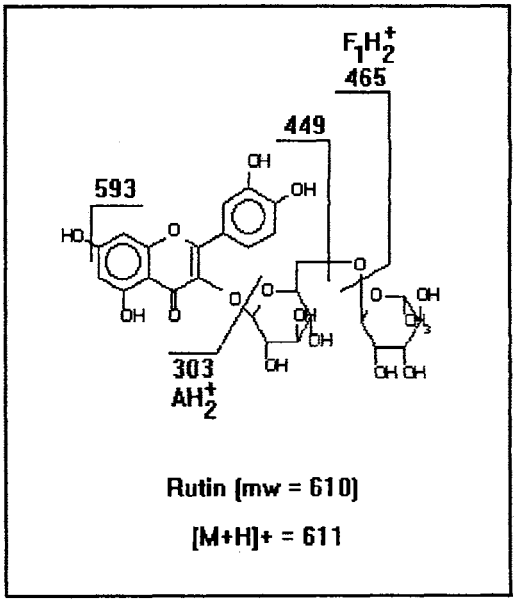

Figure 17- Fragmentation Notation and Pattern Illustrated with Rutin.

Our results varied slightly from those reported in the literature for positive ion, direct probe FAB utilizing 8 keV xenon atoms and a glycerol or acidic glycerol matrix [98]. These differences were attributed to the significantly higher primary ion energy and a difference in the matrix. The reported FAB mass spectrum of rutin yielded a relative molecular ion, $[M+H]^+$, peak intensity of 6% while the LSIMS mass spectrum yielded a relative molecular ion peak intensity of 34%. The increased relative molecular ion intensity is attributed to the optimized 1.0% TFA in thioglycerol matrix over the acidic glycerol matrix reported for the direct probe FAB experiments [98].

In addition, more fragment ion peaks were observed in the LSIMS spectra. Fragment ion peaks corresponding to the successive cleavage of the sugars from the molecular species were observed in all LSIMS mass spectra with the aglycone, $[AH_2]^+$, ion yielding the base peak. This differs from the reported FAB spectrum for naringin [98], which did not contain an aglycone peak. Thus in this case, the LSIMS spectrum yielded more chemical information than that acquired by FAB.

In addition to extensive fragment ions, peaks resulting from sodium ion adducts with the molecular species, $[M+Na]^+$, were observed at relative intensities of approximately 5% to 10% for most of the model compounds. The sodium adduct ion peak was useful in later studies for confirmation of the molecular weight by providing a known ion peak 22 mass units higher than the suspected $[M+H]^+$.

Positive-ion LSIMS spectra of genistin and daidzin are presented in Figures 18 and 19. These isoflavonoid glycosides yielded similar mass spectra to the other model flavonoid conjugates (i.e. a base peak corresponding to the $[AH_2]^+$ ion, molecular

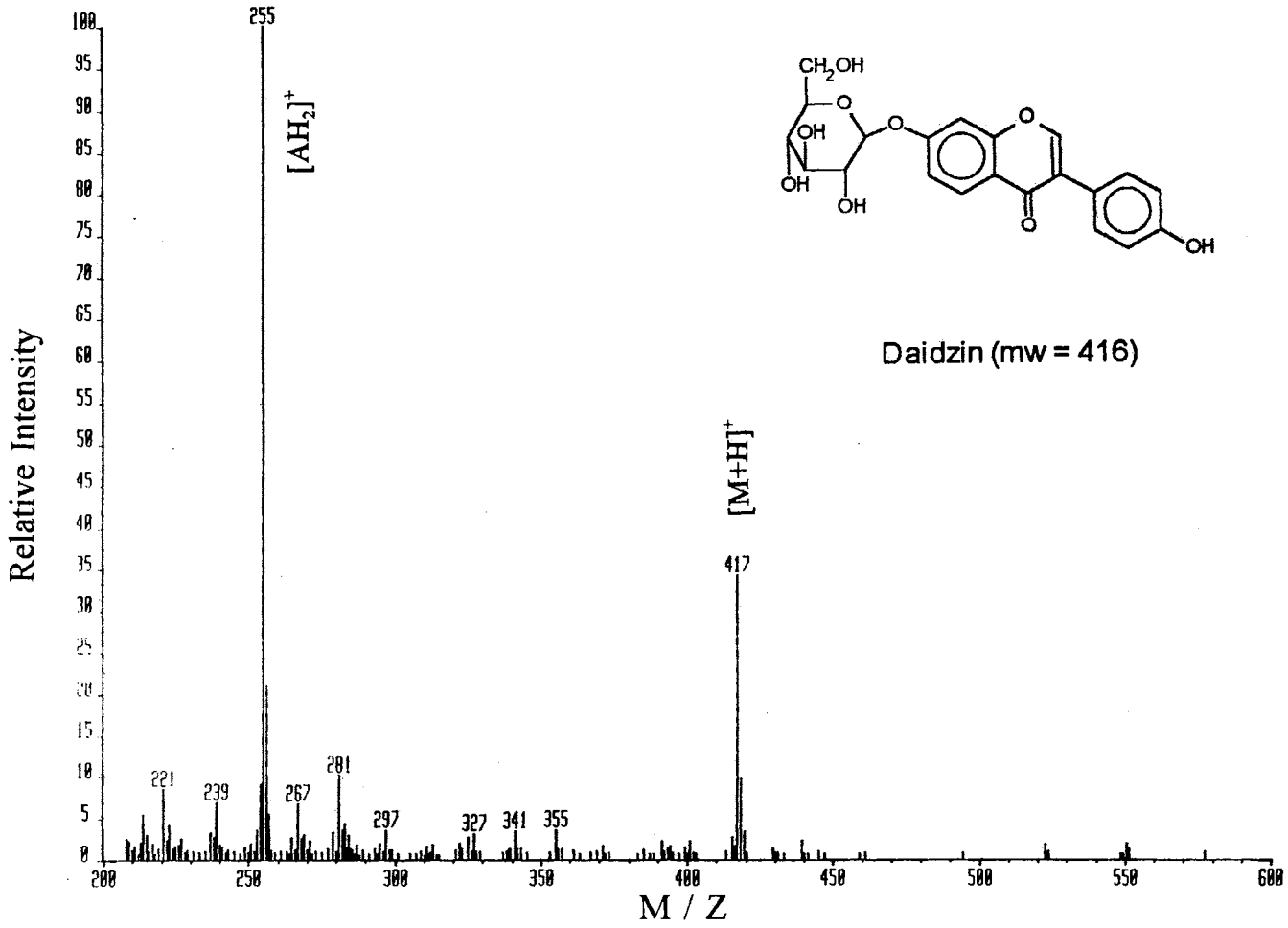

Figure 18- (+) DP-LSIMS Mass Spectrum of Daidzin

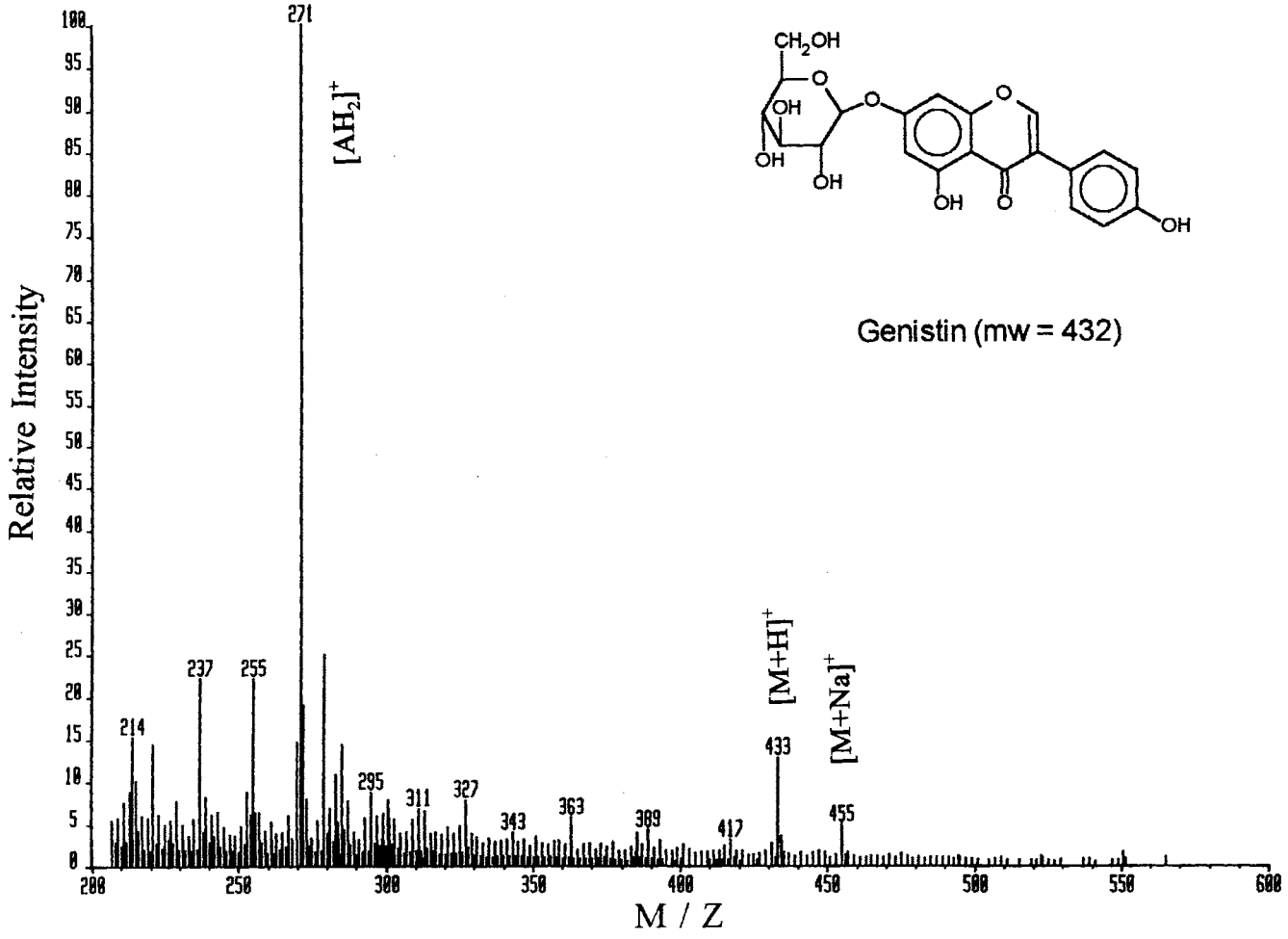

Figure 19- (+) DP-LSIMS Mass Spectrum of Genistin

ions, and sodium ion adducts with the molecular species). A summary of the ion peaks observed in the positive-ion LSIMS mass spectra of the studied flavonoids is provided in Table 1 with the relative intensities in parentheses.

To further the study of (+) DP-LSIMS analysis of flavonoids, an experiment was performed to determine the minimum detectable quantities (MDQ) for three flavonoids. Samples for mass spectral analysis were prepared by the addition of 1 μL aliquots from a series of methanol solutions containing 0.01 μg/μL to 50 μg/μL of the flavonoids to 1 μL of a 1.0% TFA in thioglycerol matrix. The samples were then submitted for (+) DP-LSIMS analysis using a 35 keV Cs+ primary ion energy. The signal-to-background (S/B) ratio was then determined by measuring the signal intensity of the [M+H]+ ion peak relative to the average intensity of background ion peaks within +/- 20 mass units. This method of S/B measurement is consistent with that described by Watson [3] for MDQ calculations of FAB spectra. Minimum detectable quantities are reported were the S/B ratio is three. Signal-to-background ratios are reported instead of signal-to-noise ratios because a substantial background is present from the matrix. The MDQ's determined are presented in Table 2. Resulting MDQ's were on the order of 1 μg. In contrast, previously reported direct probe FAB experiments typically used 20 μg to 50 μg of the flavonoid conjugates for their experiments [97,100].

Positive-ion, direct probe LSIMS experiments were then performed to study the linearity of the LSIMS response for possible quantification of flavonoid glycosides. This was accomplished using the data obtained from the MDQ study. It was found

that the ratio of the intensity of the $[M+H]^+$ ion peak of esculin at m/z = 341 relative to the background matrix ion peak intensity at m/z =391 (i.e. $I_{m/z=341}/I_{m/z=391}$), was linear with respect to the esculin concentration. A response curve of ($I_{m/z=341}/I_{m/z=391}$) versus concentration was then constructed. This response curve is presented in Figure 20 for the range of 0.73 nmol to 58.6 nmol (0.25 μg to 20 μg) esculin.

TABLE 1

POSITIVE-ION DIRECT PROBE LSIMS MASS SPECTRA OF THE MODEL COMPOUNDS

Compound	[M+H]+	$[M+Na]^+$	$[M+H-H_2O]^+$	$[F_1H_2]^+$	$[AH_2]^+$	Others
Rutin	611 (34)	633 (14)	593 (3)	465 (11)	303(100)	413 (5), 287(14), 317(5), 273(5), 239(5)
Naringin	581 (12)	---	---	403 (5)	273 (100)	551 (7), 523 (5), 435 (4), 257 (9)
Esculin	341 (100)	---	323 (3)	N/A	179 (67)	163 (7), 149 (6)
Daidzin	417 (29)	439 (3)	---	N/A	255 (100)	281 (10), 267 (7), 239 (7), 221 (8)
Genistin	433 (14)	455 (6)	---	N/A	271 (100)	255(22), 237 (22)

TABLE 2

MINIMUM DETECTABLE QUANTITIES FOR THREE MODEL FLAVONOID CONJUGATES BY POSITIVE-ION, DIRECT PROBE LSIMS

Compound	Minimum Detectable Quantity (S/B=3 for $[M+H]^+$)
Rutin	1.0 μg = 1.6 nmol
Naringin	1.0 μg = 1.7 nmol
Esculin	0.25 μg = 0.73 nmol

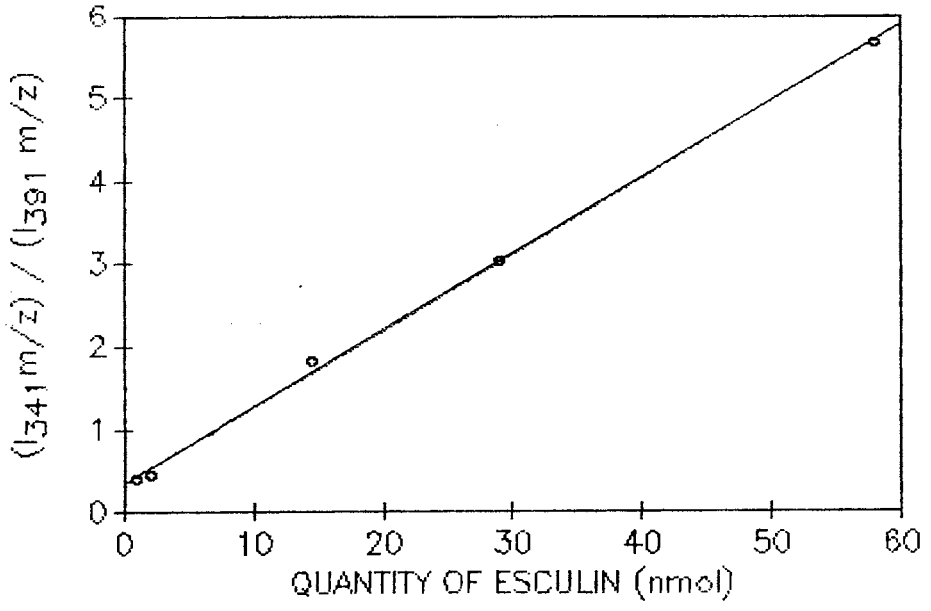

Figure 20- Response Curve for Esculin by (+) DP-LSIMS

The validity of the response curve presented above for the determination of unknown flavonoid concentrations would be dependent upon matrix effects. These effects were discussed in the introduction section, I.5.3.a, concerning hydrophobicity/hydrophilicity and their role in ion suppression. If a suspect analyte contained impurities that resulted in ion suppression of the analyte, an error in the actual concentration would be observed. This error would be reflected as a lower concentration than the true value. Therefore, quantification using (+) D-LSIMS would require a purified sample to obtain meaningful data.

III.3 Tandem (+) DP-LSIMS

Tandem mass spectrometry was investigated as a potential technique to obtain additional structural information of flavonoid conjugates. Positive-ion, direct probe LSIMS tandem mass spectrometry was performed on rutin and naringin. Tandem LSIMS experiments utilizing both metastable (MET) analysis and collisionally activated dissociation (CAD) were performed by linked scanning at a constant B/E. Samples were prepared by dissolving approximately 20 μg to 30 μg of each flavonoid conjugate in 1.5 μL of the 1.0 % TFA in thioglycerol matrix. The samples were then submitted for analysis. The results were obtained with a 35 keV, Cs^+ primary ion. Collisionally activated dissociation experiments were performed by the addition of helium gas to the first field free region gas cell in an amount sufficient to reduce the $[M+H]^+$ ion intensity by one-half. The CAD tandem mass spectra of naringin and rutin, using the $[M+H]^+$ ion as the precursor ion are presented in Figures 21 and 22.

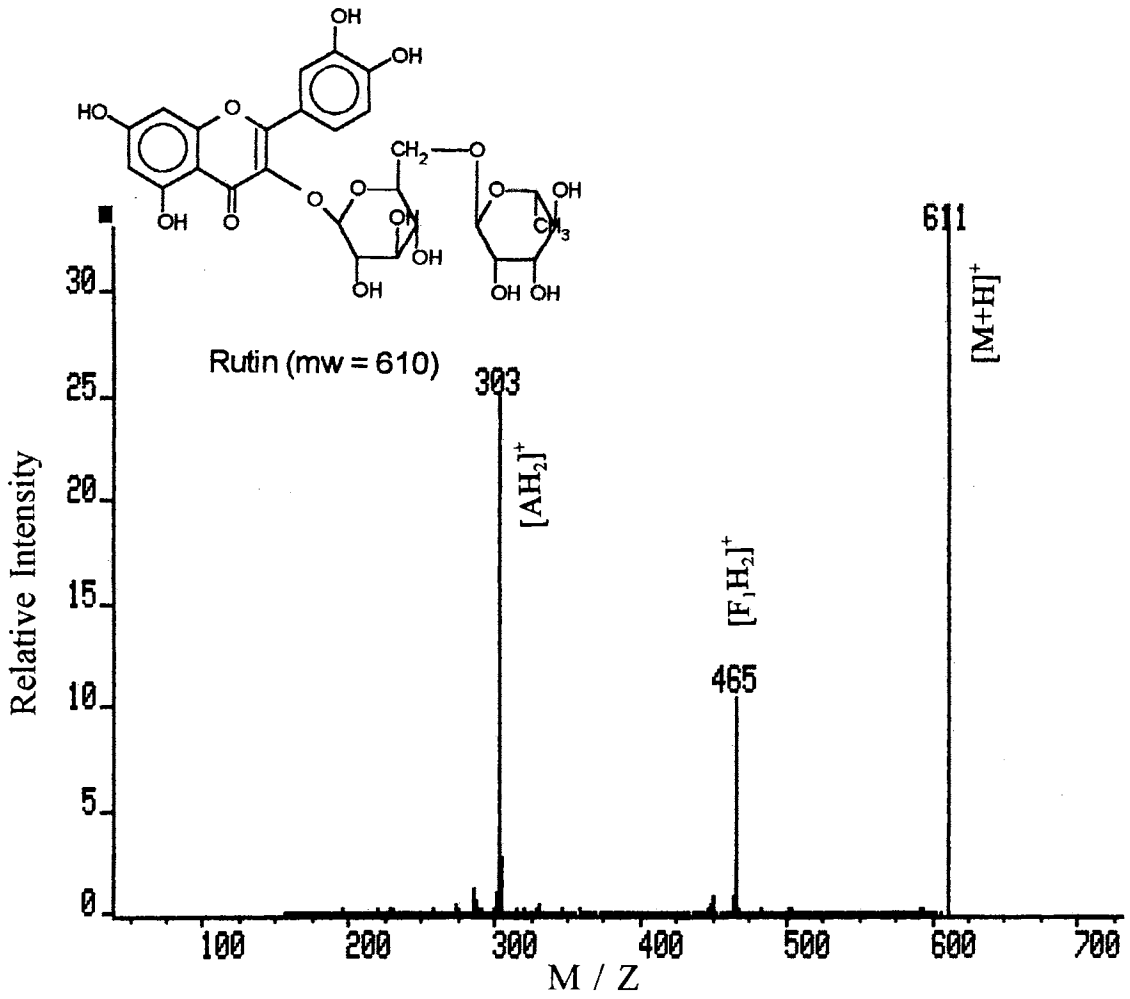

Figure 21- CAD Tandem (+) DP-LSIMS Mass Spectrum of Rutin

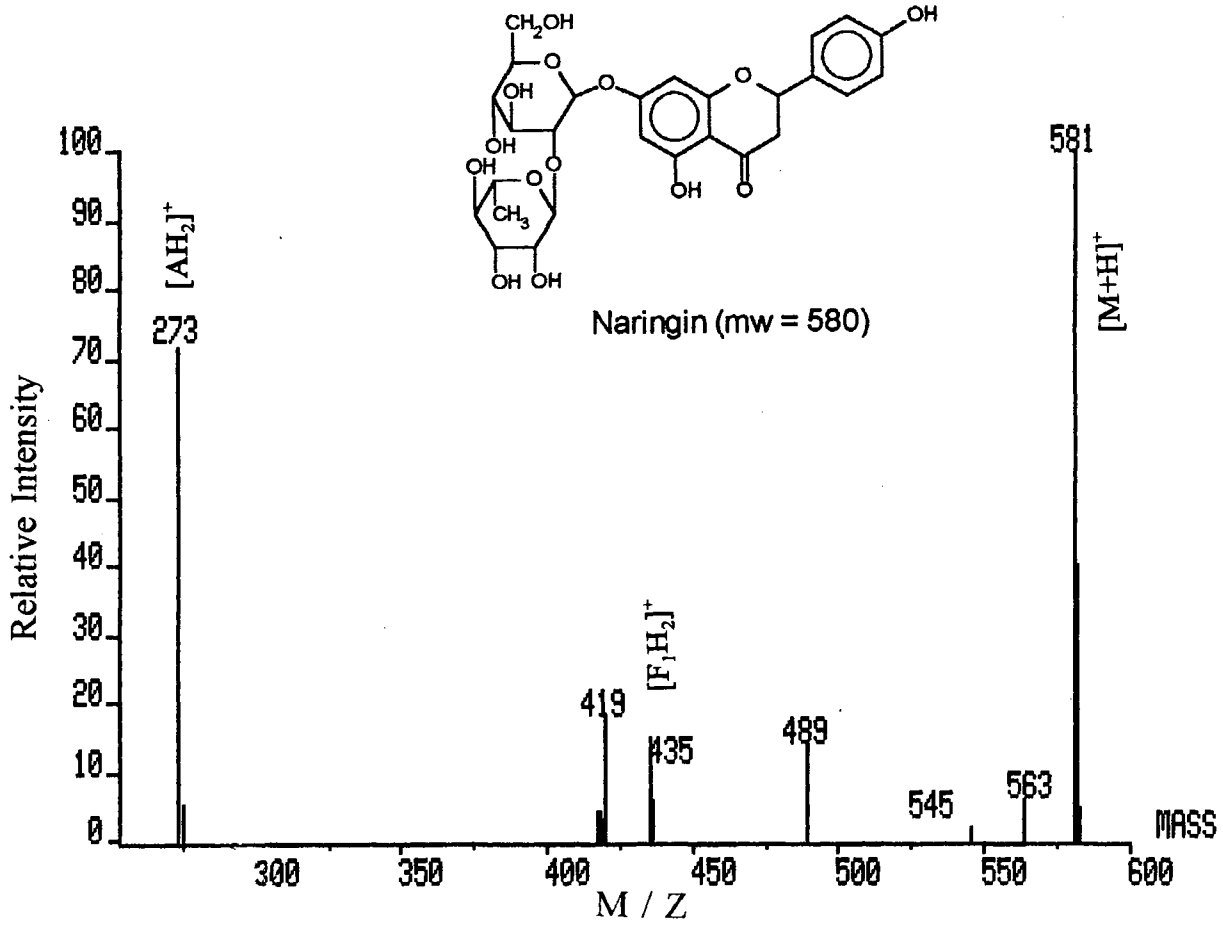

Figure 22 - CAD Tandem (+) DP-LSIMS Mass Spectrum of Naringin

These tandem (+) DP-LSIMS mass spectra are similar to those reported for direct probe FAB tandem mass spectrometry [98]. The first striking feature of the tandem mass spectra is the absence of the matrix peaks which results in much "cleaner" mass spectra. This is because only product ions originating from the selected precursor ion reach the detector as discussed in section *I.9.*.

The tandem mass spectra of rutin and naringin showed the same successive cleavage of the sugars from the $[M+H]^+$ ion as observed in direct probe LSIMS. This fact confirmed our original identification of the fragmentation ions in the direct probe LSIMS experiments. In addition, more extensive fragmentation of the sugars was observed in the MS/MS experiments. Tandem mass spectrometry was also performed by selecting the aglycone ion of rutin as the precursor ion. The MS/MS spectrum of the aglycone yielded fragmentation ions similar to those obtained by EI ionization and is shown in Figure 23. Thus, DP-LSIMS operating in the MS/MS mode can be used to provide aglycone structural information that previously required hydrolysis of the conjugates followed by EI/MS.

III.4 CF-LSIMS

The primary obstacle to successful CF-LSIMS experiments is obtaining and maintaining source stability. Source stability is described in terms of fluctuations in the source pressure which result in fluctuations in the secondary ion currents. These variations in the secondary ion currents must be maintained within +/- 10% [96-98] to perform reproducible CF-LSIMS experiments. The fluctuations are dependent upon

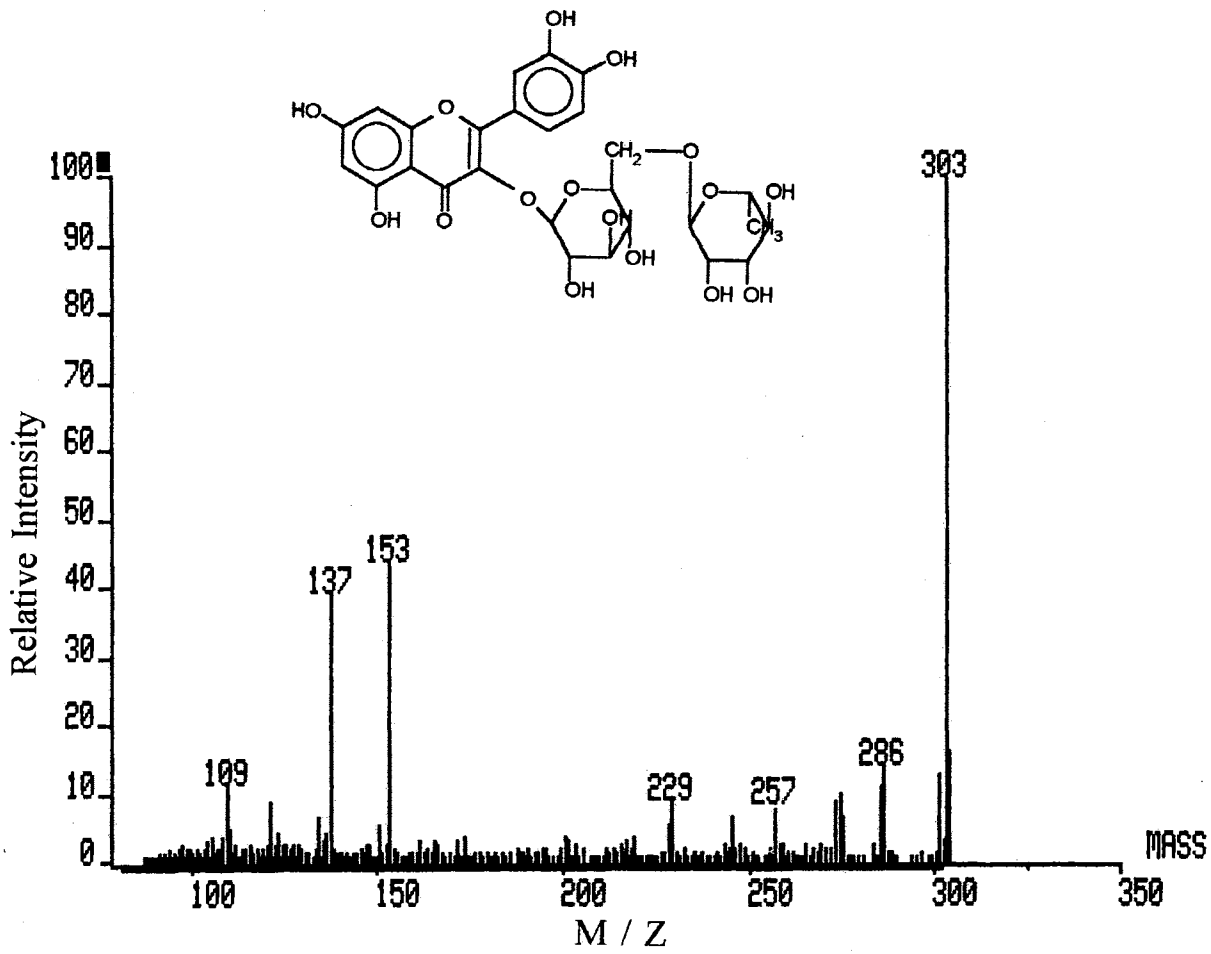

Figure 23- CAD Tandem (+) DP-LSIMS of the Aglycone of Rutin (querecetin)

the flow of the mobile phase and matrix to the probe tip and are minimized by achieving a thin film of the matrix while maintaining even evaporation of the solvents. Parameters that influence the source stability include source and probe temperature, concentration of the matrix in the mobile phase, pumping capacity of the instrument, flow rate of the mobile phase, and the transfer capillary internal diameter. Thus, our first endeavor was to establish the parameters that would produce stable source conditions for CF-LSIMS on the VG ZAB2-SE.

The first consideration was given to the glycerol concentration in the mobile phase. Reported values for glycerol concentrations range as high as 20%. At these high concentrations, an excess of glycerol builds up on the CF probe tip. The excess glycerol can be removed by increasing the probe temperature to increase the speed of evaporation or it can be removed by an absorbent pad or wick. The first is not an option since excess temperatures should be avoided for the analysis of flavonoid glycosides to minimize any possible decomposition. Incorporation of a wick requires substantial CF probe modifications. Therefore, it was decided that the glycerol concentration should be kept to a minimum. An additional parameter considered in the attempts to achieve stable source conditions was the solvents used in the mobile phase. These are generally aqueous solutions of polar organic solvents such as methanol or acetonitrile. Pure aqueous solutions of glycerol have a tendency to freeze and sputter as they emerge from the transfer capillary and evaporate into the high vacuum source region. Freezing can be controlled somewhat by slight heating of the probe tip. Freezing can also be minimized by using aqueous solutions of organic

solvents. With the above considerations, experiments were performed that investigated mobile phases consisting of solutions of 0 to 10% glycerol in acidic solutions of varying concentrations of methanol and water. It was determined that a mobile phase consisting of 49% CH_3OH, 49% H_2O, 2.0 % glycerol, and 0.1 % trifluoroacetic acid (TFA) would produce stable source conditions at a flow rate of 5.0 μL/min and a source temperature of 38°C. It should be noted that by keeping the glycerol concentration low the source temperature was also kept at a relatively low value. This will allow thermal decomposition of the conjugates to be kept to a minimum. An acid was incorporated in the mobile phase since the final objective was to perform gradient HPLC of flavonoid extracts which requires the acid modifier to achieve adequate chromatographic resolution.

III.4.1 Positive-ion CF-LSIMS Characterization of Model Flavonoid Conjugates

Once stable source conditions were obtained with the above described mobile phase and conditions, positive-ion CF-LSIMS mass spectra were acquired for the model compounds. The first experiment involved 3 repetitive injections of 2.5 μg of rutin. The total ion chromatogram (TIC) and selected ion chromatograms (SIC) of m/z = 611 and 303 from this experiment are presented in Figure 24. The mass spectrum of scan #32 corresponding to the center peak observed in the TIC and SICs is presented in Figure 25. The (+) CF-LSIMS mass spectra for naringin and esculin are presented in Figures 26 and 27. The lower m/z value of the acquisition mass range is above the m/z value 179 for the esculin aglycone, $[AH_2]^+$. The mass range limitations

TIC

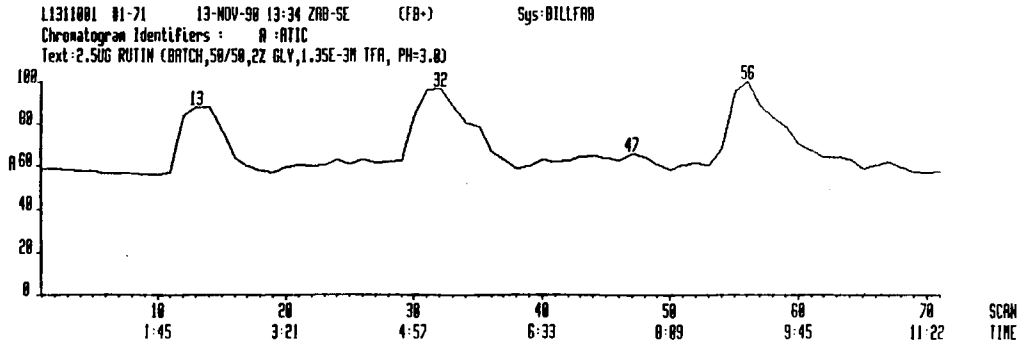

SIC of m/z = 611

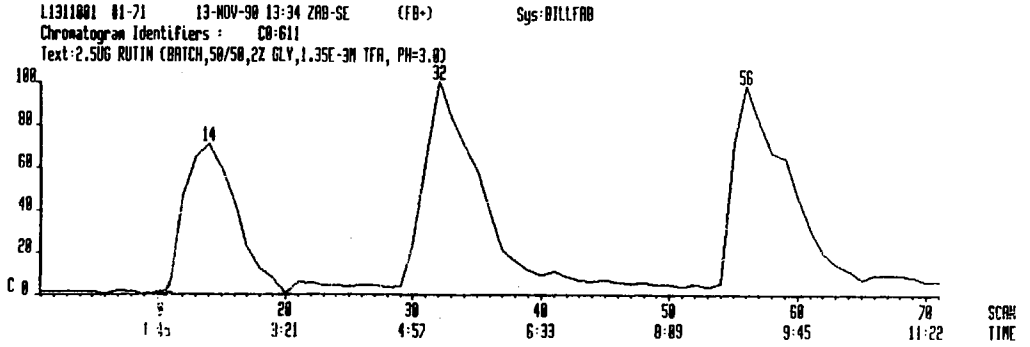

SIC of m/z = 303

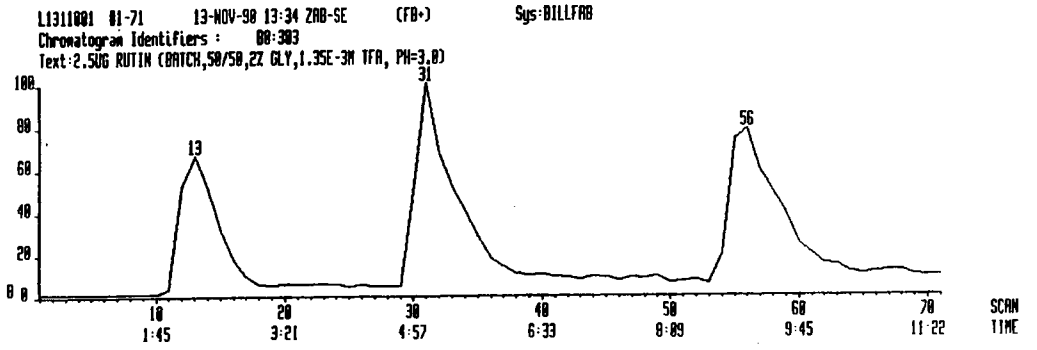

Figure 24- TIC and SICs for 3 repetitive Injections of 2.5 µg Rutin by (+) CF-LSIMS

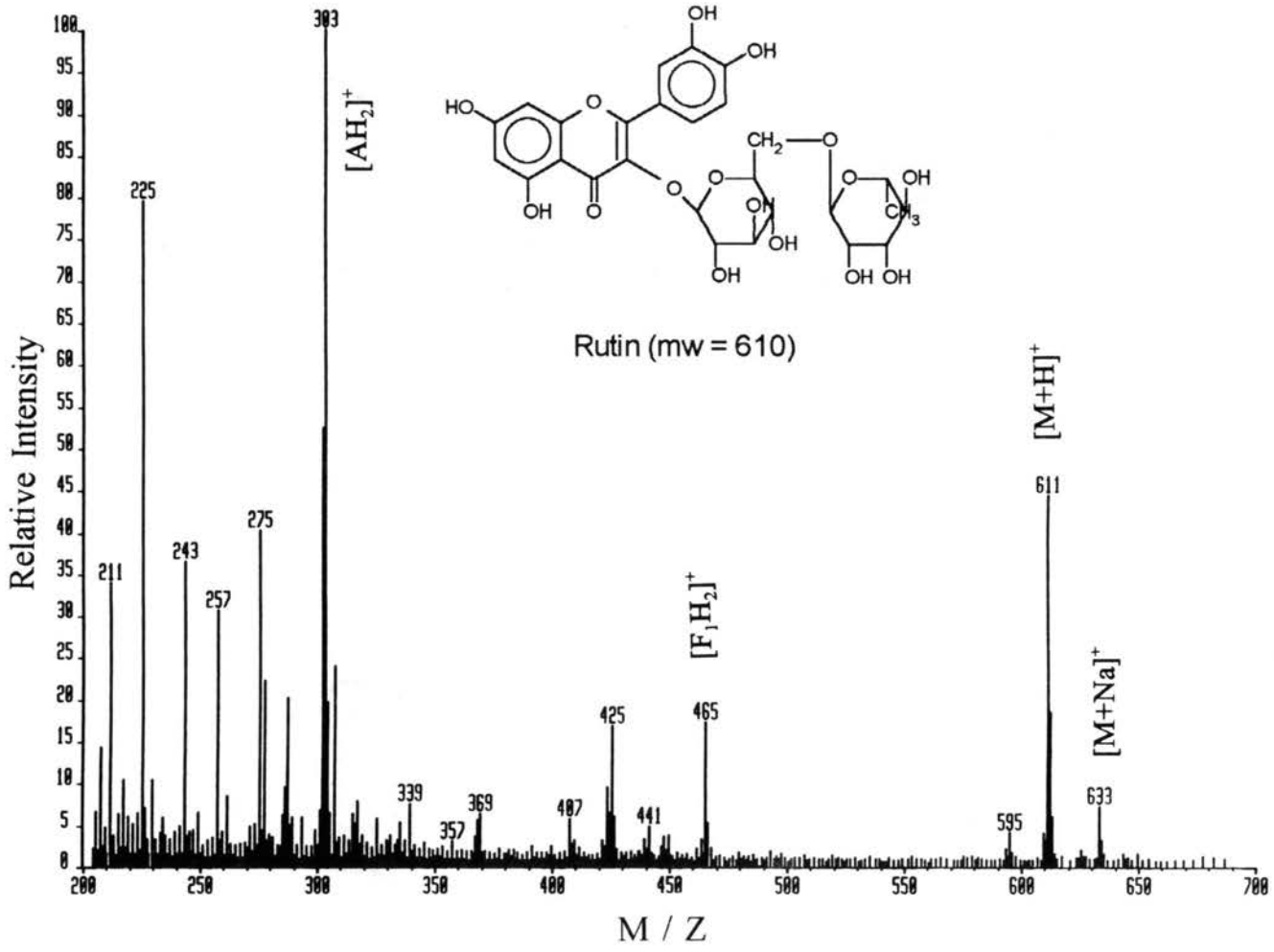

Figure 25- (+) CF-LSIMS Mass Spectrum of the Centroid Peak of Three Repetitive Injections of 2.5 µg Rutin.

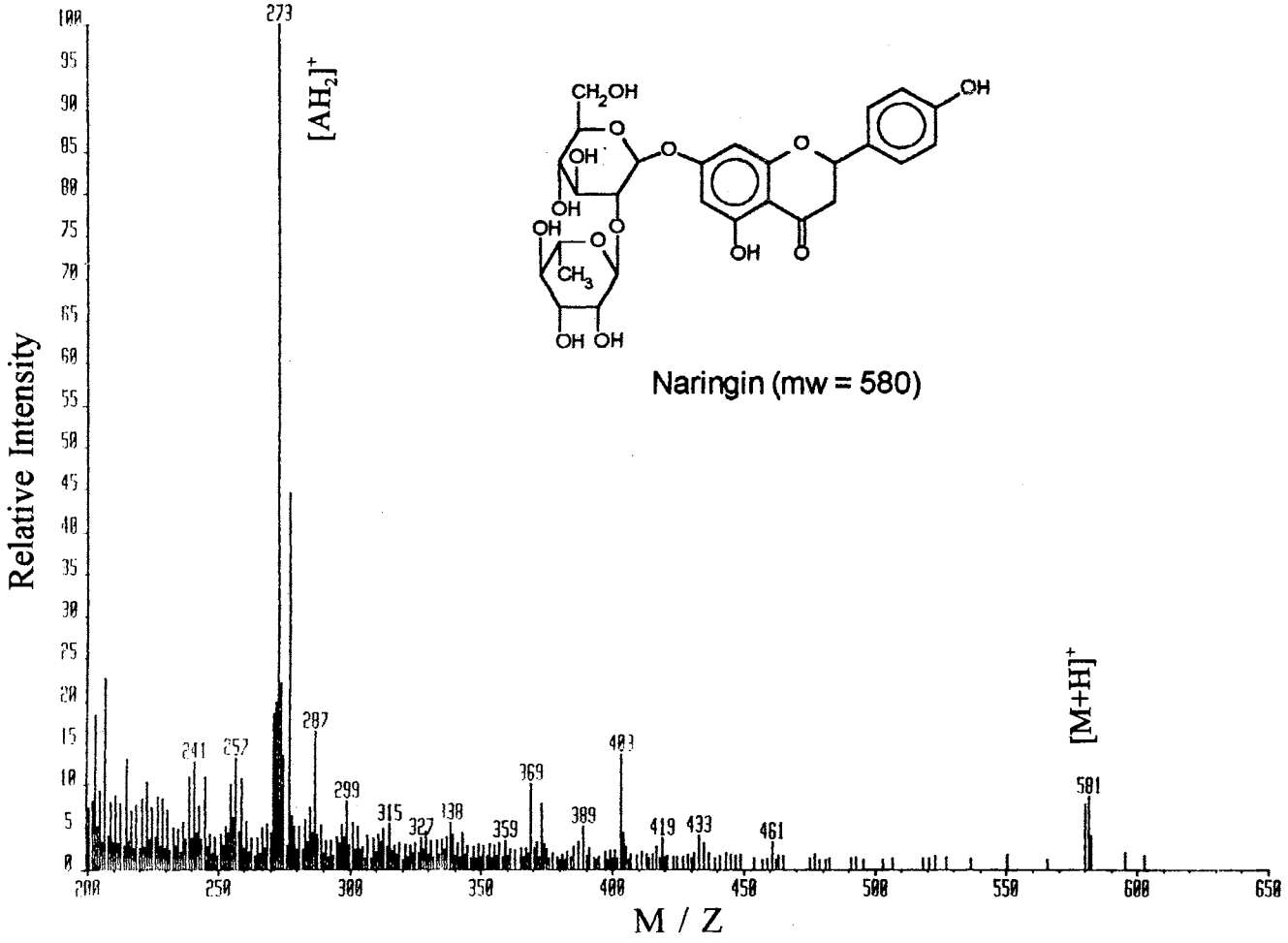

Figure 26- (+) CF-LSIMS Mass Spectrum of Naringin

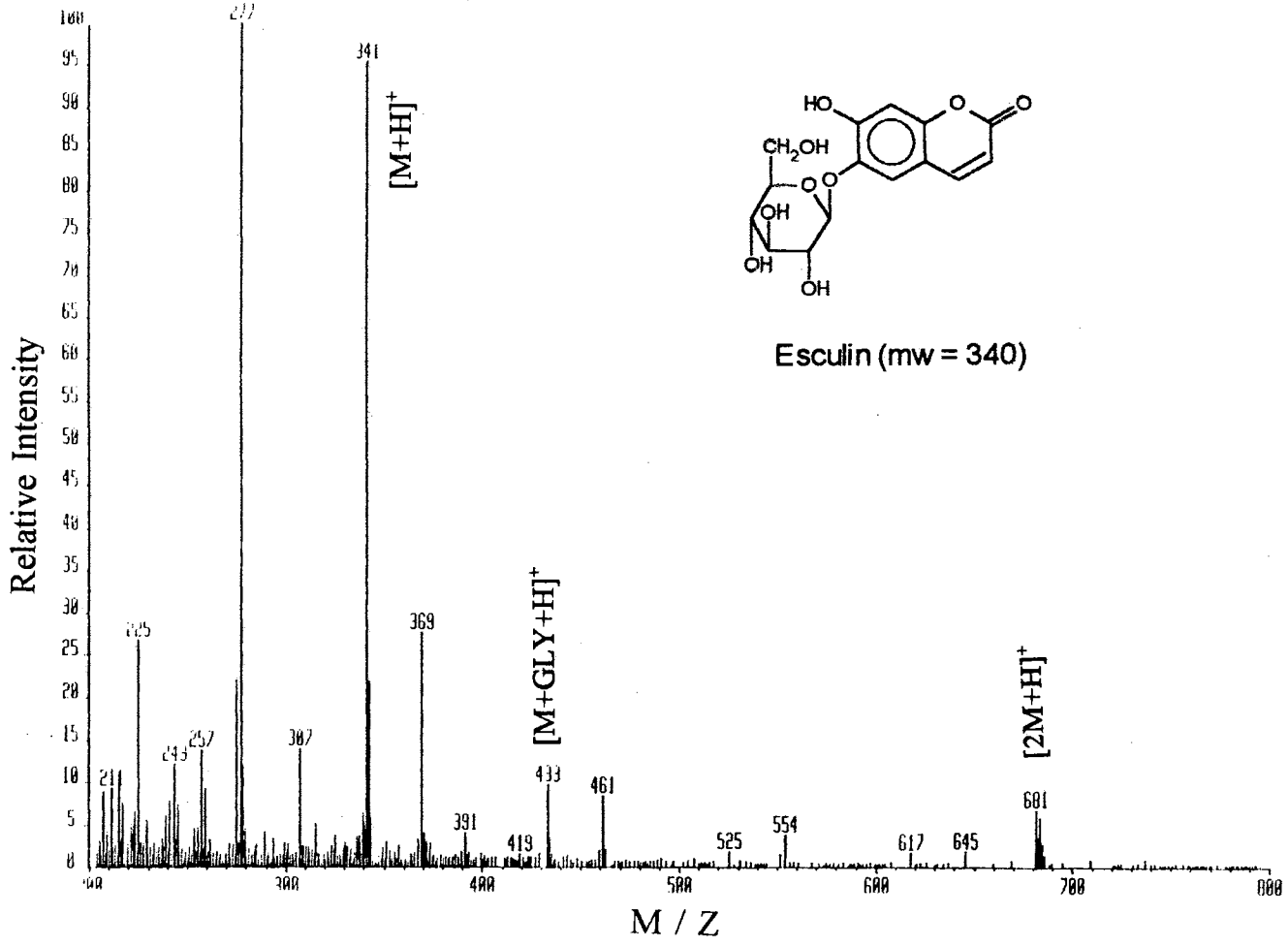

Figure 27- (+) CF-LSIMS Mass Spectrum of Esculin

described in the experimental section II.3. The (+) CF-LSIMS spectra obtained for rutin, naringin and esculin contained similar information to that obtained by (+) DP-LSIMS. Characteristic ion peaks observed for positive-ion CF-LSIMS of the model compounds correspond to $[M+H]^+$, $[M+Na]^+$, $[M+H-16]^+$, $[F_1H_2]^+$, $[AH_2]^+$ and $[A+H-16]^+$. These observed ions are summarized in Table 3. It is believed that the ions identified as the $[M+H-16]^+$ and $[A+H-16]^+$ result from the cleavage of one of the several hydroxyl groups of the A and B rings systems. These ions would be identified as $[M-OH+2H]^+$ and $[A-OH+2H]^+$ and are observed at a m/z value 15 mass units less than the molecular weight of the molecular and aglycone species. Additional ion peaks were observed for $[M+H-18]^+$ which is believed to correspond to ion generated by the loss of water, $[M+H-H_2O]^+$. This ion could also correspond to a radical molecular ion generated by the loss of a hydroxyl group, $[M-OH]^{\cdot+}$.

The study then focused on methods to increase relative ion peak intensities by background subtraction. This was performed using a computer algorithm which allowed the subtraction of a mass spectrum acquired prior to the elution of the injected sample from those spectra acquired over the entire analysis time. This process significantly reduced the intensities of the matrix ion peaks. The subtracted mass spectrum of the same 15.0 μg esculin mass spectrum reported in Figure 27 is provided in Figure 28. This spectrum shows a dramatic enhancement in spectral quality. Several other significant observations were made in the CF-LSIMS mass spectrum of esculin. The first is the presence of a peak corresponding to a glycerol adduct of the molecular ion, $[M+Gly+H]^+$, at m/z = 433. The second observation is the presence of

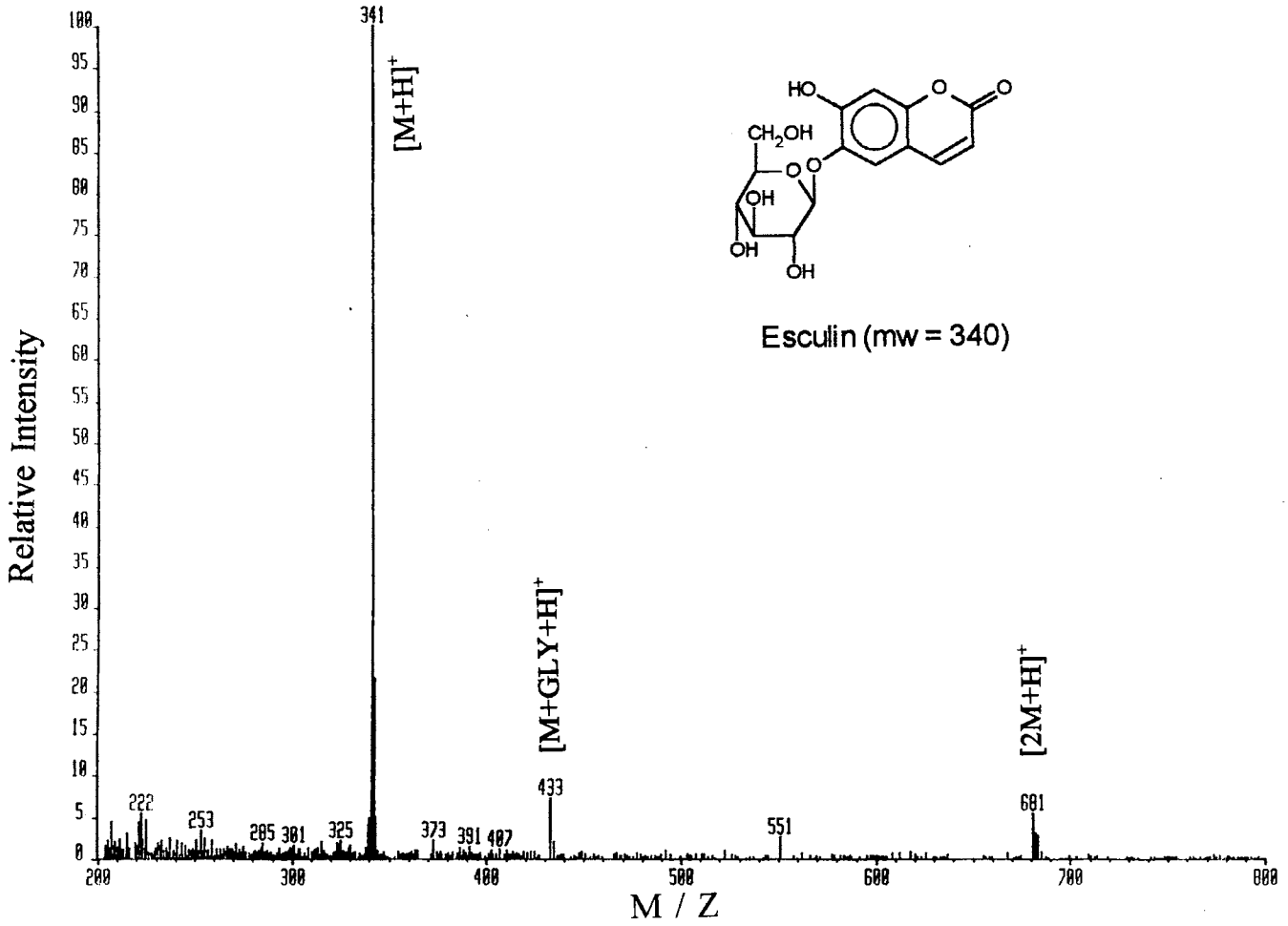

Figure 28- Background Subtracted (+) CF-LSIMS Mass Spectrum of Esculin

TABLE 3

POSITIVE-ION, CF-LSIMS OF THREE MODEL COMPOUNDS

Compound	[M+H]+	[M+Na]+	$[F_1H_2]$+	$[AH_2]$+	Others
2.5 μg Rutin	611 (45)	633 (8)	465 (18)	303 (100)	595(4),441(5),425 (18),287(20)
10.0 μg Naringin	581 (10)	603(3)	419(4)	273(100)	403(17),257(15),287(18)
15.0 μg Esculin	341(95)	—	—	—	651(6), 433(8)

a dimer ion, $[2(\text{esculin})+H]^+$, at m/z = 681. The presence of these additional ion peaks help verify the molecular weight of unknown conjugates. The presence of dimer ions was also observed in the analysis of many aglycones that will be discussed in more detail later.

After stable source conditions were obtained, a study of the reproducibility of repetitive injections was performed using the above described mobile phase and conditions. Ten repetitive 1μL injections were made with a methanol solution containing 2.5 μg/μL rutin. Alternate injections were made every 2 minutes with rutin and a blank consisting of the mobile phase. The injector was further rinsed with

methanol 30 seconds prior to all rutin and blank injections. Chromatograms were acquired in the selected ion recording (SIR) mode. The SIR data was obtained with a dwell time of 80 msec and a delay time of 20 msec while monitoring the $[M+H]^+$ ion of rutin at m/z = 611. The SIR chromatogram obtained is presented in Figure 29. The heights and area of the peaks were determined using computer functions available on the VG 11-250J data system and are reported in Table 4. The standard deviation (SD) of the areas and heights for injection #1 through #10 were calculated to be 6.90% and 10.52%, respectively. Statistical Q and T tests calculations indicate that the data point corresponding to injection #10 of the height series should be rejected. When the data point corresponding to injection #10 is rejected from both the area and height series, SDs of 5.91% and 7.13% are obtained for the peak areas and heights. These values for the SDs are well within the 10% suggested by the literature [97-100] and indicate a high degree of reproducibility.

Minimum detectable quantities (MDQ) were then determined for rutin, naringin and esculin by positive-ion, flow-injection CF-LSIMS. This was performed by injecting 1 μL aliquots of a series of methanol solutions with concentrations of 0.01 μg/μL to 50 μg/μL of the flavonoids. The mobile phase and other conditions used were as previously described. The MDQs were determined at a S/B of 3 and without background subtraction so that a valid comparison could be made with (+) DP-LSIMS data. These values are presented below in Table 5. The data shows a five fold decrease in the MDQs of naringin and rutin for the CF-LSIMS experiments over the direct probe LSIMS experiments while the MDQ enhancement for esculin was 2.5.

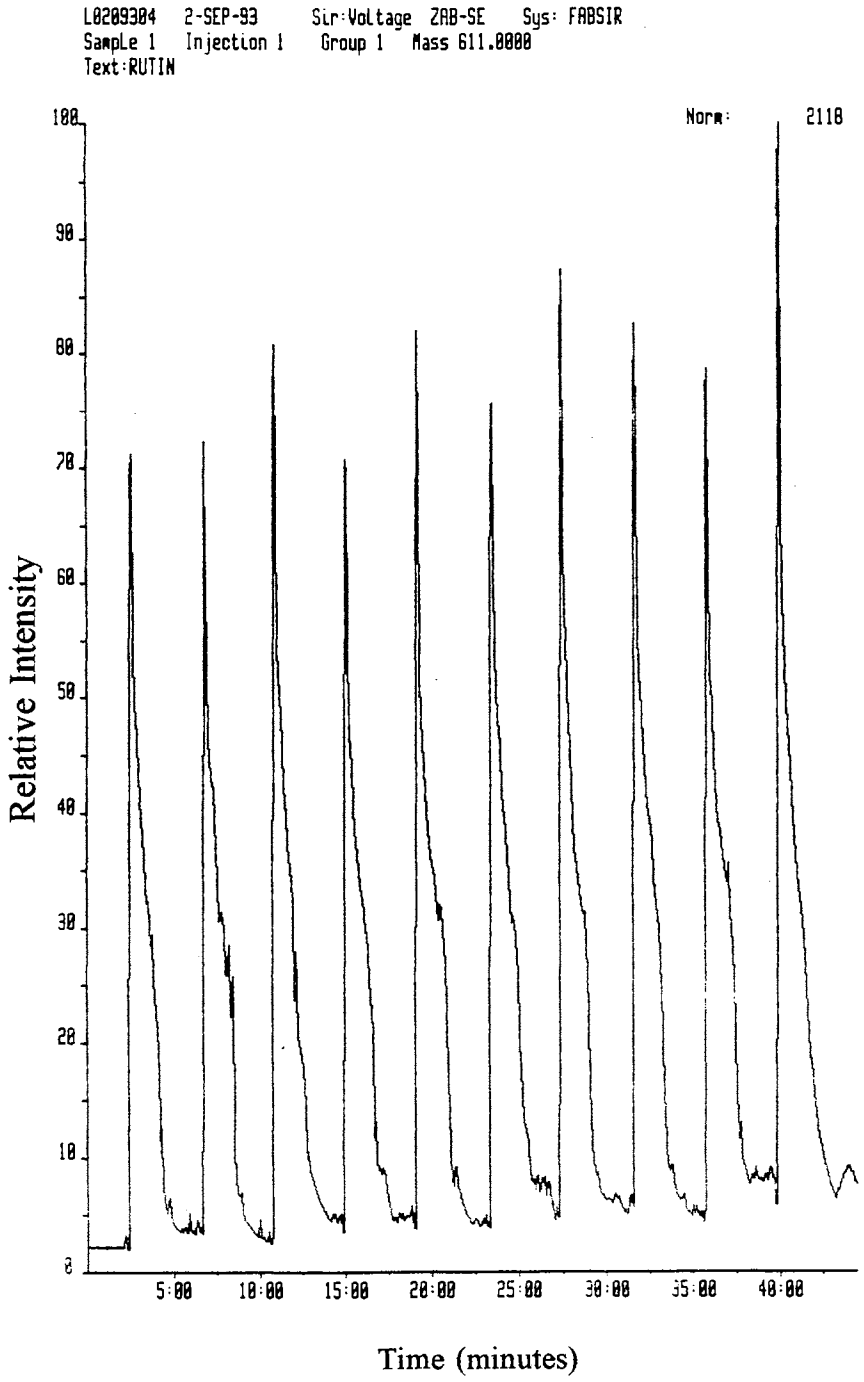

Figure 29- SIR Chromatogram of 10 Repetitive Injections of 2.5 µg Rutin

TABLE 4

AREA AND HEIGHTS OF TEN REPETITIVE INJECTIONS OF 2.5µg OF RUTIN BY POSITIVE-ION, FLOW-INJECTION, CF-LSIMS

2.5 µg Rutin	Area	Height
Injection 1	71039.70	1440.94
Injection 2	67423.84	1439.62
Injection 3	80032.16	1636.27
Injection 4	70111.59	1412.24
Injection 5	76791.59	1637.42
Injection 6	79633.69	1507.93
Injection 7	76768.3	1740.75
Injection 8	78052.33	1605.22
Injection 9	79270.84	1563.77
Injection 10	84519.29	1967.60
SD (#1-#10)	6.90%	10.52%
SD (#1-#9)	5.91%	7.13%

TABLE 5

MINIMUM DETECTABLE QUANTITIES OF MODEL FLAVONOID CONJUGATES BY POSITIVE ION, FLOW-INJECTION, CF-LSIMS

Compound	Minimum Detectable Quantity (MDQ)
Rutin	0.2 μg = 0.33 nmol
Naringin	0.2 μg = 0.34 nmol
Esculin	0.1 μg = 0.62 nmol

Due to the observance of adduct ions between the molecular species and sodium in the previous experiments, a study was performed to investigate the effect of Na^+ concentration on the CF-LSIMS mass spectra of flavonoid conjugates . This was achieved by measuring the relative intensities of the $[M+Na]^+$, $[M+H]^+$, and $[AH_2]^+$, ions of 2.5 μg rutin that had been injected into the above described mobile phase that also contained variable concentrations of 0.0 M, 0.001 M, 0.005 M, and 0.010 M NaCl. The Cs^+ primary ion energy was maintained at 35 keV. Three replicate measurements were made for each concentration of NaCl and the average relative ion intensities are reported below in Table 6 as a function of salt concentration.

The data shows that sodium adducts are formed even without the addition of sodium. This leads us to the conclusion that sodium was present in samples or mobile phase. This is a common occurrence which can not be remedied without sample clean-up and extreme precautions. The data also illustrates that the presence of Na^+ at this level is not detrimental, but provides additional confirmation of the molecular ion, $[M+H]^+$, by providing a known ion peak 22 mass units higher corresponding to $[M+Na]^+$. The presence of NaCl at higher concentrations, however, does show an adverse affect on all relative ion peak intensities. The results show a consistent decrease in both molecular ion and aglycone ion peak intensities as the salt concentration increases. At salt concentrations of 0.010 M and above, the molecular ion of rutin was no longer observable. Similar results were obtained for esculin.

TABLE 6

EFFECT OF NaCl ON POSITIVE ION INTENSITIES OF RUTIN

Compound	Conc. of NaCl	$[AH_2]^+$ Rel. Intensity	$[M+H]^+$ Rel. Intensity	$[M+Na]^+$ Rel. Intensity
2.5 μg Rutin	0.0 M NaCl	100	14	5
2.5 μg Rutin	0.001 M NaCl	100	6	16
2.5 μg Rutin	0.005 M NaCl	62	5	24
2.5 μg Rutin	0.010 M NaCl	32	---	6

III.4.2 CF-LSIMS Instrumental Optimization

During the previous experiments it was observed that variations in several instrumental parameters had significant effects on secondary ion yields. Because of these variations, it was decided that an in depth study of these parameters was necessary to determine optimum conditions for the CF-LSIMS analysis of flavonoid conjugates. No such optimization has been reported for CF-LSIMS performed on a VG ZAB2-SE for any chemical compound. Instrumental optimizations were performed using the model flavonoid conjugate, rutin. A mobile phase consisting of 49% CH_3OH, 49% H_2O, 2.0 % glycerol, and 0.1 % trifluoroacetic acid (TFA) was used at a flow rate of 5.0 μL/min and a source temperature of 38°C. The results were obtained by varying instrumental parameters and recording their effects on secondary ion production. Optimization results were quantified by calculating minimum detectable quantities (MDQs). The MDQs were determined as previously described. All CF-LSIMS optimization experiments were performed in the flow-injection mode. A summary of the instrumental optimization results is provided in Table 7.

Our optimization experiments began with a direct comparison of positive and negative secondary ion CF-LSIMS using rutin. These experiments were carried out at secondary ion acceleration voltages of +8 kV and -8 kV respectively. A four fold decrease in the MDQ was found in the negative ion mode over the positive ion mode and a MDQ of 0.05 μg determined. Although, it should be noted that the absolute ion intensities were greater in the positive-ion mode. This is consistent with the report by Beechi and co-workers [109] who found negative ion, direct probe FAB provided

lower detection limits. As a result of this observation, further optimizations were performed in the negative ion mode.

TABLE 7

INSTRUMENTAL OPTIMIZATION RESULTS

Accel. Voltage	Cs^+ Energy	% Glycerol	% Thiogly.	% TFA	MDQ for Rutin
+8 kV	33 keV	2.0%	0.0%	0.10%	0.20 µg
-8 kV	35 keV	2.0%	0.0%	0.10%	0.05 µg
-8 kV	35 keV	2.0%	2.0%	0.10%	0.10 µg
-6 kV	33 keV	2.0%	0.0%	0.10%	0.05 µg
-6 kV	30 keV	2.0%	0.0%	0.10%	5.0 n
-6 kV	30 keV	2.0%	0.0%	0.00%	1.0 n

Our initial direct probe LSIMS studies of different matrices confirmed reported observations [109] that an acidic thioglycerol matrix provided the best ionization efficiency in the positive ion mode for flavonoid glycosides. Therefore, thioglycerol was investigated as a possible matrix for CF-LSIMS experiments. It was found that using thioglycerol significantly decreased source stability. Therefore a mixture of glycerol and thioglycerol was investigated and a MDQ of 0.10 μg determined for rutin in the negative ion, CF-LSIMS mode. The data showed a decrease in the MDQ compared to 2.0% glycerol which was attributed to the continued instability of source conditions due to the presence of thioglycerol. Further investigation of thioglycerol as a matrix was discontinued from our CF-LSIMS study due to its absorbance in the UV region (λ_{max} = 237) which overlaps the UV absorption of our model compounds. The strong absorbance of thioglycerol would impair UV detection since the matrix was added directly to the mobile phases.

CF-LSIMS with a mobile phase flow rate of 5 μL/min resulted in a source pressure of 2.5 x 10^{-4} mbar, which is higher than normally encountered during EI or static LSIMS operation. Due to the increased pressure, the CF-LSIMS ionization source had a tendency to arc when the instrument was operated at acceleration voltages of +/- 8 kV or higher. It was determined that the instrument could be operated at an acceleration voltage of -6 kV with greater stability and no significant decrease in the MDQ as reflected in the equal values of the MDQs of 0.05 μg for rutin.

During instrument tuning, it was further observed that variations in the Cs^+

primary ion energy produced changes in negative secondary ion yield of both the glycerol matrix and the sample analyte. In addition, a broad primary ion beam produced more stable source conditions than a finely focused primary ion beam. It was also observed that increases in the absolute glycerol ion yield were directly correlated to increases in absolute secondary ion yield of the analyte. Therefore, an experiment was performed to determine the effect of Cs+ ion energy on the secondary ion yield. The Cs^+ primary ion energy was varied from 15 keV to 40 keV while measuring the absolute ion peak intensities of m/z = 91 and 367 which correspond to the glycerol ions $[Gly-H]^-$ and $[4Gly-H]^-$, respectively. These absolute ion intensities were obtained by measurement of the peak intensity directly from the oscilloscope of the VG ZAB2-SE and then multiplication by the appropriate amplification setting. Plots of the glycerol ion peak intensities as a function of primary ion energy are provided in Figure 30. A broad maximum glycerol ion intensity at m/z = 91 was observed in the range of 28 keV to 31 keV while the higher mass glycerol ion (m/z = 367) showed similar results with more variance. An equal and sharp spike in the m/z = 91 peak was also observed at a Cs^+ primary ion energy of 20 keV, but an average Cs^+ primary ion energy of 30 keV was used due to the broader nature of the peak in ion intensities. Under these conditions, a MDQ of 5.0 n was determined for the negative molecular ion of rutin that had been extracted and accelerated to 6 keV. These findings indicate a decrease in the MDQ and support our choice of primary ion energy. These results are consistent with those reported by Aberth and Burlingame [110] for direct probe FAB experiments.

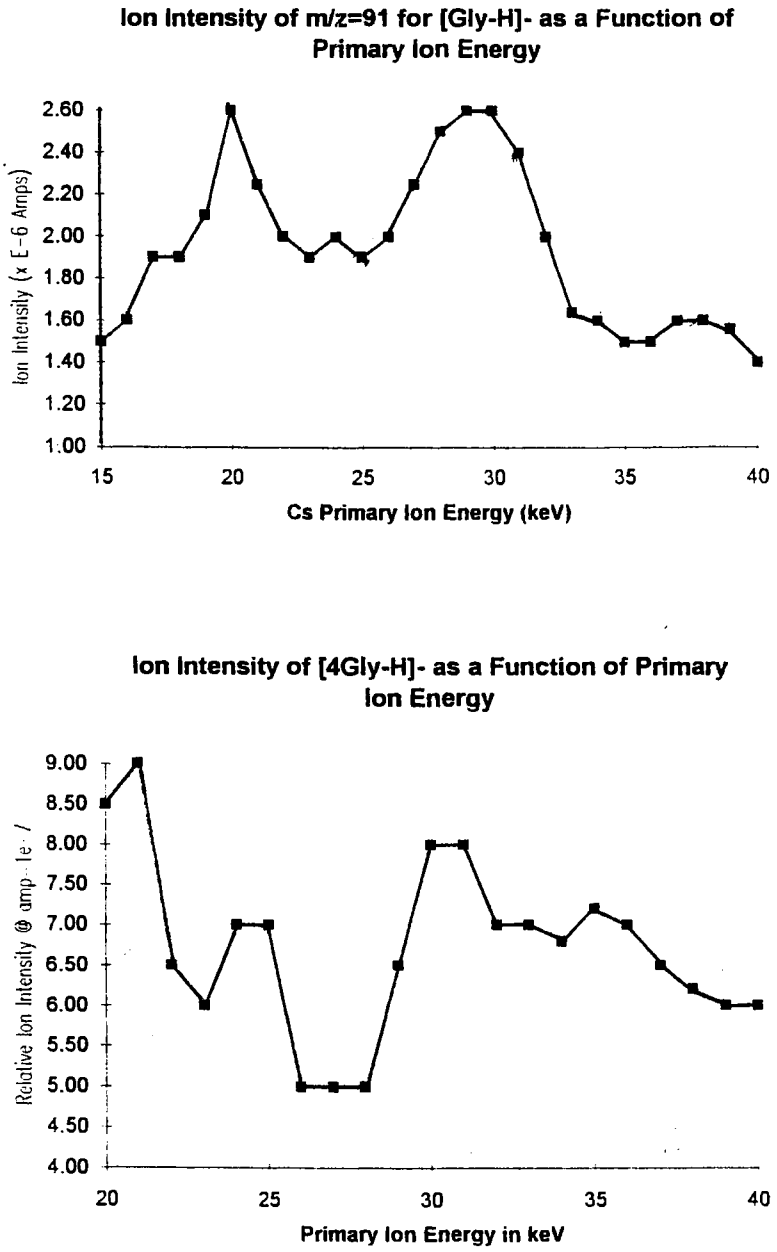

Figure 30- Plots of Glycerol Ion Intensities as a Function of Primary Ion Energy

As stated before, an acid modifier consisting of 0.1% TFA was added to the mobile phase to improve HPLC chromatographic resolution. The acid provides a source of excess protons and therefore, theoretically hinders the formation of negative ions by proton abstraction. Thus, it was postulated that a mobile phase without TFA would result in a lower MDQ for rutin in the negative-ion mode. Mass spectra were acquired of rutin without TFA in the mobile phase and a MDQ of 1.0 n determined for rutin. This indicates that if chromatographic separation was not necessary, ultimate detection limits may be obtained by omitting the acid modifier from the mobile phase.

Final instrumentation optimization yielded a MDQ of 1.0 n or 1.6 pmol for rutin by flow injection CF-LSIMS. This provides evidence that CF-LSIMS is truly a sensitive technique for the determination of isoflavonoid conjugates found in the biological systems. It further illustrates the increased sensitivity of the CF-LSIMS technique over DP-LSIMS. A mass spectrum acquired in the flow-injection (-) CF-LSIMS for 0.005 μg rutin is provided in Figures 31. The spectrum was acquired with a mobile phase consisting of 49% CH_3OH, 49% H_2O, 2.0 % glycerol, and 0.1 % trifluoroacetic acid (TFA). The flow rate was 5.0 μL/min with a source temperature of 38°C. An acceleration voltage of -6 kV was used with a primary-ion energy of 30 keV.

III.4.3 Negative-ion CF-LSIMS Characterization of Model Flavonoid Conjugates

As previously discussed, characteristic ions observed for positive ion CF-LSIMS where the $[M+H]^+$, $[M+Na]^+$, $[M+H-16]^+$, $[M+H-18]^+$, $[F_1H_2]^+$, $[F_2H_2]^+$, $[AH_2]^+$,

and $[A+H-16]^+$ ions. A similar series of characteristic negative ions were observed, consisting of $[M-H]^-$, $[M-H-16]^-$, $[F_1-H]^-$, $[A-H]^-$, and $[A-H-16]^-$. Negative-ion, CF-LSIMS mass spectra for 2.0 μg rutin, 5.0 μg naringin, and 5.0 μg esculin are presented in Figures 32 through 34. These mass spectra were acquired using a mobile phase of 49% CH_3OH, 49% H_2O, 2.0 % glycerol, and 0.1 % trifluoroacetic acid (TFA). The flow rate was 5.0 μL/min with a source temperature of 38°C. An acceleration voltage of -6 kV was used with a primary-ion energy of 30 keV. The concentrations of model compounds used for the (-) CF-LSIMS characterization were approximately ten times less concentrated than those used for (+) DP-LSIMS experiments, but provided similar quality data. A very significant difference in the molecular ion intensity was observed between positive and negative-ion CF-LSIMS. At the concentrations listed above, the (-) CF-LSIMS mass spectra yielded a molecular ion as the base peak. This is compared to a base peak corresponding to the aglycone in (+) CF-LSIMS experiments with the relative molecular ion intensity of approximately 30%.

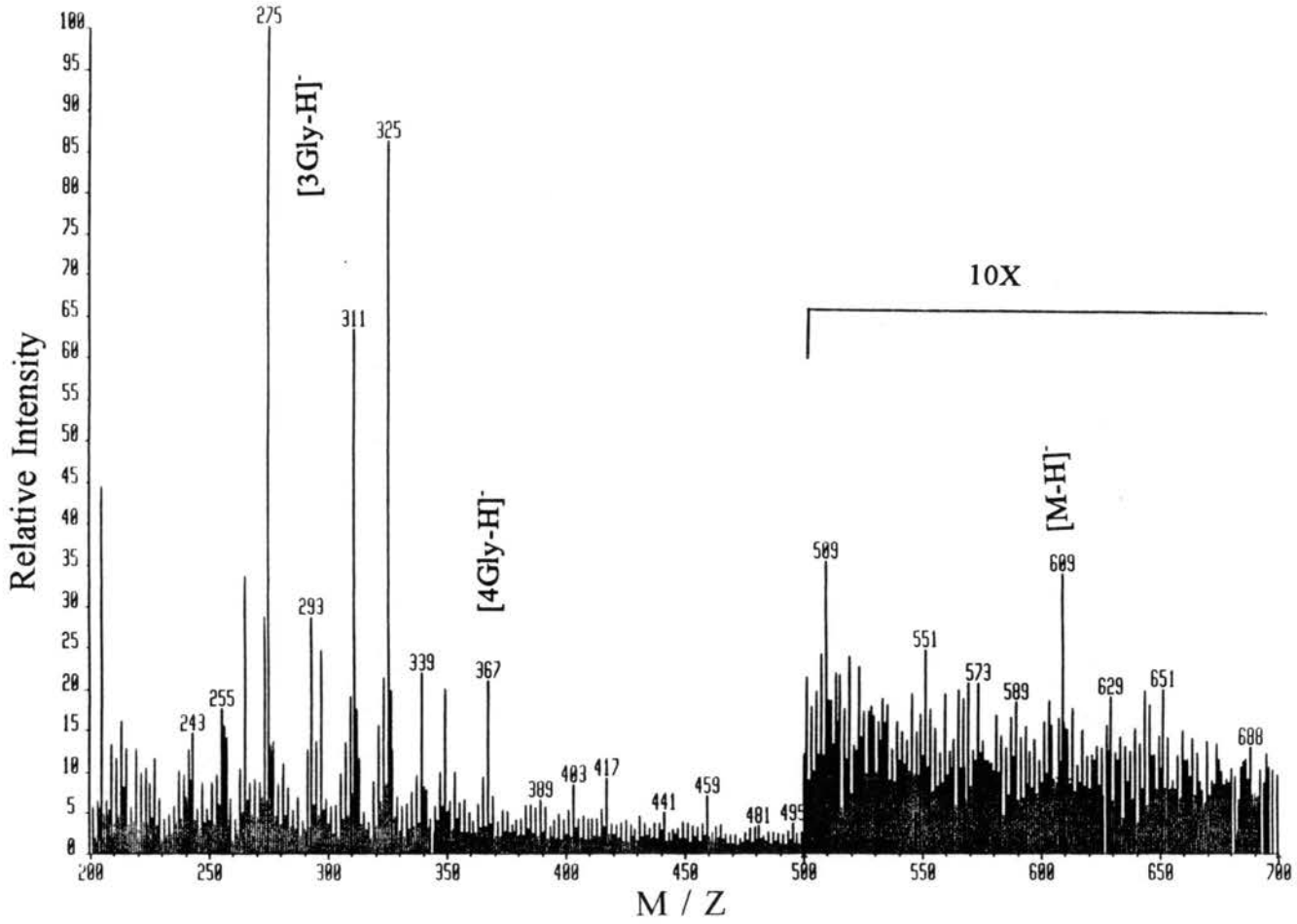

Figure 31- (-) CF-LSIMS Mass Spectrum of 0.005 µg Rutin

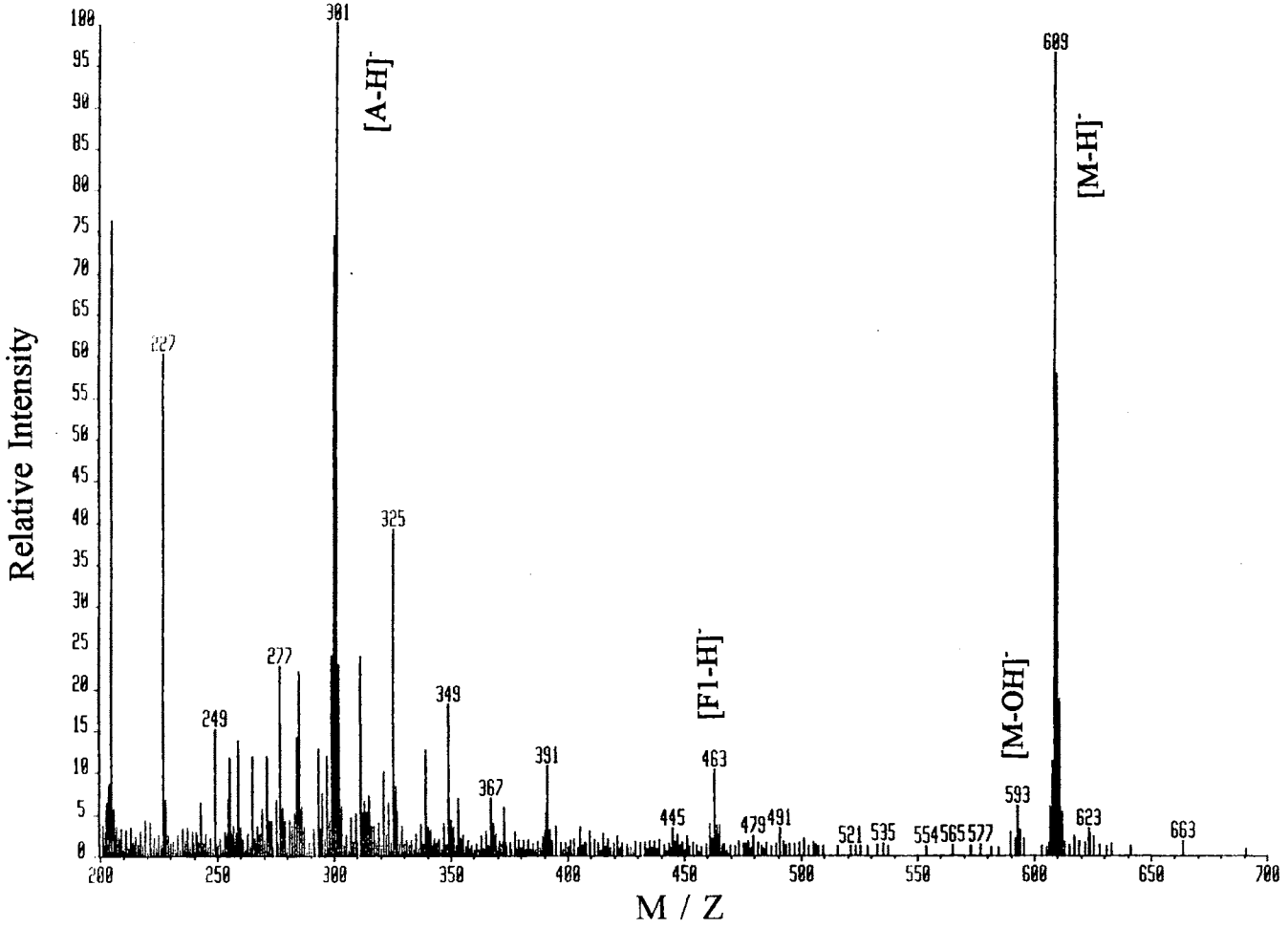

Figure 32- (-) CF-LSIMS Mass Spectrum of 2.0 µg Rutin

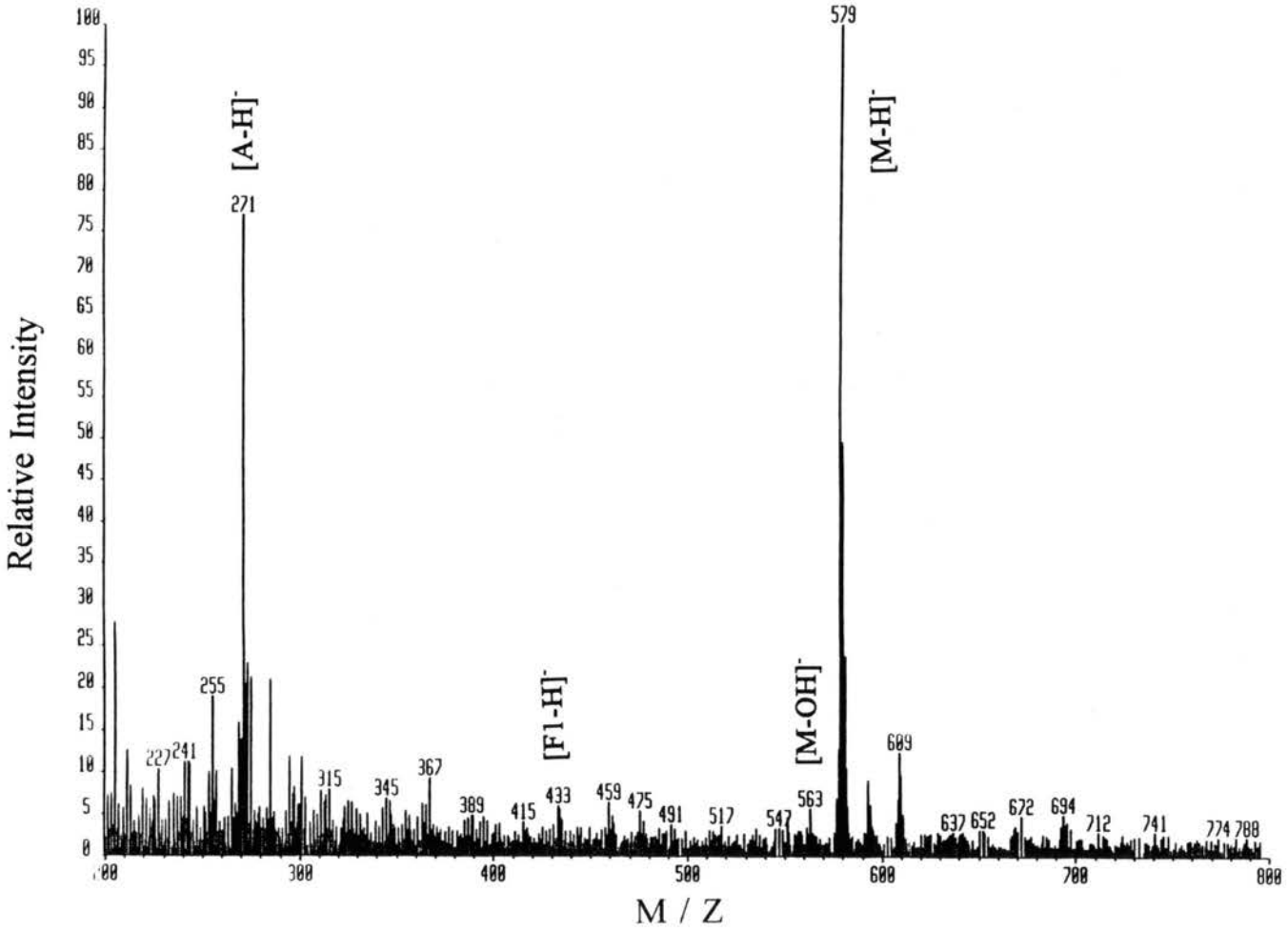

Figure 33- (-) CF-LSIMS Mass Spectrum of 5 µg Naringin

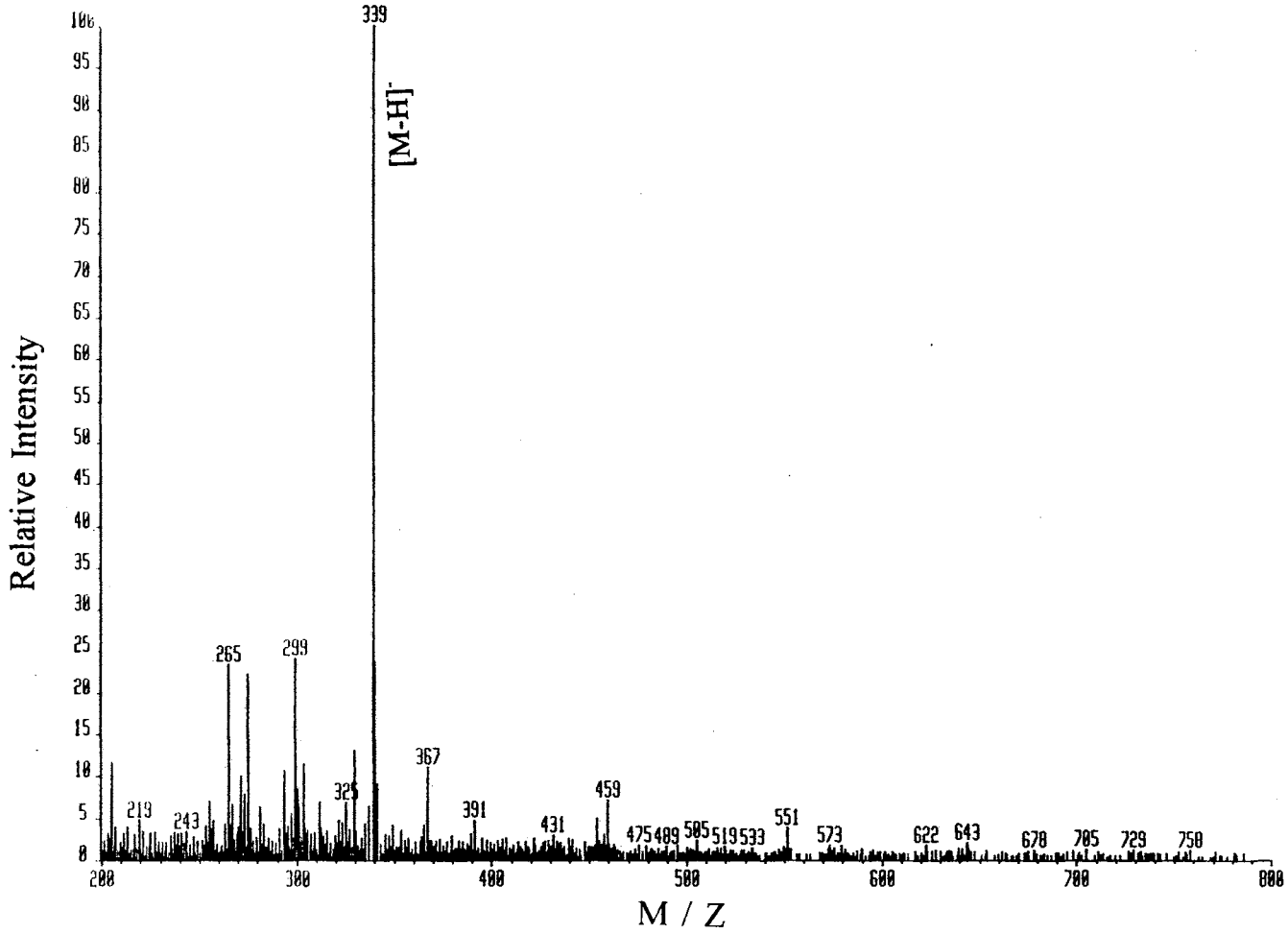

Figure 34- (-) CF-LSIMS Mass Spectrum of 5 µg Esculin

III.5 ANALYTICAL HPLC CF-LSIMS OF PLANT EXTRACTS

III.5.1 Chromatography

The literature reports several HPLC methods for the analysis of flavonoids found in plant extracts [86,111,112] . The method used in the following studies is based on a modification of that reported by Edwards and Kessmann [86]. This modification replaced the 3.0% phosphoric acid modifier with lower concentrations (0.1 to 1.0%) of more volatile TFA or acetic acid modifiers. This was found necessary to avoid the build up of inorganic salts at the probe tip which could clog the transfer fused silica capillary.

Initial attempts to separate a basic alfalfa extract were performed using a 250 mm x 4.6 mm *i.d.*, 5 μm, 300 Å pore size, octadecylsilica (ODS) HPLC column (Alltech part #71072). Gradient elution HPLC was performed using the gradient described in section II.4 with a 0.1% TFA acid modifier. It was observed that this column was unable to adequately separate the basic alfalfa extract. Gradient elution HPLC was then performed using a 4.6 mm x 150 mm Zorbax™, 5 μm, 100 Å pore size ODS column obtained from MAC-MOD Analytical, Inc. (Chadds Ford, PA) on the same basic alfalfa extract as above. The Zorbax column provided a significant increase in chromatographic resolution over the 250 mm x 4.6 mm *i.d.*, 300 Å ODS column. This increase in chromatographic resolution was attributed to the smaller pore size and of the Zorbax ODS particles. The corresponding UV chromatograms for the above comparison are provided in Figure 35. The Zorbax column was later substituted with a 4.6 mm x 250 mm Bakerbond (J.T. Baker, Phillipsburg, NJ) 5 μm,

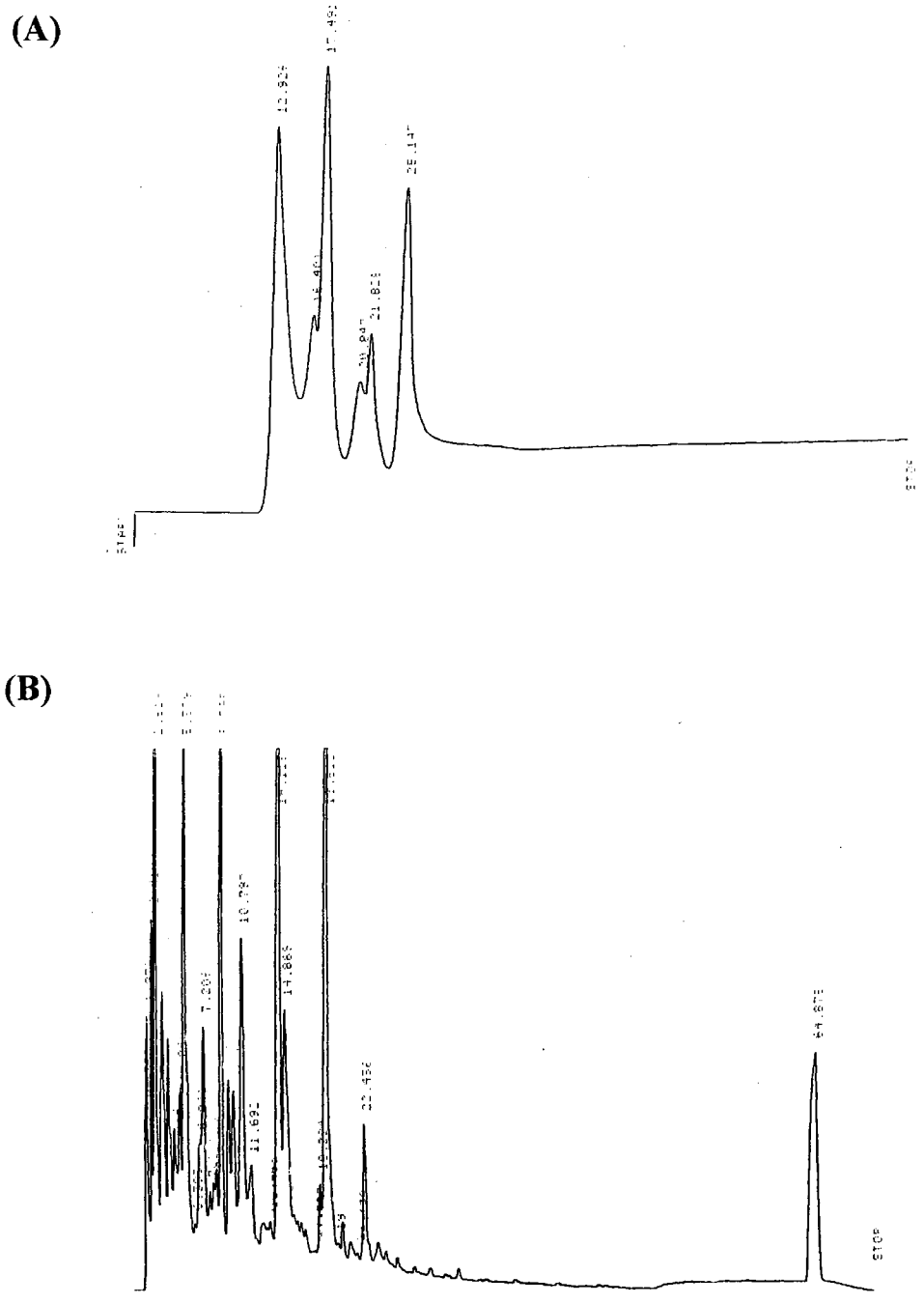

Figure 35- UV Chromatograms of a basic Apollo alfalfa extract obtained with (**A**) an Alltech 250 mm x 4.6 mm *i.d.*, 300 Å, 5 µm, ODS Column (**B**) Zorbax 150 mm x 4.6 mm *i.d.*,100 Å, 5 µm, ODS Column

120Å pore size, ODS column. This column produced similar separation efficiencies to the Zorbax column. The substitution was performed in order to correlate data obtained by LC-CF-LSIMS to that obtained at the Noble Foundation by gradient elution HPLC using a similar 4.6 mm x 250 mm Bakerbond, 5 μm, ODS Column.

III.5.2 (-) Analytical LC-CF-LSIMS of Basic Apollo Alfalfa Cell Suspension Extracts

To begin our investigation into the LC-CF-LSIMS analysis of plant extracts, negative-ion LC-CF-LSIMS was performed on a basic alfalfa (*Medicago sativa L.*, cultivar Apollo) cell suspension extract. Apollo alfalfa cell suspensions were elicited with yeast to increase isoflavonoid concentrations prior to extraction. The Apollo alfalfa was extracted and the basic fraction collected as described previously in the experimental section II.9. HPLC analysis was performed using the gradient described in the experimental section II.4 with a 0.1% TFA modifier and a Zorbax 4.6mm x 150mm ODS column. The eluent from the column was split using a Valco ZDV and differential lengths of fused silica capillaries. The measured flow delivered into the mass spectrometer was 5.2 μL/min. Mass spectral data was acquired for the mass range m/z = 100 to m/z = 700 at a scan rate of 10 seconds/decade and an interscan time of 3 seconds. The acceleration voltage was -6 kV while the primary ion energy was 30 keV. Background subtraction of scan # 5 was performed from all scans over the entire LC-CF-LSIMS acquisition.

HPLC was performed and the UV chromatogram (287nm) is presented in

Figure 36. Our attention was focused on the peaks eluting at approximately 13 to 21 minutes since enzyme hydrolysis experiments indicated that this was the elution region of suspect isoflavonoid conjugates. The UV chromatogram indicates four major peaks in the above time region. Knowing the approximate UV retention times, corresponding mass spectra could be assigned. This was done by studying the mass spectra acquired at similar retention times to those eluting in the UV. When ion peaks were observed that were not background a reconstructed ion chromatogram (RIC) could be generated of these m/z values. It was observed that intense ion peaks at m/z = 267, 269, 517, 545, and 631 were present in the mass spectra corresponding to the UV peaks. A RIC of the ions at m/z=267+269+517+545+631 was generated and is provided in Figure 37. Three major peaks were observed in the RIC at scan numbers 107, 110, and 129. The direct relationship between scan number and retention time can also be observed in Figure 37. The RIC peaks correspond to the UV peaks at 17.228, 17.221, and 20.955 minutes, respectively. A note should be made that the RIC peaks were slightly shifted to a longer retention time than the UV peaks. Since on-line UV detection had not been established yet these shifts can be attributed to slight shifts in HPLC elution times. The ions observed in the mass spectra are discussed below and summarized in Table 8. Proposed structures for the compounds to be discussed are provided in Figure 38.

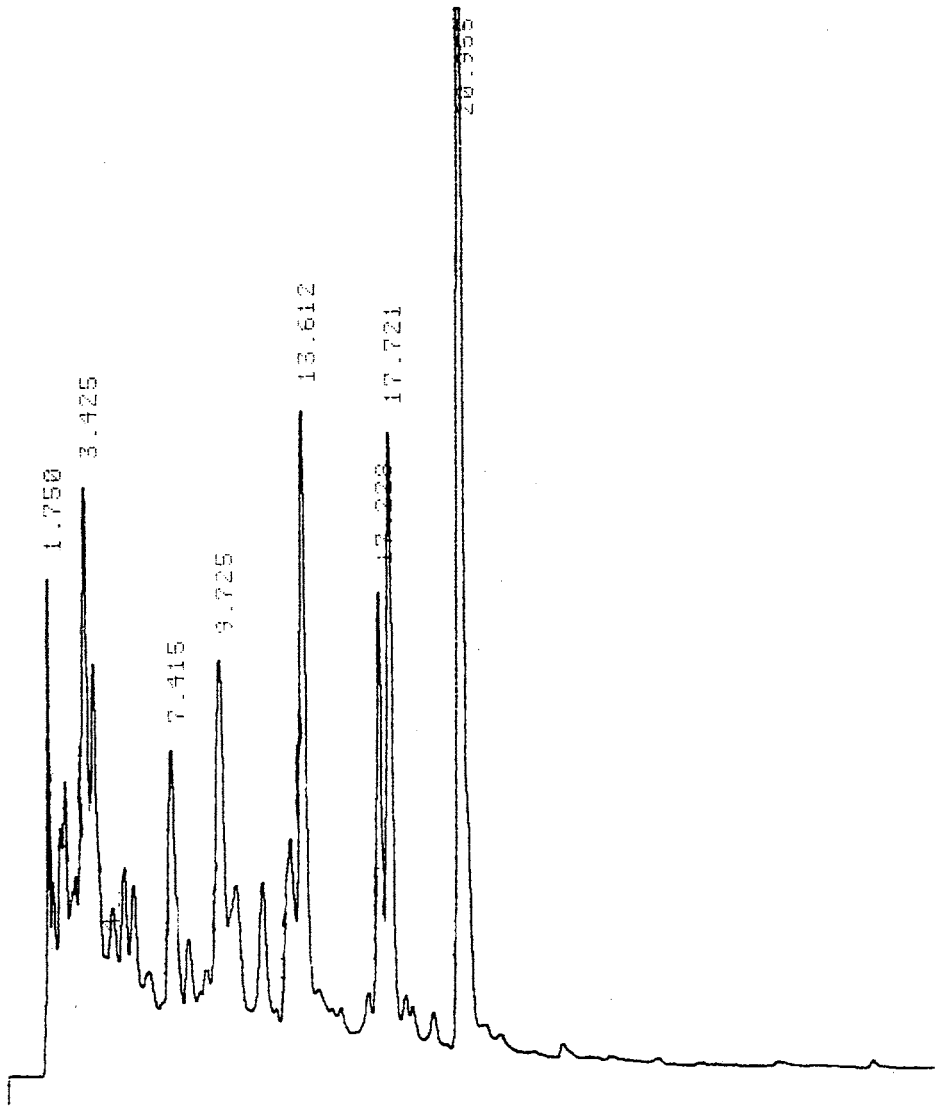

TIME (minutes)

Figure 36- UV Chromatogram of Basic Apollo Alfalfa Cell Suspension Extract

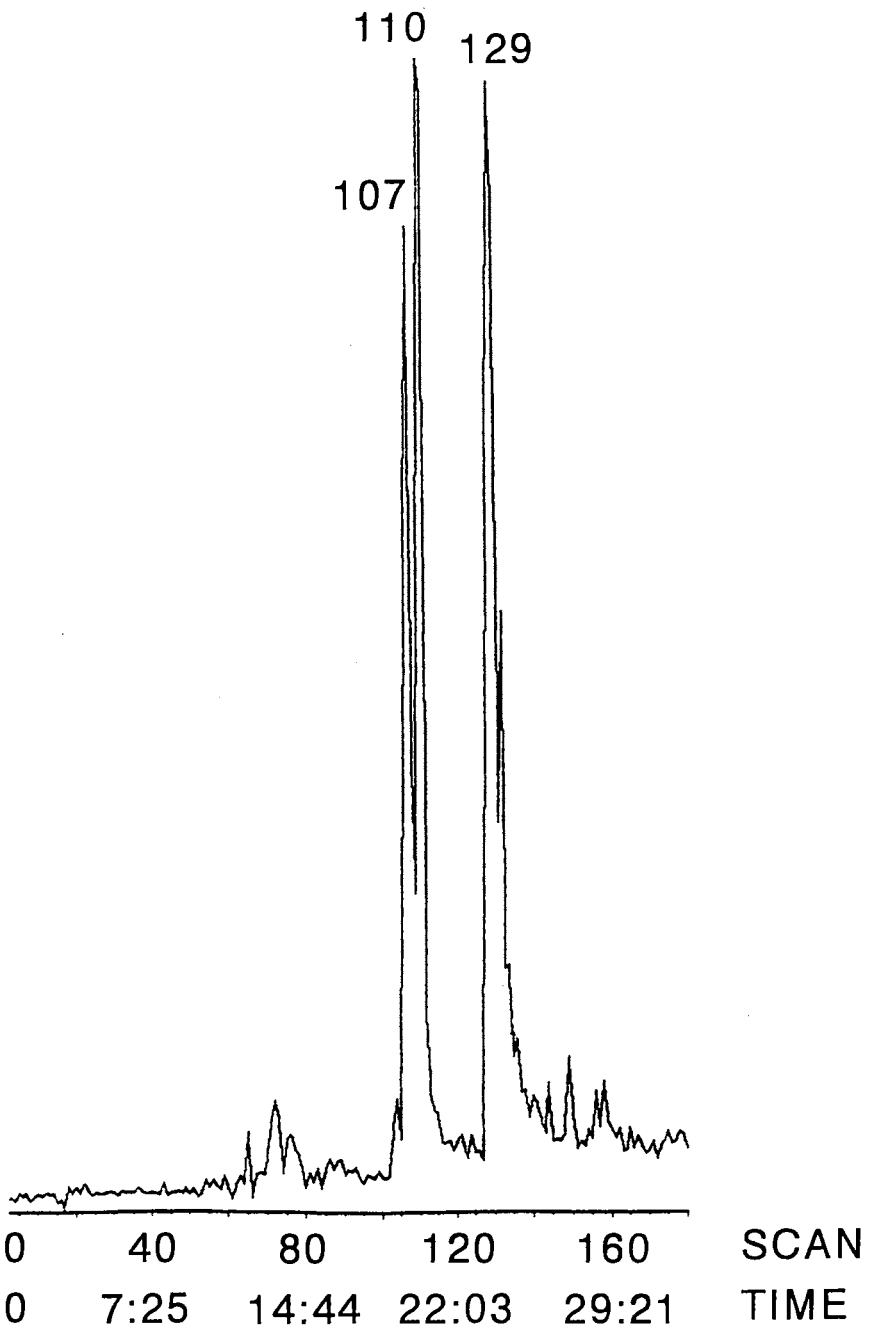

Figure 37- RIC of m/z=267+269+517+545+631 of a Basic Apollo Alfalfa Cell Suspension Extract

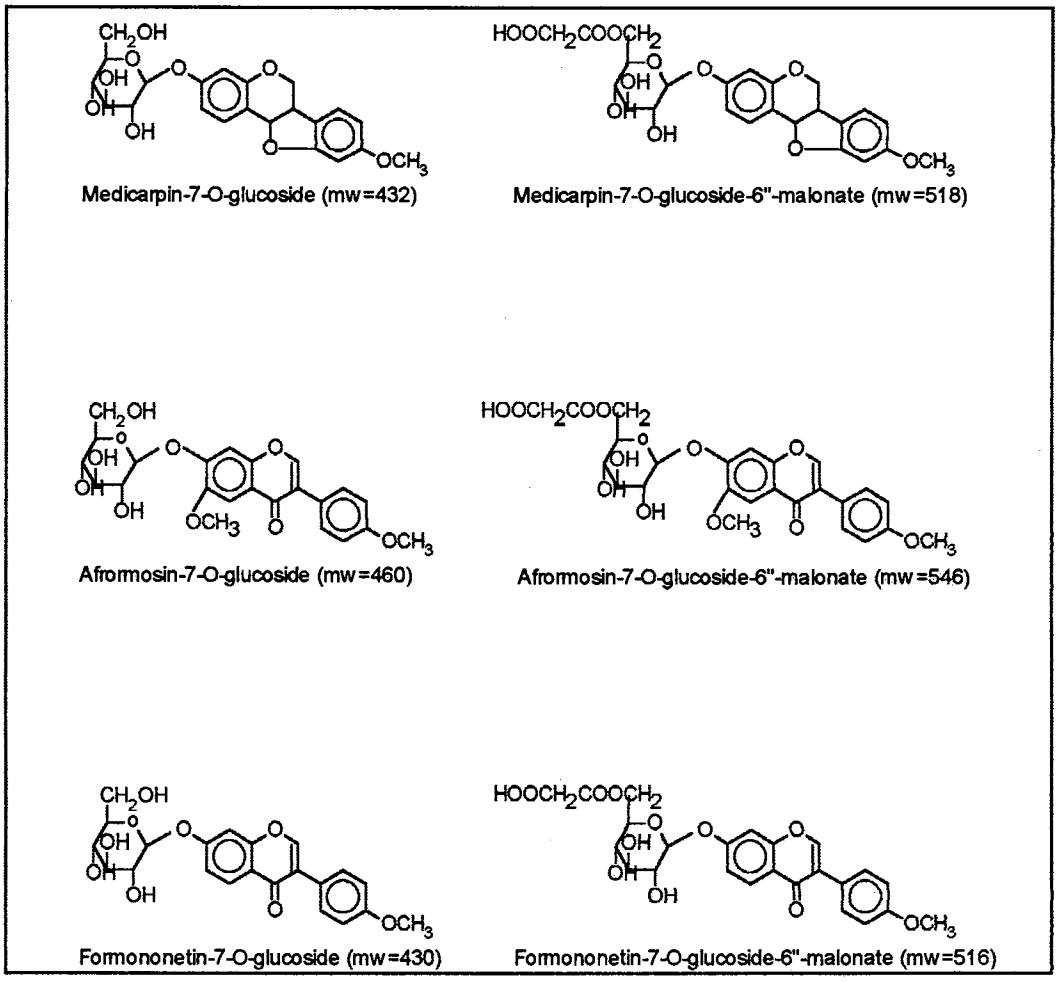

Figure 38- Proposed Molecular Structures of Isoflavonoid Conjugates in Basic Apollo Alfalfa Cell Suspension Extracts

TABLE 8

NEGATIVE-ION ANALYTICAL LC-CF-LSIMS MASS SPECTRA OF BASIC APOLLO ALFALFA EXTRACTS

Identity	FGM	MG	MGM
UV Rt	17.228	17.721	20.955
Scan #	107	110	129
[M+TFA-H]-	629 (40)	545 (17)	631 (13)
[M+GLY-H]-	607 (10)	523 (3)	609 (4)
[M-H]-	515 (21)	433 (11), [M•-] = 432 (12)	517 (15)
[M-CO_2H]-	471 (24)	---	473 (43)
[A-H]-	267 (100)	269 (100)	269 (98), [A•-] = 270 (100)
Others	309 (18), 252 (18)	254 (44), 239 (49)	254 (79), 239 (12)

The mass spectrum of the first observed peak (scan #107) is given in Figure 39. This spectrum has been tentatively identified as formononetin-7-O-glucoside-6"-O-malonate (FGM). Typical of isoflavonoid conjugates, the $[A-H]^-$ is observed as the base peak at m/z = 267. Also observed are $[M-H]^-$ at m/z = 515, $[M-CO_2H]^-$ at m/z = 471, $[M+GLY-H]^-$at m/z = 607, and an $[M+TFA-H]^-$ adduct ion peak at m/z = 629. The ion peaks corresponding to the negative ions formed by adducts of the molecular ion species with glycerol, $[M+GLY-H]^-$, and TFA, $[M+TFA-H]^-$, provide additional confirmation of the molecular weight as 516. The above ion peaks provide confirmation of the suspect compound as FGM.

The mass spectrum of scan #110 is given in Figure 40. This spectrum has been tentatively identified as medicarpin-3-O-glucoside (MG). A significant radical molecular anion, $[M]^{\bullet-}$, peak is observed at m/z = 432 with a slightly greater intensity than the $[M-H]^-$ ion peak. The formation of radical ions from flavonoid glycosides in FAB mass spectra has been discussed by Crow and co-workers [98] and is a common occurrence. From our studies, these radical ions were most commonly observed for simple glycosides of isoflavonoids. Radical ions were also observed for the aglycone and molecular species of the malonated glycosides of isoflavonoids, but were less common. An $[M-H]^-$ ion peak was observed at m/z = 431 followed by cleavage of the glucose which produced a base peak corresponding to $[A-H]^-$ at m/z = 269. Peaks corresponding to some characteristic fragments of medicarpin were also observed. These peaks were attributed to successive loses of CH_3 and OCH_3 at m/z = 254 and 239, respectively. Again, an adduct ion peak was observed for the [M+TFA-H]- and

[M+GLY-H]-. confirming the molecular weight as 432. The identification of the MG compound and the presence of the intense ion peak at m/z =545 has significant importance and will be discussed in more detail in section III.5.5.

The third RIC peak (scan #129) has been identified as medicarpin-3-O-glucoside-6"-O-malonate. The mass spectrum of scan #129 is provided in Figure 41. Ions observed include: $[M+TFA-H]^-$, $[M+GLY-H]^-$, $[M-H]^-$, $[M-COOH]^-$, $[M-CCOCH_2COOH]^-$, $[A-H]^-$, $[A-16]^-$, and $[A-OCH_3]^-$. These ion peaks show the aglycone to have a molecular weight of 270 and the malonated glycoside to have a molecular weight of 518

The mass spectra of the isoflavonoid conjugates identified in the above extract differ from those of the model flavonoid conjugates obtained by (-) CF-LSIMS. The model compounds yielded the molecular ion peak as the base peak at higher sample concentrations (c.a. 10μg). At lower concentrations (c.a. 0.10μg), the molecular ion peak intensity was similar in intensity to the aglycone ion peak. However, the isoflavonoid conjugates encountered in the basic apollo alfalfa extracts have much lower molecular ion peak intensities than the aglycone ion peak. This suggests that the malonated isoflavonoid glucosides and the isoflavonoid glucosides are somewhat less stable under particle bombardment and fragment to a greater extent than the model flavonoid conjugates. These labile nature of these malonated glycosides could possibly account for the decomposition of these conjugates previously encounter in the initial DP-LSIMS and GC/MS investigations.

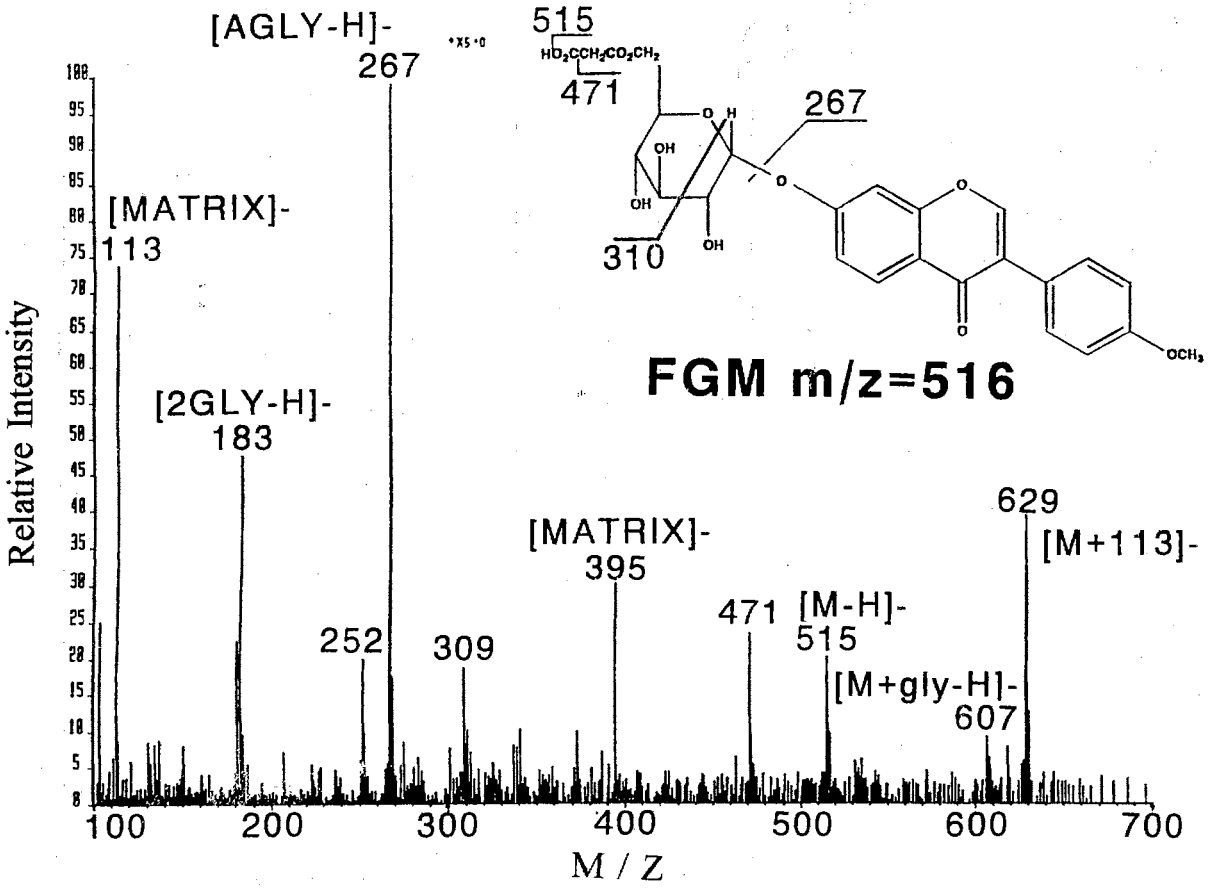

Figure 39- (-) LC-CF-LSIMS Mass Spectrum of Basic Apollo Cell Suspension Extract Scan #107 Identified as FGM.

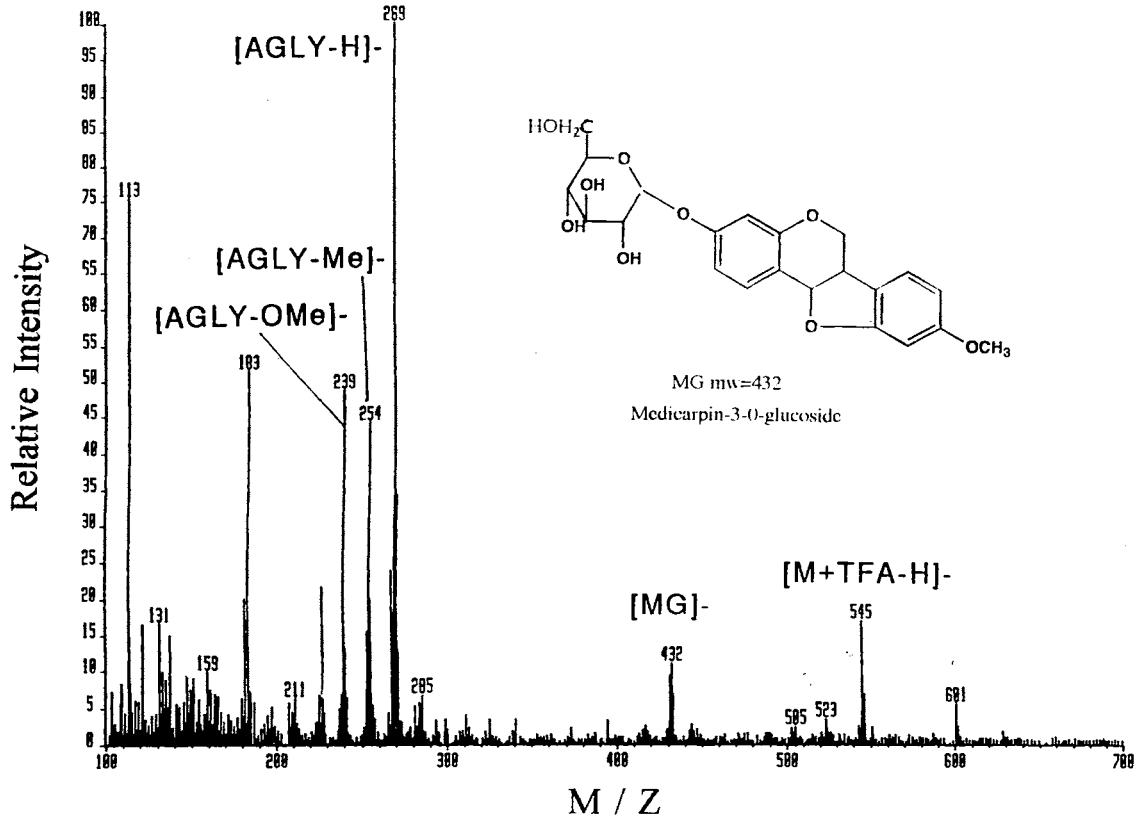

Figure 40- (-) LC-CF-LSIMS Mass Spectrum of Basic Apollo Alfalfa Cell Suspension Extract Scan #110 Identitified as MG

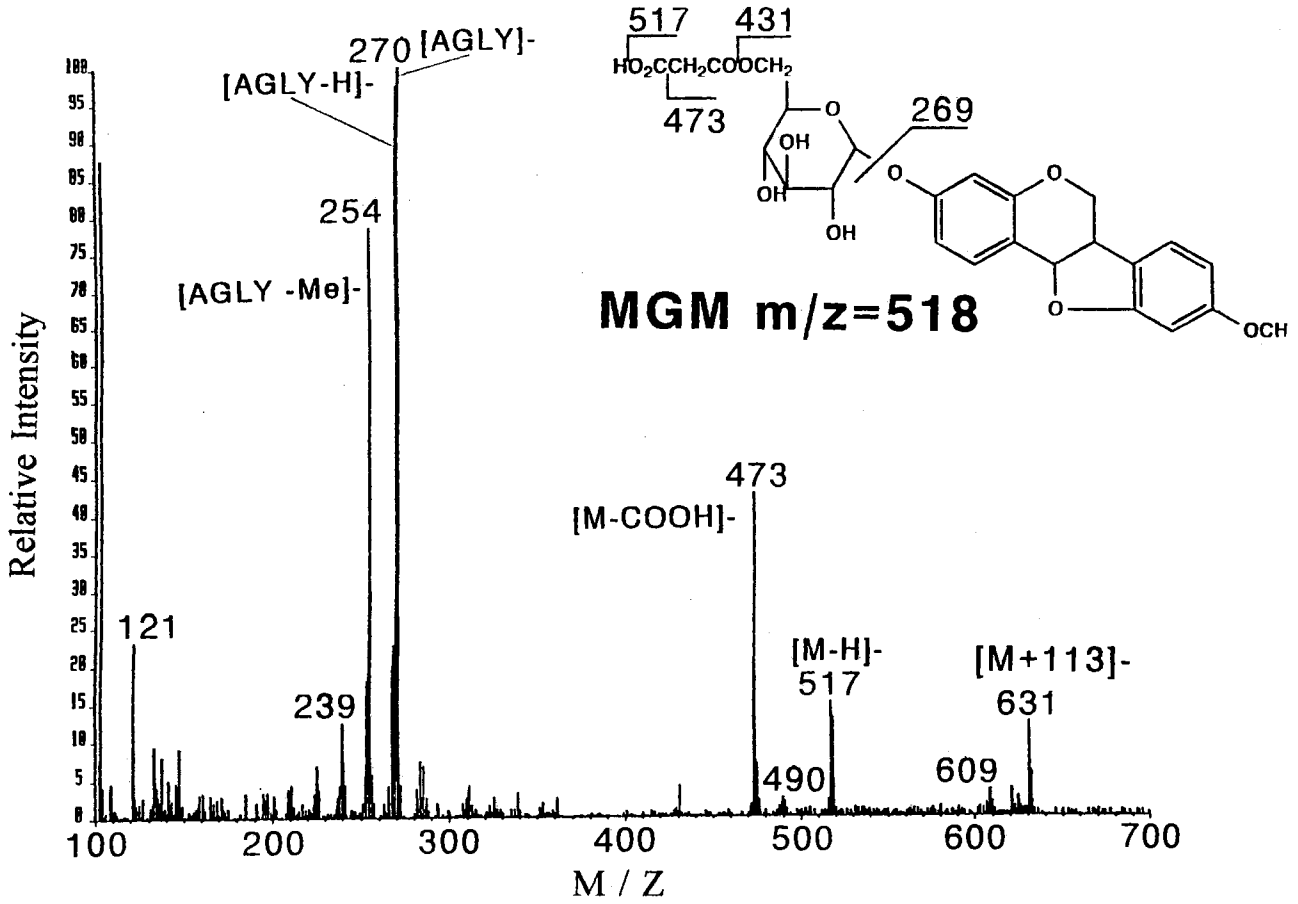

Figure 41- (-) LC-CF-LSIMS Mass Spectrum of Basic Apollo Cell Suspension Extract Scan #129 Identified as MGM.

III.5.3. (-) Tandem LC-CF-LSIMS of Basic Apollo Alfalfa Extracts

Tandem LC-CF-LSIMS analysis of the basic Apollo alfalfa extract was performed to confirm our identification of the TFA adducts with MG and MGM at m/z = 545 and 631, respectively. This was done by metastable MS/MS. Tandem LC-CF-LSIMS experiments were performed by link scanning at a constant ratio of B/E. These experiments used identical HPLC and instrumental parameters described in section *III*.5.2. Full scanning mode LC-CF-LSIMS was first performed by gradient elution of the basic apollo alfalfa extracts. From the full-scanning data, MS retention times and observed m/z values (to the hundredths decimal place) for MG and MGM were obtained. This information was then entered into the data system for acquisition of tandem LC-CF-LSIMS data. The observed m/z values (to the hundredths decimal place) of the precursor ion peak were used to accurately determined the ratio of B/E. A tandem MS acquisition time window was set for approximately 0.5 minutes prior and past the observed MS retention times. Metastable MS/MS was performed in the multichannel analysis mode (MCA) which sums all acquired mass spectra together to increase the S/B ratio. The tandem LC-CF-LSIMS experiment was then performed and a tandem spectrum of $[MGM+TFA-H]^-$ at m/z = 631 was obtained. This tandem LC-CF-LSIMS mass spectrum is presented in Figure 41. The LC-CF-LSIMS/MS spectrum produced a product ion peak at m/z = 517 corresponding to $[MGM-H]^-$ generated by the fragmentation of the TFA adduct with MGM. Other product ion peaks that were observed included: [MGM+TFA-OH]- at m/z = 614, and $[MGM+TFA-CO_2]$- at m/z = 587, $[MGM-CO_2]^-$ at m/z = 474. Further unidentified

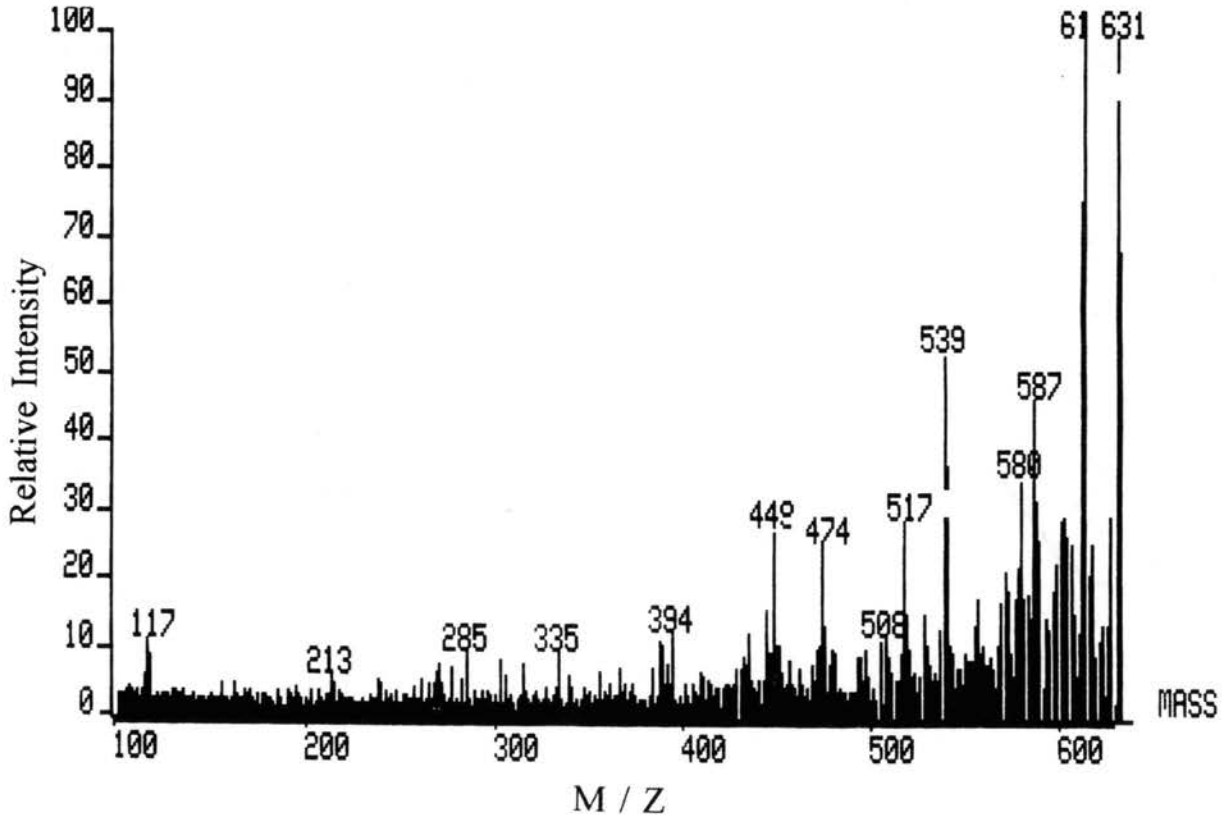

Figure 42- (-) LC-CF-LSIMS Metastable Tandem Mass Spectrum of m/z=631

ions were observed for $[MGM+TFA-92]^-$ at m/z = 539 and $[MGM+TFA-182]^-$ at m/z=449. The presence of the ion peak at m/z = 517 and other rationalized ion peaks support our identification of the ion peak at m/z = 631 as the adduct ion $[MGM+TFA-H]^-$.

The LC-CF-LSIMS experiment was then repeated and a tandem MS/MS spectrum of $[MG+TFA-H]^-$ at m/z = 545 was obtained. This spectrum is presented in Figure 43. A product ion corresponding to $[MG+TFA-H_20]^-$ was observed at m/z = 527. Additional product ions included: [MG-H]- at m/z = 517, $[MG+TFA-CO_2]^-$ at m/z = 501, and $[MG+TFA-92]^-$ at m/z =453. A product ion was also observed at m/z =515 which is believed to correspond to a dehydration of MG or $[MG-2H-H]^-$.

It was interesting that aglycone, $[A-H]^-$, product ion peaks were not observed in either of the MS/MS experiments similar to those observed in full-scanning mode LC-CF-LSIMS mode. This suggests that fragmentation of the conjugates to yield the $[A-H]^-$ ion peak must occur in the source region prior to mass analysis and little fragmentation of the conjugate occurs along the flight path of the ion. Therefore, an experiment was performed in an attempt to produce an observable product ion peak corresponding to the aglycone. This was accomplished by CAD tandem LC-CF-LSIMS of the [MGM-H]- ion at m/z=517 while link scanning at a constant ratio of B/E. A LC-CF-LSIMS experiment was first performed to establish the MS retention time and the two decimal value of MGM as described above. These values were then used to set the MS/MS acquisition window and B/E value. A collision gas consisting of helium was added to the first field-free region gas cell in an amount sufficient to

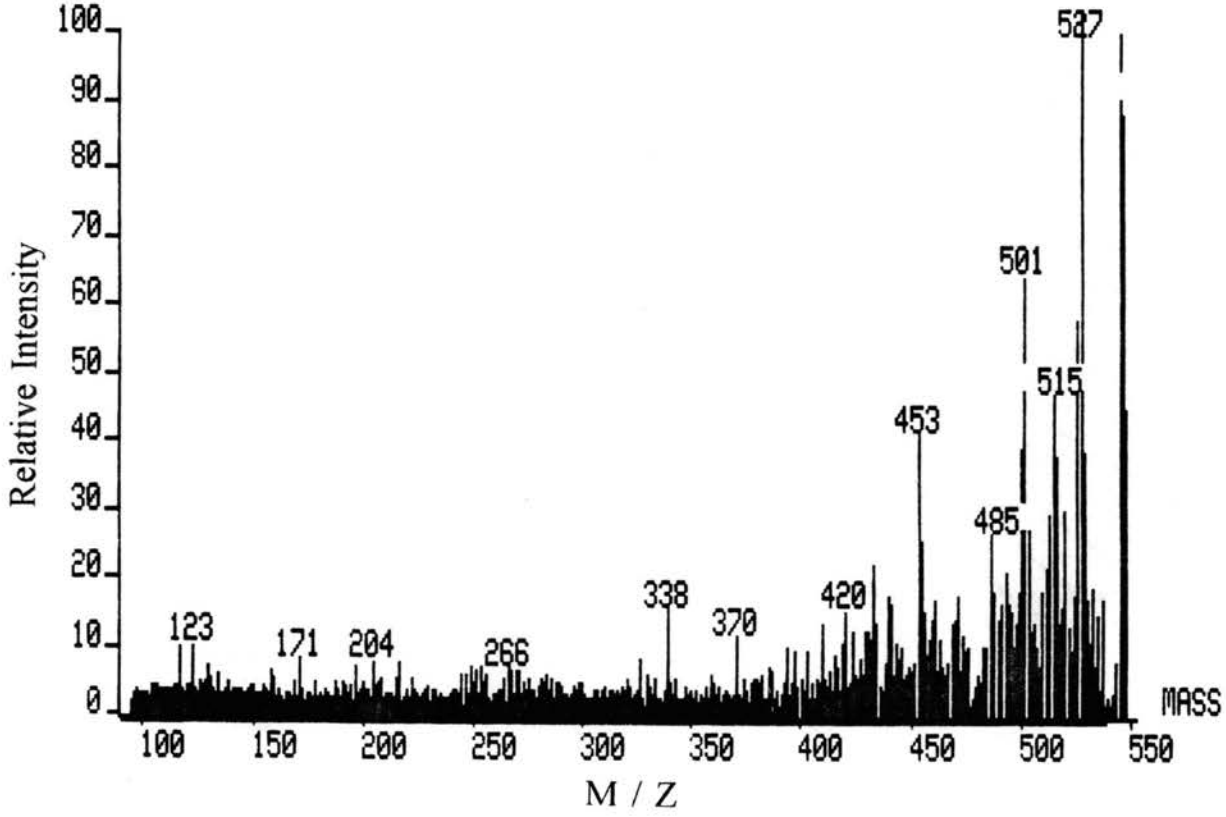

Figure 43- (-) LC-CF-LSIMS Metastable Tandem Mass Spectrum of m/z=545

reduce the glycerol ion, $[GLY-H]^-$, peak at m/z = 91 by half. The LC-CF-LSIMS experiment was repeated and a CAD LC-CF-LSIMS mass spectrum acquired in the MCA mode of MGM obtained. This spectrum is presented in Figure 44. Our experiment was successful since a product ion peak of the aglycone, [A-H]-, was observed at m/z = 269. Additional product ion peaks were observed that corresponded to $[M-CO_2H]^-$ at m/z = 473 and $[M-CO_2CH_2CO_2H]^-$ at m/z = 425. These product ions resulted from the cleavage of the malonate substituent on the glucose. The observance of these product ion peaks also confirms those identified in full-scanning LC-CF-LSIMS.

III.5.4 (+) Analytical LC-CF-LSIMS OF Basic Apollo Alfalfa Extracts

To compliment the (-) LC-CF-LSIMS analysis of the basic apollo alfalfa extract presented above, positive-ion LC-CF-LSIMS was performed on the same basic alfalfa (*Medicago sativa L.*, cultivar Apollo) cell suspension extract. A UV chromatogram at 287nm was acquired and was presented in Figure 36. HPLC analysis was performed using the gradient described in the experimental section with a 0.1% TFA modifier and a Zorbax 4.m x 150mm ODS column. Mass spectral data was acquired for the mass range m/z = 100 to m/z = 800 at a scan rate of 15 seconds/decade and an interscan time of 3 seconds. The acceleration voltage was +6 kV while the primary ion energy was 30 keV. Background subtraction of scan # 5 from all scans over the entire LC-CF-LSIMS acquisition time was performed.

Our attention was focused on the same chromatographic peaks eluting at

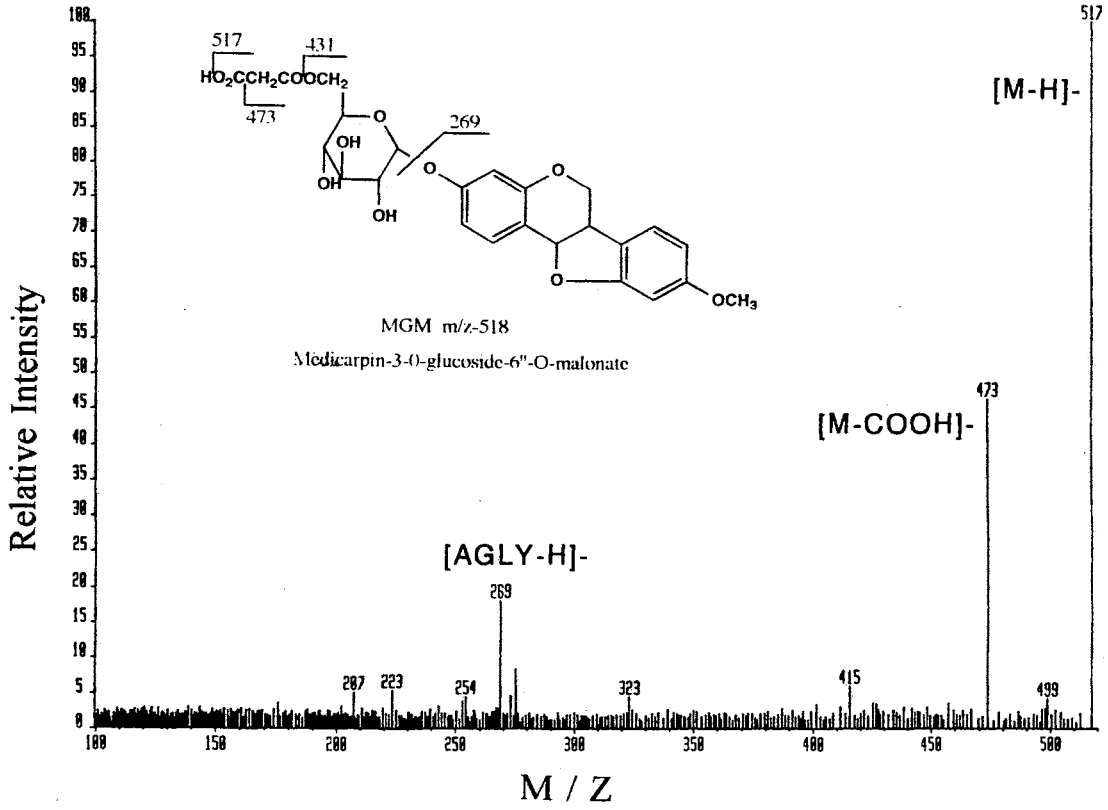

Figure 44- (-) LC-CF-LSIMS CAD Tandem Mass Spectrum of m/z=517

approximately 13 to 21 minutes that were studied previously by (-) LC-CF-LSIMS. The UV chromatogram displays four major peaks in the above time window. It was observed that intense ion peaks at m/z = 269 and 271 were present in the corresponding background subtracted mass spectra. A RIC was then generated for the m/z values of 269+271 and is presented in Figure 45. The RIC shows four intense peaks, corresponding to scans # 44, 59, 61, and 73, and strongly resembles the UV chromatogram. Observed ions in these mass spectra are presented in Table 9 along with their identification. The background subtracted mass spectra of the four RIC peaks are presented in Figures 46 through 49.

The first peak in the RIC (scan #44, UV R_t=13.612) has been identified as formononetin-7-glucoside (FG) and is believed to be the degradation product of FGM. FG yielded a molecular ion, [M+H]+ at m/z =431. The $[AH_2]^+$, was observed as the base peak similar to that found for the model compounds in the positive-ion mode. An additional peak is observed at m/z = 160 corresponding the cleavage of the B ring system through the central benzopyran ring similar to that commonly observed in EI mass spectra of flavonoids [79].

The next two peaks in the RIC (scan #59 and #61, UV Rt=17.228 and 17.721) are incompletely resolved in both the RIC and UV chromatograms. However, the mass spectra of the two peaks are different. Scan #59 yielded an $[AH_2]^+$ peak at m/z = 269 while scan #61 produced an $[AH_2]^+$ ion at m/z = 271. This illustrates that although some "memory effects" are observed, they are not significant to limit mass spectral differentiation. The extent of the memory effects can be seen in scan #61,

where the [M+H]+ ion of FGM can still be seen with a relative intensity of 7%. Scan #59 has been identified as FGM while scan #61 has been identified as MG. The MG molecular species yields both a radical molecular ion, $M^{\cdot+}$, and a proton adduct ion [M+H]+. The last peak in the RIC (scan #73, UV R_t=20.955) was identified as medicarpin-3-O-glucoside-6"-O-malonate (MGM).

TABLE 9

(+) LC-CF-LSIMS OF APOLLO ALFALFA CELL SUSPENSION EXTRACTS

Identity	UV Rt	MS Scan #	[M+H]+	$[AH_2]$+	Others
FG	13.612	#44	431	269	370,160
FGM	17.228	#59	517	269	160
MG	17.721	#61	433 432 = $M^{\cdot+}$	271	
MGM	20.955	#73	519	271	

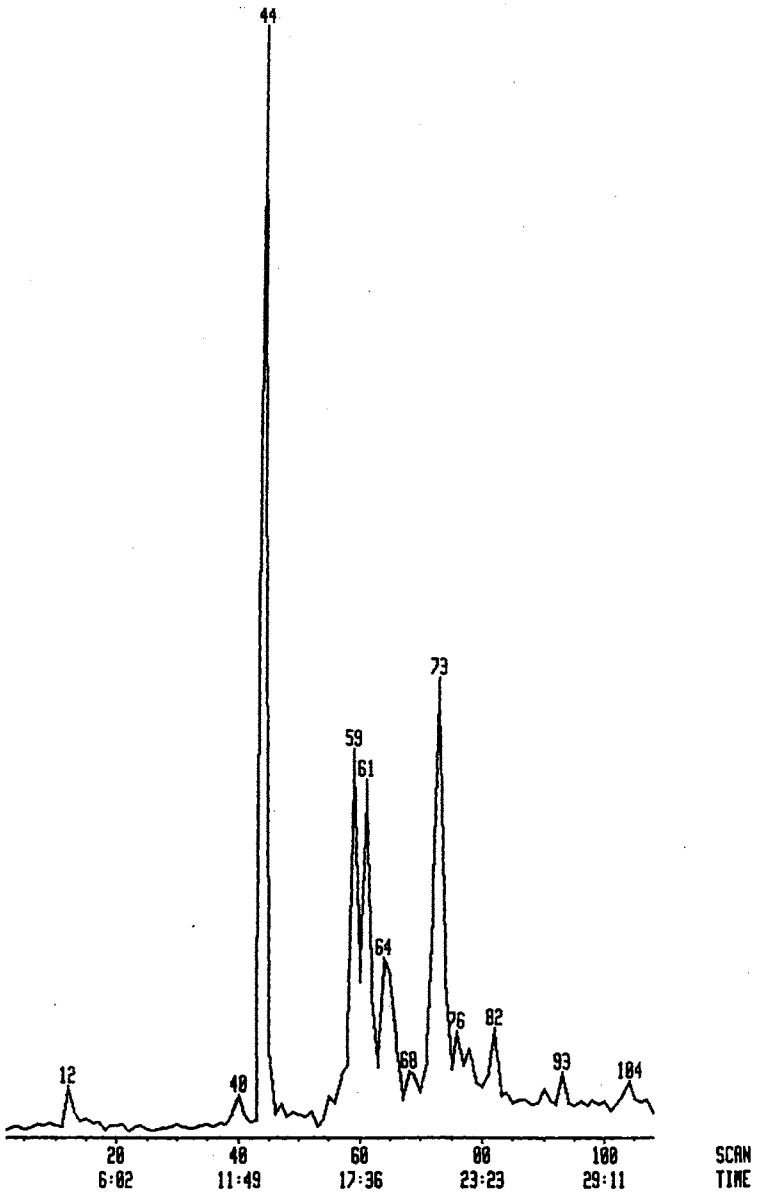

Figure 45- RIC of (+) LC-CF-LSIMS Analysis of a Basic Apollo Alfalfa Cell Suspension Extract

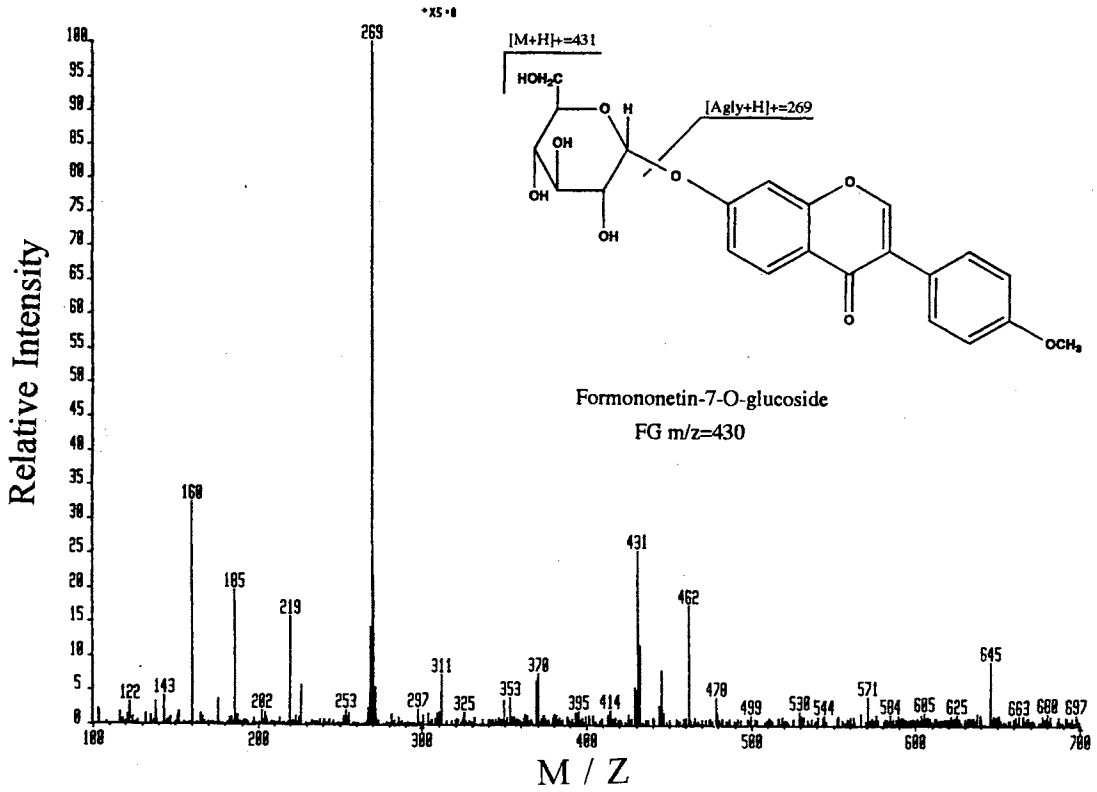

Figure 46- (+) LC-CF-LSIMS Mass Spectrum of Scan #44 from a Basic Apollo Alfalfa Cell Suspension Extract

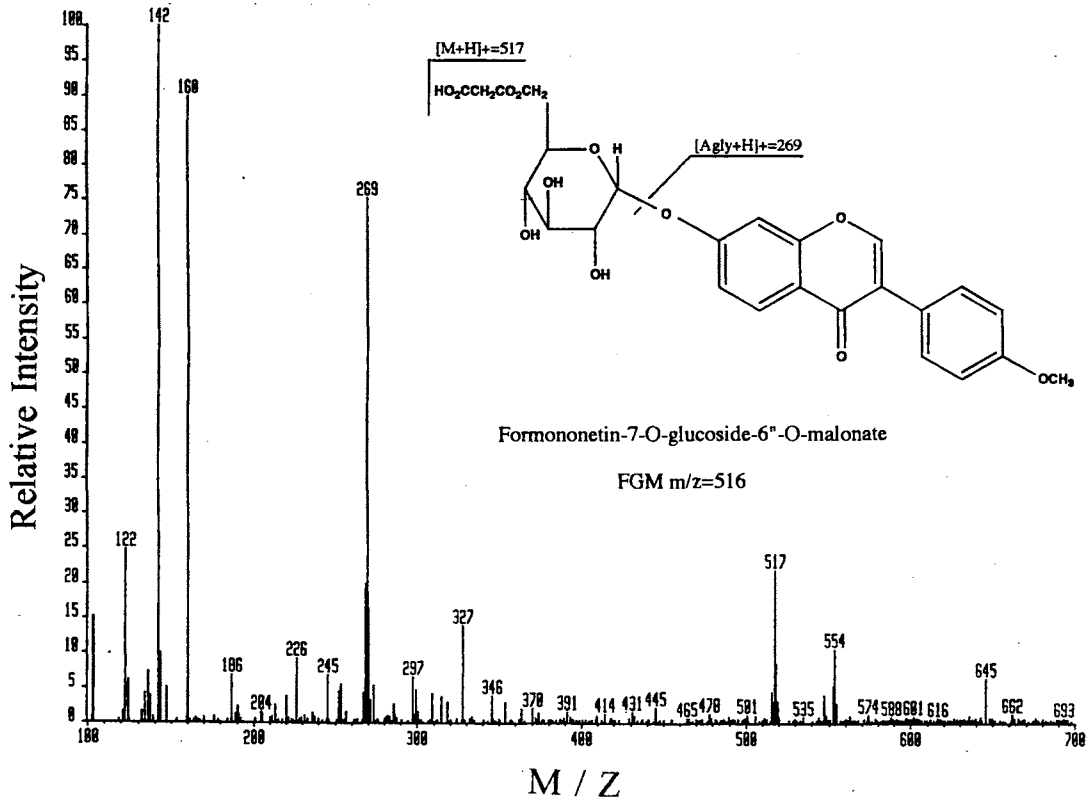

Figure 47- (+) LC-CF-LSIMS Mass Spectrum of Scan #59 from a Basic Apollo Alfalfa Cell Suspension Extract

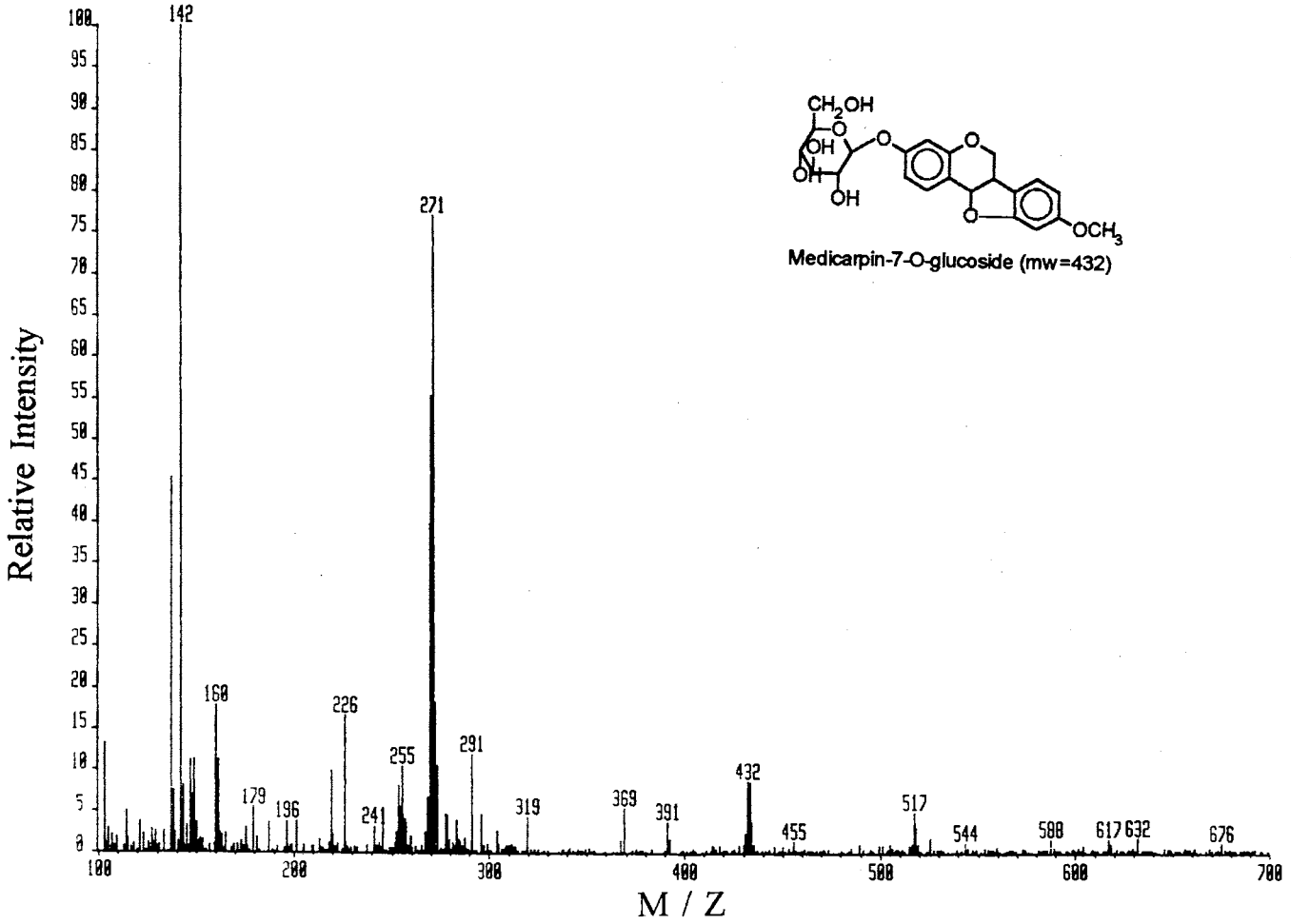

Figure 48- (+) LC-CF-LSIMS Mass Spectrum of Scan #61 from a Basic Apollo Alfalfa Cell Suspension Extract

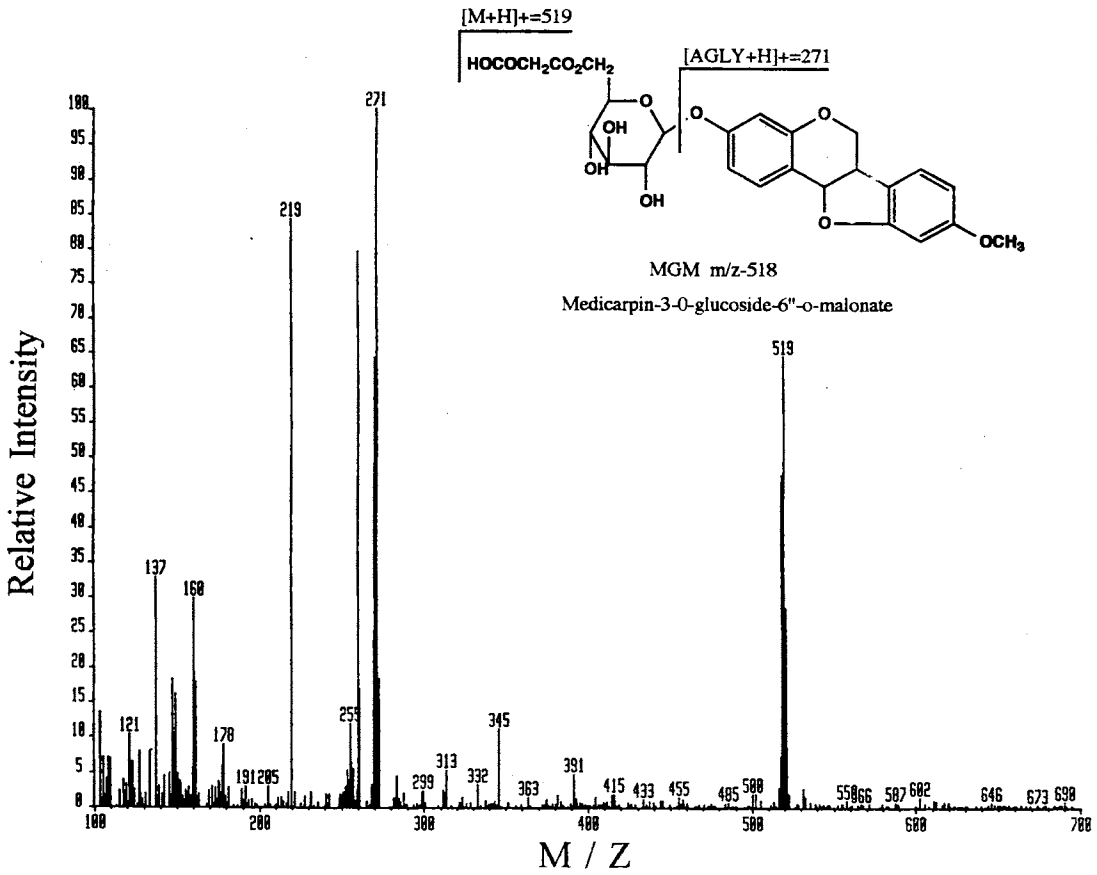

Figure 49- (+) LC-CF-LSIMS Mass Spectrum of Scan #73 from a Basic Apollo Alfalfa Cell Suspension Extract

III.5.5 Afrormosin-7-O-glucoside-6"-O-malonate

As mentioned in section III.1, (+) DP-LSIMS experiments aided in the identification of suspect isoflavonoids in basic alfalfa extracts (cultivar Calwest) as medicarpin-3-O-glucoside-6"-O-malonate (MGM), afrormosin-7-O-glucoside (AG), and afrormosin-7-O-glucoside-6"-O-malonate (AGM) [91]. Our LC-CF-LSIMS experiments were able to confirm the identification of MGM, but no such confirmation could be made for AG or AGM. The mass spectrum obtained for the suspect AGM by (+) DP-LSIMS in a 1% TFA in thioglycerol matrix is presented in Figure 50. The positive-ion peak at m/z = 547 was identified as the $[M+H]^+$ of AGM, while the peak at m/z = 299 was identified as the $[AH_2]^+$ of AGM. The mass spectrum also contains ion peaks at m/z = 269 and 517. We believe these to be the $[M+H]^+$ and $[AH_2]^+$ ion peaks of FGM.

Recall that both (+ and -) LC-CF-LSIMS experiments showed partially unresolved peaks identified as FGM and MG. Thus, if this was the fraction collected and analyzed in the above (+) DP-LSIMS experiments it would probably contain both FGM and MG. Since ions are present that are believed to from FGM, it is postulated that MG is also be present. The FGM would provide the ions at m/z =269 and 517 while it is postulated that the ion at m/z = 547 is the $[MG+TFA+H]^+$ adduct ion peak of MG. The presence of a TFA adduct with MG was observed in the (-) LC-CF-LSIMS experiments but not with significant intensity in (+) LC-CF-LSIMS. It is also suggested that the ion peak at m/z = 299 in the (+) DP-LSIMS mass spectrum is a background ion which can be seen in the matrix spectra. This ion could correspond to

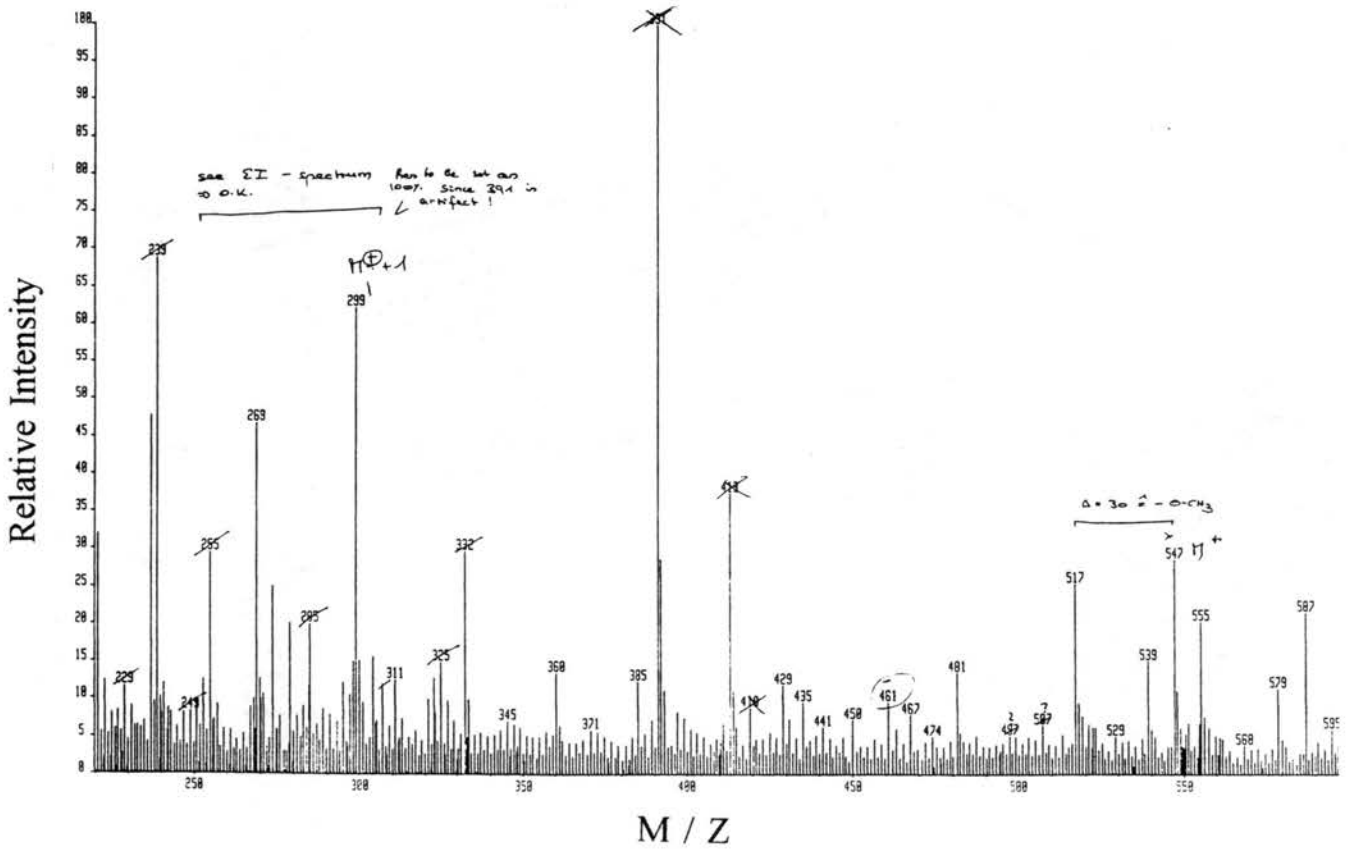

Figure 50- (+) DP-LSIMS Mass Spectrum of Suspect AGM in a matrix of 1.0 % TFA in Thioglycerol

$[2Gly+TFA+H]^+$, (184+114+1=299), since glycerol is a common contaminant of thioglycerol. The above facts generated significant doubt in the identification of AGM.

A CAD tandem LC-CF-LSIMS experiment was also performed on the selected parent ion peak at m/z = 545 in an attempt to obtain a product ion peaks corresponding to the aglycone similar to that described for MGM in section III.5.3. This experiment was unsuccessful since a product ion peak corresponding to the aglycone was not observed. These negative results were unable to confirm the aglycone as afrormosin or medicarpin.

Additional facts that support our proposed identification of the suspect AGM as FGM include the presence of formononetin in the synthetic pathway of medicarpin (see Figure 3). This pathway does not include afrormosin. Therefore, the presence of afrormosin in significant quantities is less probable. Also, the presence of large quantities of FGM in other legumes such as chickpea has been reported [113].

It should be noted that the cultivar of alfalfa used in the original experiments resulting in the identification of AGM [91] was different from that used for LC-CF-LSIMS experiments presented above. The previous (+) DP-LSIMS study used Calwest alfalfa Cell Suspensions while the LC-CF-LSIMS experiments utilized Apollo alfalfa. This difference in cultivars could possibly give rise to the presence of AGM in one cultivar and not the other. This issue will be discussed in more detail in section III.5.8

Due to the above questionable identification of AGM, experiments were designed to investigate the issue further. The first experiment proposed that if the AGM was truly present it would yield a $[M-H]^-$ ion peak at m/z = 545 in (-) LC-CF-

LSIMS experiments. A significant ion peak at m/z =545 was encountered in the (-) LC-CF-LSIMS analysis of the apollo alfalfa extract but was identified as the $[MG+TFA-H]^-$ ion of MG. The verification of this ion could be confirmed if a standard MG sample could be obtained and analyzed by (-) LC-CF-LSIMS. Thus, an experiment was designed to investigate the above logic process and is the subject of the next section.

III.5.6 Analytical (-) LC-CF-LSIMS of Crude MG Mixture with a 0.1% TFA acid modifier

Since a purified MG standard is not commercially available, a crude mixture of MG was prepared from an extract of elicited apollo alfalfa cell suspensions. The homogenized cells were extracted with acetone as described in the experimental section II.9. The peak identified as MGM was then isolated by preparative HPLC using an Alltech Econosil, 250mm x 22.5mm, 10μm, ODS column. The fraction corresponding to MGM was collected from a gradient elution of the crude extract. The gradient of 80:20 (A:B) to 40:60 (A:B) over 45 minutes at a flow rate of 10.0 mL/min was used. Solvent A was a 3.0% acetic acid in water, while solvent B was acetonitrile. The isolated MGM fraction was then subjected to mild hydrolysis conditions by autoclaving for 3 hours at 121°C in a 10% aqueous acetic acid solution to provide a crude mixture of MGM, MG, and free medicarpin. This process resulted in an approximate 60% conversion of the MGM to MG and the free medicarpin aglycone. The crude MG mixture was then analyzed by analytical LC-CF-LSIMS using a 4.6 mm x 250 mm, Bakerbond, 5 μm, ODS column. Gradient elution of the

crude mixture was performed as described in section II.4 with a 0.1% TFA acid modifier. On-line UV analysis was performed at 254nm. The eluent from the column was first passed through the UV detector and then into the fused silica capillary splitting device described in the experimental section II.5. The split eluent was delivered to the mass spectrometer at flow-rate of 5.0 μL/min. The source temperature was 38°C and the Cs^+ primary ion energy was 30 keV. Negative-ions were extracted and accelerated to 6 keV. Correlation between UV absorbance peaks and mass spectra is provided in Table 10. The resultant RIC chromatogram is presented in Figure 51. From this data four peaks were identified.

Mass spectrum #89 contained the questionable ion peak at m/z = 545 and has been identified as that of MG. The mass spectrum of scan #89 is presented in Figure 52. This identification is supported by the observance of a radical molecular anion at m/z = 432. The adduct ion peaks corresponding to $[MG+GLY-H]^-$ at m/z peak = 523, $[MG+TFA-H]^-$ at m/z =545, and $[MG+A-H]^-$ at m/z = 701 further confirm the molecular weight as 432. The aglycone, $[A-H]^-$, ion peak was observed at m/z = 269. The presence of the ion at m/z = 545 could only arise from the TFA adduct formed with MG. This is because only MGM was collected to prepare the crude MG mixture. Therefore, only conjugates of medicarpin should be present in the crude mixture.

The mass spectrum of scan #102 is provided in Figure 53 and has been identified as MGM. The identification was based on the presence of ion peaks corresponding to the following: $[MGM+TFA-H]^-$ at m/z = 631, $[MGM-H]^-$ at m/z = 517, $[MGM-CO_2H]^-$ at m/z = 473, $[A-H]^-$ at m/z = 269.

The presence of an additional medicarpin conjugate was observed in spectrum #117 which is presented in Figure 54. This conjugate has been identified as medicarpin-3-O-glucoside-6"-acetate (MGOAc). This conjugate is not found in natural extracts of alfalfa and is believed to have been generated by the hydrolysis process. The identification is based on the observation of a radical molecular ion, [MGOAc]-, peak at m/z = 474. The molecular weight identification is supported by the presence of the adduct ion peaks consistent with [MGOAc+TFA-H]- at m/z = 587 and [MGOAc+GLY-H]- at m/z = 565. The [A-H]- ion peak was observed at m/z = 269.

Finally, the medicarpin aglycone was identified in mass spectrum #148 which is presented in Figure 55. The $[A-H]^-$ ion peak was observed at m/z = 269 while the dimer, $[2A-H]^-$, ion peak was observed at m/z = 539. The presence of dimers for aglycone species was found to be a common occurrence and was beneficial in their identifications.

TABLE 10

ANALYTICAL (-) LC-CF-LSIMS OF CRUDE MG MIXTURE WITH A 0.1% TFA ACID MODIFIER

UV R_t	MS Scan # and R_t	Identification
21.400	89, 22:03	MG
24.564	102, 25:16	MGM
28.365	117, 28:58	MGOAc
35.925	148, 36:37	Medicarpin

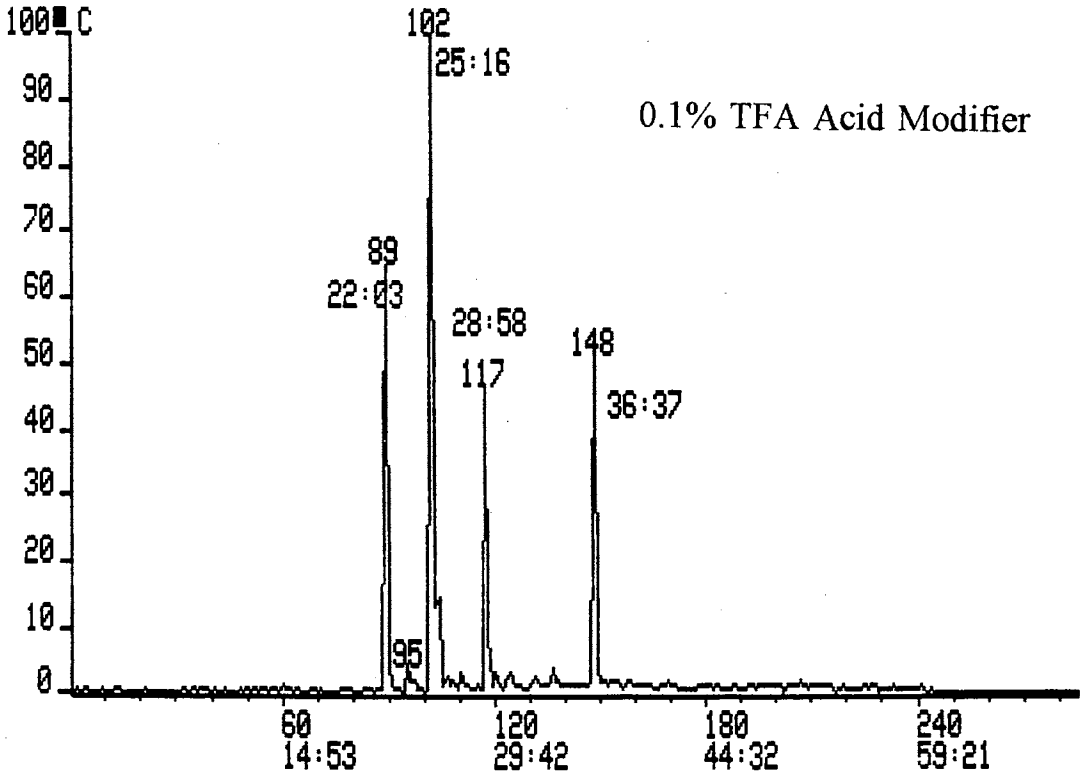

Figure 51- (-) LC-CF-LSIMS RIC of m/z=267 of a Crude MG Mixture

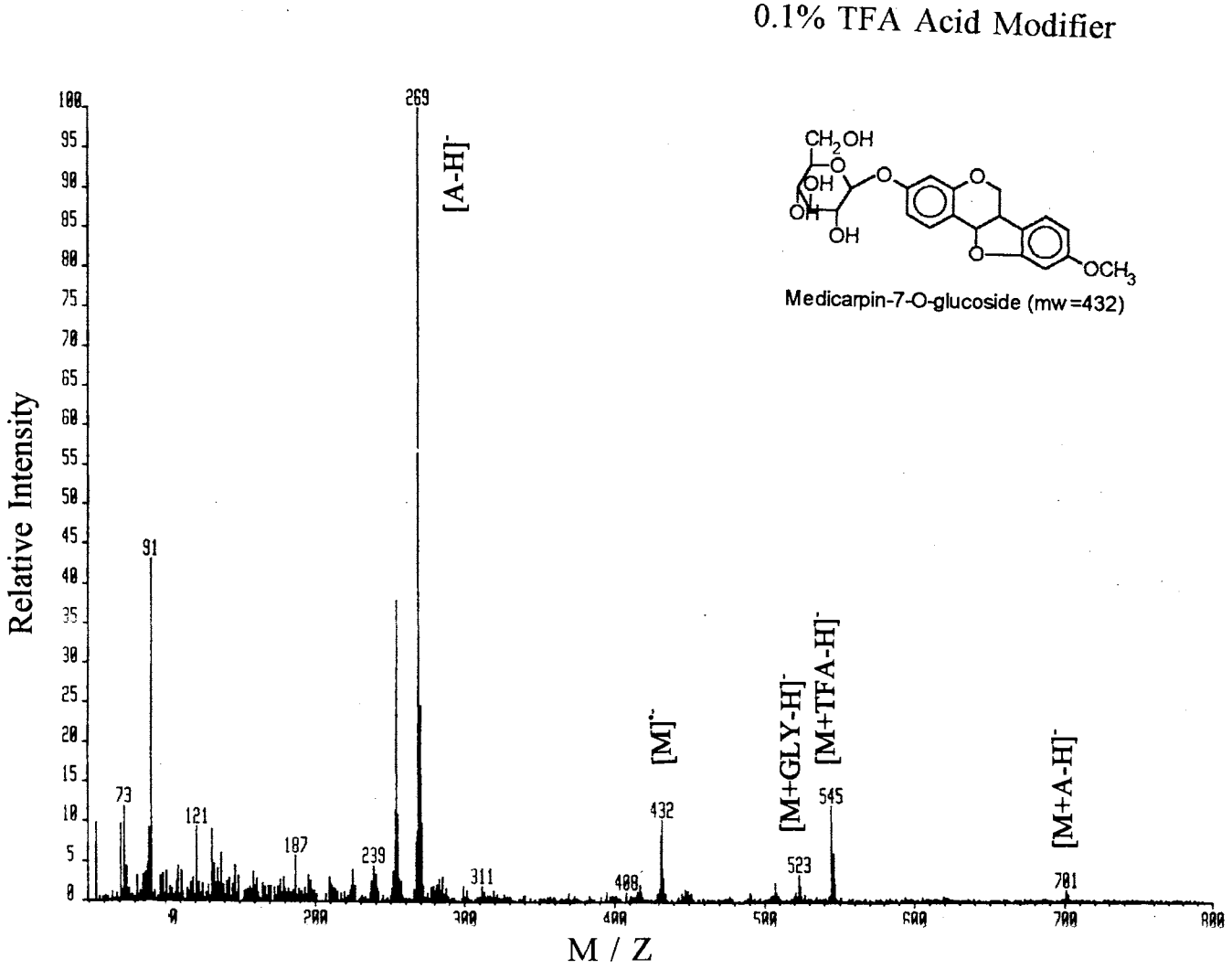

Figure 52- (-) LC-CF-LSIMS Mass Spectrum of MG from a Crude MG Mixture

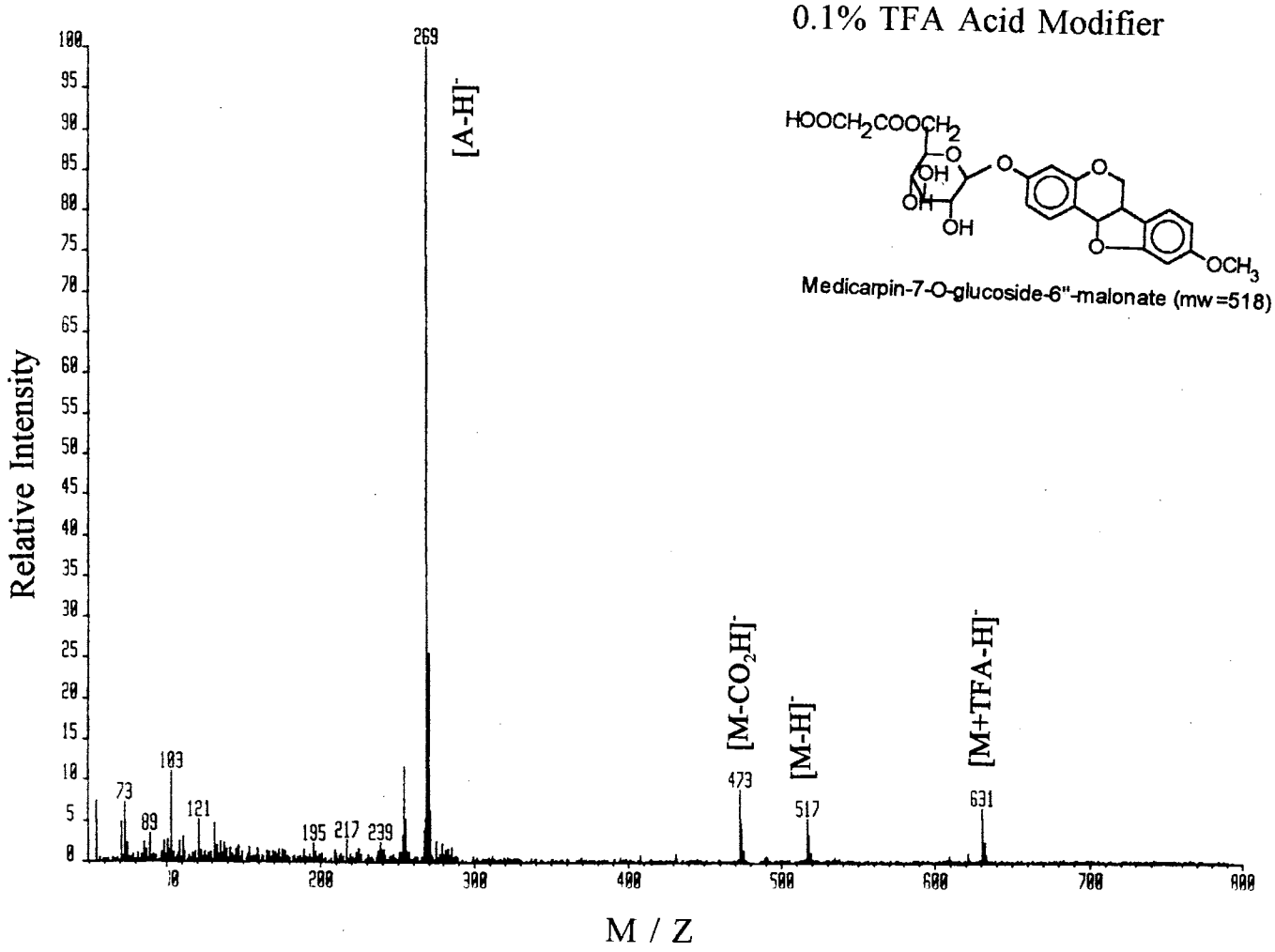

Figure 53- (-) LC-CF-LSIMS Mass Spectrum of MGM from a Crude MG Mixture

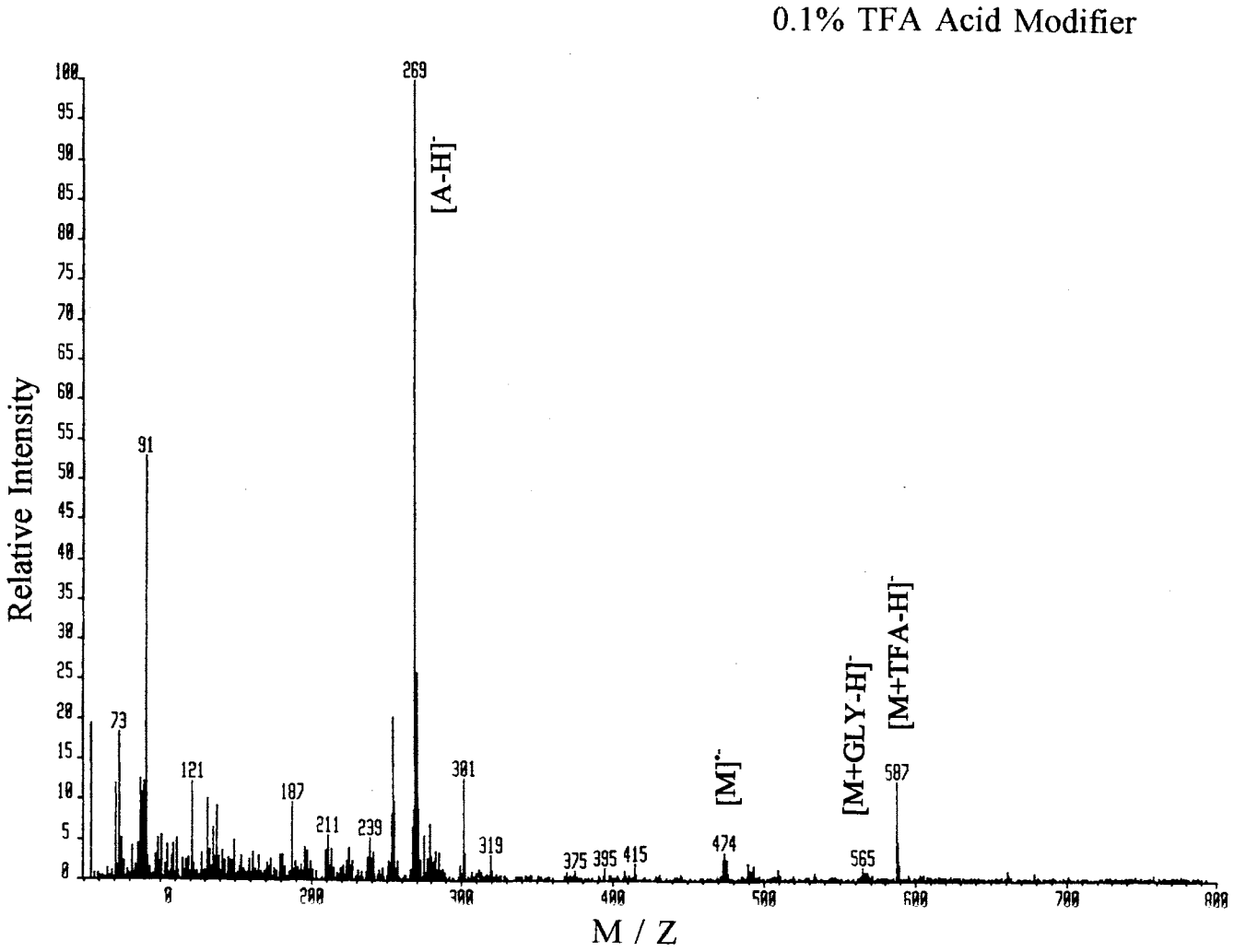

Figure 54- (-) LC-CF-LSIMS Mass Spectrum of MGOAc from a Crude MG Mixture

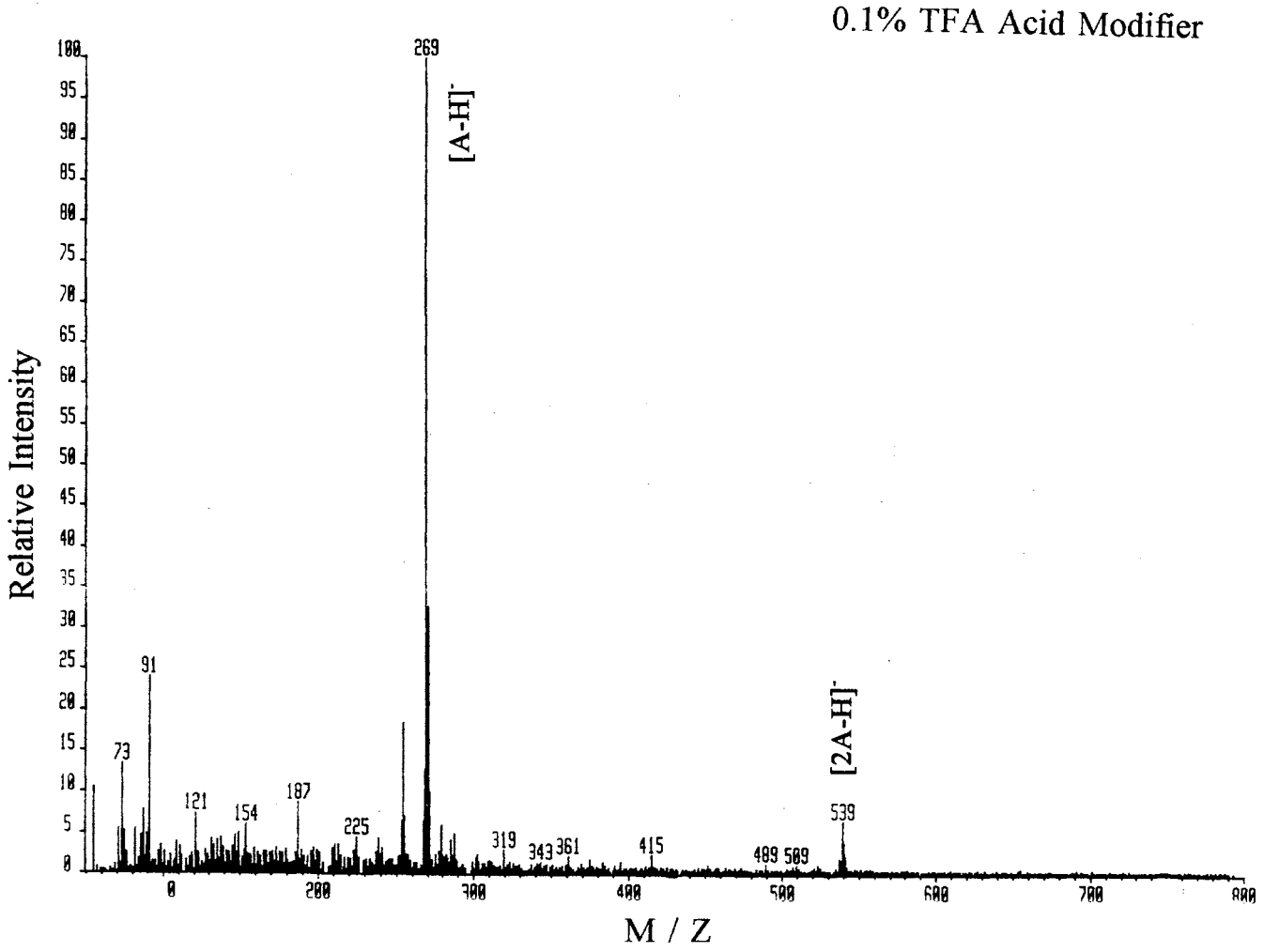

Figure 55- (-) LC-CF-LSIMS Mass Spectrum of Medicarpin from a Crude MG Mixture

III.5.7 Analytical (-) LC-CF-LSIMS of MG Reference Material with a 1.0% Acetic Acid modifier

If the ion peak at m/z = 545 corresponds to $[MG+TFA-H]^-$ and not $[AGM-H]^-$, then a change in the acidic modifier from TFA to acetic acid should produce an ion peak corresponding to $[MG+OAC]^-$ instead of $[MG+TFA-H]^-$. To confirm the above hypothesis, an experiment was performed by LC-CF-LSIMS of the crude MG mixture using a 1.0% acetic acid modifier instead of 0.1% TFA. Other experimental parameters were identical to those described above in section II.5.6. Background subtraction of scan #10 from the entire data acquisition time was performed.

The UV chromatogram and RIC chromatogram are presented in Figure 56 while the UV and MS correlation data is presented in TABLE 11. The sample yielded 5 major components which were identified by UV and LC-CF-LSIMS data.

The mass spectrum of scan #72 is presented in Figure 57 and has been tentatively identified as daidzein by both its retention time and it mass spectrum, but is yet unconfirmed by additional methods. This compound is believed to be the degradation product of medicarpin resulting from hydrolysis with 10% acetic acid. Medicarpin could decompose into daidzein by the cleavage of the methyl group from the methoxy group at 4' position. This decomposition would also include the cleavage of the furan ring system to yield an isoflavonoid. The structures of these compounds can be found in the biosynthetic pathway of medicarpin presented in chapter 1, Figure 3. The $[A-H]^-$ ion peak is present at m/z = 253 while an $[A+GLY-H]^-$ ion peak is observed at m/z = 345. One significant observation that has been made for most

aglycones is the presence of a dimer in the mass spectra. In the case of daidzein, the dimer, $[2A-H]^-$, is observed at m/z = 507. This fact is, in addition to the glycerol adduct with the aglycone, was used to confirm the aglycone molecular weight.

The second significant peak or scan #86 has been identified as MG. The mass spectrum of scan #86 is presented in Figure 58. This spectra is unique in the fact that the MG is present as a molecular radical anion similar to that encountered in the basic alfalfa extracts discussed in section III.5.2. The identity of the molecular weight as 432 is supported by the presence of matrix adduct ions between the molecular species and the acetate and glycerol anions. Those adduct ions observed corresponded to $[MG+OAc]^-$ and $[MG+GLY-H]^-$. Also, an ion peak was observed corresponding to an adduct form between MG and the medicarpin aglycone, $[MG+A-H]^-$, at m/z = 701. This type of an ion has not been previously encountered. Additional ions observed were $[A-CH_3]^-$ at m/z = 255 and $[A-OCH_3]^-$ at m/z =239.

The third major component (scan#97) was identified as MGM and its mass spectrum is presented in Figure 59. A molecular ion peak, [MGM-H]-, was observed at m/z = 517. Also present are ion peaks corresponding to successive cleavages of the malonate of MGM. These were $[MGM-CO_2H]^-$ at m/z = 473 and $[MGM-CO_2HCH_2CO]^-$ at m/z = 43.

The fourth major component has been identified as medicarpin-3-O-glucoside-6"-acetate (MGOAc). The mass spectrum of scan #115 is presented in Figure 60. This compound was not observed in the extracts of alfalfa presented above in sections II.5.2 and III.5.3 and is believed to have been synthesized in the hydrolysis of MGM

in 10.0% acetic acid. Again a radical molecular anion $[MGOAc]^-$ is noticed at m/z = 474. This ion, $[MGOAc]^-$, can be differentiated from the acetate adduct with MG, $[MG+OAc]^-$, through the series of additional adduct ions. This series includes $[MGOAc+OAc-]^-$, $[MGOAc+GLY-H]^-$, and $[MGOAc+A-H]^-$.

Also observed were the characteristic ion peaks, $[A-CH3]^-$ at m/z = 255 and $[A-OCH3]^-$ at m/z =239

Finally, the fifth major component (scan#144) of the mixture was identified as the free aglycone, medicarpin. The mass spectrum of scan #144 is presented in Figure 61. This mass spectrum provided a dimer, [2A-H]- , at m/z = 539 and the characteristic ion peaks, $[A-CH3]^-$ at m/z = 255 and $[A-OCH3]^-$ at m/z =239.

The information gained from the analysis of this crude MG mixture provided a much greater degree of characterization actual leguminous extracts then the model flavonoids described earlier. The results from this experiment further confirm that the ion peak previously encountered at m/z = 545 in the alfalfa extracts in section III.5.2 is the result of the adduct formed with MG, $[MG+TFA-H]^-$, and not from $[AGM-H]^-$.

TABLE 11

(-) ANALYTICAL LC-CF-LSIMS OF CRUDE MG MIXTURE WITH A 1.0% ACETIC ACID MODIFIER

UV R_t	MS R_t	MS Scan #	Identification
17.098	18:00	72	Daidzein
20.519	21:23	86	MG
23.269	24:05	97	MGM
27.688	28:35	115	MGOAc
34.868	35:43	144	Medicarpin

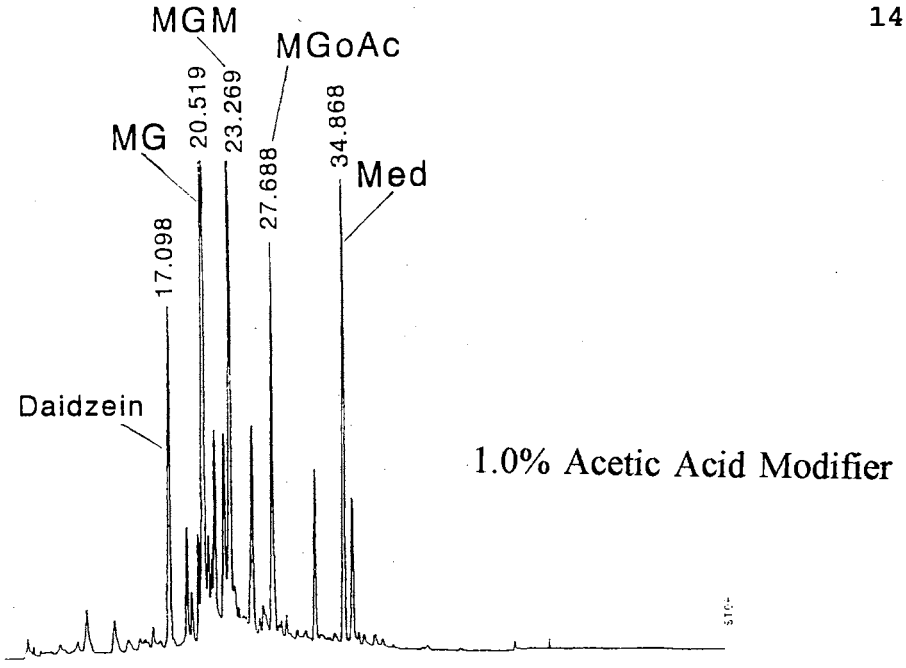

U.V. Chromatogram of MG Standard at 287nm.

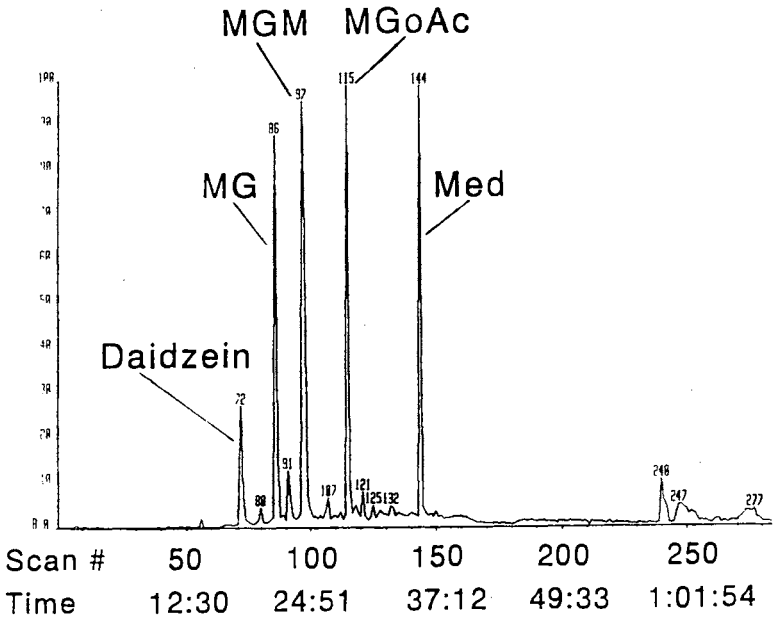

LC-CF-LSIMS SIC m/z=253+269 of MG Standard

Figure 56- On-line UV Chromatogram and RIC of m/z=253+269 of Crude MG Mixture

1.0% Acetic Acid Modifier

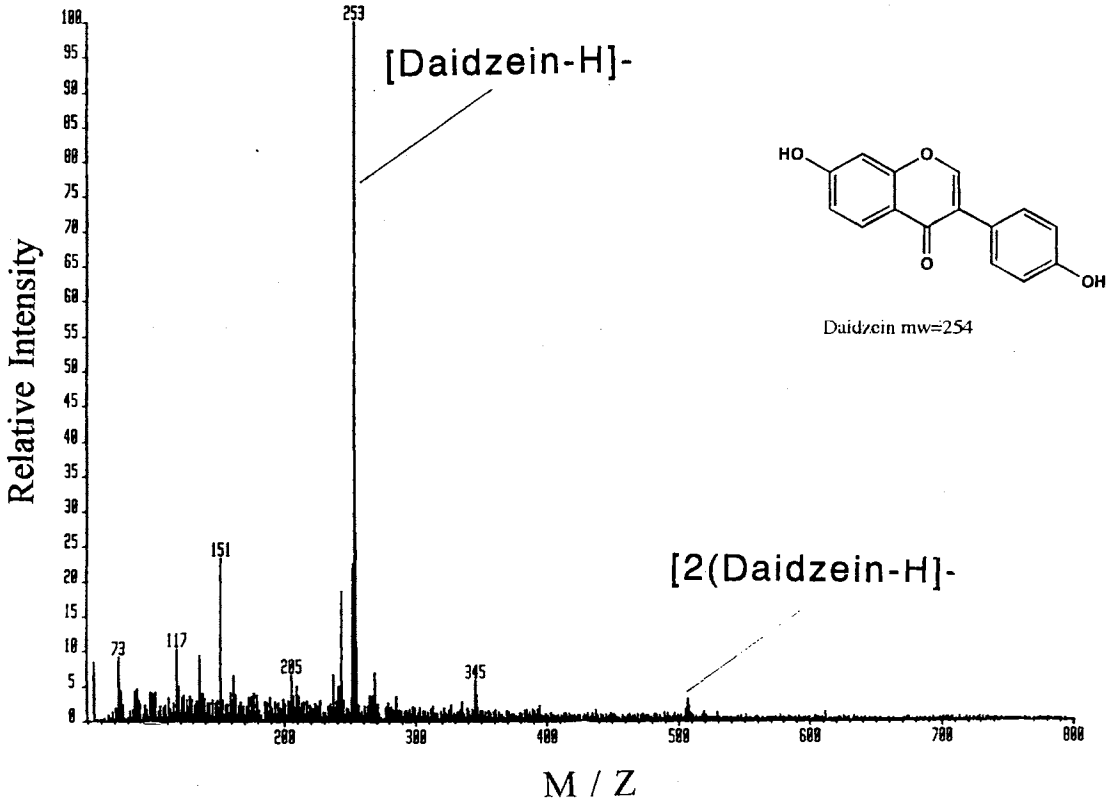

Figure 57- (-) LC-CF-LSIMS Mass Spectrum of Daidzein from Crude MG Mixture

1.0% Acetic Acid Modifier

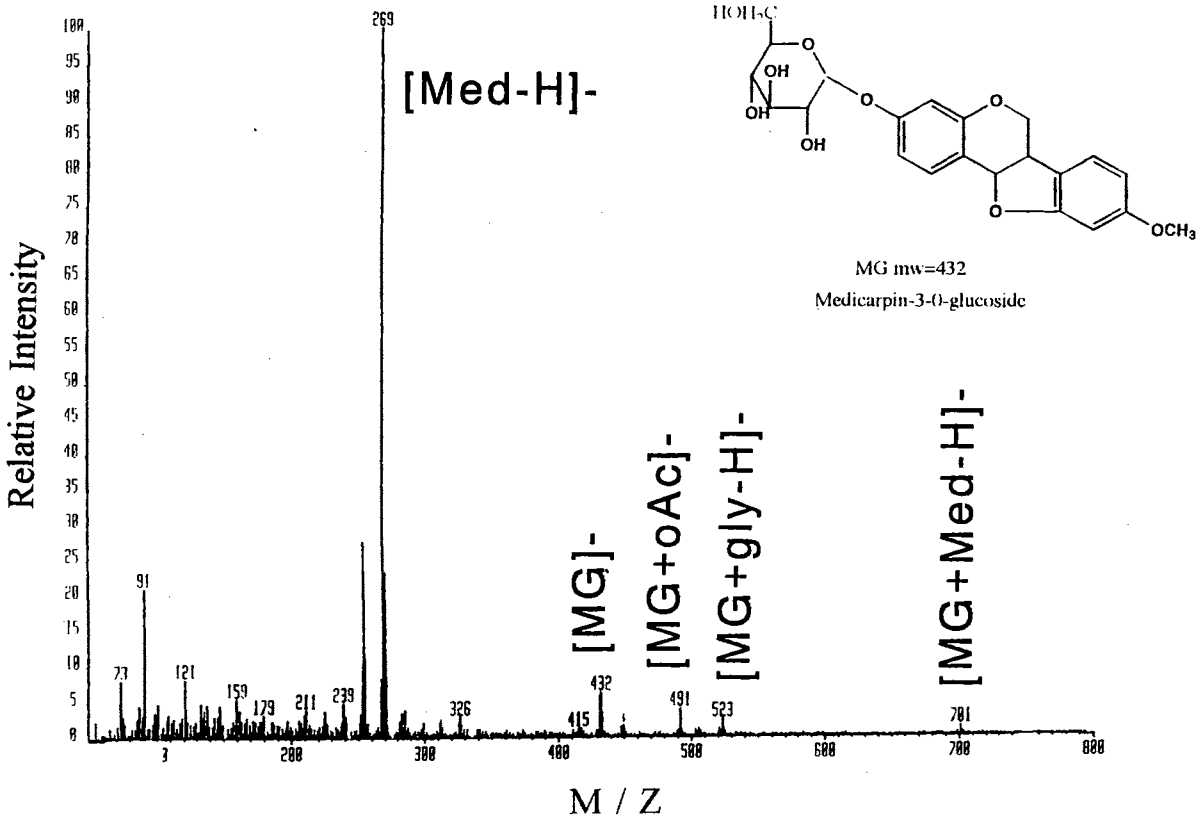

Figure 58- (-) LC-CF-LSIMS Mass Spectrum of MG from Crude MG Mixture

1.0% Acetic Acid Modifier

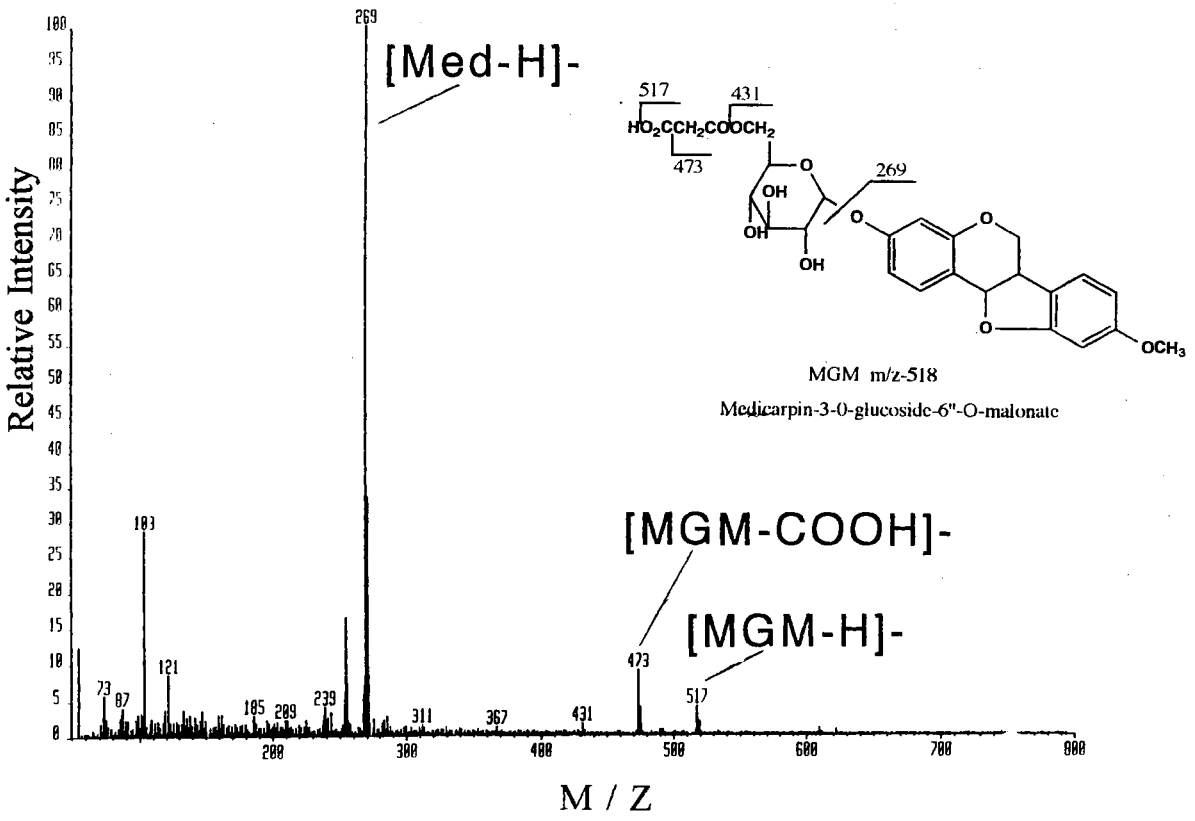

Figure 59- (-) LC-CF-LSIMS Mass Spectrum of MGM from Crude MG Mixture

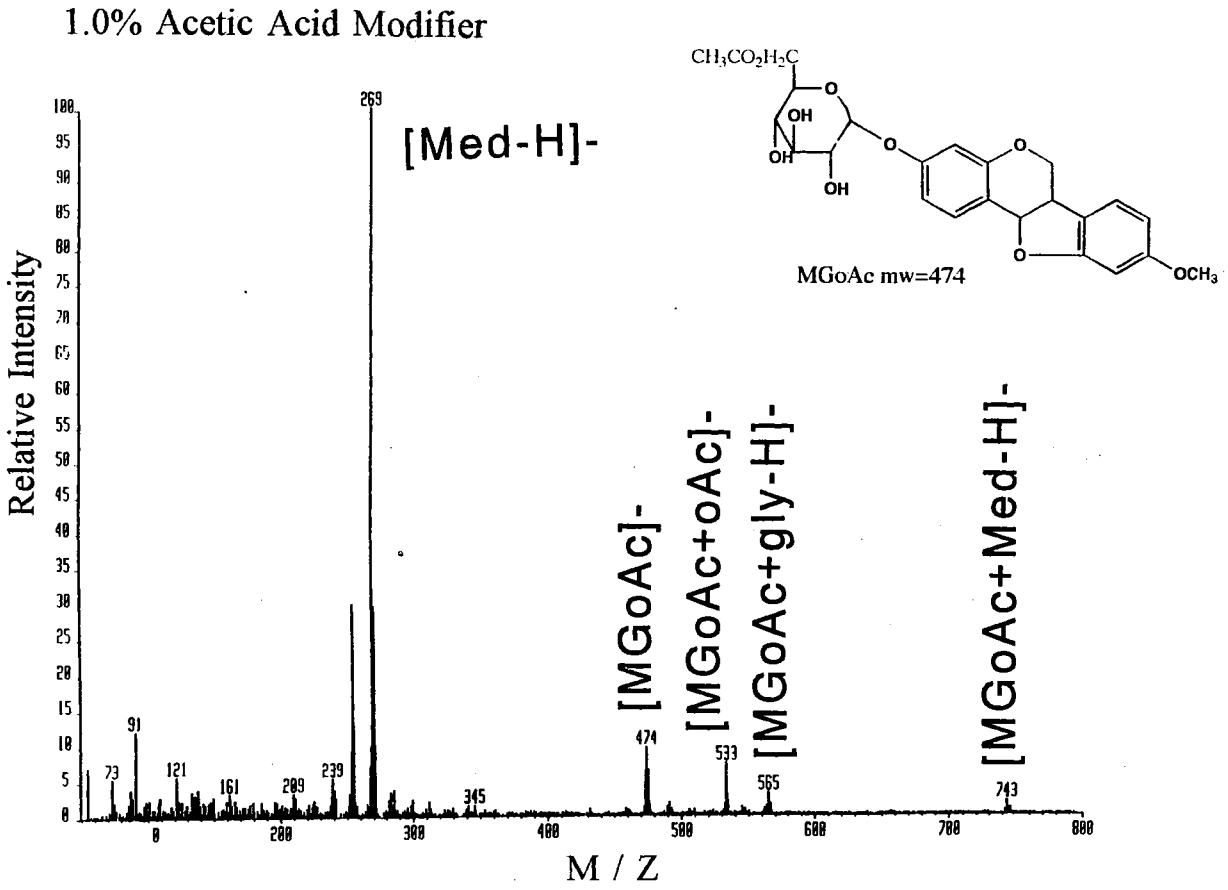

Figure 60- (-) LC-CF-LSIMS Mass Spectrum of MGOAc from Crude MG Mixture

1.0% Acetic Acid Modifier

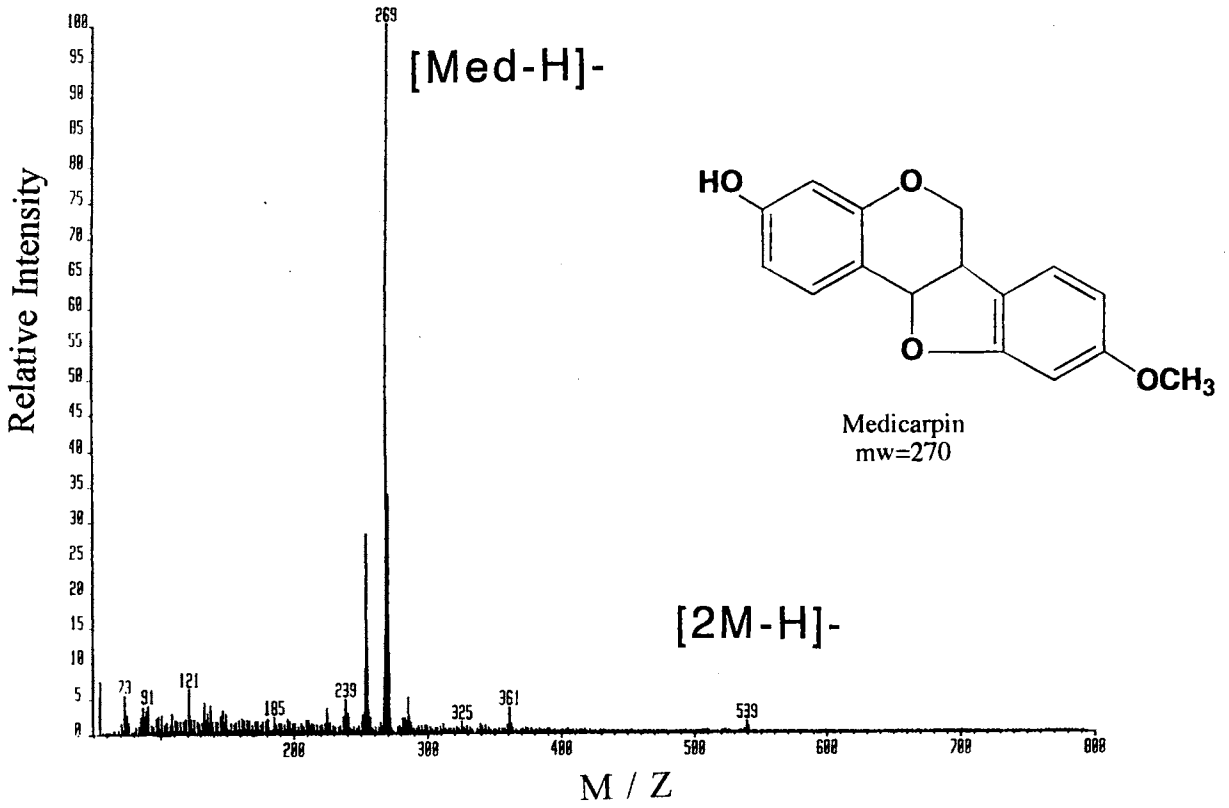

Figure 61- (-) LC-CF-LSIMS Mass Spectrum of Medicarpin from Crude MG Mixture

III.5.8 (-) LC-CF-LSIMS of Basic Calwest Alfalfa Extracts

To further qualify our identification of the questionable conjugate as FGM instead of AGM (-) LC-CF-LSIMS was performed on a basic extract of newly initiated Calwest alfalfa cell suspensions. The purpose of this experiment was to determine if different cultivars of alfalfa contain different isoflavonoid conjugates, and to further confirm that FGM is present instead of AGM. The original (+) DP-LSIMS analysis that identified the suspect conjugate as AGM was performed on basic extracts of "young" Calwest alfalfa cells suspensions. Therefore, new Calwest calluses were initiated to provided "young" Calwest alfalfa cell suspensions [86,91]. The newly initiated Calwest alfalfa cell suspensions were extracted as described in the experimental section II.9. Gradient elution (-) LC-CF-LSIMS was then performed under the conditions described in experimental section II.4 with a 1.0% acetic acid modifier. Mass spectra data were acquired in the full-scanning mode while scanning at 10 seconds/decade with an interscan time of 2 seconds. Background subtraction of scan #10 was performed over the entire acquisition time. On-line UV detection was performed at 287nm and the UV chromatogram obtained is presented in Figure 62. A RIC ion chromatogram was generated from the background subtracted mass spectra for m/z = 265+267+269+281 and is also presented in Figure 62 . Correlation of UV retention times with mass spectra was performed using the delay time method described previously.

The UV chromatogram shows an intense peak at 19.382 minutes which corresponds to the conjugate in question (AGM or FGM). This UV peak corresponds

to mass spectrum #105 which is presented in Figure 63. This mass spectra yielded a molecular ion peak, [M-H]-, at m/z = 515 that is consistent with FGM. The identification of the molecular ion at m/z = 515 is confirmed by an ion peak corresponding to $[FGM+GLY-H]^-$ at m/z = 607. Also observed were the ion peaks corresponding with $[M-CO_2H]^-$ at m/z = 471 and $[A-H]^-$ at m/z = 267.

Additional confirmation of the presence of formononetin in the Calwest alfalfa extracts was found in the UV peak eluting at 31.215 minutes. This UV peak corresponds to mass spectrum # 166. This mass spectrum yielded an [A-H]- ion peak at m/z =267 while an ion peak corresponding to the dimer of the aglycone, [2A-H]-, was observed at m/z =535 (2x268-1). As mentioned previously the presence of the dimer ion peak confirms the identification of the aglycone molecular weight as 268.

Through a similar process as described above the UV peak at 23.491 minutes corresponding to mass spectrum #125 was been identified as MGM. Mass spectrum #125 is presented in Figure 64. The molecular ion peak, [M-H]-, was observed at m/z = 517 while the ion peak corresponding to [MGM+GLY-H]- was observed at m/z = 609. The [A-H]- ion peak was observed at m/z = 269.

The identification of FGM in newly initiated calwest alfalfa cells suspension provides further evidence that the previous identification of AGM was in error.

(A)

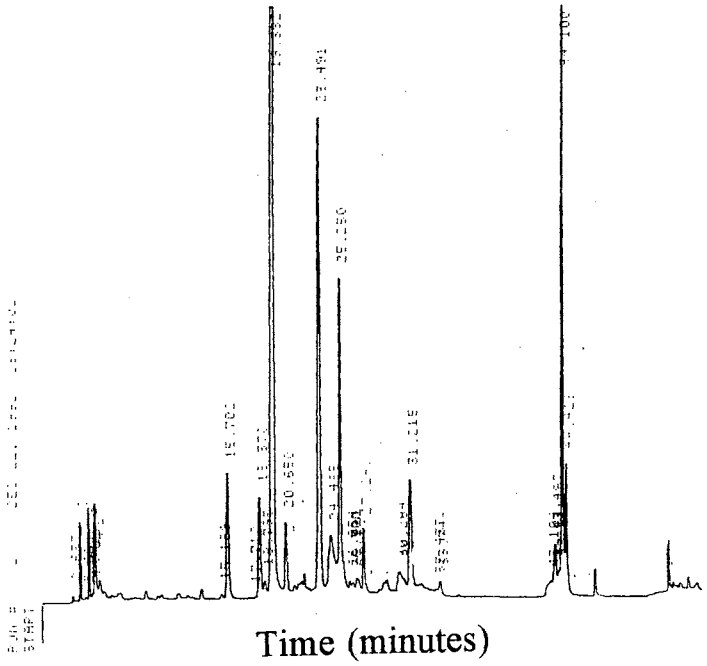

(B)

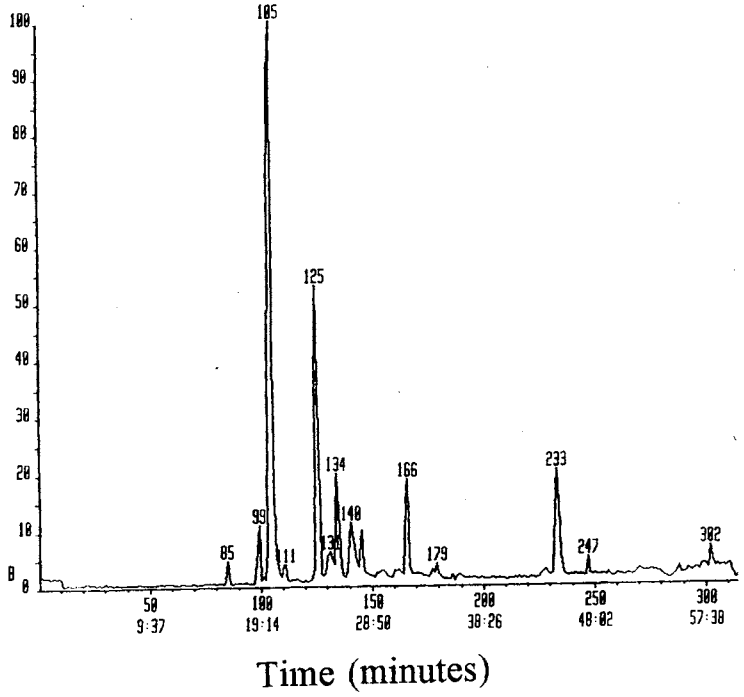

Figure 62- (**A**) On-line UV Chromatogram and (**B**) RIC of m/z=265+ 267+269+281 of Basic Calwest Alfalfa Cell Suspension Extract

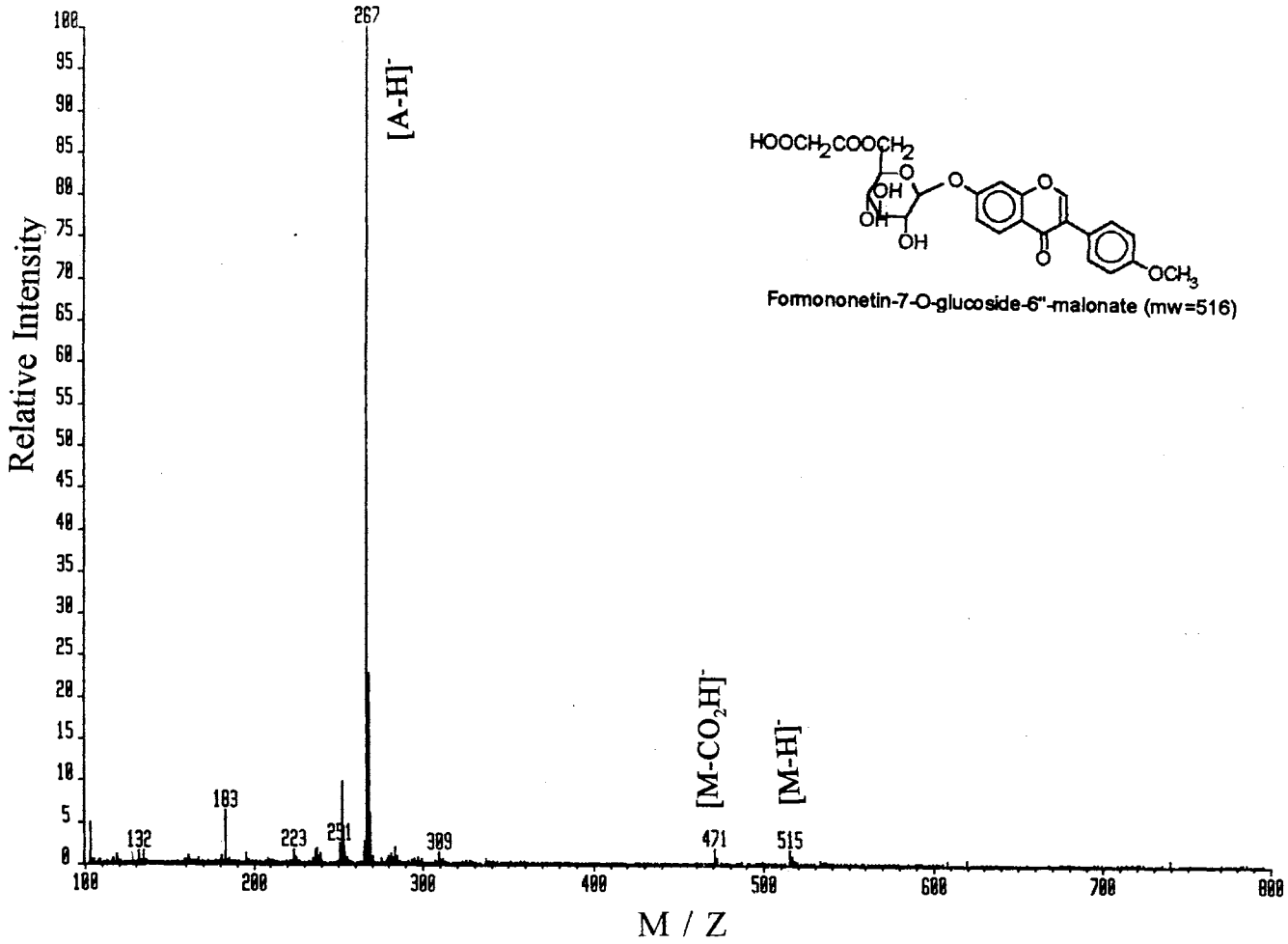

Figure 63- (-) LC-CF-LSIMS Mass Spectrum of FGM in a Calwest Alfalfa Cell Suspension Extract

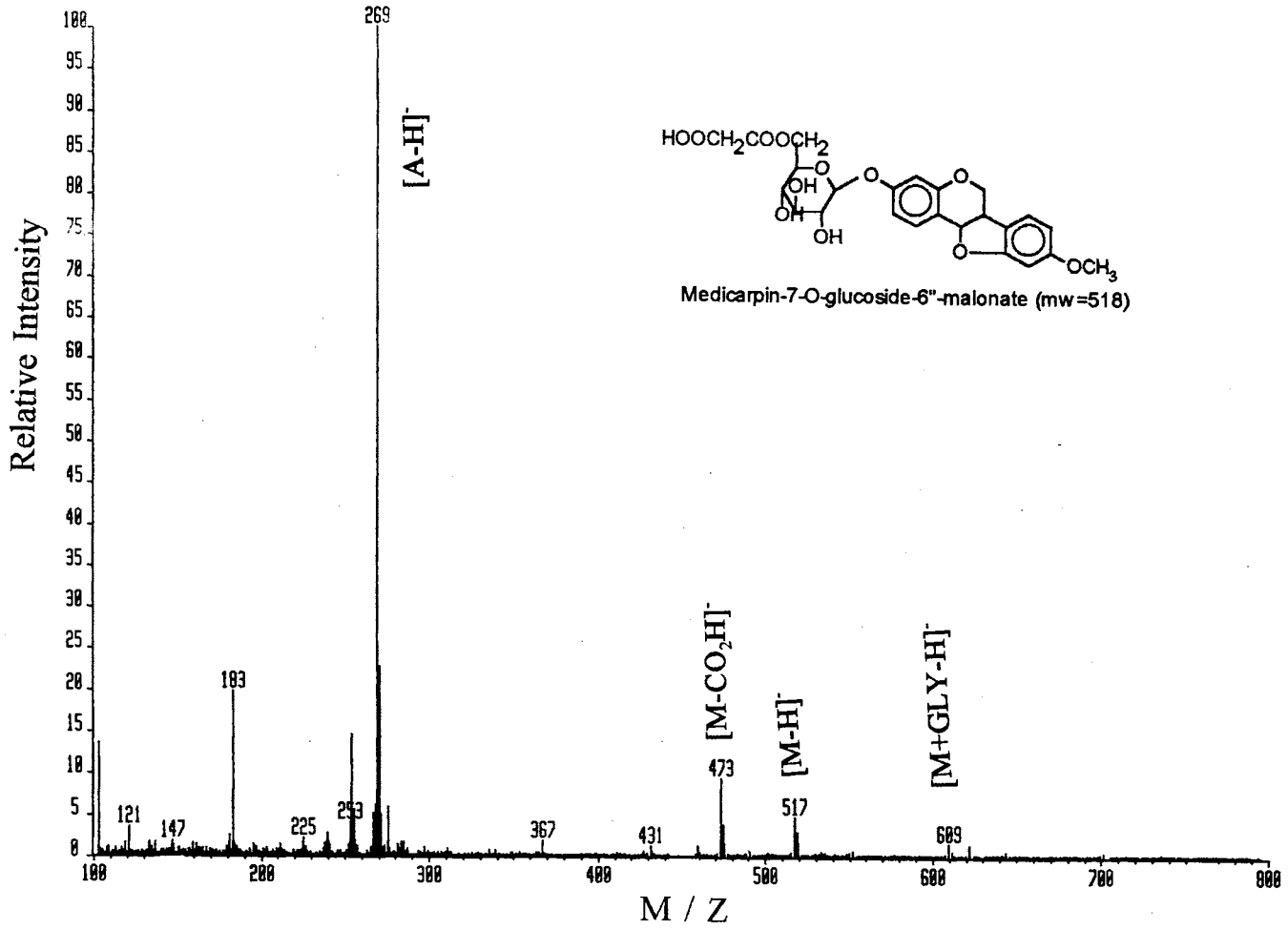

Figure 64- (-) LC-CF-LSIMS Mass Spectrum of MGM in a Calwest Cell Suspension Extract

III.5.9 Identification of Flavonoid Conjugates in Other Plant Extracts by (-)LC-CF-LSIMS

A survey of other plant systems was performed in an attempt to further illustrate to usefulness of LC-CF-LSIMS and identify additional flavonoid conjugates in plant systems. Negative-ion LC-CF-LSIMS was performed as describe above with a 1.0% acetic acid modifier. The identification process used was also as described above. All extracts were prepared as described in section II.9.

Extracts from cell suspensions and roots of several cultivars of alfalfa were analyzed by (-) LC -CF-LSIMS. The isoflavonoid conjugates FGM and MGM were identified in each of the following: Apollo alfalfa cell suspensions, Calwest 475 alfalfa cell suspensions, field grown Cimmaron alfalfa roots, field grown Apollo alfalfa roots, and field grown RegenSY alfalfa roots. The results from these experiments were similar to those already reported for Apollo and Calwest alfalfa cell suspension extracts. The only major differences were in the relative concentrations of the MG, MGM, FG, and FGM conjugates, which was expected due to the different growth environments and stress conditions.

Negative-ion analytical LC-CF-LSIMS analysis was then performed on the basic extracts of 6 day old Williams soybean (*Glycine max*) cotyledons. On-line UV detection followed by (-) LC-CF-LSIMS was performed as described in section II.4 with a 0.10% TFA acid modifier. The on-line UV chromatogram and RIC of m/z = 253+269 are presented in Figure The UV chromatogram shows three major peak which have been correlated to mass spectra as given in Table 12. The first compound

has been identified as daidzein. The mass spectrum shows a molecular ion, [M-H]-, peak at m/z = 415 which is confirmed by the adduct ion peak [DG+TFA]- at m/z = 528. The [A-H]- ion peak is present at m/z = 253. The second major peak observed in the UV chromatogram has been identified as daidzein-7-O-glucoside-6"-malonate (DGM). The mass spectrum of DGM is provided in Figure 66. The aglycone ion peak is observed at m/z = 253 while the radical molecular ion [DGM]- is observed at m/z = 502. The molecular ion confirmation is provided by the adduct ion peak [DGM+TFA-H]- at m/z = 615. Finally, the third peak present in the UV chromatogram has been identified as genistein-7-O-glucoside-6"-O-malonate (GGM). Ion peaks used for the identification of GGM include: $[GGM+TFA-H]^-$ at m/z = 631, $[GGM]^{\bullet-}$ at m/z = 518, $[GGM-CO_2H]^-$ at m/z = 473, $[A-H]^-$ at m/z = 269, and $[A-OH]^-$ at m/z = 253. The mass spectrum of GGM is provided in Figure 67. The GGM compound produces a mass spectrum very similar to MGM since they both have an aglycone molecular weight of 270. The difference in aglycones is genistein is a trihydroxy isoflavonoid while medicarpin is a hydroxy, methoxy pterocarpin. The methoxy group on medicarpin has a greater tendency to fragment than the hydroxyl group. Therefore, medicarpin usually shows a fragment ion peak at m/z = 255 for the ion $[M-CH_3]^-$, but genistein shows a fragment ion peak at m/z = 253 corresponding to $[M-OH]^-$. This fact allows the two compounds to be differentiated. This fact and additional reports in the literature [86,87] have been used to identify GGM, DG, and DGM.

(A)

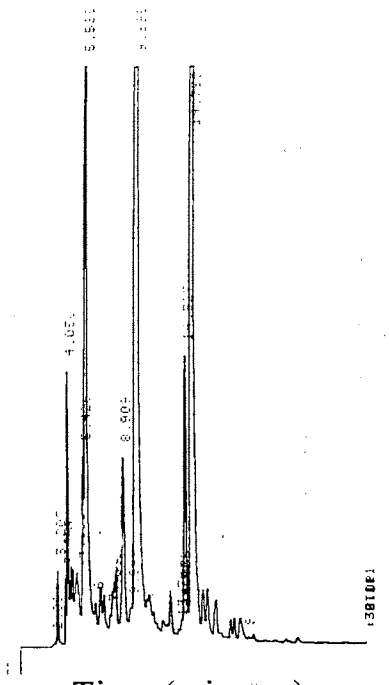

Time (minutes)

(B)

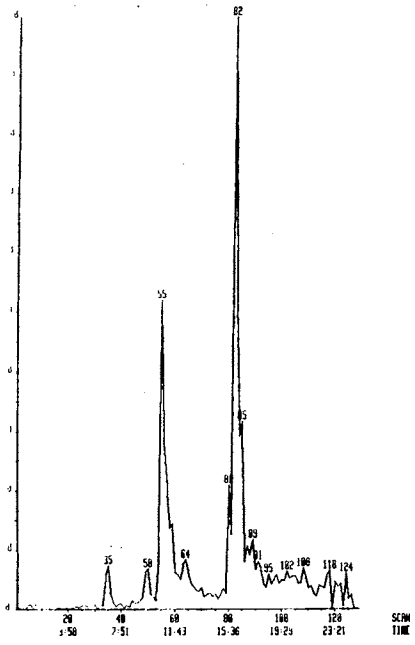

Figure 65- (**A**) On-line UV Chromatogram and (**B**) RIC of m/z=253+ 269 of Basic Williams Soybean Cotyledon Extract

TABLE 12

Correlation Data for (-) LC-CF-LSIMS of Williams Soybean Cotyledon Extracts

UV Retention Time	Mass Spectra Scan #	Identification
5.585	35	DG
9.895	55	DGM
14.739	82	GGM

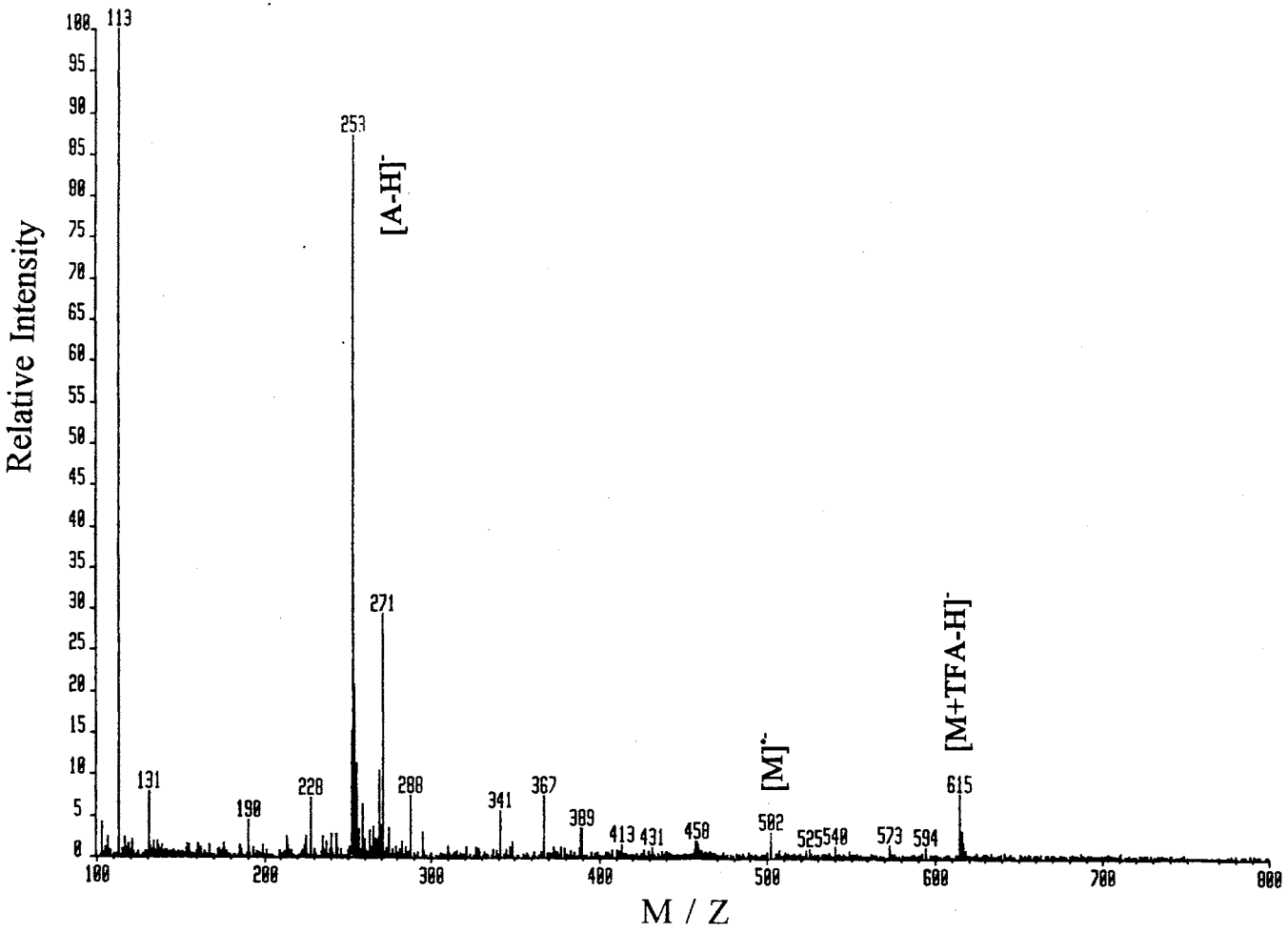

Figure 66- (-) LC-CF-LSIMS Mass Spectrum of DGM in a Basic William Soybean Cotyledon Extract

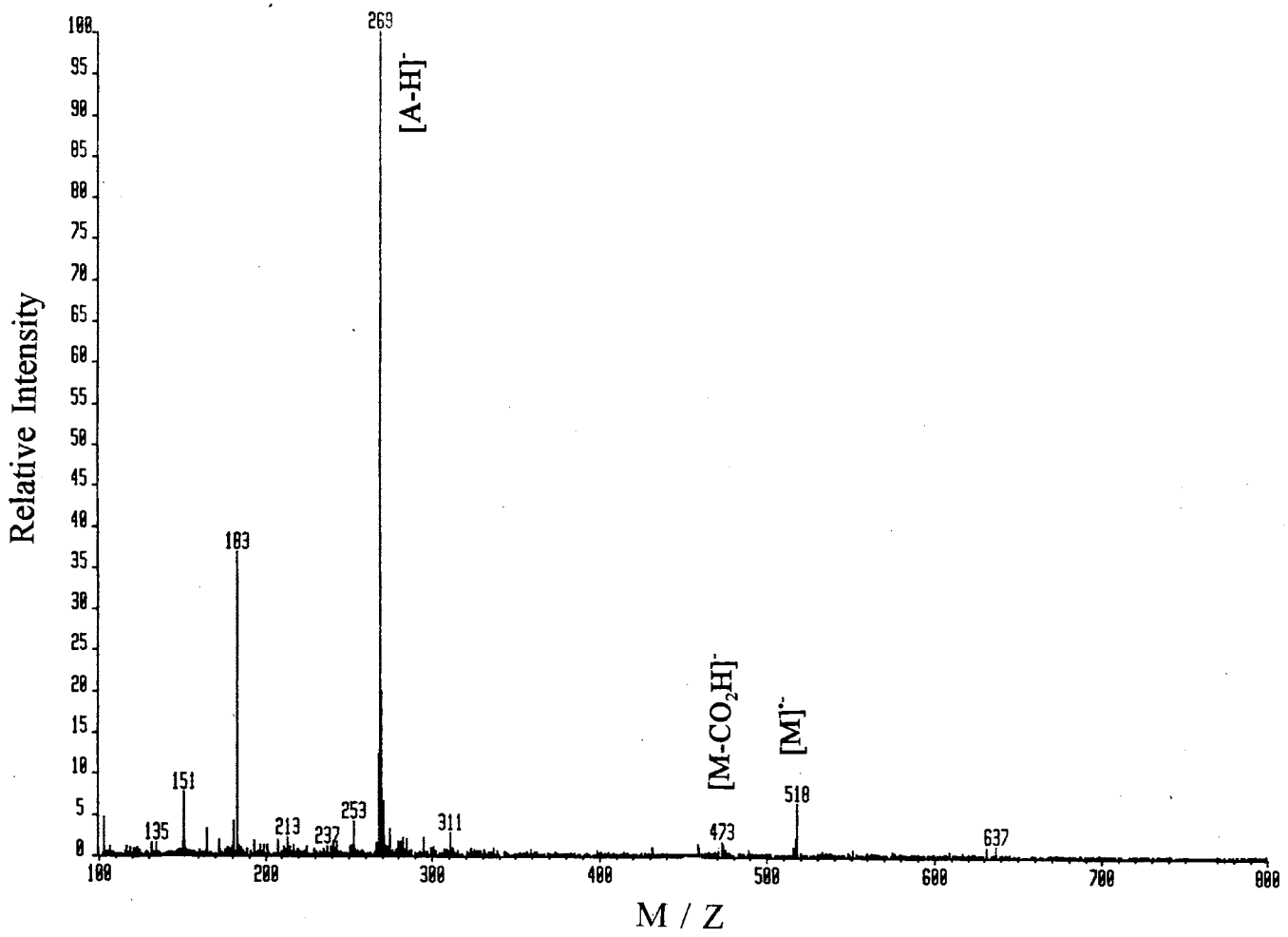

Figure 67- (-) LC-CF-LSIMS Mass Spectrum of GGM in a Basic Williams Soybean Cotyledon Extract

Negative-ion LC-CF-LSIMS analysis was also performed on extracts of 7 day old cotyledons of chickpea (Cicer arietum). Approximately 2 grams of cotyledons were extracted as described in section II.9 and the basic extract analyzed by on-line UV LC-CF-LSIMS as described in section II.4 with a 0.1% acetic acid modifier. The resultant UV chromatogram and RIC of m/z =341+255+267+269+281+283+297 are presented in Figure 68. The UV and RIC chromatogram peaks have been given numerical values that are used to correlate UV retention times to the mass spectra and are summarized in Table 13.

Three of the reported peaks have been identified by (-) LC-CF-LSIMS. The mass spectrum of peaks numbers 3, 4, and 6 are provided in Figures 69 and 70. Peak number 3 has been identified as FGM. The mass spectrum obtain for peak #3 was identical to those observed for alfalfa extracts. The presence of Biochanin A is reported in the literature [112-114]. This information aided in the identification of peak #4 as Biochanin A-7-O-glucoside (BG). A molecular ion, $[BG-H]^-$, peak was observed at m/z =445. The molecular ion peak identification was confirmed by the presence of a glycerol adduct, $[BG+GLY-H]^-$, ion peak at m/z 537. The aglycone ion, $[Bio-H]^-$, peak was present at m/z =283. Similarly, peak #6 was identified as biochanin A-7-O-glucoside-malonate (BGM). Ion peaks corresponding to the following were used in the identification of BGM: $[BGM+GLY]^-$ at m/z = 624, $[BGM]^{\bullet-}$ at m/z =532, $[BGM-CO_2H]^-$ at m/z = 487, and $[Bio-H]^-$ at m/z = 283. Ion peaks were observed in the mass spectra corresponding to the other peaks not discussed. These m/z values of these observed ions are presented in Table 13.

Three compounds are still unidentified at this time but useful data was obtained that will aid in their future identification. The LC-CF-LSIMS experiments were successful in their role in the identification of isoflavonoid conjugates in other plant systems besides alfalfa. This further emphasizes the utility of this method.

TABLE 13

CORRELATION DATA FOR (-) LC-CF-LSIMS OF A BASIC EXTRACT OF CHICK PEA COTYLEDONS

Peak #	UV Rt	MS scan #	Identification
1	16.179	86	m/z=267,299
2	18.176	97	m/z=281
3	18.975	101	FGM
4	22.275	118	BG
5	23.456	124	m/z=255,297,577, 593
6	24.505	130	BGM

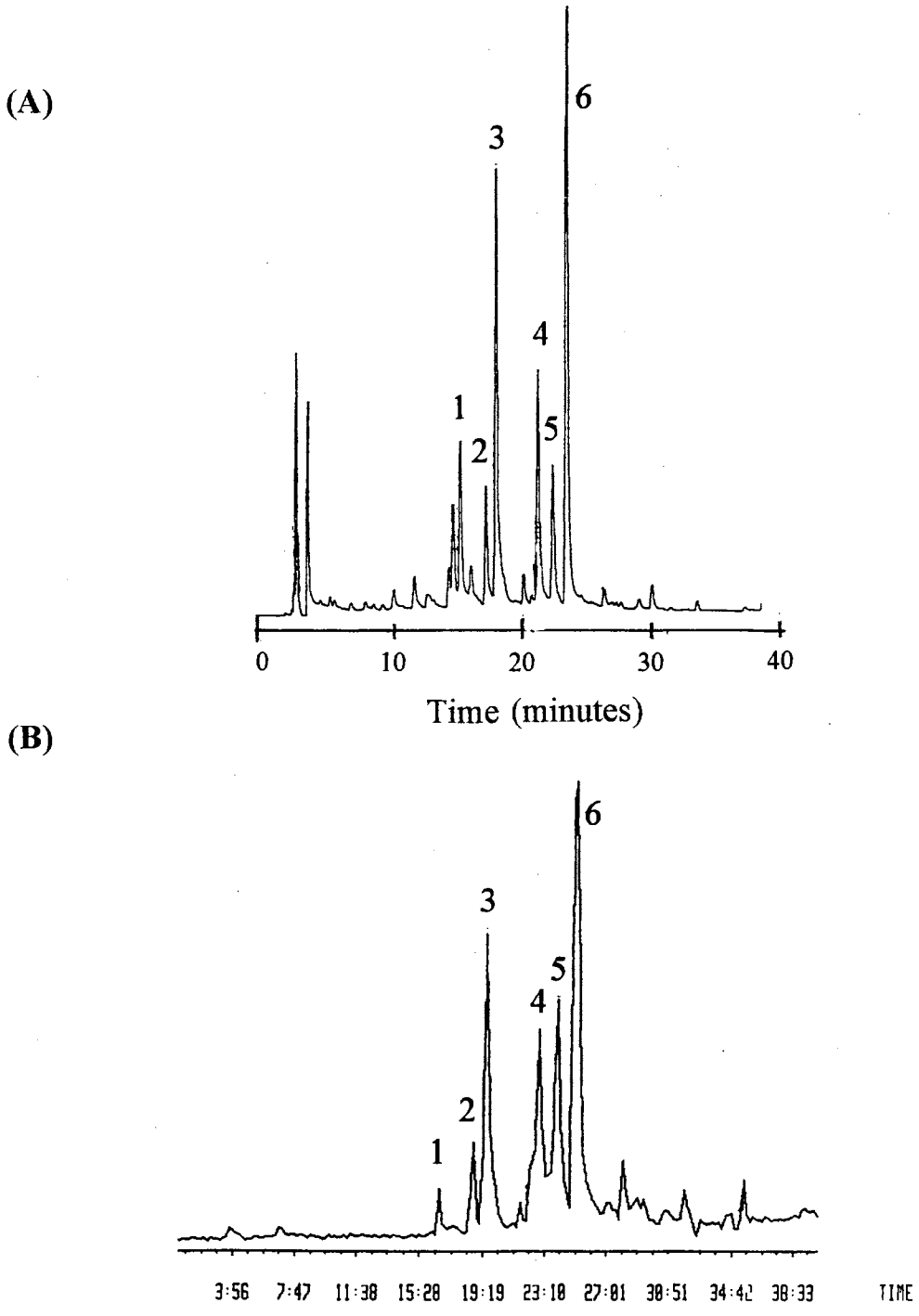

Figure 68- (**A**) On-line UV Chromatogram and (**B**) RIC of m/z=341+ 255+269+281+283+297 of Basic Chickpea Cotyledon Extract

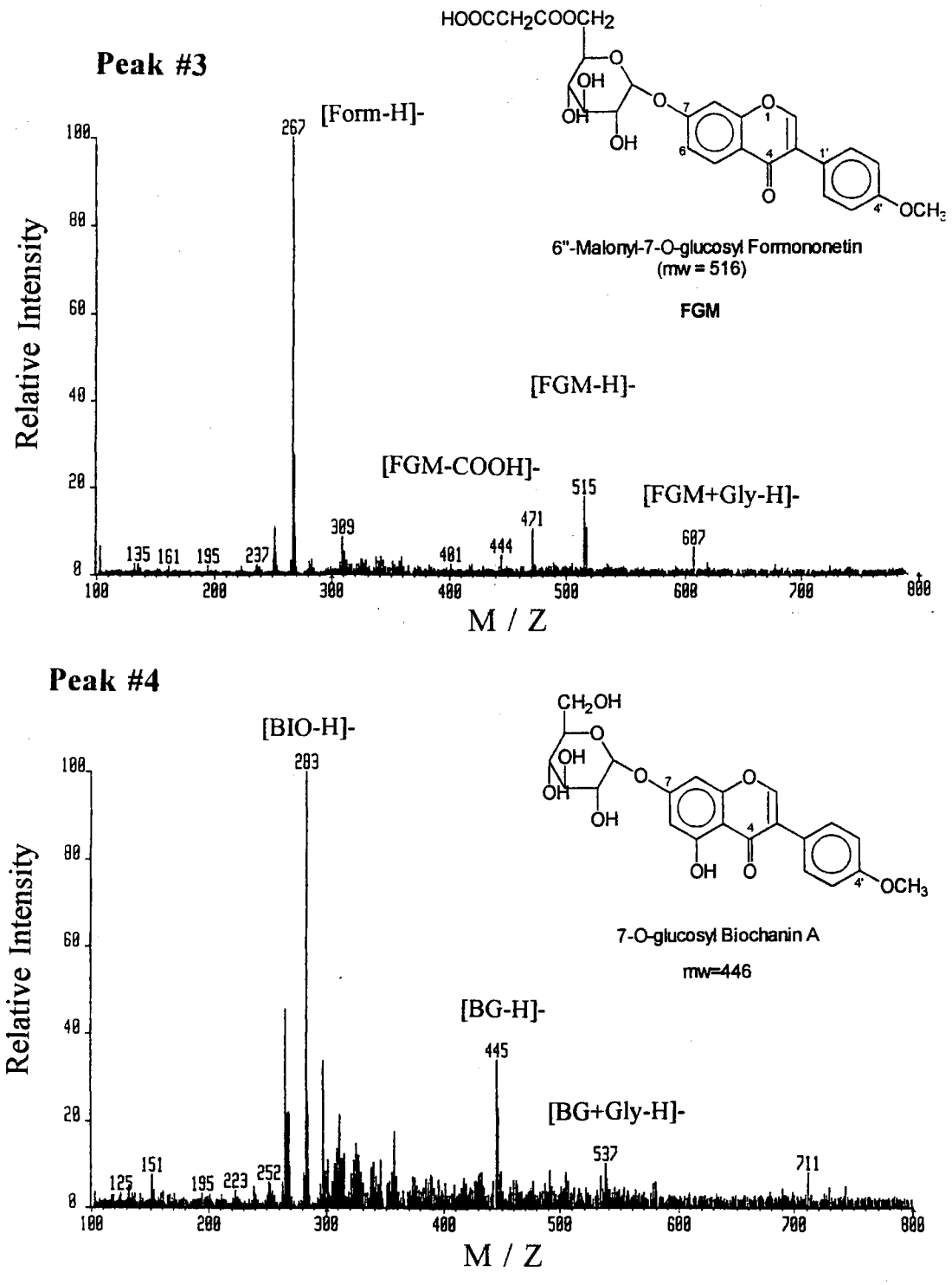

Figure 69- (-) LC-CF-LSIMS Mass Spectra of FGM and BG in a Basic Chickpea Extract

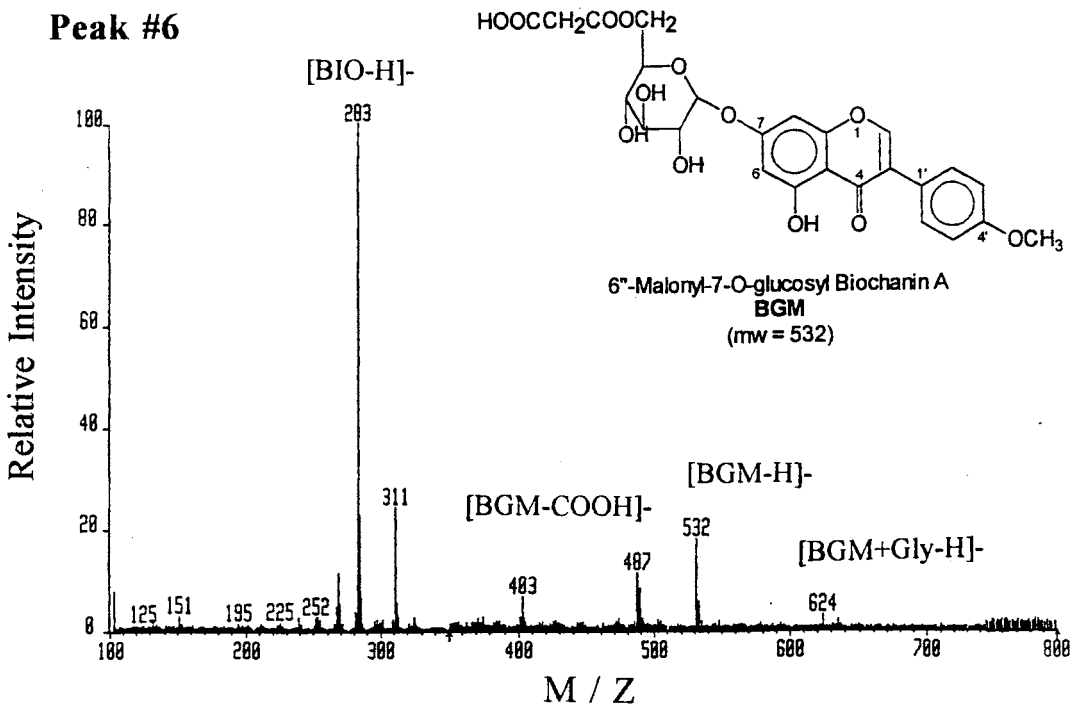

Figure 70- (-) LC-CF-LSIMS Mass Spectrum of BGM from a Basic Chickpea Cotyledon Extract

III.6 Saponins

During the (-) LC-CF-LSIMS analysis of various cultivars of alfalfa significant ion peaks were observed late in the gradient elution (i.e. 35 to 70 minutes). The ion peaks were very intense but the corresponding UV absorbance peak were rather weak. The eluting compounds are believed to be saponin derivatives which are characterized by low intensity UV absorbance. The presence of saponins in alfalfa extracts has been reported [115] which supports our suspicions. To further investigate this hypothesis a negative-ion, direct probe mass spectrum of the saponin 3-O-β-D-glucopyranosylmedicagenate (3-Glc-MA) was obtained from Mr. Paul West and is provided in Figure 71. A similar mass spectrum, which has also been identified as that of 3-Glc-MA, was obtained by analytical (-) LC-CF-LSIMS of a basic extract of calwest alfalfa is presented in Figure 72. The ion peaks observed in the (-) LC-CF-LSIMS spectrum are almost identical to those observed in the (-) DP-LSIMS mass spectrum of 3-Glc-medagenic acid. If the ion peaks observed in the (-) LC-CF-LSIMS analysis are actually saponins, then (-) LC-CF-LSIMS would provide an ideal analysis method for saponins. This method would conquer the problem encountered in HPLC detection of saponins since they show poor absorbance by UV detection.

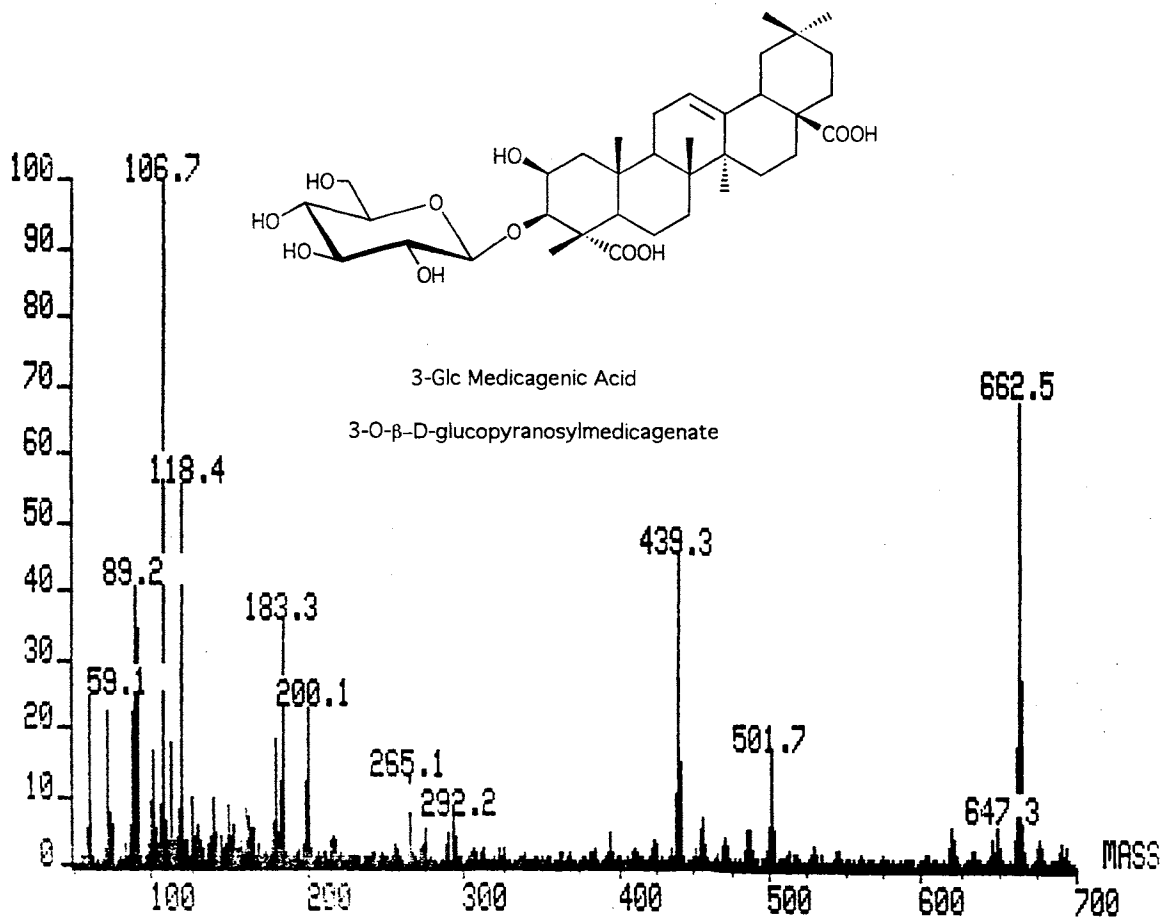

Figure 71- (-) DP-LSIMS Mass Spectrum of 3-Glc-medicagenic acid with a glycerol/thioglycerol Matrix

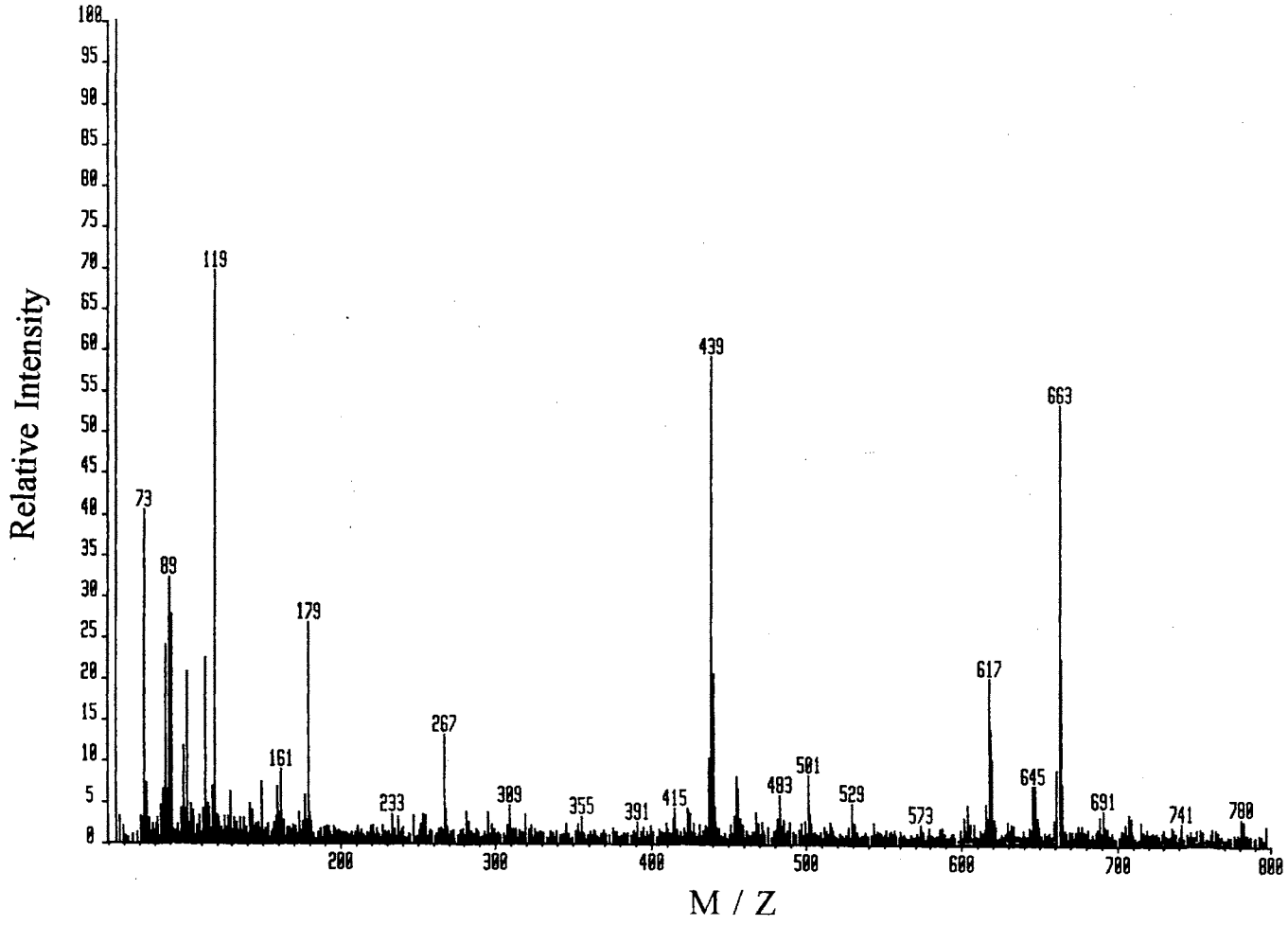

Figure 72- (-) LC-CF-LSIMS Mass Spectrum of Suspect 3-Glc-medicagenic acid

III.7 Nanoscale HPLC-CF-LSIMS

The literature reports several HPLC methods for the analysis of extracts from specific plant tissues [87,88]. One such example involves the sampling of cotyledons. These samples are obtained by removing a plug from the cotyledon and dividing it into its different tissue. These tissues include surface, subsurface, a central core material. This procedure is performed in an attempt to determine the flavonoid location in the different plant tissues. The tissues from many cotyledons are pooled and then extracted for HPLC analysis. These samples require an extensive amount of time to acquire and usually generates very small quantities (i.e. less than 2 grams) of plant material for extraction . Therefore, the waste of such samples by splitting for analytical LC-CF-LSIMS is not tolerable. These facts have prompted us to investigate nanoscale LC-CF-LSIMS of plant extracts. Nanoscale LC-CF-LSIMS analysis of these extremely small samples could be performed without waste and generate valuable mass spectral data. Thus, the purpose of our investigation into nanoscale LC-CF-LSIMS was to provide a solution to the LC/MS analysis of small quantities of plant extracts for the identification of flavonoid conjugates.

The investigation into nanoscale LC-CF-LSIMS began by packing fused silica capillaries (50 cm x 320 μm) similar to those reported in the literature [116,117]. Packing was performed on columns that had been fritted according to procedure A described in the experimental section II.6. These columns were slurry packed with isopropyl alcohol since this is a common solvent employed for packing analytical scale columns [118] which were then used for HPLC analysis. A mobile phase of

approximately 5μL/min was generated through the column by the balance column method described in section II.5. Columns that had been packed in this manner had a tendency to compress when subjected to gradient elution. Therefore, columns were then packed with a slurry solvent consisting of 59:39:2 acetonitrile, water, and glycerol [118]. This resulted in a significant decrease in compression upon gradient elution.

Two major obstacles were encountered in nanoscale HPLC. The first was detection. Most methods for nanoscale HPLC detection utilize on-column UV absorbance detection where the pathlength for on-column detectors is set by the internal diameter of the capillary used. Therefore, the pathlengths are typically between 50 and 320 μm. These short pathlengths significantly reduce the sensitivity of these detectors according to Beer's Law ($A= \varepsilon Bc$). The second major obstacle was the "fritting" of nanoscale columns. Several methods exist for fritting nanoscale columns and were discussed in section II.6. These fritting methods will be discussed below.

We were in possession of an Isco μLC-10 variable wavelength detector in which exchangeable detection cells could be placed. Due to the high cost of a commercially available detection cell, one was constructed. The constructed on-column UV detection cell for the Isco μLC-10 detector is pictured in Figure 73. This detection cell was constructed with a 3-way axis of alignment which could be adjusted to obtain optimum UV transmission through the cell. The test results obtained with this cell were insufficient due to a lack of sensitivity. Therefore, a commercial cell was purchased. The commercial cell was stationary and lacked the favorable property

of alignment. However, it did contain a collimating lens to focus the UV beam through the cell. This collimating lens considerably increased the sensitivity of the commercial detection cell as determined by removal of the lens from the cell. Therefore, our in-house constructed detection cell was modified to accept the same collimating lens. This modification significantly increased the constructed cells sensitivity. Prior to the installation of the collimating lens, UV chromatograms could not be obtained. After installation and alignment of the cell, UV chromatograms were obtained. A series of solutions containing decreasing concentrations of rutin were then injected to quantitate the detection cell's performance. These experiments were performed with a constant flow of a mobile phase composed of acetonitrile, water, and glycerol (59:39:2) at 5 μL/min. The mobile phase was provided by an Isco μLC-500 syringe pump. A detection limit of 1.0 n rutin was determined at a S/N ratio of 3. A similar experiment was performed utilizing the commercial detector that yielded a higher detection limit. This increase in sensitivity was postulated to be the result of a larger pathlength cross-section diameter and 3-way alignment of the constructed on-column detection cell. The pathlength cross-section diameter was approximately 0.180 mm for the constructed detection cell compared to that of the commercial cell with a pathlength cross-section diameter of 0.050 mm. This larger pathlength cross-section diameter provided a greater transmission of UV light through the cell. However, the commercial detection cell showed less variance in the baseline during gradient elution HPLC.

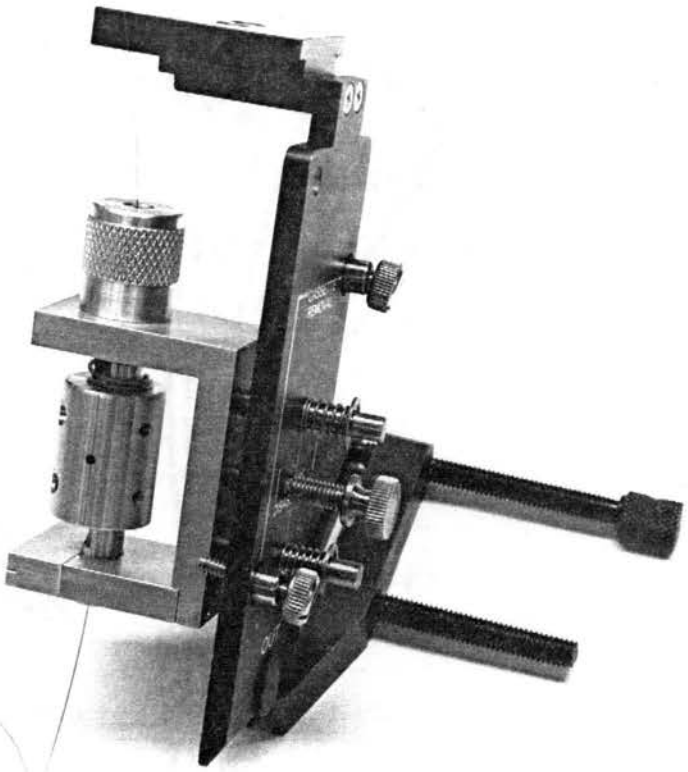

Figure 73- Photograph of the Constructed Nanoscale Detection Cell

Once the obstacle of detection was conquered investigations into nanoscale column preparation were pursued. Although, procedure A for column fritting was convenient, it could be visually observed that the frit had a large relative volume. The V-shape of the connector only allowed the capillary to be inserted a limited distance determined by its outside diameter of the capillary. Nanoscale columns fritted in this manner usually contained a frit approximately 1 cm long and 150 μm diameter.

Therefore, a procedure B using a glass sleeve was preferred. This method used a glass sleeve with an inside diameter approximately equal to the outside diameter of the fused silica capillary being packed. The glass sleeve was made by stretching a heated piece of glass capillary to the appropriate internal diameter. This procedure yielded frits approximately 1 mm in length by 320 μm in diameter.

A 15 cm x 320 μm nanoscale column was fritted with a glass sleeve and packed with 5 μm Xpertek ODS particles. This column was first washed with a constant flow of 95:5 of solvent A:B described in section II.4. The column was then conditioned by several gradient HPLC runs also described in section II.4. Three repetitive gradient HPLC analysis were then performed on a pooled basic alfalfa extract. These experiments were performed to determine the reproducibility of retention times. A chromatogram of the third analysis is provided in Figure 74. The retention times of 10 peaks observed in the three consecutive gradient elution analysis of the pooled alfalfa extract were recorded and are provided in Table 14. The standard deviation of each series of peak retention times was then calculated and is also presented in Table 14. The range of standard deviations was 0.080 min to 0.933 minutes corresponding to 0.54% to 12.69%. The average standard deviation of peaks number 1 through 10 is 6.57%. This illustrates a good degree of reproducibility. Furthermore, the columns showed a promising efficiency.

Additional attempts t pack 15 to 30 cm in length fused silica capillaries by procedure A with 3 μm ODS particles were performed. Flow rates of 5 μL/min could not be obtained with these columns since they produced a backpressure in excess of

5000 p.s.i. which was the pressure limit of the gradient pump. Therefore, further investigations of these columns was discontinued.

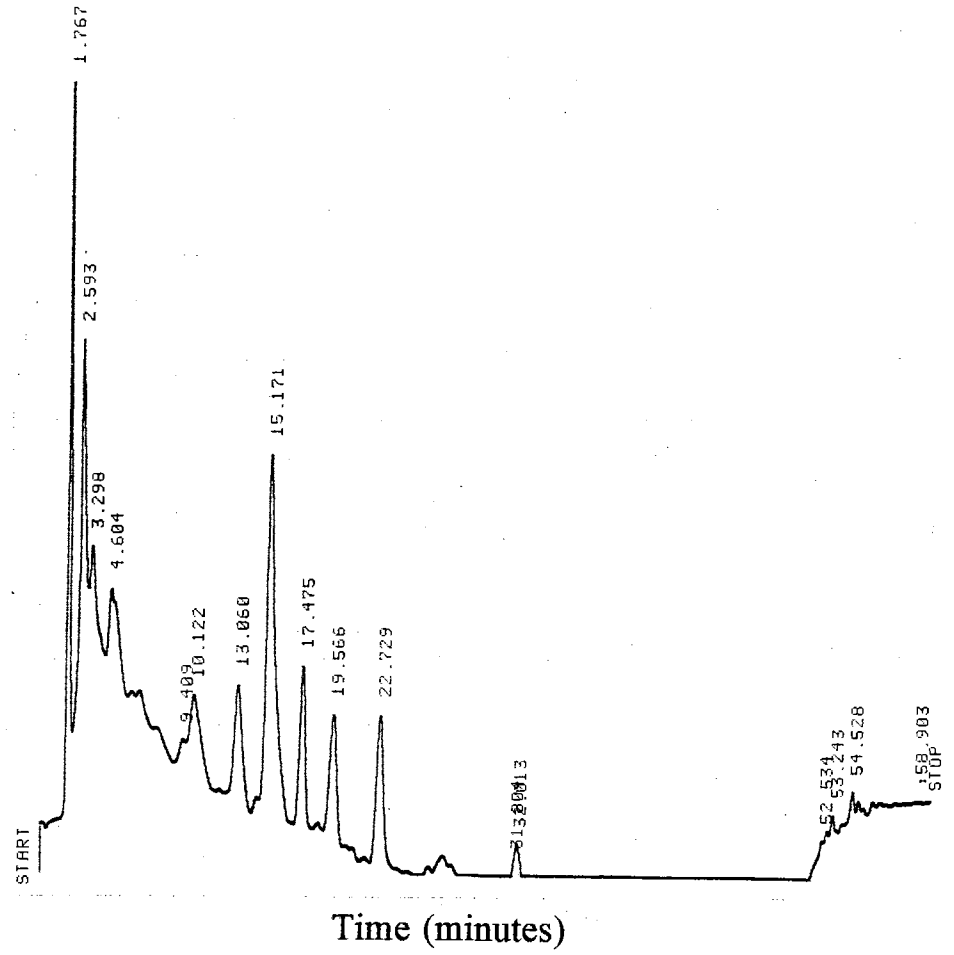

Figure 74- UV Chromatogram of Pooled Alfalfa Extract Obtained by Gradient Elution Nanoscale HPLC with 15 cm x 320 µm, ODS Packed Fused Silica Capillary Column

TABLE 14

REPRODUCIBILITY STUDY OF RETENTION TIMES FOR A NANOSCALE HPLC COLUMN

Peak #	Run #1	Run #2	Run #3	Mean	STDV	STDV %
1	1.67	1.608	1.767	1.682	0.080	4.75
2	2.354	2.268	2.593	2.405	0.168	6.99
3	2.755	---	3.298	3.027	0.384	12.69
4	3.754	3.409	4.604	3.922	0.615	15.68
5	8.802	---	10.122	9.462	0.933	9.86
6	12.081	12.229	13.060	12.457	0.528	4.24
7	14.442	14.572	15.171	14.728	0.389	2.64
8	16.989	17.160	17.475	17.208	0.247	1.44
9	19.310	190372	19.566	19.416	0.134	6.90
10	22.489	22.585	22.729	22.601	0.121	0.54
AVE STDV						6.52

To gain the durability of stainless steel capillary columns, procedure B and D were investigated for packing and fritting nanoscale HPLC columns. All attempts to pack stainless steel columns were unsuccessful. This was attributed to the imperfections of the internal walls of the stainless steel capillaries. Stainless steel analytical column interior walls are highly polished which promotes even packing. This was not the case for the stainless steel capillaries used. As a result of the imperfections in the stainless steel capillaries, channeling was postulated to be present.

Finally procedure C was investigated for fritting capillary columns. This method provided a quick and efficient method of column fritting and resembles the methods employed for commercial analytical columns. The frits in this method had the added benefit of being reusable. This method was found to give the best results and examples are presented below.

III.8 Nanoscale (-) LC-CF-LSIMS of Plant Extracts

Nanoscale (-) LC-CF-LSIMS was performed on the basic extract of Forrest soybean (*Glycine max*) cotyledons. The cotyledons were extracted and fractionated as described in section II.9. Gradient LC-CF-LSIMS analysis was performed with a 0.5 % acetic acid modifier. The balance column method was used to generate a flow rate of approximately 3 μL/min through the nanoscale column as described in section II.5. Due to the low flow rate being delivered into the mass spectrometer, the source block and probe tip were maintained at room temperature. The lower source and probe temperatures were used in an attempt to keep the probe tip from going "dry". The

nanoscale column utilized was a 75 cm x 250 μm packed fused silica capillary column. The column was slurried packed with 5 μm, Xperteck, ODS particles described in section II.9.

The UV chromatogram obtained at 287 nm is presented in Figure 75. Two major peaks were observed in the UV chromatogram at 26.463 and 31.722 minutes. These peaks correspond to mass spectra number 144 and 171 respectively. The mass spectra are presented in Figure 76. The mass spectrum of scan #144 was identified as that of DGM while the mass spectrum of scan #171 has been identified as that of GGM. The rationale and observed ion peaks used to identify these compounds were similar to those reported in section III.5.9 for Williams soybean analyzed by analytical (-) LC-CF-LSIMS. However, adduct ion peaks of the molecular ion and TFA were not observed, since an acetic acid modifier was used in this experiment.

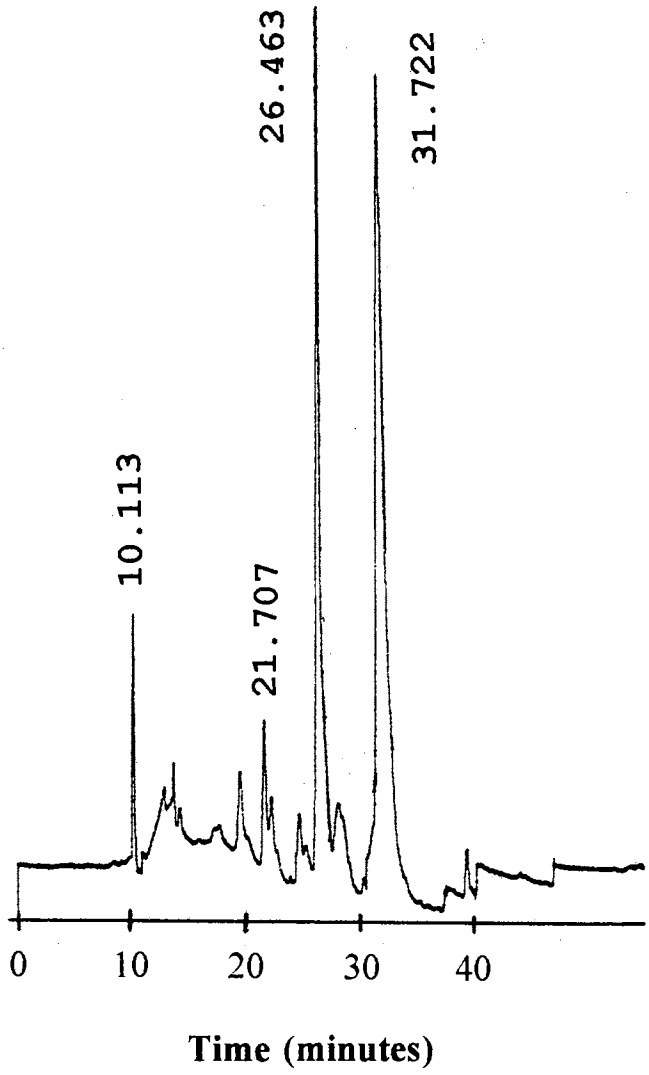

Figure 75- On-line UV Chromatogram of Nanoscale (-) LC-CF-LSIMS Analysis of a Basic Williams Soybean Cotyledon Extract.

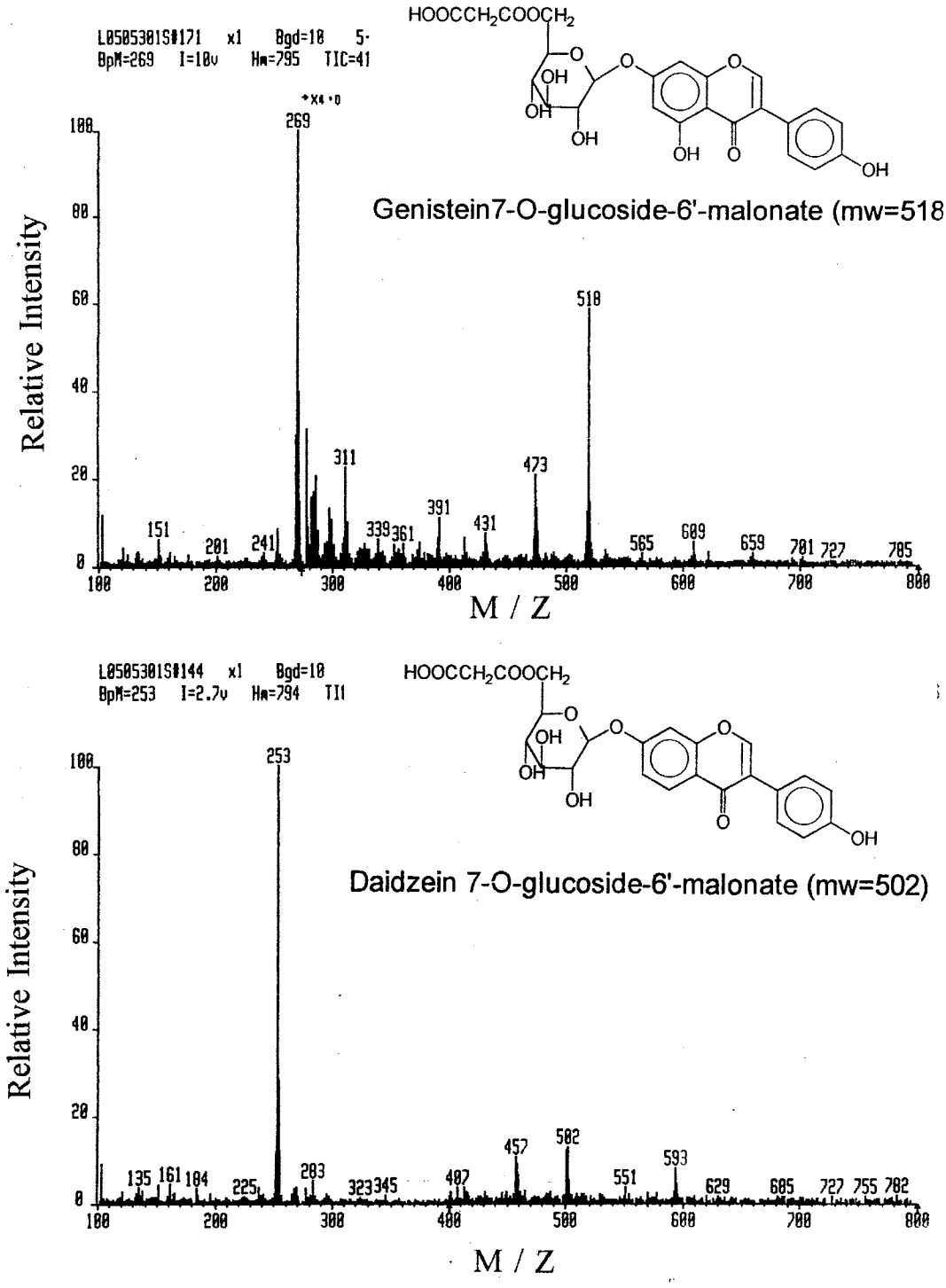

Figure 76- Nanoscale (-) LC-CF-LSIMS Mass Spectra of GGM and DGM in Basic Williams Soybean Cotyledon Extracts

An additional 50 cm x 250 μm nanoscale HPLC column was packed by procedure C with 5 μm, BakerBond ODS in an attempt to simulate the retention times obtain with a 4.6 mm x 250 mm, 5 μm, ODS BakerBond column. Gradient elution, nanoscale (-) LC-CF-LSIMS was then performed using the balance column method presented in section II.5. The basic extract of chickpea (*Cicer arietum*) cotyledons were subjected (-) LC-CF-LSIMS. The cotyledons were extracted and fractionated as described in section II.9. An injection of an amount equal to the extract of approximately 100 mg of plant material was performed. The resultant UV chromatogram is presented in Figure 77. The peaks have been labeled with roman numerals to simplify the discussion. A table presenting the abbreviations used with their appropriate chemical names is presented in Table 15. A table correlating the peak numbers, mass spectral data, and tentative identification is provided in Table 16. The mass spectra of peak numbers I through X are presented in Figures 78 through 81. The rationale utilized for the identification of these compounds has been previously presented. Therefore, and in depth discussion of observed ion peaks will not be presented. The identification of peaks in the UV chromatogram of this extract were based on the mass spectra and literature reports, but should be confirmed with additional instrumental methods. Other instrumental methods could possibly differentiate between isomers were MS is somewhat limited.

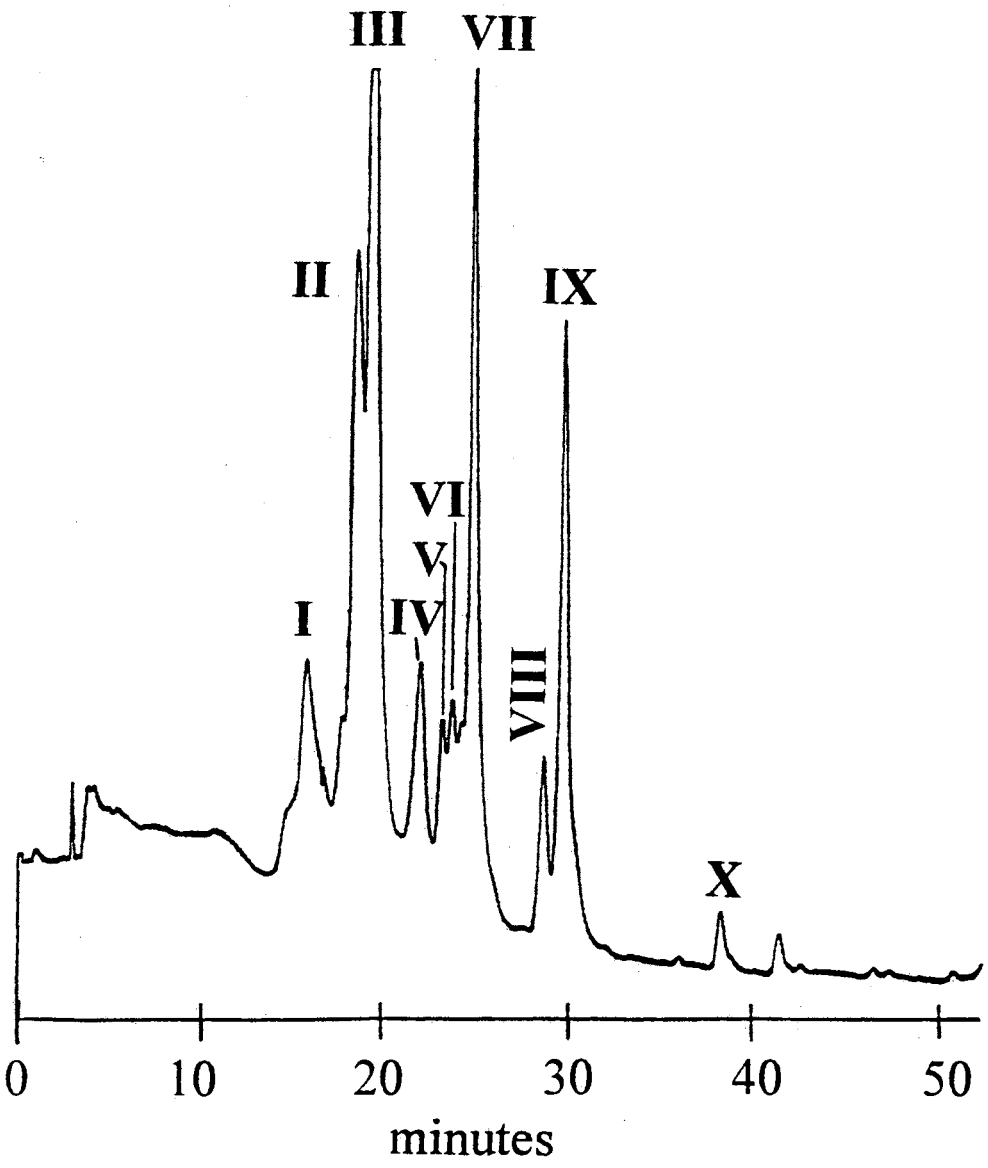

Figure 77- On-line UV Chromatogram For The Nanoscale (-) LC-CF-LSIMS Of A Basic Chickpea Extract

TABLE 15

IDENTIFICATION OF PEAKS IN THE NANOSCALE (-) LC-CF-LSIMS ANALYSIS OF A BASIC CHICKPEA EXTRACT

Peak #	Abbrv.	Name
I.	**FG**	7-O-glucoside formononetin
II.	**PGM**	7-O-glucoside-6'-malonyl pseudobaptiogenin
III.	**FGM**	7-O-glucoside-6'-malonyl Formononetin
IV.	**MaGM**	7-O-glucoside-6'-malonyl Maackiain
V.	**IGM**	7-O-glucoside-6'-malonyl trihydroxychalcone (Isoliquiritigenin)
VI.	**MeBGM**	7-O-glucoside-6'-malonyl-5-methyl Biochanin A
VII.	**BGM**	7-O-glucoside-6'-malonyl Biochanin A
VIII.	**Pseud**	Pseudobaptiogenin
IX.	**Form**	Formononetin
X.	**Bio A**	Biochanin A
	MeBio A	5-methyl-Biochanin A

TABLE 16

CORRELATION DATA FOR THE NANOSCALE (-) LC-CF-LSIMS ANALYSIS OF A BASIC CHICKPEA EXTRACT

Correlation Table

PEAK	UV R_t	MS predicted R_t	Observed R_t	Scan	Identity
I	15:30	16:18	16:05	#84	**FGM**
II	18:13	19:04	19:08	#100	**PGM**
III	19:06	19:54	19:54	#104	**FGM**
IV	21:45	22:33	22:35	#118	**MaGM**
V	23:00	23:48	23:56	#125	**IGM**
VI	23:30	24:18	24:19	#127	**MeBGM**
VII	24:42	25:30	25:27	#133	**BGM**
VIII	28:28	29:16	29:17	#153	**Psued**
IX	29:31	30:19	30:15	#158	**Form**
X	38:03	38:51	38:52	#203	**Bio A**

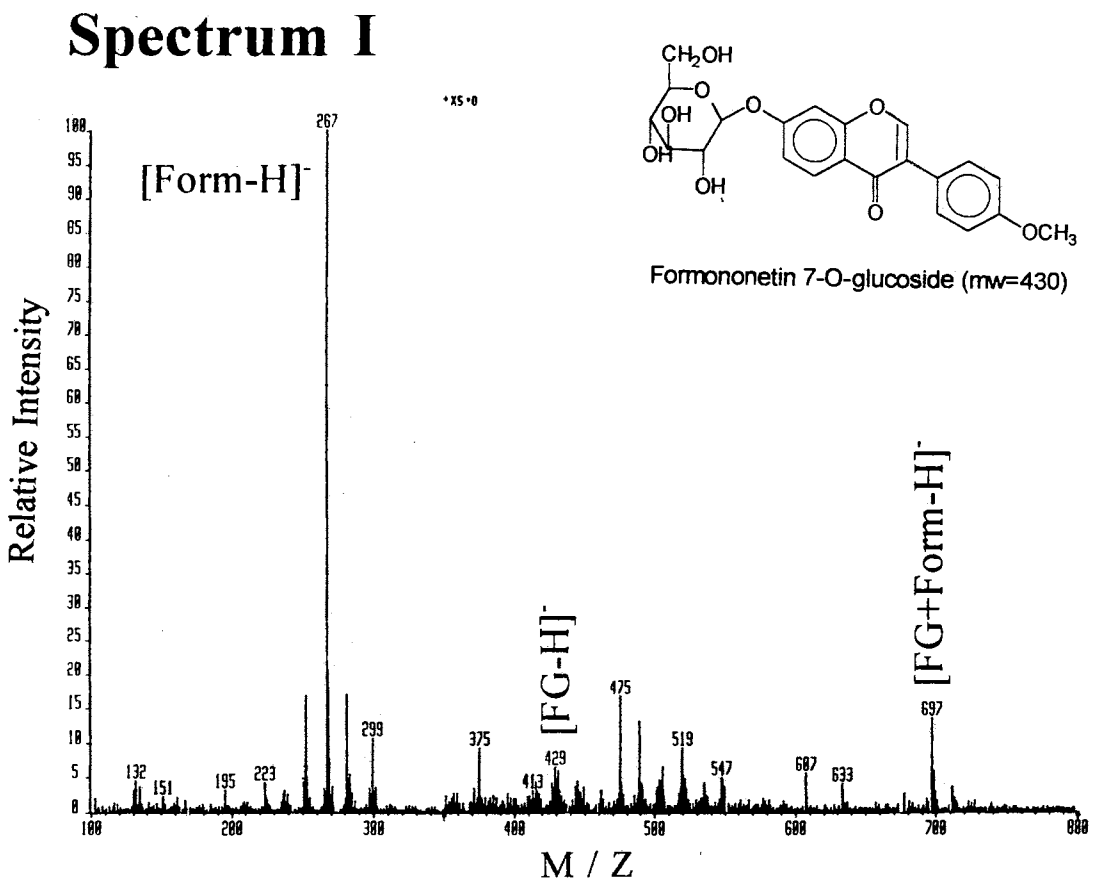

Figure 78- Nanoscale (-) LC-CF-LSIMS Mass Spectrum of Peak #I of a Basic Chickpea Cotyledon Extract

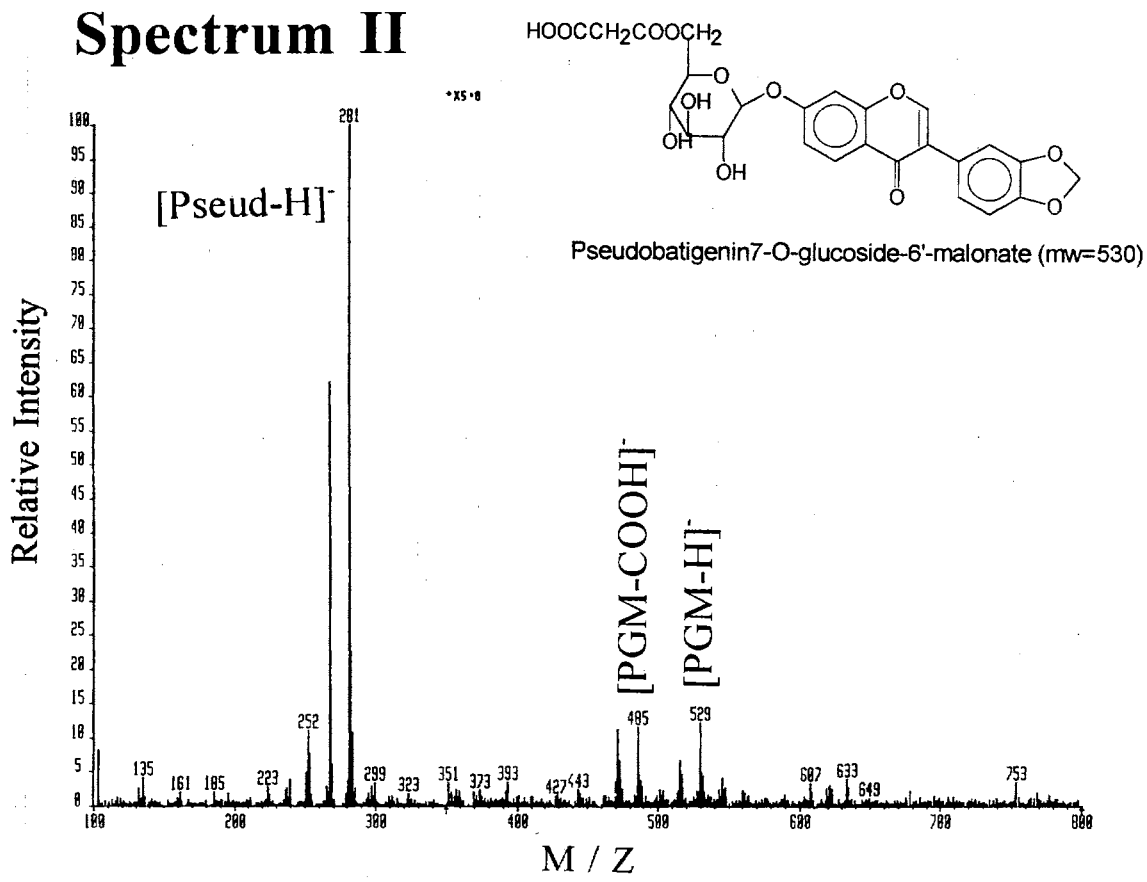

Figure 79- Nanoscale (-) LC-CF-LSIMS Mass Spectrum of Peak #II of a Basic Chickpea Cotyledon Extract

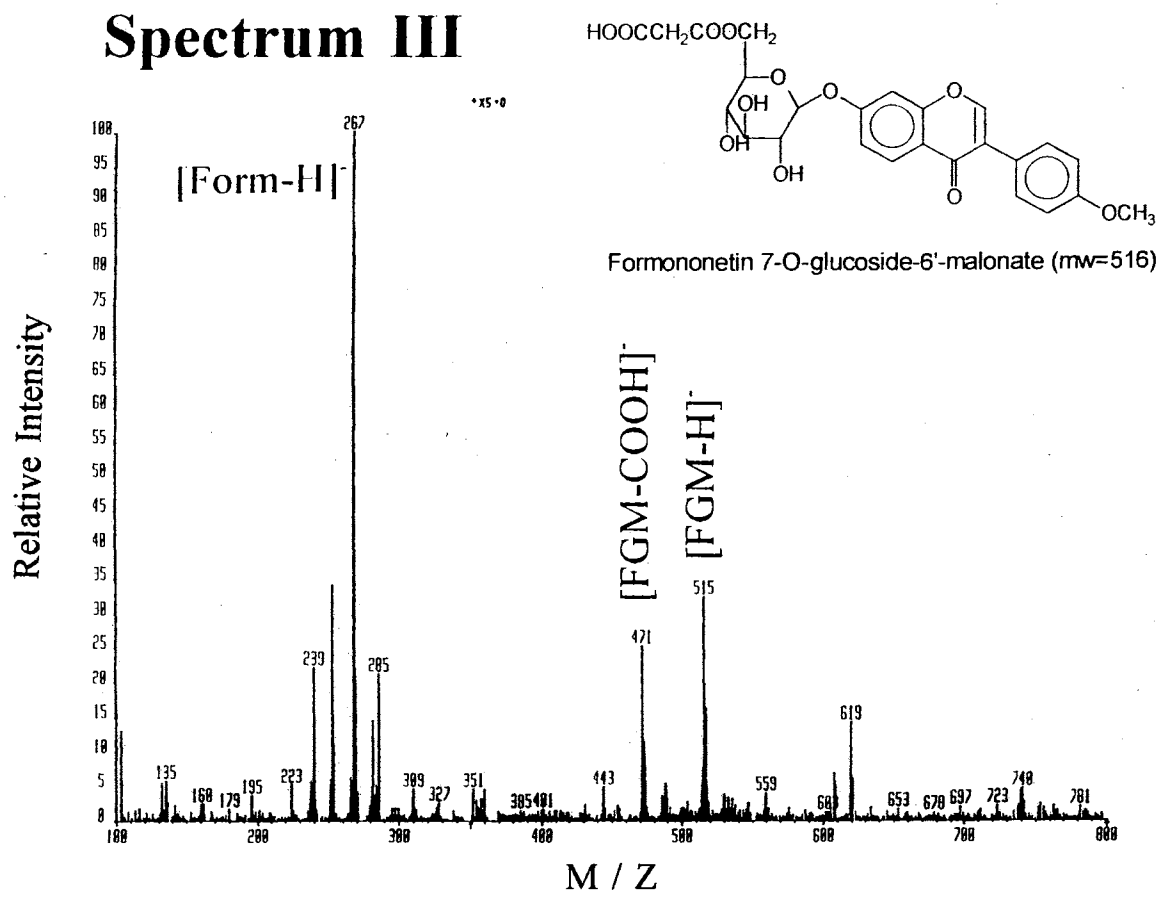

Figure 80- Nanoscale (-) LC-CF-LSIMS Mass Spectrum of Peaks #III of a Basic Chickpea Cotyledon Extract

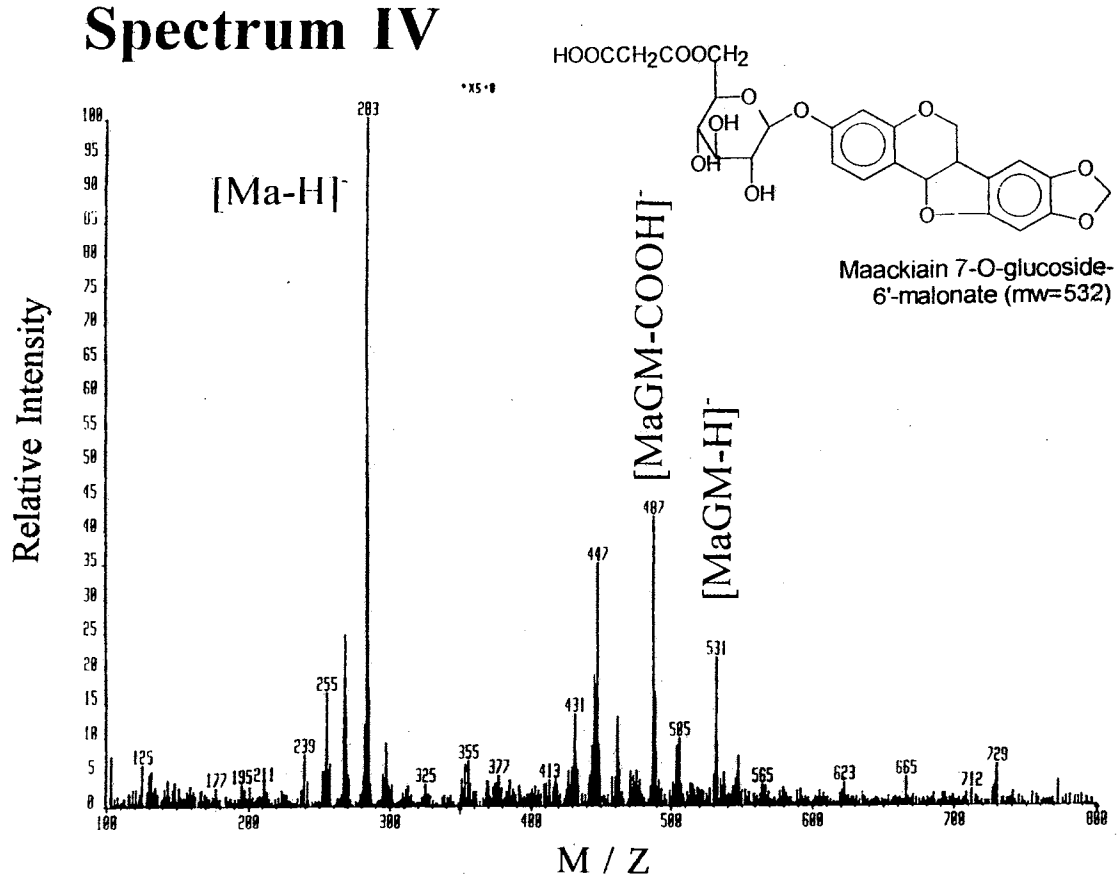

Figure 81- Nanoscale (-) LC-CF-LSIMS Mass Spectrum of Peaks #IV of a Basic Chickpea Cotyledon Extract

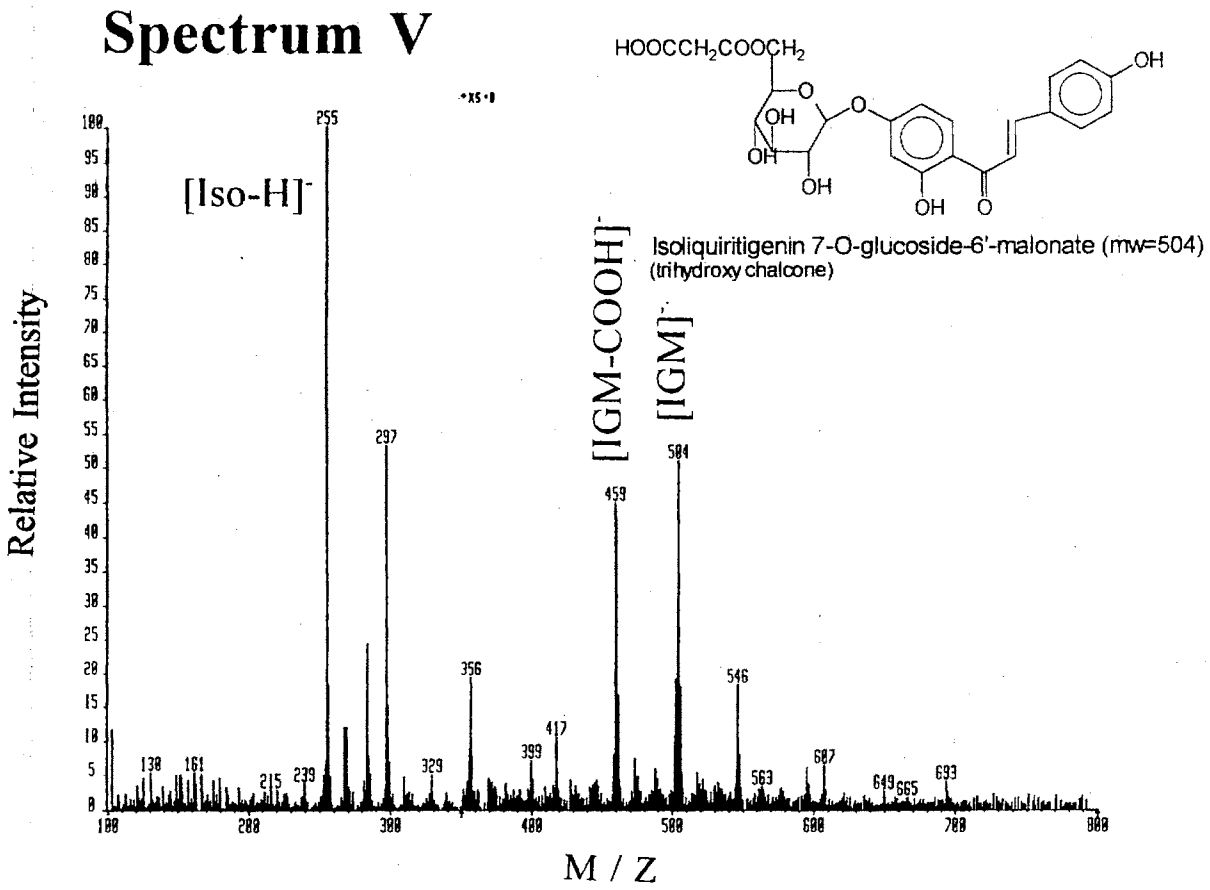

Figure 82- Nanoscale (-) LC-CF-LSIMS Mass Spectrum of Peaks #V of a Basic Chickpea Cotyledon Extract

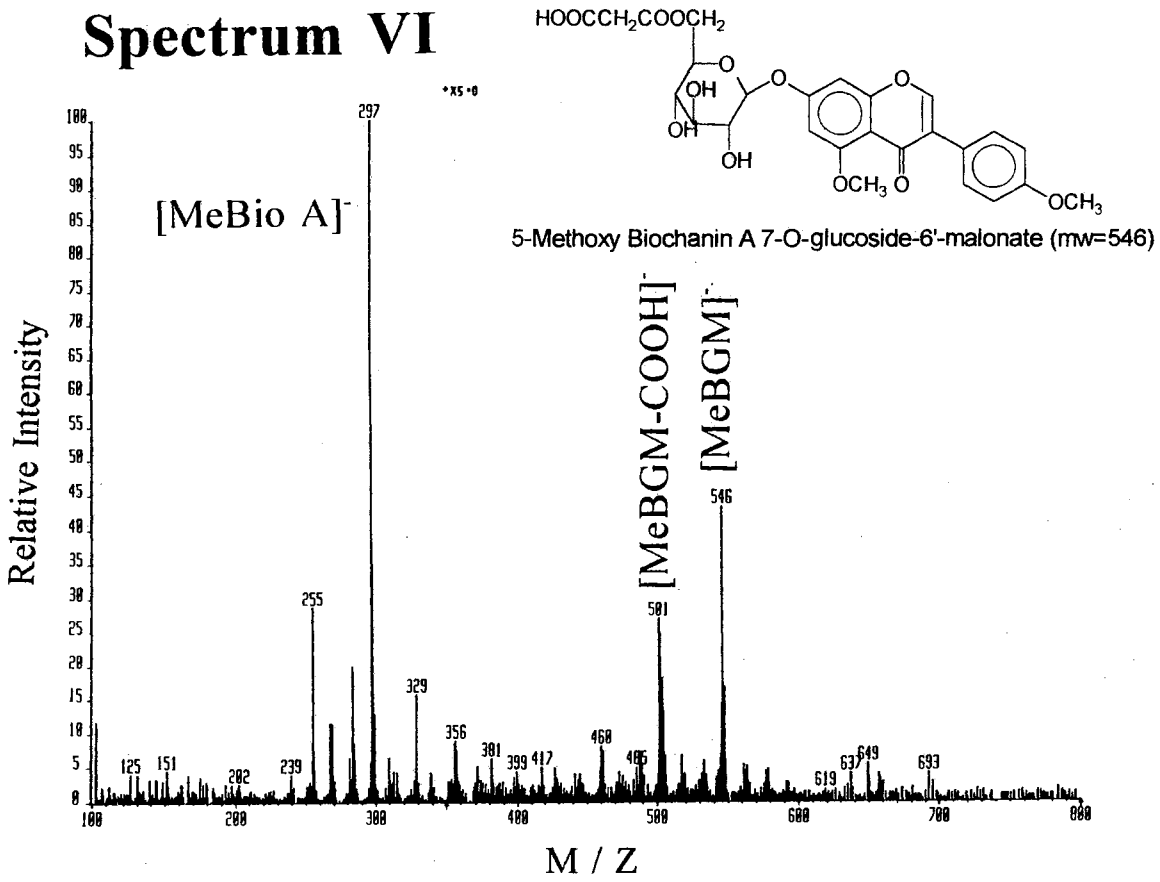

Figure 83- Nanoscale (-) LC-CF-LSIMS Mass Spectrum of Peaks #VI of a Basic Chickpea Cotyledon Extract

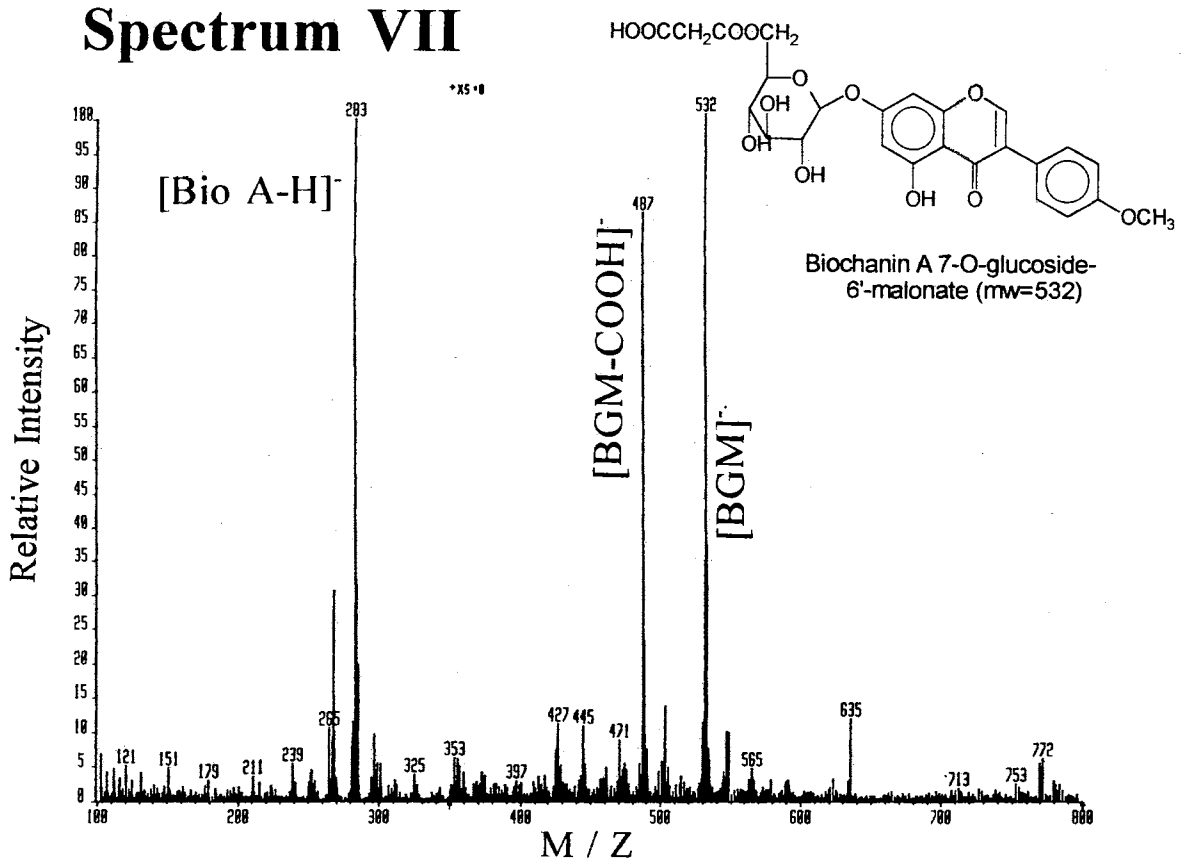

Figure 84- Nanoscale (-) LC-CF-LSIMS Mass Spectrum of Peaks #VII of a Basic Chickpea Cotyledon Extract

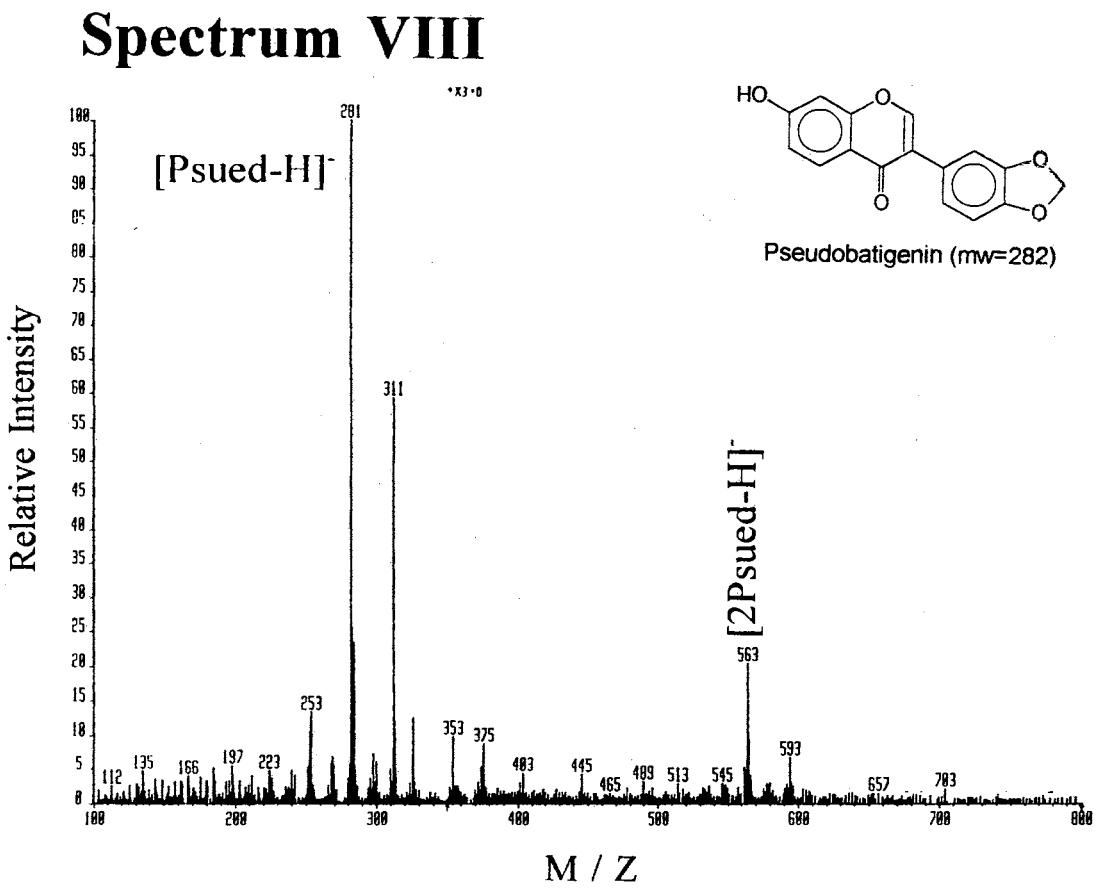

Figure 85- Nanoscale (-) LC-CF-LSIMS Mass Spectrum of Peaks #VIII of a Basic Chickpea Cotyledon Extract

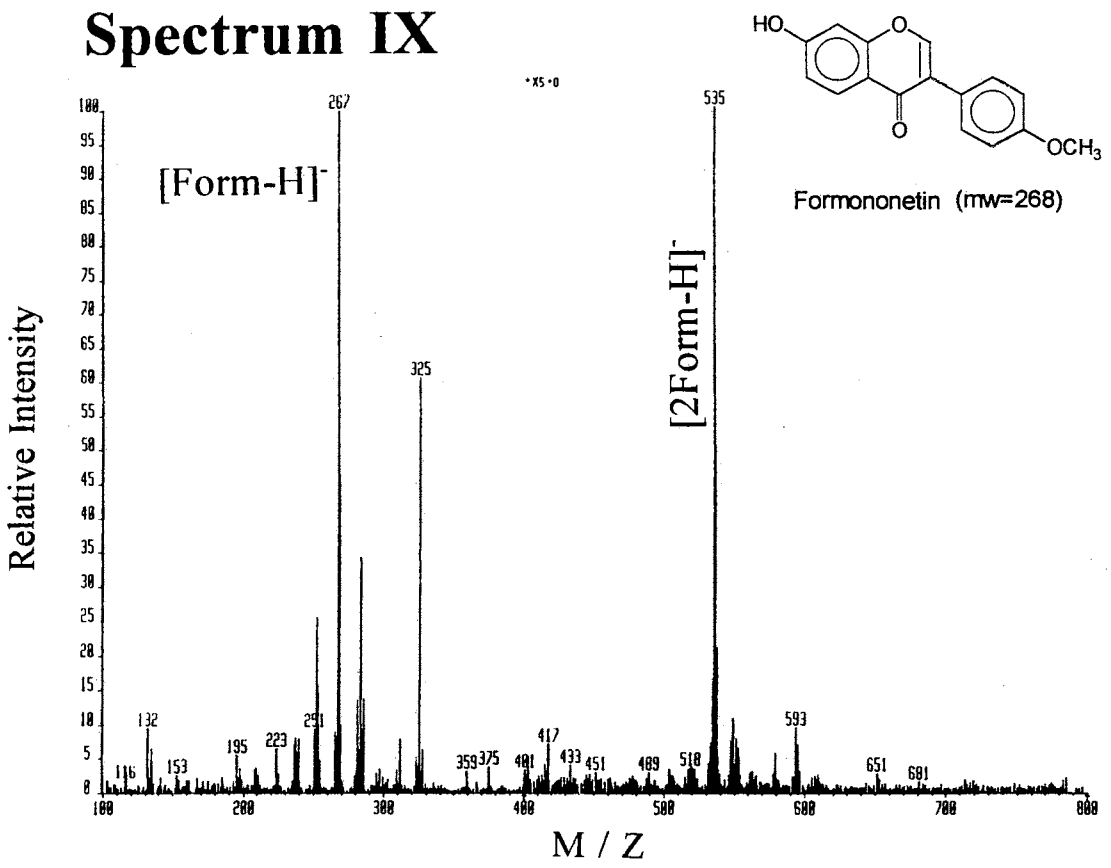

Figure 86- Nanoscale (-) LC-CF-LSIMS Mass Spectrum of Peaks #IX of a Basic Chickpea Cotyledon Extract

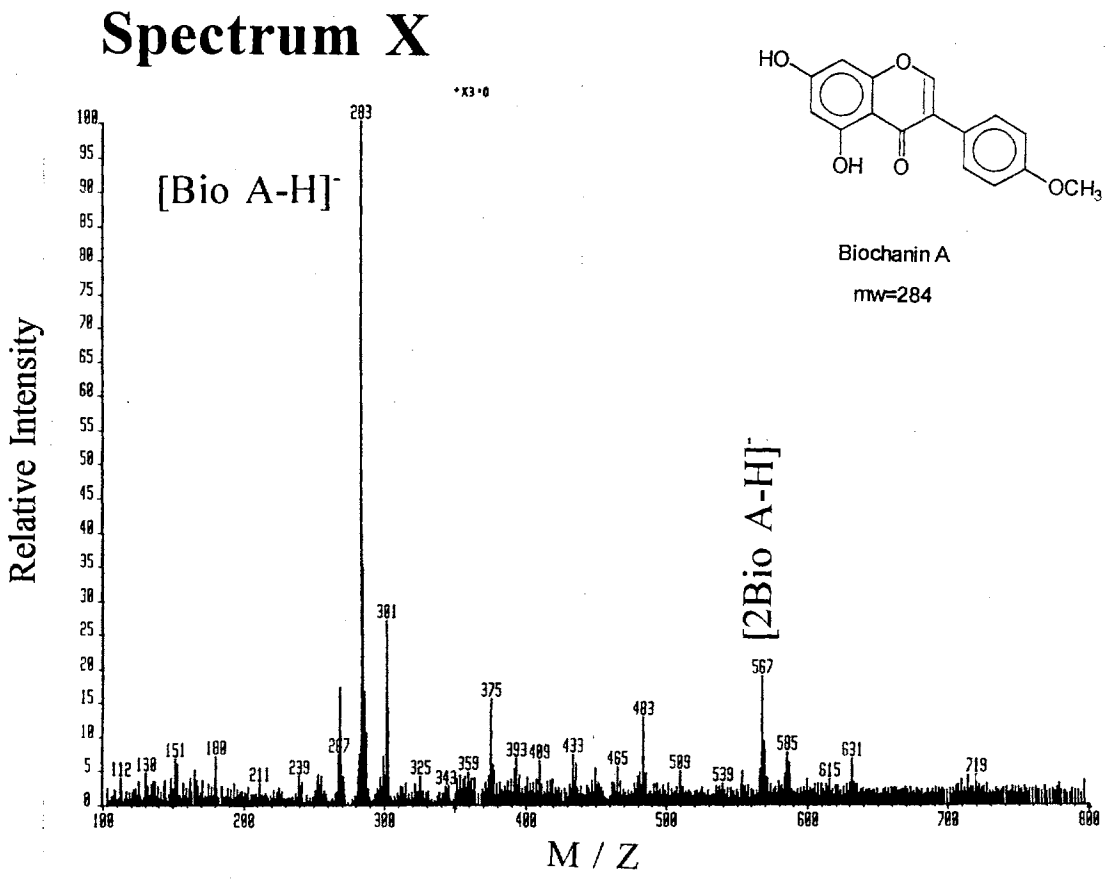

Figure 87- Nanoscale (-) LC-CF-LSIMS Mass Spectrum of Peaks #X of a Basic Chickpea Cotyledon Extract

CHAPTER IV

CONCLUSION

The project presented in this thesis focused on the development of mass spectrometry techniques that would aid in the identification of flavonoid conjugates isolated from plant extracts.. The project investigated many MS techniques which included: direct probe EI, GC/MS, (+) DP-LSIMS, (+) and (-) flow-injection CF-LSIMS, (+) and (-) analytical LC-CF-LSIMS, (-) tandem LC-CF-LSIMS, and nanoscale (-) LC-CF-LSIMS. Due to the poor results obtained for the initial direct probe and GC/MS experiments utilizing EI ionization, the investigation was turned towards DP-LSIMS and CF-LSIMS. The techniques were studied in an attempt to gain from the benefits of these techniques as discussed in the introduction. A study was performed that compared DP-LSIMS and CF-LSIMS using model flavonoid conjugates. The results of this comparison showed that an approximate 5 fold decrease in the limit of detection could be obtained by the use of CF-LSIMS over DP-LSIMS. Positive and negative-ion CF-LSIMS were then performed to characterize the mass spectra of model flavonoid conjugates. This characterization provided the basis for identification of unknown flavonoid conjugates in plant extracts. The investigation then focused on the reproducibility of the CF-LSIMS operated in the

flow-injection mode. This experiment calculated a standard deviation of 5.91% in the areas of peaks observed in a SIR chromatogram which was generated by 10 repetitive injections of 2.5 μg of rutin. The low standard deviation demonstrated CF-LSIMS to be a very reproducible means for the determination of flavonoid conjugates. The project further investigated instrumental parameters encountered during normal CF-LSIMS operation. A systematic optimization of these parameters was performed to determine the optimum conditions for the CF-LSIMS determination of flavonoid conjugates. These instrumental parameters included the concentration of glycerol in the mobile phase, source temperature, acceleration voltage, and primary ion energy. The optimization experiments were original in the sense that no such optimizations have been reported for CF-LSIMS performed on a VG ZAB2-SE. The results of the optimization experiments provided a dramatic increase in the MDQ's of the model flavonoid conjugates and yielded a MDQ of 1.0 ng for rutin. This was the determining factor to continue further studies. The low MDQ illustrated that useful mass spectrometric data could be readily obtained for naturally occurring quantities of flavonoid conjugates in plant extracts.

The information gained through the characterizations and optimizations were then applied to LC-CF-LSIMS. The utilization of LC-CF-LSIMS allowed the coupling of an on-line separation technique immediately followed MS. This minimized the decomposition of the flavonoid conjugates previously encountered during fraction collection followed by MS analysis. Both positive and negative-ion LC-CF-LSIMS were illustrated as useful means for the identification of flavonoid conjugates in

alfalfa. Full-scanning LC-CF-LSIMS and tandem LC-CF-LSIMS were also used to solve a substantial analytical problem. The problem arose due to the identification of a suspect isoflavonoid conjugate as AGM from (+) DP-LSIMS data. Although the first LC-CF-LSIMS analysis provided the true identification of the suspect isoflavonoid conjugate as FGM, extensive LC-CF-LSIMS experiments were performed to sufficiently negate the identification of the suspect isoflavonoid conjugate as AGM and confirm its identification as FGM. The ability of the LC-CF-LSIMS technique to solve the AGM controversy best justifies this project.

LC-CF-LSIMS was also used to identify flavonoid conjugates in other plant systems to further document the technique's application range. The project concluded with the development of nanoscale LC-CF-LSIMS. This method was shown to be a very useful technique in the analysis of small quantity extracts generated from as little as 100 mg of plant material. Nanoscale LC-CF-LSIMS eliminated the sample waste encountered in traditional analytical HPLC-CF-LSIMS which saved a significant amount of time, material, and cost necessary for sample preparation. Furthermore, nanoscale LC-CF-LSIMS yielded high quality MS data for the limited sample quantities when traditional LC-CF-LSIMS would have failed.

The author would like to suggest several paths for expansion or continuation of the presented project. The first expansion would involve the utilization of on-line UV/ visible diode array detection. This would provide an additional qualitative dimension for the identification of unknown flavonoid compounds since the use of UV spectroscopy in the identification of flavonoids has been extensively documented

[78,79]. This modification could be achieved at a relatively low cost when compared to the cost of mass spectrometers. Other routes for suggested research would include continued efforts into tandem LC-CF-LSIMS/MS. This technique is very instrumentally difficult but could provide solutions to many problems.

Future research should also include a comparison of the presented LC-CF-LSIMS method for identification of flavonoid conjugates to other LC/MS techniques such as ESI, APCI, and TSP. Thermospray is suggested since the literature does provide indications of some success in the analysis of simple flavonoid glycosides. Also, it would be interesting to investigate the use of the LC-CF-LSIMS methods described in this thesis as a possible means for the detection and identification of saponins. The LC-CF-LSIMS of saponins would yield a solution to the problem of UV detection of the extremely poor chromaphores. Another suggestion for future research would include the adaptation of the LC-CF-LSIMS method reported here to a coaxial matrix delivery setup. This would remove the glycerol from the mobile phase and provide greater chromatographic resolution in both analytical and nanoscale HPLC. Finally, it is strongly suggested that nanoscale HPLC interfaced with ESI or APCI be investigated for the identification of flavonoid conjugates.

REFERENCES

1. J. J. Thompson, *Rays of Positive Electricity and Their Application to Chemical Analyses*, F. Horton, Ed., Longmans, Green and Co., London, 1913.

2. F. W. McLafferty, *Interpretation of Mass Spectra*, 3rd Ed., University Science Books, Mill Valley, CA, USA, 1980.

3. J. T. Watson, *Introduction To Mass Spectrometry*, 2nd Ed., Raven Press, New York, 1985.

4. M. S. B. Munson and F. H. Field, *J. Am. Chem. Soc.*, **88**, 2621 (1966).

5. F. H. Field, *J. Am. Soc. Mass Spectrom.*, **1**, 277 (1990).

6. A. Benninghoven, F. G. Rudenauer, and H. W. Werner, *Secondary Ion Mass Spectrometry - Basic Concepts, Instrumental Aspects, Applications and Trends*, John Wiley & Sons, New York, 1987.

7. R. D. Macfarlane and D. F. Torgerson, *Science*, **191**, 920 (1976).

8. M. Barber, R. S. Bordoli, G. J. Elliot, R. D. Sedgewick, and A. N. Tyler, *Anal. Chem.*, **54**, 645A (1982).

9. W. Aberth, K M. Straub and A. L. Burlingame, *Anal. Chem.*, **54**, 2029 (1982).

10. S. J. Pachuta and R. G. Cooks, *Chem. Rev.*, **87**, 647 (1987).

11. P. Sigmund, Phy. Rev., 184, 383 (1969).

12. P. Sigmund, *Sputtering by Particle Bombardment I*, in *Topics in Applied Physics, Vol. 47*, R. Behrisch (Ed.), Springer-Verlag, Berlin, 1981,p 9.

13. R. Stoll, U. Schade, U. Giessman, and D. Barofsky, *Int. J. Mass Spectrom. Ion Phys.*, **43**, 227 (1982).

14. B. J. Garrison, *J. Am. Chem. Soc.*, **105**, 373 (1983).

15. H. Munster, F. Theobald, H. Budzikiewicz, and E. Schroder, *Int. J. Mass Spectrom. Ion Processess*, **79**, 73 (1987).

16. R. Stoll, U. Schade, U. Giessman, and D. Barofsky, *Int. J. Mass Spectrom. Ion Phys.*, **43**, 227 (1982).

17. G. Bojessen and J. Moller, *Int. J. Mass Spectrom. Ion Processess*, **68**, 239 (1986).

18. S. Naylor, A. F. Findeis, B. W. Gibson, and D. H. Williams, *J. Am. Chem. Soc.*, **108**, 6359 (1986).

19. D. H. Williams, C. V. Bradley, S. Santikarn, and G. Bojesen, *Biochem. J.*, **201**, 105 (1982).

20. W. V. Ligon, Jr., and S. B. Dorn, *Int. J. Mass Spectrom. Ion Processess*, **78**, 99 (1986).

21. A. Dell, P. Azadi, P. Tiller, and J. Thomas-Oates, *Carbohydr. Res.*, **200**, 59 (1990).

22. M. Barber, R. S. Bordoli, R. D. Sedgewick, and A. N. Tyler, *Biomed. Mass Spectrom.*, **87**, 105 (1987).

23. E. De Pauw, *Mass Spec. Rev.*, **5**, 191 (1986).

24. C. Fenselqu and R. J. Coter, *Chem. Rev.*, **87**, 501 (1987).

25. L. Stryer, *Biochemistry*, 2nd Ed., W. H. Freeman & Co., San Fransisco, 1981, p 129.

26. D. Voet and J. G. Voet, *Biochemistry*, John Wiley & Sons, New York, 1990, p 32.

27. J. G. Pavlovich, T. Yen, D. F. Barofsky, J. Kopniczky, B. U. R. Sundquist, proceeding of the 40th Annual American Society for Mass Spectrometry Conference on Mass Spectrometry and Allied Topics, Washington, DC, May 31-June 5, 1992.

28. M. A. Baldwin and F. W. McLafferty, *Org. Mass Spectrom.*, 7, 1111 (1973).

29. J. W. Serum and A. Melera, Paper No. 589 presented at the 29th Pittsburgh Conference on Analytical Chemistry and Applied Spectroscopy, 27 Feb. - 3 March 1978.

30. A. Melera, *Adv. Mass Spectrom.*, **8B**, 1597 (1980).

31. R. P. W. Scott, C. G. Scott, M. Munroe, and J. Hess, Jr., *J. Chromatogr.*, **99**, 395 (1974).

32. W. H. McFadden, H. L. Schwartz, and S. J. Evans, *J. Chromatogr.*, **122**, 389 (1976).

33. W. H. McFadden, D. C. Bradford, D. E. Games, and J. L. Gower, *Am. Lab.*, **October**, 55 (1976).

34. J. G. Stroh, J. C. Cook, R. M. Milberg, L. Brayton, T. Kigara, Z. Huang, K. L. Rinehart, Jr., and I. A. S. Lewis, *Anal. Chem.*, **57**, 985 (1985).

35. C. R. Blakely and M. L. Westal, *Anal. Chem.*, **55**, 750 (1983).

36. M. L. Vestal and G. J. Fergusson, *Anal. Chem.*, **57**, 2373 (1985).

37. R. D. Voyksner and C. A. Haney, *Anal. Chem.*, **57**, 991 (1985).

38. M. R. Clench, R. Owen, V. C. Parr, O. Weir, and D. Wood, "Application of Plasmaspray LC-MS", VG Tritech Applications Note (1987).

39. R. C. Willoughby and R. F. Browner, *Anal. Chem.*, **56**, 2626 (1984).

40. P. C. Winkler, D.D. Perkins, W. K. Williams, and R. F. Browner, *Anal. Chem.*, **60**, 489 (1988).

41. J. D. Kirk and R. F. Browner, *Biomed. and Environ. Mass Spectrom.*, **18**, 355 (1989).

42. D. H. Russell, Dept. of Chemistry, Texas A & M University, personal communication.

43. Y. Ito, T. Takeuchi, D. Ishi and M. J. Goto, *J. Chromatogr.*, **346**, 161 (1985).

44. R. M. Caprioli, T. Fan and J. S. Cottrell, *Anal. Chem.*, **58**, 2949 (1986).

45. R. M. Caprioli and T. Fan, *Biochem. Biophys. Res. Commun.*, **141**, 1058 (1986).

46. R. M. Caprioli, W. T. Moore, and T. Fan, *Rapid Commun. Mass Spectrom.*, **1**, 15 (1987).

47. R. M. Caprioli and W. T. Moore, *Int. J. Mass Spectrom. Ion Processess*, **86**, 187 (1988).

48. R. M. Caprioli, *Biochemistry*, **27**, 513 (1988).

49. R. M. Caprioli, *Trends Anal. Chem.*, **7**, 328 (1988).

50. R. M. Caprioli and B. B. DaGue, *J. Chromatogr. Sci.*, **26,** 640 (1988).

51. W. E. Seifert, Jr., A. Ballatore, and R. M. Caprioli, *Rapid Commun. Mass Spectrom.*, **3**, 117 (1989).

52. R. M. Caprioli, *Anal. Chem.*, **62**, 477A (1990).

53. T. L. Wang, M. Shish, and S. P. Markey, *Anal. Chem.*, **61**, 1013 (1989).

54. P. Kokkonen, W. M. A. Niessen, U.R. Tjaden and J. van der Greef, *J. Chromatogr.*, **474**, 59 (1989).

55. J. S. M. de Wit, L. J. Deterding, M. A. Moseley, K. B. Tomer, and J. W. Jorgenson, *Rapid Commun. Mass Spectrom.*, **2**, 100 (1988).

56. M. A. Moseley, L. J. Deterding, J. S. M. de Wit, K. B. Tomer, R. T. Kennedy, N. Bragg, and J. W. Jorgenson, *Anal. Chem.*, **61**, 1577 (1989).

57. S. Pleasance, P. Thibault, M. A. Mosely, L. J. Deterding, K. B. Tomer, and J. W. Jorgenson, *J. Am. Soc. Mass Spectrom.*, **1**, 312 (1990).

58. J. P. Gagne, A. Carrier, and M. J. Bertrand, *J. Chromatogr.*, **554**, 47, (1991).

59. J. P. Gagne, A. Carrier, and M. J. Bertrand, *J. Chromatogr.*, **554**, 61, (1991).

60. R. M. Caprioli in *Continuous-Flow Fast Atom Bombardment Mass Spectrometry*, R. M. Caprioli, Ed., John Wiley & Sons, Chichester, West Sussex, England, 1990, chapter 1, p 11.

61. T. Takeuchi and D. Ishii, *J. Chromatogr.*, **213**, 25 (1981).

62. C. Borra, S. M. Han, and M. Novotny, *J. Chromatogr.*, **385**, 75 (1987).

63. R. T. Kennedy and J. W. Jorgenson, *Anal. Chem.*, **61**, 1128 (1989).

64. M. Dole, L. L. Mack, R. L. Hines, R. C. Mobley, L. D. Ferguson, and M. B. Alice, *J. Chem. Phys.*, **49**, 2240 (1968).

65. L. L. Mack, P. Kralik, A. Rheude, and M. Dole, *J. Chem. Phys.*, **52**, 4977 (1970).

66. D. Teer and M. Dole, *J. Polym. Sci.*, **13**, 985 (1975).

67. M. Yamashita and J. B. Fenn, *J. Phys. Chem.*, **88**, 4451 (1984).

68. M. Yamashita and J. B. Fenn, *J. Phys. Chem.*, **88**, 4671 (1984).

69. C. M. Whitehouse, R. N, Dreyer, M. Yamashita, and J. B. Fenn, *Anal. Chem.*, **57**, 675 (1985).

70. R. D. Smith, J. A. Loo, R. R. O. Loo, M. Busman, and H. R. Udseth, *Mass Spectrom. Rev.*, **10**, 359 (1991).

71. M. Mann, S. F. Wong, and J. B. Fenn In *Ion Formation from Organic Solids*, IFOS V, A. Hedin, Ed.; John Wiley & Sons: New York, 1990: p 139.

72. R. D. Smith, J. A. Loo, C. G. Edmonds, C. J. Barinaga, and H. R. Udseth, *Anal. Chem.*, **62**, 882 (1990).

73. S. F. Wong, C. K. Meng, and J. B. Fenn, *J. Phys. Chem.*, **92**, 546 (1988).

74. *The API Book* by Perkin Elmer Sciex, Central Reproductions, Mississauga, Ontario, Canada, 1990.

75. Y. Kato. S. Takahashi, H. Hirose, M. Skairi, and H. Kambara, *Biomed. Mass Spectrom.*, **14**, 129 (1987).

76. K. L. Busch, G. L. Glish, and S. A. McLuckey in *Mass Spectrometry/Mass Spectrometry Techniques and Applications of Tandem Mass Spectrometry*, VCH Publishers, New York, 1988.

77. *Tandem Mass Spectrometry*, ed. by F. W. McLafferty, Johy Wiley & Sons, New York, 1983.

78. T. J. Mabry and K. R. Markham in *The Flavonoids* ed. by J. B. Harborne, T. J. Mabry and H. Mabry, Academic Press, New York, 1975, p 78.

79. T. J. Mabry and A. Ulubelen in *Biochemical Applications of Mass Spectrometry*, ed. by G. R. Waller and O. C. Dermer, First Supplementary Volume, Wiley-Interscience, 1976, p 1131.

80. T. R. Baker, L. H. Tulich, K. R. Wehmeyer, and G. R. Kelm poster presented at the 41st Annual Amercian Society for Mass Spectrometry Conference on Mass Spectrometry and Allied Topics.

81. R. A. Dixon, *Biol. Rev.*, **61**, 239 (1986).

82. J. W. Blount, R. A. Dixon and N.L. Paiva, *Physiol. Mol. Plant Path.*, **41**, 333 (1992).

83. D. G. Smith, A. G. McInnes, V. J. Higgins and R. L. Miller, *Physiol. Plant Pathology*, **1**, 41 (1971).

84. K. Dalkin, R. E. Edwards, B. Edington and R. A. Dixon, *Plant Physiol.*, **92**, 440 (1990).

85. P. M. Dewick, *Phytochem.*, **16**, 93 (1977).

86. R. Edwards and H. Kessmann in *Molecular Plant Pathology: A Practical Approach,* ed. by J. J. Gurr, M. J. McPherson, and D. J. Bowls, Oxford University Press, Vol. 2, 1992, p 45-62.

87. T. L. Graham and M. Y. Graham, *Molecular Plant-Microbe Interactions*, **4**, 60 (1991).

88. T. L. Graham, J. E. Kim and M. Y. Graham, *Molecular Plant-Microbe Interactions*, **3**, 157 (1990).

89. Y. Sakagami, S. Kumai, and A. Suzuki, *Agr. Biol. Chem.*, **38**, 1031 (1974).

90. P. Kamalarvilas and A. Mort, *Carb. Res.*, **89**, 261 (261)

91. H. Kessman, R. Edwards, P.W. Geno and R.A. Dixon, *Plant Physiol.*, **94**, 227 (1990).

92. M. S. Ahmed, R. H. Dobberstein, and N. R. Farnsworth, *J. Chromatogr.*, **192**, 387 (1980).

93. T. J. Mabry, K. R. Markham, and M. B. Thomas in The Systematic Identification of Flavonoids, Springer-Verlag, New York, 1970.

94. P. A. Hedin and V. A. Phillips, *J. Agric. Food Chem.*, **40**, 507 (1992).

95. M. Stobiecki, W. Olechnowiez-Stepien, H. Rzadkowks-Bodalska, W. Cisowski and E. Budko, *Biomed. and Environ. Mass Spectrom.*, **15**, 589 (1988).

96. J. A. Page and T. Beer, *J. Chromatogr.*, **474**, 51 (1989).

97. J. Wolfender, M. Mailard, A. Marston, and K. Hostettman, *Phytochem. Anal.*, **3**, 193 (1992).

98. F. R. Crow, K. B. Tomer, J. H. Looker and M. L. Gross, *Anal. Biochem.* **155**, 286 (1986).

99. C. G. de Koster, W. Heerma, G. Dijkstra and G. J. Niemann, *Biomed. Mass Spectrom.*, **12**, 596 (1985).

100. Q. M. Li, H. Van den Heuvel, L. Dillen and M. Claeys, *Biolog. Mass Spectrom.*, **21**, 213 (1992).

101. Q. Li, H. Van den Heuvel, O. Delorenzo, J. Corthout, L. A. C. Peters, A. J. Vlietinck and M. Claeys, *J. Chromatogr.*, **562**, 435 (1991).

102. W. Greenaway, I. Gumusdere, and F. R. Whatley, *Phytochem.*, **30**, 1883 (1991).

103. J. D. Orr, L. W. Sumner, R. Edwards, and R. A. Dixon, *Phytochem. Anal.*, **4**, 124 (1993).

104. D. E. Games, M. A. McDowall, K. Evsen, K. H. Schafer, P. Dobberstein, and J. L. Gower, *Biomed. and Environ. Mass Spectrom.*, 11, 87 (1984).

105. Y. Y. Lin, K. J. Ng and S. Yang, *J. Chromatogr.*, **629**, 389 (1993).

106. E. Schröder and I. Merfort, *Biolog. Mass Spectrom.*, **20**, 11 (1991).

107. C. E. M. Heeremans, R. A. M. van der Hoeven, W. M. A. Niessan, U. R. Tjaden, and J. van der Greef, *J. Chromatogr.*, **474**, 149 (1989).

108. M. P. Balogh and C. Stacey, *J. Chromatogr.*, **562**, 73 (1991).

109. M. Beechi and D. Fraisse, *Biomed. and Environ. Mass Spectrom.*, **18**, 122 (1989).

110. W. H. Aberth and A. L. Burlingame, *Anal. Chem.* **60**, 1426 (1988).

111. F. Dondi, Y. D. Kahie, G. Lodi, G. Blo, C. Pietrogrande, and P. Reschiglian, *J. Chromatogr.*, **461**, 281 (1989).

112. J. Koster, A. Zuzok, and W. Barz, *J. Chromatogr.*, **270**, 392 (1983).

113. U. Jaques, J. Koster, and W. Barz, *Phytochem.*, **24**, 949 (1985).

114. J. Koster, D. Strack, and W. Barz, *Plant Med.*, **48**, 131 (1983).

115. W. Olesek, K. R. Price, I. J. Colqhoun, M. Jurzysta, M. Ploszynski, and G. R. Fenwick, *J. Agric. Food Chem.*, **38**, 1810 (1990).

116. A. C. Barefoot, R. W. Reiser, and S. A. Cousins, *J. Chromatogr.*, **474**, 39 (1989).

117. A. C. Barefoot and Reiser, *J. Chromatogr.*, **398**, 217 (1987).

118. Personal communication with Z. El Rassi..

APPENDIX A

B/E LINK SCAN TANDEM MASS SPECTROMETRY DERIVATION

Tandem mass spectrometry performed on a reverse-geometry (Nier-Johnson) dual sector instrument consisting of a magnetic sector followed by an electric sector is based on the ion transmission properties of the individual sectors. A brief discussion of these ion transmission properties will be presented followed by a discussion of tandem MS techniques.

The energy imparted to an accelerated ion leaving the source is given by:

$$\text{K.E.} = mv^2/2 = zV \tag{1}$$

where K.E. is the kinetic energy of the ion, m is the mass of the ion in kilograms, v is the velocity of the ion in meters per second, z is the charge in Coulombs (i.e. $z'e$, where z' is an integer number of unit charges and e is the fundamental unit of charge), and V is the acceleration voltage. When the acceleration voltage and ion mass are known, the ion velocity can be calculated by:

$$v = (2zV/m)^{1/2} \tag{2}$$

The motion of an ion in a magnetic field is a circular path normal to the magnetic field and is described by:

$$mv^2/r = zvB \tag{3}$$

where m, v, and z have been previously described, r is the radius of deflection in a magnetic field, and B is the magnetic field strength in units of tesla. Rearrangement of equation 3 demonstrates that ions are dispersed in a magnetic field according to their momentum-to-charge ratio:

$$mv/z = Br \tag{4}$$

Substitution of equation 2 into equation 4 yields:

$$m/z = B^2r^2/2V \tag{5}$$

Equation 5 can be used to describe the various techniques of separating ions with a magnetic sector based on their mass-to-charge value. Mass spectra can be obtained with a magnetic instrument by scanning or varying B, V, or r. Since r is generally fixed, the magnetic field is most commonly scanned at constant V to transmit ions of varying m/z ratio. Similarly at a constant B, V can be scanned to transmit ions of varying m/z values.

The dispersion of ions through an electrostatic sector is given by:

$$mv^2/r = zE \tag{6}$$

where r is the radius of deflection in meters and E is the electrostatic field strength in volts per meter. Rearrangement of equation 6 yields:

$$mv^2/z = rE \tag{7}$$

Since r is typically a fixed value, the above equation shows that ion transmission through the electric sector is a function of the ion's kinetic energy-to-charge ratio (mv^2/z). Thus, an electric sector is an energy analyzer and at a set acceleration potential and electrostatic field strength, ion transmission through an

electric sector is independent of mass since from equation 1, K.E.= $mv^2/z = 2V$.

The above equations describe general ion transmission through magnetic and electric sectors. The presented equations will now be used to discuss tandem mass spectrometry on reverse-geometry sector instruments.

If an ion (parent ion) fragments after it has been accelerated out of the source to produce a product or daughter ion, the product ion no longer has the same kinetic energy-to-charge ratio as the parent ion since the ion's mass (m) has changed. Although, the product ion still has the same velocity as the parent ion. Since the kinetic energy of the product ion has changed, it will no longer pass through the electric sector set at the energy of the parent or E_p but at a value of E_d. E_d can be calculated using equation 7 to set up a ratio of the parent and product ion energies (E_p and E_d) and then solving the ratio for E_d to yield:

$$E_d = E_p m_d z_p / m_p z_d \qquad (8)$$

Thus, tandem mass spectra can be obtained by selecting a parent ion with the magnetic sector followed by fragmentation of the ion in the region between the magnet and electric sector (i.e. field free region 2, FFR2). The product or daughter ions formed after fragmentation are then scanned with the electric sector according to equation 8. This method of tandem mass spectrometry is called mass-analyzed ion kinetic energy microscopy (MIKES). MIKES generates low resolution mass spectra (<500) which might be unsatisfactory for all occasions.

If an ion fragments after acceleration from the ion source and before entering the magnetic field (field free region 1, FFR1), the velocity of the daughter ion (v_d) is

the same as the parent ion (v_p) since it was originally accelerated to the parent ion's velocity prior to fragmentation. In addition, the velocity of the daughter ion is not the same as an ion of similar mass accelerated from the source. The velocity of the daughter ion is given by:

$$v_d = (2zV/m_p)^{1/2} \tag{9}$$

Substituting equation 9 into equation 4 yields:

$$(m_d^2/m_p)/z = B^2r^2/2V \tag{10}$$

Therefore, the daughter ion will pass through the magnetic sector at an apparent mass of m*. This ion is referred to as a metastable ion and produces a broad peak at a mass m* described by:

$$m^* = m_d^2/m_p \tag{11}$$

Tandem mass spectra may also be obtained on a reverse geometry by link scanning or scanning the magnetic and electric sector simultaneously (B/E link scan). This is illustrated by dividing the equation of ion transmission through a magnetic sector (4) by that of ion transmission through an electric sector (7) to produce:

$$B/E = 1/v \tag{12}$$

If fragmentation occurs in FFR1 the product ion will have the same velocity as the parent ion. If the ratio of B/E is set to allow transmission of the parent and then scanned at this same ratio, a product ion spectrum will be obtained. B/E tandem mass spectra are preferred over MIKES due to their higher resolution.

VITA

Lloyd W. Sumner

Candidate for the Degree of

Doctor of Philosophy

Thesis: IDENTIFICATION OF ISOFLAVONOID CONJUGATES BY HIGH PERFORMANCE LIQUID CHROMATOGRAPHY CONTINUOUS-FLOW LIQUID SECONDARY ION MASS SPECTROMETRY

Major Field: Chemistry

Biographical:

Personal Data: Born in Fort Hood, Texas, May 1, 1965, the son of Kenneth and Lynnette Sumner. Married Sherry A. Gilley on September 27, 1985.

Education: Graduated from Lawton High School, Lawton, Oklahoma, May of 1983; received Bachelor of Science Degree with a major in Chemistry and a minor in Mathematics from Cameron University, Lawton, Oklahoma, in May of 1989: completed requirements for the Doctor of Philosophy degree at Oklahoma State University in December, 1993.

Professional Experience: Graduate Teaching Assistant, Department of Chemistry, August, 1989 to May 1990; Graduate Research Assistant, May 1990 to September, 1993; Analyst for the Oklahoma State University Mass Spectrometry Facility, September, 1991, to September, 1993.

Professional Organizations: Member of the American Chemical Society, member and former Vice-President of the Alpha Delta Chapter of Phi Lambda Upsilon, member of the American Society for Mass Spectrometry.